The 17th International Workshop on the Physics of Compressible Turbulent Mixing

Atlanta, GA, USA
July 18 – 22, 2022

Georgia Tech

UNIVERSITY OF NORTH CAROLINA CHARLOTTE

Welcome

The 17th International Workshop on the Physics of Compressible Turbulent Mixing will be held in Atlanta, USA from July 18 – July 22, 2022, and will be jointly hosted by Georgia Tech and the University of North Carolina at Charlotte.

This workshop has been held approximately biennially since 1988, and brings together researchers from universities and research laboratories around the world to discuss the state-of-the-art in theory, modelling, experiment and simulation of compressible and variable-density turbulent mixing induced by hydrodynamic instabilities in multi-material hydrodynamic flows. This meeting was originally planned for 2020, but was postponed due to the COVID 19 pandemic. The workshop will include invited lectures, oral and poster presentations, together with informal round table discussion sessions. A total of 70 abstracts for oral presentations, and 10 poster presentations have been received. In addition, six plenary lectures will be presented.

The organizing committee is grateful to the *Atomic Weapons Establishment, UK,* the *Commissariat à l'énergie atomique et aux énergies alternatives*, *France,* and the *Office of the Executive Vice-President for Research at Georgia Tech* for their generous sponsorship of the workshop.

We thank you for joining us in Atlanta, and for your contributions to this workshop. We wish you an enjoyable stay in Atlanta, and a productive workshop with many fruitful discussions.

Warmest regards,

Local Organizing Committee

Local Organizing Committee

Praveen Ramaprabhu, University of North Carolina at Charlotte (Co-Chair)
Devesh Ranjan, Georgia Tech (Co-Chair)

Oleg Schilling, Lawrence Livermore National Laboratory (Member)
Jacob McFarland, Texas A&M University (Member)
Arindam Banerjee, Lehigh University (Member)
Susan Kurien, Los Alamos National Laboratory (Member)

Time	Sunday, July 17	Monday, July 18	Tuesday, July 19	Wednesday, July 20	Thursday, July 21	Friday, July 22
8:00-8:30		Breakfast				
8:30-8:50		Welcome Remarks	Plenary Lecture: R. Williams, Chair: F. Grinstein	Plenary Lecture: R. Bonazza, Chair: D. Ranjan	RM Simulations & Theory IV, Chair: B. Thornber	Plenary Lecture:S. Balachandar, Chair: J. McFarland
8:50-9:10						
9:10 - 9:30		Plenary Lecture: T. Ma, Chair: B. Remington	RT Simulations & Theory, Chair: F. Grinstein	General Instability & Mixing, Chair: D. Aslangil		Shock Particle & Multiphase Flows I, Chair: J. McFarland
9:30 - 9:50					RM Experiments, Chair: T. Desjardins	
9:50 - 10:10		HEDP I, Chair: B. Remington				
10:10 - 10:30						
10:30 - 10:50						
10:50 - 11:10		Coffee Break				
11:10 - 11:30		Turbulence Modeling I, Chair: O. Schilling	Plenary Lecture: O. Durand, Chair: J. Charonko	HEDP II, Chair: G. Malamud	Turbulence Modeling III, Chair: T. Kaman	Shock Particle & Multiphase Flows II, Chair: J. Capecelatro
11:30 - 11:50						
11:50 - 12:10			Ejecta, EOS & Strength I, Chair: J. Charonko			
12:10 - 12:30						
12:30 - 13:40		Lunch				
13:40 - 14:00		Plenary Lecture: D. Livescu, Chair: R. Williams	RM Simulations & Theory II, Chair: M. Groom	Poster Session	HEDP III, Chair: B. Haines	Turbulence Modeling IV, Chair: Z. Li
14:00 - 14:20						
14:20 - 14:40		RM Simulations & Theory I, Chair: R. Williams				
14:40 - 15:00						Conclusion
15:00 - 15:20				Turbulence Modeling II, Chair: I. Boureima	RT Experiments, Chair: A. Lawrie	Notes: 1. Sci. Comm. Lunch will be held on Tues. 2. Student networking lunch will be on Thurs.
15:20 - 15:40						
15:40 - 16:00		Coffee Break				
16:00 - 16:20		Discussion: O. Schilling, A. Shimony	Ejecta, EOS & Strength II, Chair: O. Durand	RM Simulations & Theory III, Chair: B. Olson	Discussion: J.W. Jacobs, A. Lawrie	
16:20 - 16:40						
16:40 - 17:00						
17:00 - 17:20			Discussion: O. Durand, B. Morgan	Discussion: B. Olson, R. Bonazza		
17:20 - 17:40						
18:00 - 20:00	Welcome Reception					
19:00 - 22:00		Banquet				

Technical Program

Sunday, July 17, 2022

Welcome Reception at the Club Room of the Georgia Tech Hotel and Conference Center (18:00 – 20:00)

Monday, July 18, 2022

Session: Welcome Remarks (08:30 – 09:10)

Introduction and Welcome, Praveen Ramaprabhu, Devesh Ranjan
Presiding remarks, Chaouki Abdallah, Executive Vice-President for Research, Georgia Tech

Session: Plenary Lecture (09:10 – 09:50) 1

Chair: Bruce Remington (LLNL)

09:10 – 09:50 *Advancing High-Energy-Density (HED) Science with Short-Pulse, High-Intensity Lasers*
Tammy Ma, LLNL (ma8@llnl.gov)

Session: High Energy Density Physics I (09:50 – 10:50) 3

Chair: Bruce Remington (LLNL)

09:50 – 10:10 *Hydrodynamic instabilities and mixing in high energy density settings*
Bruce A. Remington (remington2@llnl.gov)

10:10 – 10:30 *Accessible Turbulent HED Plasma Experimental Platforms for Studying Heterogeneous Mix on ICF Fusion Reactions*
K. A. Flippo, H. Li, A. S. Liao, S.T. Li, A. Rasmus, Y. C. Lu, S. R. Kline, J. M. Levesque, C. Kuranz and C. K. Li (kflippo@lanl.gov)

10:30 – 10:50 *Asymptotic Rayleigh-Taylor Instability Experiments on the National Ignition Facility*
Asaf Shimony, Dov Shvarts, Yonatan Elbaz, Kirk A. Flippo, Channing H. Huntington, Stephan A. MacLaren and Guy Malamud (shimonya@gmail.com)

Coffee Break (10:50 – 11:10)

Session: Turbulence Modeling I (11:10 – 12:30) 6

Chair: Oleg Schilling (LLNL)

11:10 – 11:30 *A multispecies turbulence model for restabilized mixing layers*
N. O. Braun, R. A. Gore (nbraun@lanl.gov)

11:30 – 11:50 *Advection vs. Diffusion in Richtmyer-Meshkov and Rayleigh-Taylor Mixing*
Forrest W. Doss (fdoss@lanl.gov)

11:50 – 12:10 *On the Assessment of Two-Level Simulation Model for Numerical Study of Compressible Turbulent Scalar Mixing*
H. Chandrasekhar, R. Ranjan and S. Menon (reetesh-ranjan@utc.edu)

12:10 – 12:30 *Derivation and evaluation of a Reynolds stress model designed to simulate reacting mixing layers*
Denis Souffland, Olivier Soulard and Jérôme Griffond (denis.souffland@cea.fr)

Lunch (12:30 – 13:40)

Session: Plenary Lecture (13:40 – 14:20) 10

Chair: Robin Williams (AWE)

13:40 – 14:20 *Turbulent mixing in flows with large density variations*
Daniel Livescu, LANL (livescu@lanl.gov)

Session: Richtmyer-Meshkov Simulations & Theory I (14:20 – 15:40) 12

Chair: Robin Williams (AWE)

14:20 – 14:40 *Buoyancy-Drag modelling and spike-to-bubble ratios for single-shock Richtmyer-Meshkov mixing*
David Youngs, Michael Groom and Ben Thornber (david.l.youngs.uk@gmail.com)

14:40 – 15:00 *Numerical Simulation of the Broadband Richtmyer-Meshkov Instability and Comparison with Shocktube Experiments*
Michael Groom and Ben Thornber (michael.groom@sydney.edu.au)

15:00 – 15:20 *The Effect of Axial Strain on the Richtmyer-Meshkov Instability*
Bradley Pascoe, Michael Groom, Ben Thornber (b.thornber@sydney.uni.edu.au)

15:20 – 15:40 *A study of modal interaction between different scales of the turbulent Richtmyer-Meshkov instability using high-resolution three-dimensional FLASH simulations*
Mohammad Mohaghar, Jacob McFarland and Devesh Ranjan (mohaghar@gatech.edu)

Coffee Break (15:40 – 16:00)

Session: Discussion (16:00 – 16:40)

Chair: Oleg Schilling (LLNL), Asaf Shimony (U. Michigan)

Banquet at the Fox Theatre (19:00 – 22:00)

Tuesday, July 19, 2022

Session: Plenary Lecture (8:30 – 9:10) 16

Chair: Fernando Grinstein (LANL)

08:30 – 09:10 *The Validity of MILES Simulations*
Robin Williams, AWE (Robin.Williams@awe.co.uk)

Session: Rayleigh-Taylor Simulations & Theory (09:10 – 10:50) 17

Chair: Fernando Grinstein (LANL)

09:10 – 09:30 *Rayleigh-Taylor instability with variable acceleration reversal(s)*
Denis Aslangil, Andrew G.W. Lawrie and Arindam Banerjee (arb612@lehigh.edu)

09:30 – 09:50 *Numerical Study of Plasma Rayleigh-Taylor Instability with Realistic Transport Phenomena*
Zhaorui Li and Daniel Livescu (zhaorui.li@tamucc.edu)

09:50 – 10:10 *Heat Transfer and Variable Transport Property Effects on the Compressible Rayleigh-Taylor Instability*
K. Cherng, S. K. Lele and D. Livescu (kcherng@stanford.edu)

10:10 – 10:30 *Direct numerical simulations of 2D multi-mode compressible Rayleigh-Taylor instability to explore the effects of different iso-thermal stratification strengths*
Man Long Wong and Denis Aslangil (denis.aslangil@ua.edu)

10:30 – 10:50 *Energy Pathways of Rayleigh-Taylor driven Mixing and Implications on Implosion Modeling*
Dongxiao Zhao, Riccardo Betti and Hussein Aluie (hussein@rochester.edu)

Coffee Break (10:50 – 11:10)

Session: Plenary Lecture (11:10 – 11:50) 22

Chair: John Choronko (LANL)

11:10 – 11:50 *Molecular dynamics simulations as a helpful tool to understand the phenomenology of formation and fragmentation of shock-induced hydrodynamic instabilities*
Olivier Durand, CEA (olivier.durand@cea.fr)

Session: Ejecta EOS & Strength I (11:50 – 12:30) 24

Chair: John Choronko (LANL)

11:50 – 12:10 *Modeling the Shell Growth and Breakup of Hydriding Ejecta Particles*
Frederick Ouellet, Alan K. Harrison and Jonathan D. Regele (f.ouellet@lanl.gov)

12:10 – 12:30 *LES of ejecta from irregular surfaces*
M. A. Brown, R. J. R. Williams (matthew.a.brown@awe.co.uk)

Lunch and Scientific Committee Meeting (12:30 – 13:40)

Session: Richtmyer-Meshkov Simulations & Theory II (13:40 – 15:40) 26

Chair: Michael Groom (U. Sydney)

13:40 – 14:00 *Dependence of Enstrophy Transport and Mixed Mass on Dimensionality and Initial Conditions in the Richtmyer–Meshkov Instability Induced Flows*
Ye Zhou, Michael Groom and Ben Thornber (michael.groom@sydney.edu.au)

14:00 – 14:20 *Study of turbulence statistics and transport for Richtmyer-Meshkov instability with re-shock*
Man Long Wong, Jon R. Baltzer, Daniel Livescu, and Sanjiva K. Lele (mlwong@alumni.stanford.edu)

14:20 – 14:40 *Permanence of large eddies in variable-density Richtmyer-Meshkov turbulent mixing zones*
O. Soulard and J. Griffond (olivier.soulard@cea.fr)

14:40 – 15:00 *Linear stability investigations of the Richtmyer-Meshkov instability in an ideal two-fluid plasma*
Yuan Li, Abeer Bakhsh, Ravi Samtaney (ravi.samtaney@kaust.edu.sa)

15:00 – 15:20 *Numerical Simulations of a Perturbed Diffuse Interface Subjected to the Richtmyer-Meshkov Instability: Early Time and Transition to Turbulence*
Sam Pellone, Tiffany Desjardins, Carlos Di Stefano, John Charonko, Forrest Dos (sampellone@lanl.gov)

15:20 – 15:40 *Linear Stability Simulations of Magnetohydrocynamic Richtmyer-Meshkov Instability of Double Interfaces in Cylindrical Geometry*
Abeer Bakhsh, Ravi Samtaney (ahbaksh@uqu.edu.sa)

Coffee Break (15:40 – 16:00)

Session: Ejecta, EOS & Strength II (16:00 – 17:00) 32

Chair: Olivier Durand (CEA)

16:00 – 16:20 *A high-order, localized artificial diffusivity method for Eulerian simulation of multi-material elastic-plastic deformation with strain hardening*
Jacob R. West, Michael C. Adler and Sanjiva K. Lele (jrwest@stanford.edu)

16:20 – 16:40 *Ejecta physics induced by a downward impinging supersonic jet*
Juan Sebastian Rubio, Miguel X. Diaz Lopez, Matt Gorman and Rui Ni (rui.ni@jhu.edu)

16:40 – 17:00 *Transition to Stable Plastic Regime of Rayleigh-Taylor Instability in Elastic-Plastic Solids*
Aren Boyaci and Arindam Banerjee (arb612@lehigh.edu)

Session: Discussion (17:00 – 17:40)

Chair: Olivier Durand (CEA), Brandon Morgan (LLNL)

Wednesday, July 20, 2022

Session: Plenary Lecture (08:30 – 09:10) 35

Chair: Devesh Ranjan (Georgia Tech)

08:30 – 09:10 *The RM Instability After Reshock*
Riccardo Bonazza, U. Wisconsin, Madison (riccardo.bonazza@wisc.edu)

Session: General Instability & Mixing (09:10 – 10:50) 37

Chair: Denis Aslangil (U. Alabama)

09:10 – 09:30 *Diagnostics in extreme environments: a methodology for coupled velocity and scalar measurement*
A. G. W. Lawrie, J. T. Horne, R. J. R. Williams (andrew.lawrie@bristol.ac.uk)

09:30 – 09:50 *Recent Progress on Coarse Grained Simulations of Turbulent Mixing*
Fernando F. Grinstein (fgrinstein@lanl.gov)

09:50 – 10:10 *The subcritical transition to turbulence of Faraday waves in miscible fluids*
M. Cavelier, B.-J. Gréa, A. Briard and L. Gostiaux
(benoit-joseph.grea@cea.fr)

10:10 – 10:30 *Experimental 3D turbulent statistics in non-Boussinesq jet flows*
D. Fratantonio, E. G. Connor, A. Martinez, J. J. Charonko
(dfratantonio@lanl.gov)

10:30 – 10:50 *Different initial composition ratio effects on variable-density turbulent mixing*
Denis Aslangil, Daniel Livescu and Arindam Banerjee
(denis.aslangil@ua.edu)

Coffee Break (10:50 – 11:10)

Session: High Energy Density Physics II (11:10 – 12:30) 42

Chair: Guy Malamud (NRCN)

11:10 – 11:30 *The impact of temperature and material mixing heterogeneities on thermonuclear reactions*
Brian M. Haines, B. J. Albright, T. J. Murphy, M. R. Douglas, J. H. Cooley, T. H. Day, N. A. Denissen, C. Di Stefano, P. Donovan, S. L. Edwards, J. Fincke, C. Forrest, V. Yu. Glebov, L. M. Green, L. Goodwin, R. A. Gore, M. A. Gunderson, J. R. Haack, C. E. Hamilton, E.P. Hartouni, K. C. Henderson, N. V. Kabadi, S. Khan, P. M. Kozlowski, Y. Kim, M. N. Lee, R. Lester, T. Morrow, J. A. Oertel, R. E. Olson, B. M. Patterson, T. Quintana, R. B. Randolph, D. W. Schmidt, R. C. Shah, J. M. Smidt, A. Strickland, C. Wilson, and L.Yin (bmhaines@lanl.gov)

11:30 – 11:50 *Transition to Turbulence and Multiphysics in 3D ICF Capsule Implosions*
F.F. Grinstein, V. Chiravalle and B.M. Haines (fgrinstein@lanl.gov)

11:50 – 12:10 *Computational study of shock-induced instability growth and mixing at high energy density*
Jason D. Bender, Oleg Schilling, Kumar S. Raman, Robert A. Managan, Britton J. Olson, and Shon T. Prisbrey (jbender73@gmail.com)

12:10 – 12:30 *Code Validation of Radiative Shock Propagation through a Porous Foam*
Lauren M. Green, Brian M. Haines, Yong Ho Kim, Pawel M. Kozlowski, Thomas J. Murphy, Brian J. Albright (lgreen@lanl.gov)

Lunch (12:30 – 13:40)

Session: Poster Presentations (13:40 – 15:00) 46

Miscible Experiments on the Rayleigh-Taylor Instability in the Linear Induction Motor Drop Tower
C. J. Withers, M. J. Mokler and J. W. Jacobs (claytonwithers@email.arizona.edu)

Single-mode Richtmyer-Meshkov Instability
R. J. R. Williams, M. G. Probyn, B. Thornber, D. Drikakis, D. L. Youngs (robin.williams@awe.co.uk)

Plasma transport dissipation in turbulent instability mixing
Erik Vold, Jan Velechovsky and Susan Kurien (elv@lanl.gov)

Experimental investigation of Rayleigh-Taylor mixing in gases using simultaneous PIV-LIF
Prasoon Suchandra, Mark Mikhaeil, Gokul Pathikonda, Devesh Ranjan (prasoon.suchandra@gmail.com)

Simulations of Multimode Perturbations Driven by Same-Sided Successive Shocks
R.F. Sacks, F.W. Doss, C.A. Di Stefano, E.C. Merritt, H. Robey (rsacks@lanl.gov)

A density fluctuation analysis for HED Richtmyer-Meshkov experiments
E.C. Merritt, F.W. Doss, J.M. Levesque, T. Desjardins, C.A. Di Stefano, K.A. Flippo, H. F. Robey, R. Sacks, D.W. Schmidt, L. Kot and T. Perry (emerritt@lanl.gov)

Wall Vortices Induced by Re-Shock in RMI Shock Tube Experiments
Raymond McConnell, Chris Noble, Alex Ames, Jason Oakley, David Rothamer and Riccardo Bonazza (rmcconnell2@wisc.edu)

Simulation of shock-tube experiments using a well-characterised initial gas separation
Jérôme Griffond, Marta Rasteiro dos Santos, Yannick Bury, Stéphane Jamme and Denis Souffland (jerome.griffond@cea.fr)

Exploring Shock and Interface Physics to Measure Viscosity
Sonya Dick, Tyler Perez, June Wicks, Marius Millot and Eric Johnsen (scdick@umich.edu)

Numerical investigation of compressibility and Atwood number effects on the single-mode iso-thermally stratified Rayleigh-Taylor Instability
Tyler Prine, Denis Aslangil and Man Long Wong (denis.aslangil@ua.edu)

Session: Turbulence Modeling II (15:00 – 15:40) 56

Chair: Ismael Boureima (LANL)

15:00 – 15:20 *Novel PANS model for variable density turbulence*
Filipe S. Pereira, Fernando Grinstein and Daniel Israel (fmsoarespereira@gmail.com)

15:20 – 15:40 *Learning closure models for turbulence*
Ismael Boureima, Vitaliy Gyrya, Juan Saenz, Susan Kurien, and Marianne Francois (iboureima@lanl.gov)

Coffee Break (15:40 – 16:00)

Session: Richtmyer-Meshkov Simulations & Theory III (16:00 – 17:00) 58

Chair: Britton Olson (LLNL)

16:00 – 16:20 *High−Resolution Simulations of Transitional Triple−Point Shock Interactions*
Alboreno Voci, Sanjiva Lele, Fernando Grinstein, Vincent Chiravalle and Jonathan Regele (albovoci@stanford.edu)

16:20 – 16:40 *Implicit large Eddy Simulations and Analytical Modelling of Shock-Induced Turbulent Mixing in Spherical Implosions*
Moutassem El Rafei and Ben Thornber (ben.thornber@sydney.edu.au)

16:40 – 17:00 *High-resolution front tracking simulations of single-mode Richtmyer-Meshkov Instability*
Tulin Kaman (tkaman@uark.edu)

Session: Discussion (17:00 – 17:40)

Chair: Britton Olson (LLNL) and Riccardo Bonazza (U. Wisconsin)

Thursday, July 21, 2022

Session: Richtmyer-Meshkov Simulations & Theory IV (08:30 – 09:30) 61

Chair: Ben Thornber (U. Sydney)

08:30 – 08:50 *Ejection of vortex rings from shock-accelerated interfaces*
Michael Wadas and Eric Johnsen (mwadas@umich.edu)

08:50 – 09:10 *On the stability of non-isolated steady shock waves*
Andrés Calvo-Rivera, César Huete, Gustavo Wouchuk, and Alexander L. Velikovich (chuete@ing.uc3m.es)

09:10 – 09:30 *Shock Acceleration of a Multifluid Vortex Ring*
Alex Ames, Chris Noble, Ray McConnell, Jason Oakley, David Rothamer, and Riccardo Bonazza (aames@wisc.edu)

Session: Richtmyer-Meshkov Experiments (09:30 – 10:50) 64

Chair: Tiffany Desjardins (LANL)

09:30 – 09:50 *Investigating high-speed velocity measurements in the Blast-Driven Instability*
Samuel J. Petter, Dr. Benjamin C. Musci, Dr. Gokul Pathikonda, and Dr. Devesh Ranjan (devesh.ranjan@me.gatech.edu)

09:50 – 10:10 *Influence of the Shock-To-Reshock Time on the Richtmyer-Meshkov Instability in a Dual-Driver Vertical Shock Tube*
K. J. Ferguson and J. W. Jacobs (kjfergus@email.arizona.edu)

10:10 – 10:30 *Shocked Variable-Density Turbulence Studies*
Tiffany Desjardins, Erin Connor, Adam Martinez and John Charonko (tif_des@lanl.gov)

10:30 – 10:50 *Experimental study of the Richtmyer-Meshkov instability in spherical geometry*
M. Brasseur, C. Mariani, D.C. Barros, G. Jourdan, M. Vandenboomgaerde, D. Souffland (mathieu.brasseur@univ-amu.fr)

Coffee Break (10:50 – 11:10)

Session: Turbulence Modeling III (11:10 – 12:30) 68

Chair: Tulin Kaman (U. Arkansas)

11:10 – 11:30 *Local Wavenumber Model for Inhomogeneous Two-Fluid Mixing*
Nairita Pal, Ismael Boureima, Noah Braun, Susan Kurien, Praveen Ramaprabhu, Andrew Lawrie (nairita@lanl.gov)

11:30 – 11:50 *Advances in Reynolds-averaged Navier-Stokes modeling for reacting turbulent mixing*
Brandon E. Morgan (morgan65@llnl.gov)

11:50 – 12:10 *Calibration of Local Wave-Number Turbulence Model using Machine Learning Techniques*
Ismael Boureima, Vitaliy Gyrya, Juan Saenz, Susan Kurien (vitaliy_gyrya@lanl.gov)

12:10 – 12:30 *Multi-fidelity validation of variable-density turbulent mixing models*
Britton Olson, Benjamin Musci and Devesh Ranjan (olson45@llnl.gov)

Lunch and Student Networking Event (12:30 – 13:40)

Session: High Energy Density Physics III (13:40 – 15:00) 72

Chair: Brian Haines (LANL)

13:40 – 14:00 *Plasma kinetic effects on the deceleration Rayleigh-Taylor instability*
Jan Velechovsky, Erik Vold and Susan Kurien (jan@lanl.gov)

14:00 – 14:20 *Analysis of Mix Using the Method of Separated Reactants on Indirect Drive Gas-Fill Implosions at the National Ignition Facility*
A.R. Vazsonyi, J.E. Pino, B.E. Morgan, and K.K. Mackay (vazsonyi1@llnl.gov)

14:20 – 14:40 *Demonstration of a Divergent Shock-Bubble Interaction in a High Energy Density Plasma*
Pawel M. Kozlowski, Yongho Kim, Brian M. Haines, Joseph M. Smidt, Tana Morrow, Shaun G. Newman, Thomas J. Murphy, Melissa R. Douglas, Brian J. Albright (pkozlowski@lanl.gov)

14:40 – 15:00 *The Impact of Fill Tube Geometry on Recent High Yield Implosions on the National Ignition Facility*
John Kuczek, Brian M. Haines (jkuczek@lanl.gov)

Session: Rayleigh-Taylor Experiments (15:00 – 15:40) 76

Chair: Andrew Lawrie (U. Bristol)

15:00 – 15:20 *Experimental investigation of the multilayer Rayleigh-Taylor instability*
Prasoon Suchandra, Devesh Ranjan (prasoon.suchandra@gmail.com)

15:20 – 15:40 *Stratified flows under variable global acceleration*
J. T. Horne, A. G. W. Lawrie (jonathan.horne@bristol.ac.uk)

Coffee Break (15:40 – 16:00)

Session: Discussion (16:00 – 16:40)

Chair: Jeff Jacobs (U. Arizona), Andrew Lawrie (U. Bristol)

Friday, July 22, 2022

Session: Plenary Lecture (08:30 – 09:10) 78

Chair: Jacob McFarland (Texas A&M)

08:30 – 09:10 *Shock-Particle Interaction and Explosive Dispersal of Particles*
Sivaramakrishnan Balachandar, U. Florida (bala1s@ufl.edu)

Session: Shock Particle Interactions & Multiphase Flows I (09:10 – 10:50) 79

Chair: Jacob McFarland (Texas A&M)

09:10 – 09:30 *Numerical investigation of drag and turbulence in compressible flows through particle suspensions*
Archana Sridhar, Mehdi Khalloufi and Jesse Capecelatro (arsridha@umich.edu)

09:30 – 09:50 *An Euler--Lagrange Approach for Turbulent Particle-laden Compressible Flows*
Meet Patel and Jesse Capecelatro (meetm@umich.edu)

09:50 – 10:10 *Comparisons of Explosive Dispersal in Static and Supersonic Conditions*
Bradford Durant, Frederick Ouellet, S. Balachandar and T. Jackson (neoncrash@ufl.edu)

10:10 – 10:30 *Break up and Evaporation in Shock Driven Multiphase Mixing*
Vasco O. Duke W., Calvin J. Young, Jacob A. McFarland (mcfarlandja@tamu.edu)

10:30 – 10:50 *Modeling of Droplet Breakup and Impact in Supersonic Flight*
Sam Briney, S. Balachandar (bala1s@ufl.edu)

Coffee Break (10:50 – 11:10)

Session: Shock Particle Interactions & Multiphase Flows II (11:10 – 12:30) 84

Chair: Jesse Capecelatro (U. Michigan)

11:10 – 11:30 *Multiphase Phenomena in Heterogeneous Detonations*
Calvin J. Young, Vasco O.D. Walker, Jacob A. McFarland (mcfarlandja@tamu.edu)

11:30 – 11:50 *Jet initiation from shock wave-induced microbubble collapse*
Guillaume T. Bokman, Luc Biasiori-Poulanges, Daniel W. Meyer and Outi Supponen (bokmang@ethz.ch)

11:50 – 12:10 *Shock-induced release of a gas-encapsulated droplet*
Luc Biasiori-Poulanges, Guillaume Bokman, Enea Baumann and Outi Supponen (lbiasiori@ethz.ch)

12:10 – 12:30 *Effect of surface instabilities on evaporation rates of shock-driven droplets*
Prashant Tarey, Praveen Ramaprabhu and Jacob McFarland (pramapra@uncc.edu)

Lunch (12:30 – 13:40)

Session: Turbulence Modeling IV (13:40 – 14:40) 88

Chair: Zhaorui Li (Texas A&M University – Corpus Christi)

13:40 – 14:00 *Buoyancy–Shear–Drag–Scalar-Based Turbulence Modeling for Rayleigh–Taylor, Reshocked Richtmyer–Meshkov, and Kelvin–Helmholtz Mixing: Applications*
Oleg Schilling (schilling1@llnl.gov)

14:00 – 14:20 *Three- and Four-Equation Reynolds-Averaged Navier−Stokes Modeling of a Small Atwood Number, Transitional Rayleigh−Taylor Mixing Experiment*
N. J. Mueschke and Oleg Schilling (schilling1@llnl.gov)

14:20 – 14:40 *Convergence problem of Reynolds-averaged Navier-Stokes modeling in case of shock waves*
Maksim Igorevich Boldyrev, I.V. Glazyrin and N.A. Mikhailov (boldyrevmi@vniitf.ru)

Concluding Remarks (14:40 – 15:00)

Advancing High-Energy-Density (HED) Science with Short-Pulse, High-Intensity Lasers

T. Ma[1,*], D. Mariscal[1], S. Ade[1], R. Anirudh[1], T. Bremer[1], H. Chen[1], B. Djordjevic[1], S. Feister[2], E. Grace[1,3], A. Kemp[1], S. Kerr[1], J. Kim[4], N. Lemos[1], A. J. Mackinnon[1], P. Poole[1], B. Remington[1], D. Rusby[1], D. Schneider[1], G. Scott[1], R. Shepherd[1], M. Sherlock[1], R. Simpson[1,5], B. Spears[1], K. Swanson[1], T. Spinka[1], J. Thiagarajan[1], B. Van Essen[1], S. Wilks[1], G. J. Williams[1], G. Zeraouli[6], A. Zylstra[1], and V. Tang[1]

[1]Lawrence Livermore National Laboratory, Livermore, CA, USA
[2]California State University, Channel Islands, Camarillo, CA, USA
[3]Georgia Institute of Technology, Atlanta, GA, USA
[4]University of California, San Diego, La Jolla, CA, USA
[5]Massachusetts Institute of Technology, Boston, MA, USA
[6]Colorado State University, Fort Collins, CO, USA

[*]**Corresponding Author: ma8@llnl.gov**

High Energy Density Science (HEDS) represents a rich and diverse portfolio of research spanning from the laboratory scale to the astrophysical scale within the broader field of plasma physics. As succinctly stated in the 2003 report, *Frontiers in High Energy Density Physics: The X-Games of Contemporary Science*, "A new generation of sophisticated laboratory systems ("drivers"), now existing or planned, creates matter under extreme high energy density conditions (exceeding 10^{11} J/m^3), permitting the detailed exploration of physical phenomena under conditions not unlike those in astrophysical systems"[1]. High-intensity (irradiance) lasers (>10^{18} W/cm^2) represent one such type of driver that has opened up an entirely new set of discoveries. Their ability to precisely heat, compress, generate, and probe extreme states of matter provides a versatile and powerful tool to explore and grow the field[2].

Soon after the chirped pulse amplification (CPA) scheme was invented by Morou and Strickland[3], Lawrence Livermore National Laboratory (LLNL) demonstrated the first implementation of CPA at the petawatt level in 1996, which subsequently ushered in a new realm of physics. At 1.3 PW (1,300,000,000,000,000 watts of power), and a peak intensity > 10^{21} W/cm^2, the Nova Petawatt[4] launched an unanticipated revolution in laser plasma physics, demonstrating for the first time 10-100 MeV electron beams[5], laser-generated proton beams[6], hard x-rays and gamma-rays, and photo-fission[7].

Innovative photonics technologies today continue to push the boundaries to ever higher laser energies, intensities, and average powers, and with them come a range of new research opportunities in creating and probing extreme states of matter, the development of secondary particle and photon sources, and advanced plasma photonics. In this talk, we will discuss research efforts at LLNL, from exploring fundamental short-pulse physics on the world's most energetic short-pulse laser, to developing the full integrated HED experimental system necessary to take advantage of high-repetition-rate lasers, to bridging over to application space with laser-driven secondary sources.

LLNL's National Ignition Facility-Advanced Radiographic Capability (NIF-ARC)[8] is currently the most energetic (4.8 kJ) short-pulse laser in the world. It further distinguishes itself by sitting in a different parameter space from most other short-pulse lasers: four separate beamlets, relatively long (multi-picosecond), large focal spot, and quasi-relativistic (~10^{18} W/cm^2) intensities. Despite these relatively low intensities, highly relativistic electron acceleration is possible[9], and protons have been generated that exceed the conventional scaling[10] by 5x[11]. Coupled to the 192 long-pulse beams of the NIF, the ARC offers exciting possibilities for HED and astrophysics such as proton isochoric heating of dense plasmas to several 100's of eV temperatures and 3D tomography of evolving plasma conditions. Another unique feature of the NIF-ARC is its high-fidelity, on-shot laser characterization which allows for precise multi-step modeling of the time-dependent laser-plasma interaction to establish a short-pulse physics predictive capability.

Also of particular interest is the development of high-repetition-rate laser science. Whereas most of today's high-energy lasers are single-shot (i.e., typically ~ 1 shot/hour), higher-rep-rate (10 Hz) intense short-pulse and (shot/min) high-energy long-pulse lasers are rapidly being brought online around the world and promise a radical paradigm shift in the way HED physics is done by dramatically increasing shot rates. This will herald a new era where HED conditions and high-energy particle sources can be produced at unprecedented pace, increasing not only the phase space that can be explored, but enabling increased robustness, repeatability, error bar reduction, faster data acquisition, and *accelerated learning in HED science.* The integration and development of high-throughput targetry and diagnostics, data analytics and machine learning, rapid simulation and feedback control will be required to harness this potential. At LLNL, work is currently ongoing to combine interdisciplinary expertise in everything from advanced optics to cognitive computing to additive manufacturing to simultaneously accelerate both empirical discovery and model development.

Another major thrust is the use of short-pulse, high-intensity lasers for the development of laser-driven particle (proton, electron, neutron, ion) and radiation (x-ray, gamma ray) beams, aka secondary sources[12]. Such sources offer unique properties that are not accessible with conventional radiofrequency accelerators, such as ultrashort duration allowing time-resolution of dynamic processes, small source size for high resolution imaging, directional beams, and high compactness. Here, R&D continues in improving the fundamental understanding of the laser-plasma interaction, scaling physics of beam

characteristics with laser parameters, and novel schemes for increasing flux or achieving on-demand tunability.

Via an integrated experimental, theoretical, and modeling effort, the LLNL high-intensity laser HED science program seeks to provide new capability in, and drive forward frontier HED, high-intensity applications, and future light sources.

Acknowledgments: This work was performed under the auspices of the U.S. Department of Energy by Lawrence Livermore National Laboratory under contract DE-AC52-07NA27344, and supported in part by LDRDs 17-ERD-039, 20-ERD-048, 21-ERD-015, and 22-ERD-022, and DOE SCW1722 and DOE Early Career SCW1651.

References

[1] National Research Council. 2003. Frontiers in High Energy Density Physics: The X-Games of Contemporary Science. Washington, DC: The National Academies Press. *https://doi.org/10.17226/10544.*
[2] P. Bucksbaum *et al., The Science and Applications of Ultrafast Intense Lasers* (2002)
[3] Strickland and Mourou, *Optics Comm.* **56**, 219 (1985).
[4] February 1985 issue of *Energy & Technology Review,* UCRL-52000-85-2, Lawrence Livermore National Laboratory
[5] M.H. Key *et al.,* in *Proceedings of the 1st International Conference on Inertial Fusion Sciences and Applications*, Bordeaux, France, 1999 (Elsevier, Paris, 2000).
[6] R. A. Snavely, *et al*., *Phys. Rev. Lett.* **85**, 2945 (2000)
[7] M. Roth *et al.*, in *Proceedings of the 1st International Conference on Inertial Fusion Sciences and Applications*, Bordeaux, France, 1999 (Elsevier, Paris, 2000).
[8] J. K. Crane, *et al.*, *J. Phys.: Conf. Ser.* **244**, 032003 (2010).
[9] G. J. Williams, *et al., Phys. Rev. E* **101**, 031201 (2020).
[10] J. Fuchs, *et al., Nature Phys.* **2**, 48 (2006).
[11] D. Mariscal, *et al., Phys. Plasmas* **26**, 043110 (2019).
[12] M. Borghesi, *et al., Fusion Sci. Tech.* **49**, 412 (2006).

Hydrodynamic instabilities and mixing in high energy density settings

Bruce A. Remington[1]

[1]Lawrence Livermore National Laboratory, Livermore, CA, USA

[*]**Corresponding Author: remington2@llnl.gov**

Hydrodynamic instability experiments are being developed and carried out on the National Ignition Facility (NIF) laser at LLNL through the NIF Discovery Science (basic science) program and the high energy density science (HEDS) program. The motivations are many, including supernova explosion dynamics [1, 2]; supernova remnant evolution [3, 4]; planetary formation dynamics [5, 6, 7]; and asteroid impact and breakup dynamics [8]. Examples include single-mode and multimode classical (non-stabilized) Rayleigh-Taylor (RT) experiments in planar geometry [9, 10]; classical RT in single-mode cylindrically convergent geometry [11, 12]; RT mixing into the hot spot at high compression in inertial confinement fusion (ICF) capsule implosions [13, 14, 15, 16]; ablation front RT experiments in direct drive [17]; in indirect drive [18]; and in the nonlinear RT bubble merger regime [19]. Radiative shock stabilized RT instability experiments have been developed [4]; as well as material strength stabilized RT experiments at high pressures and strain rates in solid-state ductile metals [20]. Examples will be given, connections to astrophysical and planetary science settings made; and future directions will be discussed.

Acknowledgments: The experiments described were done, in part, through the NIF Discovery Science Program.

References

[1]. K. Kifonidis *et al.*, "Non-spherical core collapse supernovae: neutrino-driven convection, Rayleigh-Taylor instabilities, and the formation and propagation of metal clumps", Astronomy & Astrophysics 408, 621 (2003).

[2]. E. Müller, B. Fryxell, D. Arnett, "Instability and clumping in SN 1987A", Astronomy & Astrophysics 251, 505 (1991).

[3] F. Fraschetti et al., "Simulation of the growth of the 3D Rayleigh-Taylor instability in supernova remnants using an expanding reference frame," Astronomy & Astrophysics 515, A104 (2010).

[4] C.C. Kuranz et al., "How high energy fluxes may affect Rayleigh–Taylor instability growth in young supernova remnants," Nat. Commun. 9, 1564 (2018).

[5] Shigeru Ida et al., "The Earth's core formation due to the Rayleigh-Taylor instability," Icarus 69, 239 (1987)

[6] Takanori Sasaki and Yutaka Abe, "Rayleigh-Taylor instability after giant impacts: imperfect equilibration of the Hf-W system and its effect on the core formation age," Earth Planets Space, 59, 1035 (2007).

[7] Trudi Hoogenboom and Gregory A. Houseman, "Rayleigh–Taylor instability as a mechanism for corona formation on Venus," Icarus 180, 292 (2006).

[8] D.G. Korycansky et al., "High-resolution calculations of asteroid impacts into the Venusian atmosphere," Icarus 146, 387 (2000).

[9] S.R. Nagel et al., "A platform for studying the Rayleigh–Taylor and Richtmyer–Meshkov instabilities in a planar geometry at high energy density at the National Ignition Facility," Phys. Plasmas 24, 072704 (2017).

[10] A. Shimoni et al., "Determining the self-similar stage of the Rayleigh-Taylor instability through NIF Discovery Science experiments," PRL, in preparation (2022).

[11] J.P. Sauppe et al. "Demonstration of scale-invariant Rayleigh-Taylor instability growth in laser-driven cylindrical implosion experiments," Phys. Rev. Lett. 124, 185003 (2020).

[12] S. Palaniyappan et al., "Hydro-scaling of direct-drive cylindrical implosions at the Omega and the National Ignition Facility," Phys. Plasmas 27, 042708 (2020).

[13] V.A. Smalyuk et al., "Recent and planned hydrodynamic instability experiments on indirect-drive implosions on the National Ignition Facility," HEDP 36, 100820 (2020).

[14] V.A. Smalyuk et al., "Review of hydrodynamic instability experiments in inertially confined fusion implosions on NIF," PPCF 62, 014007 (2020).

[15] T. Ma et al., "Onset of hydrodynamic mix in high-velocity, highly compressed inertial confinement fusion implosions," PRL 111, 085004 (2013).

[16] B. Bachmann et al., "Localized mix-induced radiative cooling in a capsule implosion at the National Ignition Facility," PRE 101, 033205 (2020).

[17] A. Casner et al., "Long-duration planar direct-drive hydrodynamics experiments on the NIF," Plasma Phys. Control. Fusion 60, 014012 (2018).

[18] D.T. Casey et al., "Reduced instability growth with high-adiabat high-foot implosions at the National Ignition Facility," PRE 90, 011102(R) (2014).

[19] D. A. Martinez et al., "Evidence for a bubble-competition regime in indirectly driven ablative Rayleigh-Taylor instability experiments on the NIF," PRL 114, 215004 (2015).

[20] A. Krygier et al., "Extreme hardening of Pb at high pressure and strain rate," Phys. Rev. Lett. 123, 205701 (2019).

Accessible Turbulent HED Plasma Experimental Platforms for Studying Heterogeneous Mix on ICF Fusion Reactions

K. A. Flippo[1*], H. Li[1], A. S. Liao[1], S.T. Li[1], A. Rasmus[1],Y. C. Lu[1,2], S. R. Kline[3], J. M. Levesque[3], C. Kuranz[3] and C. K. Li[4]

[1]Los Alamos National Laboratory, Los Alamos, NM, USA
[2]Rice University, Houston, TX, USA
[3]University of Michigan, Ann Arbor, MI, USA
[4]Massachussetts Institute of Technology, Cambridge, MA, USA

[*]**Corresponding Author: kflippo@lanl.gov**

Our team at LANL has developed a laser-driven plasma plume experiment as a means of studying the turbulent magnetic dynamo[1]. Such dynamos are thought to have amplified the weak, primordial magnetic fields generated in the Early Universe to present-day strengths seen in the cosmos. Our recent experiments on the OMEGA-EP laser have recreate the turbulent dynamo in the laboratory. Here, we present the data from this turbulent dynamo and look at ways to study turbulent mixing as a way to gain insight into Inertial Confinement Fusion (ICF) implosions.

It is now generally accepted that the ICF experiments like those using the NIF laser to compress a small capsule suffer major yield degradation due to mix [2,3] caused by "jets" (from the fill-tube) and "meteors" (from tent supporting the target). Mix of material into the fusing hot-spot (see Fig. 1) is one primary reason that prevents ignition in the standard design. LANL's ICF portfolio's main ignition-like platform is the double-shell concept[4], which also uses a fill-tube, and in addition, has a joint in the two outer hemispheres to allow assembly of the inner parts. These features can feed-through to the inner shell as a jet or jetted ring if not properly designed. The way these jets propagate and mix, either as bulk material or atomic mixtures, is unknown, as the diagnostics resolution of 20-30 microns is on order of the hot-spot itself (Fig. 1, middle and left).

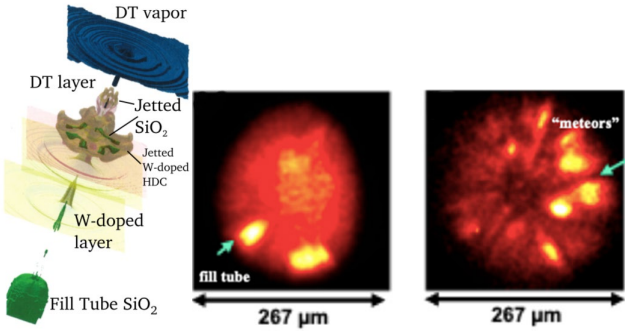

Figure 1: (left) A RAGE simulation [5] of the fill tube jetting into the compressed ICF fuel. An x-ray image (middle) from a NIF implosion, showing the fill tube glowing, and (right) multiple hot x-ray objects ,"meteors," mixing into the fuel region of a perturbed ICF capsule.

We present a new HED turbulent mix platform containing a turbulent plasma jet. Using three powerful Omega EP lasers (Fig. 2 left, blue) in long-pulse (10 ns) mode, we strike the cone's inner surface, producing an outflowing turbulent jet. The magnetic field structure in the dynamo region has been measured using proton radiography (Fig. 2, right) from a 4th short-pulse laser beam. Each long-pulse laser is a 351 nm, 3ω UV beam delivering ~4-5 kJ over a 10 ns-long square pulse

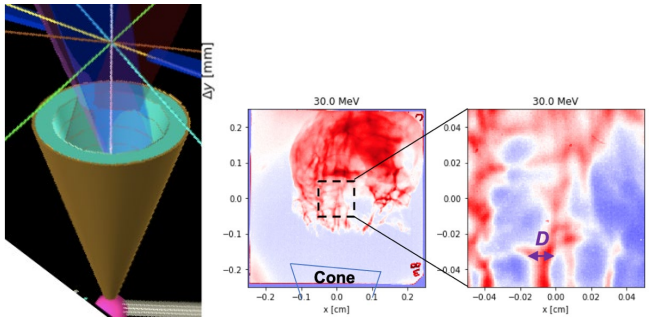

Figure 2: (left) The design of our Omega EP experiment. Laser beams strike the inner surface of a cone. A turbulent jet is formed along the cone axis. (right) Proton radiographs of the turbulent plasma using the dynamo produced fields to diagnose the turbulence. The region ~mm in size, with a density ~ $10^{19\text{-}20}$/cc lasts for ~ 5 ns.

focused with a SG8-750 DPP, that is a supergaussian of degree 4.5 and e-folding radius of 438 μm.

The ablated cone plasmas converge to form a turbulent, magnetized jet directed along the target axis. Heat, momentum and matter fluxes in this jet are quasi-steady along significant lengths above the lip of the cone for times greater than about 5 ns and last until the lasers turn off. Structure takes the form of dynamic, turbulent filaments of enhanced vorticity. Seed magnetic fields can be amplified in this region of ~ mm^3 kept hot by the lasers. Density is low enough that the lasers heat this region to 1.5 keV, but do not suffer from significant laser-plasma instabilities. The plasma flows progressively upward, and fast local amplification of the magnetic field occurs in this heated turbulent dynamo region (Prandtl number > 1). We show that the field structure in Fig.2 can be used to measure the turbulent spectrum in dynamo region.

Acknowledgments: This work was performed under the auspices of Los Alamos National Laboratory operated by Triad National Security, LLC for the U.S. DOE under contract 89233218CNA000001. This work was funded by LDRD.

References

[1] A. S. Liao, et al., Physics of Plasmas **26** 032306 (2019)
[2] Ma, T. et al., Physics of Plasmas **24**, 056311 (2017)
[3] V. A. Smalyuk, et al., Physics of Plasmas **25**, 072705 (2018)
[4] D. S. Montgomery, et al., Physics of Plasmas, **25**, 092706 (2018)
[5] B. M. Haines, B.M. , et al., Physics of Plasmas **26**, 102705 (2019)

Asymptotic Rayleigh-Taylor Instability Experiments on the National Ignition Facility

Assaf Shimony[1,2,*], Dov Shvarts[1,3], Yonatan Elbaz[4], Kirk A. Flippo[5], Channing H. Huntington[6], Stephan A. MacLaren[6] and Guy Malamud[1,2]

[1]Nuclear Research Center Negev, Beer Sheva, Israel
[2]University of Michigan, Ann Arbor, Michigan, USA
[3]Ben Gurion University of the Negev, Beer Sheva, Israel
[4]Israel Atomic Energy Commission, Tel Aviv, Israel
[5]Los Alamos National Laboratory, Los Alamos, New Mexico, USA
[6]Lawrence Livermore National Laboratory, Livermore, California, USA

[*]**Corresponding Author: shimonya@gmail.com**

The asymptotic self-similar evolution of the Rayleigh-Taylor instability (RTI) is ubiquitous in natural and engineering systems of different length scales such as inertial confinement fusion (ICF) and supernovae. In this regime, the evolution of the width of the mixing zone is dominated by the dimensionless scaling parameter, α_B, and the bubble size distribution is of a log-normal shape[1].

Experiments to determine the value of α_B, have presented challenges for many years. In many cases, these experiments have had limited control over the range of initial conditions present at the interface. As a results, high modes might not reach three bubble merger generations, which are needed for self-similarity[2], or low modes could break an achieved self-similarity[3]. Moreover, persistent discrepancies in the value of α_B between experiments (α_B~0.06) and simulations[4] (α_B~0.03) highlight the need for experiments that can be accurately characterized, for direct comparison to models and simulations.

To this end, we have developed two laser-driven experimental platforms, fielded on the National Ignition Facility (NIF), to explore deeply non-linear, multimode hydrodynamic growth of a planar interface. In these experiments, well-characterized initial conditions were machined onto a plastic surface, which was mated to a low-density foam and constituted the unstable interface. This interface was first shocked, promoting a phase of rapid Richmyer-Meshkov instability (RMI) growth, followed by a longer period of blast-wave driven RTI growth and eventual decompression. The mixing materials are miscible (plasma state) as in most simulations and the Reylnolds number is high, so that turbulent mixing and entrainment effects[5] might be significant. The two platform differ by the laser drive which initiated the main shock wave. One platform used a hohlraum (indirect drive, IDD) while in the other platform[6] the laser beams targeted directly to the physical package (direct drive, DD). Both platforms included a side-on radiograph diagnostic for the measurement of the width of the mixing zone, while the DD platform also included a face-on radiograph diagnostic for the measurement of the bubble distribution. Figure 1 presents typical raw images from the two platforms.

For the IDD platform, accurate measurements of the shock, spike, and bubble were made, yielding a mix-width growth curve. We account for each of the growth mechanisms (RMI, RTI, and decompression) with a set of buoyancy-drag force-balancing equations[7]. A range of initial conditions was studied, each with a unique initial amplitude. The value of α_B is being extracted these days for each initial conditions' setup separately, while focusing on the case of the smallest initial wavelength since it reaches the highest bubble merger generation.

The side-on measurements in the two platforms were compared, showing a good agreement. The bubble size distribution is extracted from the face-on radiograph in the DD platform. This distribution is in a log-normal shape and being compared to theory.

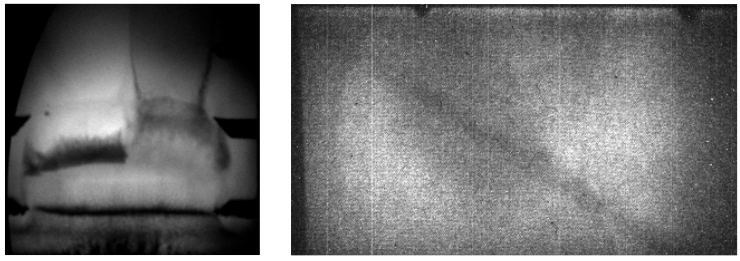

Figure 1: Typical raw images of a side-on radiograph of the IDD platform (left) and a face-on radiograph of the DD platform (right).

Acknowledgments: This work performed under the auspices of the U.S. Department of Energy by Lawrence Livermore National Laboratory under Contract DE-AC52-07NA27344, National Science Foundation through the Basic Plasma Science and Engineering program NSF 16-564, grant number 1707260, and with support from UM-LLNL collaborative contract and from NRCN.

References

[1] D. Oron et al., Phys. Plasmas **8**, 2883–2889 (2001).
[2] Y. Elbaz and D. Shvarts, Phys. Plasmas **25**, 062126 (2018).
[3] D. L. Youngs, Philos. Trans. Royal Soc. A **371**, 20120173 (2013).
[4] G. Dimonte et al., Phys. Fluids **16**, 1668–1693 (2004).
[5] A. Shimony et al., J. Fluids Eng. **140**, 050906 (2018).
[6] G. Malamud et al., High Energy Density Phys. **11**, 17–25 (2014).
[7] Y. Srebro et al., Laser Part. Beams **21**, 347–353 (2003).

A multispecies turbulence model for restabilized mixing layers

N. O. Braun* and R. A. Gore

Los Alamos National Laboratory, Los Alamos, NM, USA

*Corresponding Author: nbraun@lanl.gov

Conventional Reynolds-Averaged Navier-Stokes (RANS) models for turbulent mixing have often assumed that mixing layers act to smooth material gradients, yielding diffusion-like behavior at material interfaces. This is a reasonable approximation for many flows, such as the classical Rayleigh-Taylor (RT) instability problem of a heavy fluid sitting above a light fluid with a constant downward gravitational body force, but other problems may observe more complex mixing behavior. One example of this is in reversed-gravity RT in which a material interface is initially subjected to an unstable gravitational body force that drives the development of a mixing layer, but after some time the direction of gravity reverses to stabilize the interface. This type of transition from an unstable to a stable interface may generally occur in the presence of a time-varying acceleration, and the resulting stabilization can yield a steepening of the interface as unmixed chunks of fluid coalesce back towards their original heavy-on-light configuration.

Cihonski et al. [1] proposed a modification of the BHR3.1 RANS model [2] for incompressible flows that would allow it to capture the anti-diffusive behavior observed in reversed-gravity RT. Multi-fluid models, e.g. [3], have also been able to capture this behavior, but Cihonski's model retains the conventional single-point closure form of BHR3.1, while introducing closure equations for all remaining second order moments except pressure fluctuations.

We propose an extension of Cihonski's model to address compressible flow regimes. The proposed multispecies BHR model, BHR4, retains the BHR3.1 equations for turbulent mass flux, a, and density-specific volume covariance, b, while introducing equations for a species mass-fraction turbulent flux, a^k, and fluctuation, b^k. In incompressible flows simple summation properties relate a^k and b^k to a and b, respectively, and the requirement to preserve these relations largely defines the closures needed for a^k and b^k. This means there is minimal model complexity introduced by tracking the additional terms in BHR4, although computational cost may be increased relative to BHR3.1. Additionally, BHR4 does not introduce new empirically fit coefficients and requires only limited recalibration of the BHR3.1 coefficients.

Figure 1 compares the BHR4 model to DNS [4] in an Atwood number $A_t = 0.75$ reversed-gravity RT instability problem. BHR4 agrees reasonably well with the DNS, including capturing the limited amount of mixing layer steepening that occurs shortly after gravity is reversed. The three fluid RT problem considered by Youngs [5] is also tested, in which a band of heavy fluid is suspended in lighter fluid both above and below it. In the presence of gravity, the lower interface of the heavy fluid is unstable and develops growing mixing layer that eventually impinges on the stable upper interface of the heavy fluid band. Relative to BHR3.1, BHR4 is better able to capture the reduction in mixing that occurs at the stable interface in comparisons with DNS. The proposed model is discussed in further detail in Braun & Gore [6].

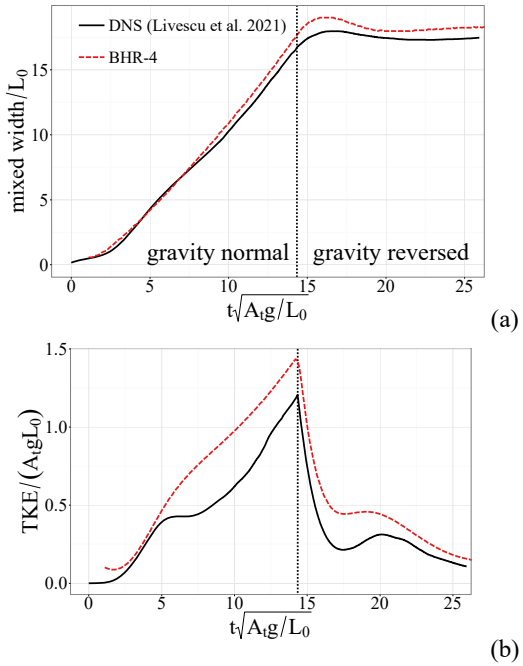

Figure 1: Mixing layer width based on a 95% volume fraction threshold (a) and maximum turbulent kinetic energy (b) in reversed-gravity $A_t = 0.75$ Rayleigh-Taylor simulations. The DNS is of Livescu, Wei, and Brady [4] and the dotted line marks when gravity is reversed. Results are non-dimensionalized by gravity, g, and the reference lengthscale of the DNS, L_0.

Acknowledgments: This work was supported by the US Department of Energy through the Los Alamos National Laboratory. Los Alamos National Laboratory is operated by Triad National Security, LLC, for the National Nuclear Security Administration of U.S. Department of Energy (Contract No. 89233218CNA000001).

References

[1] A. J. Cihonski, T. T. Clark and R. A. Gore, Tech. rep., Los Alamos National Lab LA-UR-15-20485 (2015).

[2] J. D. Schwarzkopf, D. Livescu, J. R. Baltzer, R. A. Gore and J. R. Ristorcelli, *Flow, Turb. Comb.*, **96**, 1 2016.

[3] D. L. Youngs, *Physica D: Nonlinear Phen.*, **37**, 270 (1989).

[4] D. Livescu, T. Wei and P. Brady, *Phys D: Nonlin Phenom,* **417** (2021).

[5] D. L. Youngs, *Philos. Trans. Royal Society A: Math., Phys. and Eng. Sci.*, **367**, 1899 (2009).

[6] N. O. Braun, and R. A. Gore, *Journal of Turbulence*, **22**, 12 (2021).

Advection vs. Diffusion in Richtmyer-Meshkov and Rayleigh-Taylor Mixing

Forrest W. Doss

Los Alamos National Laboratory, Los Alamos, New Mexico, USA

*Corresponding Author: fdoss@lanl.gov

In the field of mathematical analysis of PDEs, *a priori* estimation is the deduction of certain properties obeyed by solutions of differential equations even when the solutions themselves are unknown or unobtainable. The utility of this technique applied to turbulent solutions of the Navier-Stokes equations has been known for a long time, and has been used to derive, for instance, bounds on the permissible dissipation rates in shear flows [1]. This is possible because in turbulent solutions dissipation is 'anomalous,' that is, because it is controlled not by the physical viscosities of the problem but by the efficiency of nonlinear cascades in transporting energy to fine scales.

Less known until recently, the technique can also be used to estimate the implied mixing of dissimilar materials in flows, including flows introduced by instabilities [2]. In a simple statistical (i.e. Reynolds-Averaged) model of the Richtmyer-Meshkov instability (RMI), such an *a priori* result exists for the resulting equation which implies the strong suppression of mixing for certain regimes of flow [3]. In particular, for the broadband RMI this predicts the observed decrease in the asymptotic mix efficiency as the long wavelength content of the instability is increased. This matches trends in observations from DNSs recently performed by others [4].

The predicted cutoff in mixing efficiency also implies that to second-order different regimes of the RMI may either efficiently lose information regarding the initial conditions, or may retain their imprint indefinitely.

This presentation reports and expands upon the analysis in [2]. In addition, it will describe how the same methodology can be used to predict unconditional mixing in the Rayleigh-Taylor case.

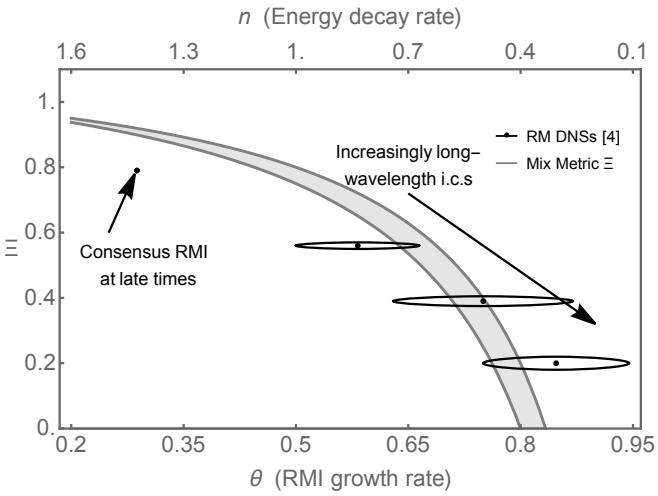

Figure 1: Mix metric Ξ vs. RMI growth rate

Acknowledgments: This work was supported by the U.S. Department of Energy at Los Alamos National Laboratory operating under contract 89233218CNA000001 with Triad National Security LLC. The author also thanks the Pulsed Power Sciences Center at the Sandia National Laboratories for their hospitality during recent years. LA-UR-22-21583

References

[1] C. R. Doering, J. D. Gibbon, *Applied Analysis of the Navier Stokes Equations*, Cambridge University Press(1995)

[2] F. W. Doss, *Physics Letters A,* **430** 127976 (2022)

[3] J. Wirth, *Math. Methods Appl. Sci.*, **27**, 101 (2003)

[4] M. Groom, B. Thornber, *Physica D* **407** 132463 (2020)

On the Assessment of Two-Level Simulation Model for Numerical Study of Compressible Turbulent Scalar Mixing

H. Chandrasekhar[1], R. Ranjan[1,*] and S. Menon[2]

[1]Department of Mechanical Engineering, University of Tennessee, Chattanooga, TN, USA
[2]School of Aerospace Engineering, Georgia Institute of Technology, Atlanta, GA, USA

[*]**Corresponding Author: reetesh-ranjan@utc.edu**

Turbulent scalar mixing under compressible conditions is key for the design of high-speed aerospace applications. Past studies [1-9] have characterized the role of compressibility on the scalar mixing, which in comparison to an incompressible counterpart leads to a reduced rate of growth of the mixing layer, suppression of fluctuations associated with the flow and the scalar fields, reduced efficiency of scalar mixing, structural changes, etc. Apart from the experimental studies, which are limited by the resolution needed to resolve scalar mixing, computational studies such as direct numerical simulation (DNS) have helped to gain further insight into such flows. While DNS is suitable for fundamental studies, large eddy simulation (LES) is a computationally tractable approach for the study of practical applications. Although, LES based studies have captured the key features of such flows [6,8], there are still challenges that need to be addressed. For example, LES employing eddy viscosity/diffusivity-based approaches disregard key aspects of subgrid scale (SGS) physics such as counter-gradient transport, small-scale anisotropy, backscatter, etc. An alternate strategy based on the two-level simulation (TLS) model [10] has shown promise in capturing a wide range of SGS physics [11]. The past studies using TLS model focused on incompressible flows and this study focuses on modeling of compressible scalar mixing.

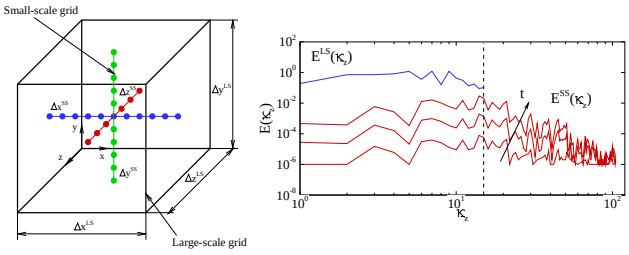

Figure 1 SS grid within a LS cell and (b) the time evolution of the SS energy spectrum within the LS energy spectrum [13].

The TLS model performs scale separation of a field variable ϕ using a scale decomposition through: $\phi = \phi^{L} + \phi^{S}$, where superscripts 'L' and 'S' denote large scale (LS) and small-scale (SS) components of ϕ, respectively. The resulting governing equations for ϕ^{L} and ϕ^{S} are solved in a coupled manner by simplifying the SS equations by employing the TLS modeling assumptions. The simplified SS equations are solved locally on three orthogonal 1D lines embedded within a 3D grid on which the LS equations are solved (see Fig. 1). Thus, in the TLS model both LS and SS (albeit in a modeled simulation) fields are recovered locally to capture the complete spectrum (see Fig. 1). No classical LES filtering and eddy viscosity/diffusivity closure are needed in TLS, and in the past, this model has been used to study a wide range of flows such as isotropic turbulence, temporal mixing layer, wall-bounded flows, etc. [10-13].

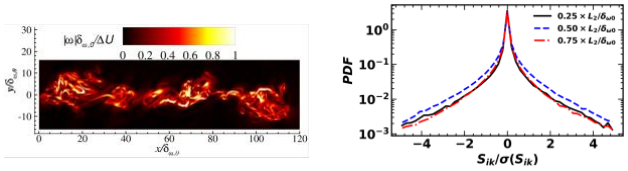

Figure 2 Normalized vorticity magnitude at $t\frac{\Delta U}{\delta_{\omega,0}} = 350$ in the central x-y plane in a compressible mixing layer (left) and *a priori* assessment of TLS model assumption for the viscous term.

In the present study, the SS modeling assumptions are re-assessed for compressible scalar mixing since, in the past, the assumptions have been assessed only under incompressible conditions. The initial *a priori* assessment is performed using the DNS data corresponding to a compressible scalar mixing layer at convective Mach number $M_c = 0.7$ and initial Reynolds number based on vorticity thickness $Re_{\delta_{\omega,0}} = 640$. The computational setup follows a past study [7] and is simulated (see Fig. 2) using a fully compressible solver. The flow is initialized with a hyperbolic-tangent profile for the mean streamwise velocity and density fields. Streams of oxygen and nitrogen in the top and bottom halves of the domain, respectively, are considered at constant pressure and temperature. Results from DNS are being used to assess the accuracy of the modeling assumptions of the TLS model under compressible conditions (see Fig. 2). Further studies will be conducted using other convective Mach numbers to assess the generality and limitation of the underlying assumptions in the TLS model.

Acknowledgments: The computational resources provided by the SimCenter at UTC are greatly appreciated.

References

[1] D. Papamoschou, & A. Roshko. J. Fluid Mech., **197**, 453 (1988).
[2] G.S. Elliott & M. Samimy. Physics of Fluids A: Fluid Dynamics, **2**, 1231, (1990).
[3] S.G. Goebel & J.C. Dutton. AIAA J., **29**(4), 538 (1991).
[4] A.W. Vreman, N.D. Sandham & K.H. Luo. J. Fluid Mech., **320**, 235(1996).
[5] C. Pantano & S. Sarkar. J. Fluid Mech., **451**, 329 (2002).
[6] V. Sankaran & S. Menon. Proc. Comb. Inst., **30**, 2835 (2005).
[7] I. Mahle, H. Foysi, S. Sarkar & R. Friedrich. J. Fluid Mech., **593**, 171-180 (2007).
[8] C. Le Ribault. I. J. Heat Mass Transfer, **51**, 3514 (2008).
[9] J. O'Brien, J. Urzay, M. Ihme, P. Moin, & A. Saghafian. J. Fluid Mech., **743**, 554 (2014).
[10] K.A. Kemenov & S. Menon. J. Comp. Phys., **220**, 290 (2006).
[11] R. Ranjan & S. Menon. J. Turbulence, **19**, 334 (2018).
[12] A.G. Gungor & S. Menon. Prog. Aero. Sci., **46**, 28 (2010).
[13] R. Ranjan & S. Menon. J. Turbulence, **14**, 1 (2013).

Derivation and evaluation of a Reynolds stress model designed to simulate reacting mixing layers

Denis Souffland[1,*], Olivier Soulard[1] and Jérôme Griffond[1]

[1]CEA, DAM, DIF, Arpajon F-91297, France

[*]**Corresponding Author: denis.souffland@cea.fr**

One of the most deleterious phenomena during the implosion of Inertial Confinement Fusion capsules is the development of hydrodynamic instabilities at the interface between the fuel and the plastic shell. These instabilities induce the interpenetration of the two materials and can lead, eventually, to the creation of a turbulent mixing layer. The modification in the burn efficiency of the capsule is primarily a function of the widening of the mixing layer, but it depends also on its homogeneity.

In the framework of Reynolds stress models (RSM) an accurate way to characterize the mixture homogeneity is to use the covariance of the mass fraction of the involved species. With this aim in view, we have extended the GSG-R model [1,2] with transport equations for the mass fraction fluctuations correlations. GSG-R is a probability density function (pdf) - based RSM, where stochastic partial differential equations for the velocity components and the specific volume fluctuations ($u_i^{"}$, $\tau^{"}$) have been set up. In the same way, we derived stochastic equations for the mass fraction of the materials in presence ($Y_a^{"}$) that allows us to reconstruct additional transport equations for second-order moments such as the mass fraction turbulent fluxes $\widetilde{Y_a^{"}u_i^{"}}$ and co-variances $\widetilde{Y_a^{"}Y_b^{"}}$. We have called GSG-Y this extension of our model.

As the instantaneous reaction rates between light ions are proportional to the particle number densities of the two reactants (n_α, n_β), the calculation of their means requires the knowledge of the Reynolds averages $\overline{n'_\alpha n'_\beta}$. A β-pdf model has been developed to express the desired quantities thanks to the correlations followed by GSG-Y, i.e. based on the Favre averaging of the mass fractions of the materials. Then we can estimate a segregation parameter θ, that quantifies the heterogeneity of the mixture. It is used to calculate the correction of the mean reaction rates when reactants are premixed as well as nonpremixed.

In 2018, Morgan et al. [3] have documented test cases in spherical geometry. They consist, as a first stage, in the widening of Rayleigh-Taylor induced mixing layers between an inner gas and a plastic shell, until they reach self-similar states. The second stage is the burn of the obtained mixture, triggered off by the rise of the temperature up to 1keV. Two main cases are considered. The first one is a premixed configuration, where a deuterium-tritium (DT) gas is surrounded by a CH plastic shell. In the second one, a nonpremixed configuration is considered: the gas contains tritium but no deuterium and the plastic shell has been deuterated. The authors carried out reference large-eddy simulations (LES) of the development of the mixing layers to self-similar states with the Miranda code. For the calculation of the burn in the mixtures, they use the ARES code with the new *k-L-a-V* model, extension of their previous model with the addition of an equation for the variance of the fluid mass fractions.

In order to evaluate the behavior of GSG-Y, we have simulated the same configurations as in [3] with our 1D code. We will focus on the evolution of the turbulent correlations involved in the determination of the mixing layer homogeneity and on their relative contributions on the reaction rates.

During the talk, we will present the principles of the derivation of the GSG-Y model, and the β-pdf model adopted to close the segregation parameter and take into account heterogeneity in the reaction rates calculation. The results obtained with this set of models on the configurations defined and documented by Morgan *et al.* will also be detailed.

References

[1] J. Griffond, O. Soulard and D. Souffland, Physica Scripta, **T142**, 014059 (2010).
[2] D. Souffland, J. Griffond and O. Soulard, J. Fluids Eng., **136**, 091102 (2014).
[3] B.E. Morgan, B.J. Olson, W.J. Black and J.A. McFarland, Phys. Rev. E, **98**, 033111 (2018).

Turbulent mixing in flows with large density variations

Daniel Livescu[1]

[1]CCS-2, Los Alamos National Laboratory, Los Alamos, NM USA

[*]**Corresponding Author: livescu@lanl.gov**

Flow systems with large density variations are ubiquitous in technology and nature. Sources of variable-density (VD) effects include compressibility phenomena such as acoustic fluctuations and shock waves, temperature variations due to differential heating or chemical/nuclear reactions, mixing between fluids with different molar masses or phases, and phase transformations. At very large scales, all astrophysical explosions, accretion disks, and mergers, as well as convection in stars, involve turbulent flows with significant density variations. Detailed measurements of the flow characteristics under the most extreme conditions are not possible; only observations that are inherently limited in the timescales and phenomena they capture are available to inform numerical and theoretical models. At the opposite end of length- and timescale ranges are manmade implosions inside inertial confinement fusion (ICF) capsules at the National Ignition Facility. The implosions are measured in nanoseconds, and the capsules are only about a millimeter in diameter. While measurements are being performed for the flow within such capsules, the overlap of fluid [e.g., Richtmyer–Meshkov (RM), Rayleigh–Taylor (RT), ablative], laser beam, and plasma instabilities; phase changes; plasma and magnetic effects; and kinetic effects makes it extremely difficult to understand the flow. Between these limits, significant variations in fluid density are encountered in, for example, high-speed flight; combustion; convection regions in oceans, the atmosphere, and Earth's mantle; and industrial flows. Such a large variety of applications may seem overwhelming and all but impossible to understand. However, starting from conservation equations, one can identify canonical flows that exhibit aspects shared across applications [1]. Designing canonical flows has facilitated the development of laboratory-sized experiments that expose relevant phenomena at widely different scales, such as in astrophysics or ICF. These canonical flows have been studied in some cases for more than a century and have developed communities that have diverged as the fields grew.

There is a vast body of literature addressing density variations associated with acoustic fluctuations. However, there are significantly fewer studies addressing turbulence with density fluctuations subsequent to mixing between different molar mass fluids. Here, I will give an overview of recent results concerning variable density effects arising from mixing between fluids with different molar masses in various flows, including shock-variable density isotropic turbulence interaction [2], Richtmyer-Meshkov [3] and Rayleigh-Taylor [4] instabilities, homogeneous buoyancy-driven variable-density turbulence [5], and shear driven mixing layers [6]. In particular, I will use some of the largest DNS to date to highlight mixing and turbulence asymmetries, as well as changes in the structure of mixing layers in the presence of large density variations.

In general, large density variations lead to strong differential inertial effects in heavy and light fluid regions. For example, a quasi-homogeneous non-premixed binary mixture of different density fluids will present a very different flow structure in the heavy and light fluid regions after passing through a shock wave [2]. Due to the rapid compression across the shock, there is a tendency towards two-dimensionalization (i.e. the flow becomes axi-symmetric) of single fluid turbulence following the interaction with the shock. For the variable density case, light fluid regions recover the three-dimensional structure a short distance downstream from the shock, as their reduced inertia responds fast to changes in the local strain. On the other hand, heavy fluid regions retain the two-dimensional structure for a much longer distance downstream of the shock. These differences can be highlighted using the joint Probability Density Function (PDF) of the second (Q) and third (R) invariants of strain rate tensor. Figure 1 shows that post-shock light fluid regions exhibit the characteristics tear-drop shape of the (Q,R) joint PDF encountered in 3D fully developed turbulence, while the heavy fluid regions retain for a longer distance the fully symmetric joint PDF obtained immediately after the shock.

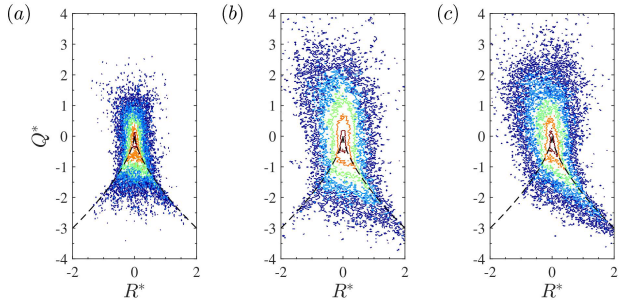

Figure 1: Variable density effects change the post-shock flow morphology: Heavy fluid regions (a) show a full symmetrization of the (Q,R) joint PDF, while light fluid regions (c) retain the characteristic tear-drop shape. Mixed fluid regions (b) show some weak symmetrization [2].

The lower inertia of the light fluid regions also allows them to become turbulent faster than heavy fluid regions if a non-premixed binary mixture of different density fluids initially at rest is subjected to acceleration. These differences can be easily identified using Direct Numerical Simulations of buoyancy driven variable density turbulence in triply-periodic domains [5], but they can be seen in turbulent flows generated by all basic flow instabilities (RT/RM, shear driven). For example, fig. 2 shows that the density isosurfaces present significantly more fragmentation near the light fluid stream compared to the heavy fluid stream in a temporal simulation of variable-density shear driven mixing layers [6]. The higher turbulent intensities in light fluid regions leads to faster stirring and ultimately faster molecular mixing in these regions [see 1 and references therein]. Thus, pure light fluid vanishes faster from the flow in the triply periodic configuration, while mean density profile becomes more

elongated on the light fluid side and transitions faster to the pure fluid density on the heavy fluid side [6]. Similar differences between the mean density variations near the heavy and light fluid sides are seen in the mixing layers generated by RT [4] and RM [3] instabilities.

When mixing layers are formed between parallel streams of fluids with different densities, the entrainment properties are also different on the two sides of the mixing layer. This results in the light fluid side becoming wider than the heavy fluid side, while the neutral velocity point (the location where the mean velocity is zero) moves to the light fluid side of the interface.

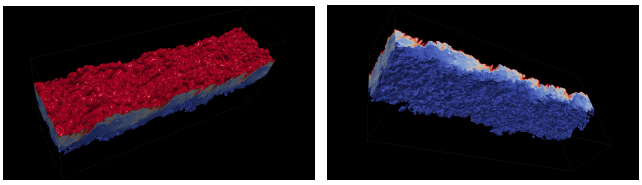

Figure 2: Density isosurfaces near the heavy-fluid (a) and light-fluid (b) streams from a temporal mixing layer DNS with 7:1 density ratio (Atwood number A = 0.75) [4].

Finally, I will also discuss some of the challenges and open questions regarding variable density effects, and prospects for exa-scale computing to address these issues.

Acknowledgments: Los Alamos National Laboratory is operated by Triad National Security, LLC, for the National Nuclear Security Administration of the US Department of Energy (contract number 92689233218CNA000001).

References

[1] D. Livescu, Annu. Rev. Fluid Mech. **52**, 309-341, (2020).
[2] Y. Tian, F.A. Jaberi and D. Livescu, J. Fluid Mech. **880**, 935-968 (2019).
[3] M.L. Wang, D. Livescu and S.K. Lele, Phys. Rev. Fluids **4**, 104609 (2019).
[4] D. Livescu, T. Wei and P.T. Brady, Physica D **417**, 132832 (2021).
[5] D. Aslangil, D. Livescu and A. Banerjee, J. Fluid Mech. **895**, A12(2020).
[6] J.R. Baltzer and D. Livescu, J. Fluid Mech. **900**, A16 (2020).

Buoyancy-Drag modelling and spike-to-bubble ratios for single-shock Richtmyer-Meshkov mixing

David Youngs*, Michael Groom and Ben Thornber

Department of Aerospace, Mechanical and Mechatronic Engineering, University of Sydney, NSW 2006, Australia

*Corresponding Author: david.l.youngs.uk@gmail.com

The Buoyancy-Drag model is a simple model, based on ordinary differential equations, for estimating the growth of a turbulent mixing zone at an interface between fluids of different density due to Richtmyer-Meshkov and Rayleigh-Taylor instabilities. The early stages of the mixing process are very dependent on the initial conditions and modifications to the Buoyancy-Drag model are needed to obtain correct results. Recent papers [1,2] have used ILES results (from the FLAMENCO code) to construct the modifications required to represent the evolution of the integral width ($W = \int \overline{f}_1 \overline{f}_2 dx$) due to single-shock Richtmyer-Meshkov mixing evolving from narrowband initial random perturbations. This presentation extends the analysis to broadband initial perturbations with power spectra $P(k) \sim k^s$, $s = -1$ and -2 [3] which are likely to be more representative of typical applications. Results are also given for the variation of the spike to bubble ratio, h_s / h_b, with time. Novel integral definitions [2] of the bubble and spike distances are used which vary smoothly with time. For example, if the spike region is $x > 0$ and $\overline{f}_1$ is the layer averaged dense fluid volume fraction, the spike distance is based on measures of the mean distance of the dense fluid from the interface:

$$h_s^{(m)} \sim \left(\int_0^\infty x^m \overline{f}_1 dx \Big/ \int_0^\infty \overline{f}_1 dx \right)^{1/m}$$

Results are presented for two pre-shock density ratios, $\rho_1 / \rho_2 = 3$ and 20.

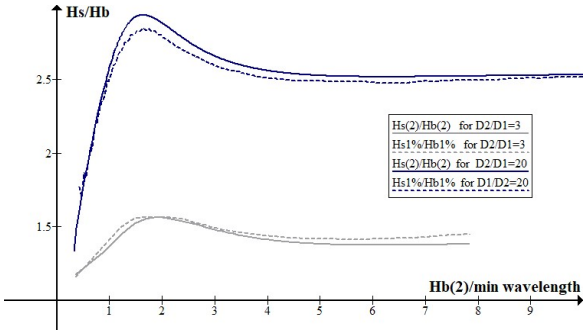

Figure 1: Spike-to-bubble ratios versus scaled bubble distance based on integral distances (*m*=-2) and 1% volume fraction limits for the broadband case *s* =-1 at $\rho_1 / \rho_2 = 3 (\text{grey}) \text{ and } 20 (\text{black})$.

New insights are given for the variation of asymmetry of the mixing zone with time. For the broadband cases with minimum wavelength $\lambda_{\min}$ at $\rho_1 / \rho_2 = 3$ and 20, the variation of h_s / h_b with $h_b^{(2)} / \lambda_{\min}$ is shown if fig. 1. The asymmetry rises to a peak value and reduces as mixing proceeds.

The method used to analyse the integral width data provides a new way of estimating the self-similar growth exponent θ ($W \sim t^\theta$). The values obtained for the narrowband case are approximate as it is likely that the ILES has not fully reached the self-similar regime. For results obtained so far, estimates of $\theta \sim 1/3$ are consistent with the model of Elbaz & Shvarts [4]. For the broadband cases estimates are close to the theoretical values of $\theta = 2/(s+5)$ [5,6]. The corrected forms of the Buoyancy-Drag model gives accurate fits to the data for W over the whole time range with model constants which depend on θ but are similar at the two density ratios. Fig. 2 shows the results for broadband perturbations at $\rho_1 / \rho_2 = 3$.

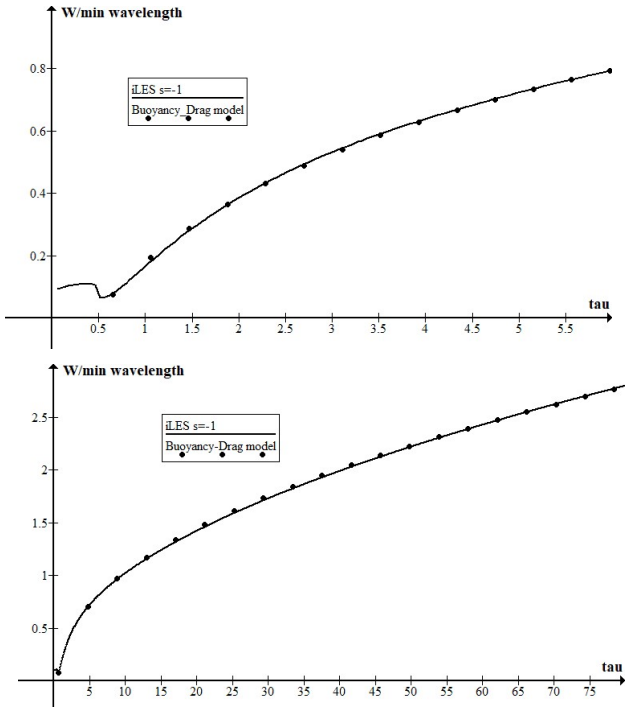

Figure 2: Mix distances versus scaled time. Solid lines: ILES. Dots: buoyancy-drag model, top (early time), bottom (late time)

References

[1] D.L. Youngs and B. Thormber, J. Fluids Eng. **142**(12), 121107 (2020).
[2] D.L. Youngs and B. Thornber, Physica D, **410**, 132517 (2020).
[3] M. Groom and B. Thornber, Physica D, **407**,132463 .(2020)
[4] Y. Elbaz and D. Shvarts, Physics of Plasmas , **25**, 062126 (2018).
[5] B. Thornber et al., J. Fluid Mech., **654**, 99-139 (2010)
[6] O. Soulard et al., Phys. Rev. Fluids, **3**, 104603 (2018)

Numerical Simulation of the Broadband Richtmyer-Meshkov Instability and Comparison with Shocktube Experiments

Michael Groom[1] and Ben Thornber[1,*]

[1]School of Aerospace, Mechanical and Mechatronic Engineering, The University of Sydney, Sydney, New South Wales, Australia

[*]**Corresponding Author: michael.groom@sydney.edu.au**

1. Introduction

The effects of initial conditions in shock-induced turbulent mixing are analysed using both implicit large eddy simulations (ILES) and direct numerical simulations (DNS). In particular, this study considers 3D initial perturbations of a planar interface which follow a power spectrum of the form

$$P(k) = Ck^m. \quad (1)$$

In Equation 1, k is the radial wavenumber of the perturbation, C is a constant that dictates the overall amplitude of the perturbation and m is the spectral scaling exponent, taken here to be an integer. Two classes of initial conditions are considered; narrowband perturbations containing length scales in the range $\lambda_{max} = L/16$ to $\lambda_{min} = L/32$ (where $L = 2\pi$ is the width of the computational domain) and a constant power spectrum (i.e. $m = 0$) and broadband perturbations that contain a greater range of initial length scales, ranging from $\lambda_{max} = L/2$ to $\lambda_{min} = L/32$, and with spectral exponents $m = -1$ or $m = -2$. In both cases the constant C is set such that the initial amplitudes of each mode in the perturbation are in the linear growth regime; all cases have the amplitude of the smallest wavelength in the perturbation set to be $0.1\lambda_{min}$. For the DNS cases, the initial Reynolds number is defined as

$$Re_0 = \frac{\overline{\rho^+}\dot{W}_0\bar{\lambda}}{\bar{\mu}}, \quad (2)$$

where $\overline{\rho^+}$ is the mean post-shock density, $\bar{\mu}$ is the mean dynamic viscosity, $\bar{\lambda}$ is a weighted-average initial wavelength and $\dot{W}_0$ is the initial growth rate of the integral width W. ILES are performed for the narrowband and two broadband perturbations, using a computational setup that is representative of shocktube experiments performed by Jacobs et al. [1]. Specifically, a $M = 1.5$ shock wave is initialised in air and impacts the prescribed surface perturbation at the interface between air and SF_6 ($p_0 = 0.915$ atm and $T_0 = 298$ K for both gases). Only the initial shock interaction is simulated; the reshock that occurs at an intermediate time in the shocktube experiments is not considered here. DNS is also performed for each surface perturbation at Reynolds numbers that are capable of being fully grid resolved but are lower than those of the experiments. This is used to bound the experimental results as the effective Reynolds numbers in the ILES cases are likely higher than those of the experiments (recently estimated in [2]). The initial Reynolds numbers for each DNS case are given in Table 1.

Quantity	$Re_0 = 122$	$Re_0 = 261$	$Re_0 = 526$	$Re_0 = 1051$
m	0	-1	-2	-2
$\bar{\lambda}$	0.278	0.463	0.785	0.785
$\dot{W}_0$	15.67	20.03	23.84	23.84
$\bar{\mu}$	0.3228	0.3228	0.3228	0.1614

Table 1: Reference length and velocity scales for each DNS case.

2. Results

The following non-dimensionalisation is used to compare results at different times between the simulations and experiments,

$$\tau = \frac{(t-t_0)A^+\Delta u}{\lambda_{min}}, \quad (3)$$

where $t_0 = 0.0011$ s is the shock arrival time in the simulations, $\Delta u = 158.08$ m/s is the initial impulse imparted by the shock and $A^+ = 0.72$ is the post-shock Atwood number. A visualisation of the heavy fluid volume fraction field for the three ILES cases at a similar dimensionless time to the point at which reshock occurs in the experiments is given in Figure 1. The effects of additional long wavelength perturbations are clearly visible at this time, particularly for the $m = -2$ broadband case.

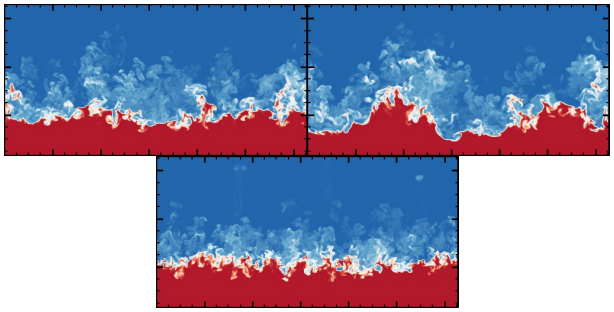

Figure 1: Visualisations of the narrowband case (bottom), $m = -1$ (left) and $m = -2$ (right) broadband cases at time $\tau = 98$.

Using nonlinear regression to fit a model of the form $W = \beta(\tau - \tau_0)^\theta$, the growth exponent θ is estimated for each simulation to be 0.34 for the narrowband ILES case, 0.44 for the $m = -1$ broadband ILES case and 0.49 for the $m = -2$ broadband ILES case. Similar values are obtained for the equivalent DNS cases, indicating that the effects of viscosity on θ are small even at relatively low Reynolds numbers. These results demonstrate that for perturbations of moderate bandwidth (~1 order of magnitude between λ_{min} and λ_{max}) typical of most shocktube experiments, values of θ are obtained that are in between those expected for purely narrowband perturbations ($\theta = 1/3$) and large bandwidth broadband layers ($\theta = 1/2$ to $\theta = 2/3$). These results are also still compatible with the predictions of just-saturated mode theory in the infinite bandwidth limit; saturation of the longest wavelength in the broadband cases occurs at times of $\tau = 49$ for $m = -1$ and $\tau = 10$ for $m = -2$. If the nonlinear fit is restricted to these times, the values for θ that are obtained are very close to the theoretical values of $\theta = 1/2$ and $\theta = 2/3$ respectively.

References

[1] Jacobs, J. W. et al., *Shock Waves*, **23**, 407-413 (2013).
[2] Sewell, E.G. et al., *J. Fluid Mech.*, **917**, A41 (2021).

The Effect of Axial Strain on the Richtmyer-Meshkov Instability

Bradley Pascoe[1], Michael Groom[1], Ben Thornber[1,*]

[1]University of Sydney, Sydney, New South Wales Australia

[*]**Corresponding Author: b.thornber@sydney.uni.edu.au**

The Richtmyer-Meshkov [1,2] and Rayleigh-Taylor [3,4] instabilities are understood to behave differently in cylindrical and spherical geometries. Denoted the Bell-Plesset [5,6] effect, the amplitude growth rates are dependent upon the compression ratio and convergence ratio. In a planar analogue, the Richtmyer-Meshkov instability is analysed under the effects of axial strain, in essence isolating the radial strain component experienced by the converging/diverging instabilities. Using a velocity potential formulation, the effects of axial strain on the Richtmyer-Meshkov instability are considered to derive a differential equation for growth rate in the linear regime. This modelling equation is the same as derived by Epstein [7] for an arbitrary compression ratio in planar geometry. The linear regime model is validated by performing a 2D numerical simulation of a single mode instability at Re = 2048 and Atwood = 0.5, initialized by a velocity perturbation. There are two strain cases presented, defined by either a constant strain rate or a constant boundary velocity. These cases are simulated for compression (negative strain rate) and expansion (positive strain rate). The systems are defined by a non-dimensional strain rate:

$$\tilde{S} = \bar{S}\lambda/U_0 \qquad (1)$$

Here $\bar{S}$ is the mean axial strain, λ is the perturbation wavelength, and U_0 is the impulsive velocity of RMI. The linear regime model shows good agreement across the non-dimensional strain values, with amplitude growth diverging away from the unstrained solution as the magnitude of $\tilde{S}$ increases.

These results for the 2D single-mode are then extended to an 3D implicit large eddy simulation case with a narrowband multi-mode spectrum. The effects of the axial strain on the development of the turbulent mixing layer are analysed. The growth of the mixing layer is compared to the predictions of a buoyancy-drag model, which utilises ordinary differential equations to calculate the bubble and spike heights. In turn, the implications for turbulence models to describe the flow is also discussed.

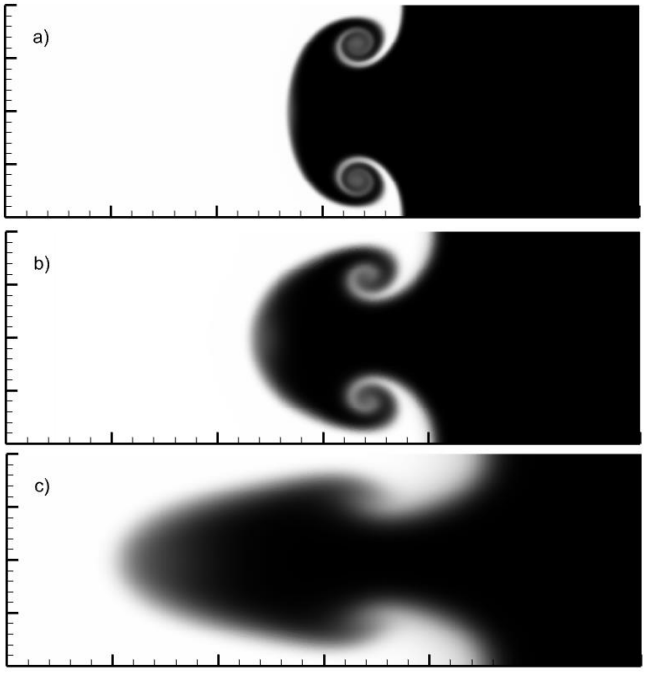

Figure 1. Richtmyer-Meshkov instability at t = 0.2s, $\lambda = 0.2$, $U_0 = 1$. a) compression with $\tilde{S} = -1.2$, b) no strain, c) expansion with $\tilde{S} = 1.2$

Acknowledgments: The authors acknowledge the Sydney Informatics Hub and the use of the University of Sydney's high performance computing cluster, Artemis.

References

[1] R.D. Richtmyer, Commun. Pure Appl. Math. **13**, 297 (1960).
[2] E.E. Meshkov, Fluid Dyn. **4**, 101 (1969).
[4] Lord Rayleigh, Proc. London Math. Soc. **s1**, 170 (1900)
[5] G. Taylor, Proc. R. Soc. London, Ser. A **201**, 192 (1950)
[6] G. Bell, Report LA-1321, Los Alamos National Laboratory, Los Alamos, NM, 1951
[7] M.S. Plesset, J. Appl. Phys. **25**, 96 (1954)
[8] R. Epstein, Phys. Plasmas **11**, 5114 (2004).

A study of modal interaction between different scales of the turbulent Richtmyer-Meshkov instability using high-resolution three-dimensional FLASH simulations

Mohammad Mohaghar[1,*], Jacob McFarland[2] and Devesh Ranjan[1]

[1]George W. Woodruff School of Mechanical Engineering, Georgia Institute of Technology, Atlanta, GA, USA
[2]Department of Mechanical and Aerospace Engineering, University of Missouri, Columbia, Missouri, USA

[*]**Corresponding Author: mohaghar@gatech.edu**

In this study, three-dimensional simulations of inclined-interface Ritchmyer-Meshkov instability are presented using adaptive mesh refinement (AMR) code, FLASH. The dimensions of the simulations are compatible with those of the shock-tube experiments at the inclined shock tube at Georgia Institute of Technology.[1, 2] The current work is a complementary study to the previous computational and experimental studies on investigation of modal interactions between inclined interface perturbation and small wave-length perturbations. [1, 2, 3] Variations in the rate of mixing width, mixedness and mixed-mass are compared with experimental data first for code validation. The main interest of the current study is to understand flow behavior in the out-of-plane dimension, the modal content and the interaction between a large-wavelength inclined interface perturbation and small-wavelength multi-mode perturbations before and after reshock to help future experimental and computational studies. The mass fraction, vorticity, enstrophy and density iso-surfaces are presented to investigate flow structures before and after reshock.

The computational domain is exactly the same as experimental shock tube, 11.43 cm in both Y and Z directions and 175 cm in the X direction. The initial perturbations are computed directly from PLIF images of single- and multi-mode perturbations of experimental results to model the Mach 1.55 N_2/CO_2 shock tube experiment (Figure 1). The experimental PLIF images for the initial conditions are modeled by directly implementing the equation of interface detected using Canny-edge detection method. The initial diffusion layer thickness is prescribed by an error function based on the average of experimental measurements for 200 PLIF realizations with a thickness of 0.96 cm and 1.54 cm for single- and multi-mode initial conditions. [1, 2] AMR with 6 levels of refinement and a base resolution of 2.85 cm is used during the simulation, and the highest computed resolution is $\Delta x = \Delta y = \Delta z = 446\ \mu$m.

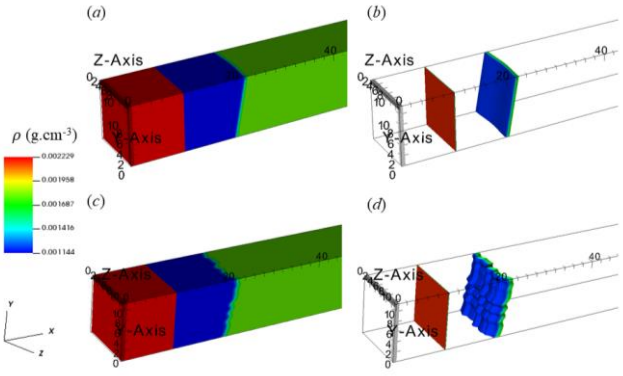

Figure 1: Illustration of the shock tube test section having a square cross-sectional width of 11.43 cm considered in the computational domain, showing initialization of the interface, shock wave and coordinate system for (a, b) pre-dominantly single-mode interface, and (c, d) multi-mode interface.

The preliminary results, which are shown in Figures 2 and 3, indicate that although the magnitude of several quantities in the third dimension is insignificant compare to the $x-y$ plane before reshock, after reshock all three dimensions are contributing to the mixing and the small modes in the $z-$perturbation is playing an important role in the flow mixing. The iso-surfaces of both density and vorticity in the three dimensions suggest that the primary vortex has become very well mixed, and the magnitude of vorticity is similar in all three directions specially in the multi-mode case.

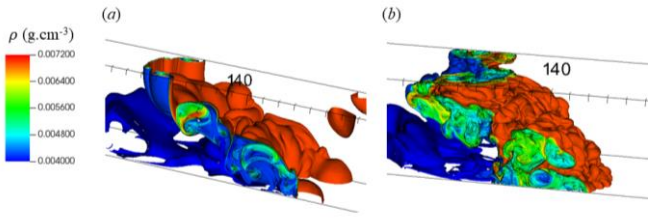

Figure 2: Iso-surfaces of density corresponding to (a) single- and (b) multi-mode interfaces after reshock at $\tau = 2.105$.

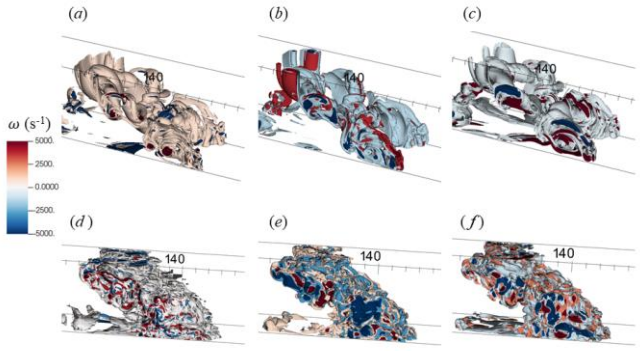

Figure 3: Iso-surfaces of vorticity in (a, d) z-, (b, e) y- and (c, f) x-direction corresponding to (a, b and c) single- and (d, e and f) multi-mode interfaces after reshock at $\tau = 2.105$.

References

[1] M. Mohaghar, J. Carter, B. Musci, D. Reilly, J. McFarland, D. Ranjan, Journal of Fluid Mechanics **831**, 779-825 (2017)
[2] M. Mohaghar, J. Carter, G. Pathikonda, D. Ranjan, Journal of Fluid Mechanics **871**, 595-635 (2019)
[3] J.A. McFarland, D. Reilly, W. Black, J.A. Greenough, D. Ranjan, Physical Review E **92** (1), 013023

The Validity of MILES Simulations

R. J. R. Williams[1,*]

[1]AWE, Aldermaston, Reading, RG7 4PR, United Kingdom

[*]**Corresponding Author: robin.williams@awe.co.uk**

The numerical method of Monotone Implicit Large Eddy Simulation (MILES) is widely used in studies of compressible turbulence, as discussed in detail in [1], but its application remains the subject of some controversy. Recently, for example, Bian *et al.* [2] have made a detailed and comprehensive study of single-mode Rayleigh-Taylor instability (RTI) using a direct numerical simulation (DNS) code, finding that for low viscosities, the bubble continues to accelerate at late times, without breakdown of the symmetry of the initial conditions. They suggest that the breakdown of symmetry found in previous MILES results means that the results of these codes, applied to both to single mode RTI and other problems, should be treated with skepticism.

In this presentation, we will discuss the validity of the MILES modeling approach by comparing results for a number of different test cases and numerical schemes. This study utilizes two workhorse codes: an incompressible flow scheme capable of both spectral and high-order upwind advection, and a two-dimensional compressible hydrodynamics code which uses the same staggered-mesh Lagrange-remap algorithm as TURMOIL [3]. Each code is capable of both MILES and DNS calculations.

We have used a variety of test cases to validate the 3D incompressible code, including single-mode Kelvin-Helmholtz instability, incompressible Richtmyer-Meshkov instability and decaying homogeneous isotropic turbulence. The results confirm the non-locality of Fourier-based schemes [4], the effect of algorithm choices on, e.g., the energy present in fine-scale structures, and the realizability of passively advected scalar fields.

Our 2D compressible DNS calculations of single-mode RTI closely replicate the previous results of [2]. We find that in MILES mode, symmetry can be maintained with sufficiently careful coding, as previously discussed for single-mode RTI calculations using a range of WENO schemes [5]. Symmetry breakdown can however be driven by even the smallest numerically-resolvable change in conditions, with the rate of symmetry breakdown and rate of material interpenetration strongly dependent on the level of perturbation applied. As the rate of entropy production increases as the symmetry breaks, it appears that the symmetry breakdown corresponds to a physical instability in the single mode RTI system. Hence it could be argued that the breaking of symmetry is more representative of the behaviour which would be found in a physical system at sufficiently high Reynolds number than the case where symmetry is retained. This situation is comparable, for example, to the growth of asymmetry in the wake of a cylindrical obstacle, forming a vortex street, where mirror symmetry is broken in experiments for Reynolds numbers as low as 40 [6] as a result of unstable asymmetric modes [7].

In 2D MILES mode, with periodic boundary conditions and any finite level of symmetry-breaking perturbation, the flow after breakdown for the RTI problem evolves to a 'zonal' structure which expands rather slowly.

As G. E. P. Box observed, "All models are wrong but some are useful" [8]. We attempt to clarify the contexts in which MILES and DNS modeling are wrong, or should at least be treated with healthy skepticism, and those in which they are useful.

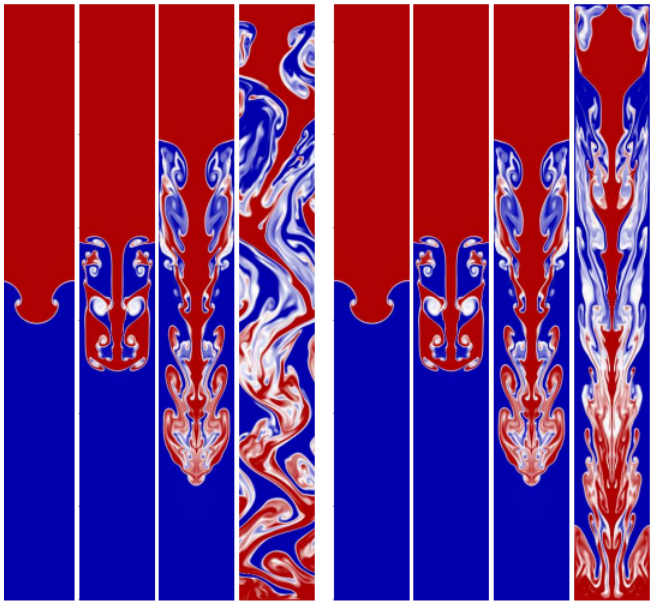

Figure 1: At = 0.04 single-mode RT in MILES mode. With asymmetry caused by rounding errors (left), compared with discretely symmetric scheme (right).

References

[1] F. F. Grinstein, L. G. Margolin, W. J. Rider, eds, *Implicit Large Eddy Simulation*, Cambridge University Press (2007).
[2] X. Bian, H. Aluie, D. Zhao, H. Zhang, D. Livescu, Physica D: Nonlinear Phenomena **403**, 232250 (2020).
[3] D. L. Youngs, Physics of Fluids A **3**, 1312 (1991).
[4] S. S. Ray, U. Frisch, S. Nazarenko, T. Matsumoto, Phys. Rev. E **84**, 016301 (2011).
[5] N. Fleischmann, S. Adami, N. A. Adams, Computers & Fluids **189**, 94 (2019).
[6] M. Coutanceau, R. Bouard, J. Fluid Mech. **79**, 231 (1977).
[7] A. Zebib, J. Engineering Math. **21**, 155 (1987).
[8] G. E. P. Box, in *Robustness in Statistics*, Academic Press (1979), pp. 201-236.

UK Ministry of Defence © Crown Owned Copyright 2022/AWE

Rayleigh-Taylor instability with variable acceleration reversal(s)

Denis Aslangil[1], Andrew G.W. Lawrie[2] and Arindam Banerjee[3*]

[1]Department of Aerospace Engineering and Mechanics, The University of Alabama, Tuscaloosa, AL, USA
[2]Department of Mechanical Engineering, University of Bristol, UK
[3]Department of Mechanical Engineering and Mechanics, Lehigh University, Bethlehem, PA, USA

[*]**Corresponding Author: arb612@lehigh.edu**

Classical Rayleigh-Taylor instability (RTI) with constant acceleration is observed in geophysical flows, oceanic flows, and chemical reactor processes. RTI under variable acceleration histories occurs in blast waves, inertial confinement fusion, and pulsating stars and is thus of interest to the turbulence community (see [1, 2] and references therein). Compared with classical RTI (constant gravity), which has been studied extensively, RTI with acceleration reversal is an uncharted but important problem. To date, there exists only one experiment [3] and a few numerical studies [2, 4, 5]. The numerical studies have mainly employed a step function with constant deceleration periods. It is noted that the deceleration period may lead to internal waves like motions within the mixing layer [1], and as a result, the second acceleration may show dependency on these dynamics.

In this study, we explore the sensitivity of reacceleration time on subsequent RTI growth with 12 different ADA simulations. Different deceleration histories are selected to elucidate the deceleration dynamics on the reacceleration phase of RTI mixing and late time RTI growth using a massively parallel implicit large eddy simulation (ILES) method (see figure 1 for an acceleration profile).

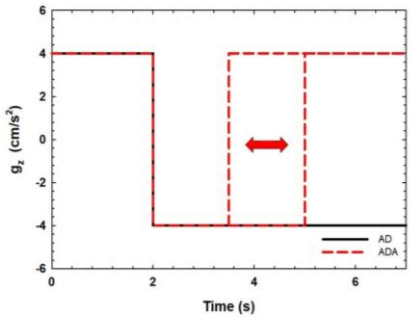

Figure 1. Representative *accel-decel* (AD) and *accel-decel-accel* (ADA) profiles were used for the current study. For the ADA cases, the deceleration time is varied, as indicated in the figure.

In RTI with variable acceleration studies, the commonly used length scale $Z(t)$ is defined as[3]:

$$Z(t) = \int_0^t \int_0^{t''} g_z(t')dt'dt''. \qquad (1)$$

where, g_z is the time-dependent acceleration of a given profile. Instead, to accommodate for variable periods of t_2, we redefine the length scale $Z_{ADA}(t)$ shifted in time-origin as

$$Z_{ADA}(t) = Ag_0(t-t_2)^2 \qquad (2)$$

This definition ensures that $Z(t)$ does not reach non-physical negative values during deceleration. In addition, $Z_{ADA}(t)$ grows from t_2 (reacceleration time) at the same rate as the constant acceleration RTI and allows for comparison between the two cases.

The time instants (t_2) for reacceleration cases are chosen to explore the effects of residual kinetic energy distribution between the vertical and horizontal components during the deceleration. This is measured by the vertical component of the anisotropy tensor B_{33}. The ADA cases are labeled as increasing (I), peak (P), decreasing (D), and trough (T) based on the vertical component (B_{33}) of the anisotropy tensor.

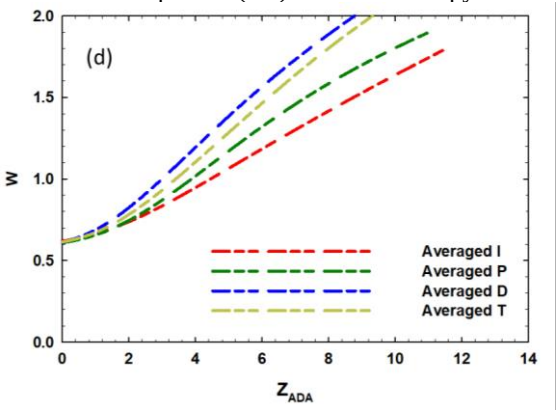

Figure 2: The integral mixing width, W, scaled by Z_{ADA} for the (a) first period of B_{33}; during the RTI ADA reacceleration phase.

Figure 2 presents the integral mix width plotted as a function of Z_{ADA} for the I, P, D, T cases for the first oscillation of B_{33} behavior. The integral mix width for the different I, P, D, and T cases indicates a significant difference in the growth rate upon reacceleration. Once self-similar length scales are adjusted to account for the variation in t_2, we note that growth rates follow the pattern |D|>|P|~|T|>|I| and our simulations suggest that although their short-term development may be substantially different, in the long-term, any I, P, T, or D choice within an oscillation period is likely to produce a similar long-term trajectory. A Similar ranking is observed in the I, P, D, T cases selected from the following oscillations. We will discuss the details of flow dynamics, first and second order statistics in detail for deceleration period and different ADA cases.

Acknowledgment: Arindam Banerjee acknowledges financial award from the U.S. National Science Foundation Grant #1453056.

References:

[1] Aslangil, D., Livescu, D., and Banerjee, A., *Effects of Atwood and Reynolds numbers on the evolution of buoyancy-driven homogeneous variable-density turbulence.* Journal of Fluid Mechanics, 2020. **895**.

[2] Aslangil, D., Banerjee, A., and Lawrie, A., *Numerical investigation of initial condition effects on Rayleigh-Taylor instability with acceleration reversals.* Physical Review E, 2016. **94**(5): p. 053114.

[3] Dimonte, G., and Schneider, M., *Turbulent Rayleigh-Taylor instability experiments with variable acceleration.* Physical Review E, 1996. **54**: p. 3740-3743.

[4] Ramaprabhu, P., Karkhanis, A., and Lawrie, A., *The Rayleigh-Taylor Instability driven by an accel-decel-accel profile.* Physics of Fluids (1994-present), 2013. **25**(11): p. 115104.

[5] Aslangil, D., Lawrie, A., and Banerjee, A., *Effects of variable deceleration periods on Rayleigh-Taylor instability with acceleration reversals,* under revision Physical Review E, 2022.

Numerical Study of Plasma Rayleigh-Taylor Instability with Realistic Transport Phenomena

Zhaorui Li[1*] and Daniel Livescu[2]

[1]Texas A&M University-Corpus Christi, Corpus Christi, Texas, USA
[2]Los Alamos National Laboratory, Los Alamos, New Mexico, USA

[*]**Corresponding Author: zhaorui.li@tamucc.edu**

It is generally believed that the development of Rayleigh-Taylor instability (RTI) is one of the main obstacles in achieving economically controlled fusion, however, due to the presence of complex plasma physics and their interaction with magnetic field, accurate simulations of RTI in regimes directly relevant to the inertial confinement fusion (ICF) coasting stage are still scarce. In this study, direct numerical simulation (DNS) of plasma RTI has been conducted under ICF coasting stage conditions by using a high-order two-fluid plasma solver [1] in which all realistic plasma transport terms [2] are included.

The numerical results show that, for any given Atwood number and hot-spot temperature, the RTI development or lack thereof can be characterized by two critical hot-spot number densities (fig.1), which increase exponentially with hot-spot temperature and decrease with Atwood number. When the hot-spot number density is smaller than the lower threshold value, RTI is completely suppressed by the electron thermal diffusion and viscous dissipation. Instead, fully developed RTI into chaotic stage (single-mode) or turbulence (multimode) is observed only when the hot-spot number density is larger than the upper threshold value.

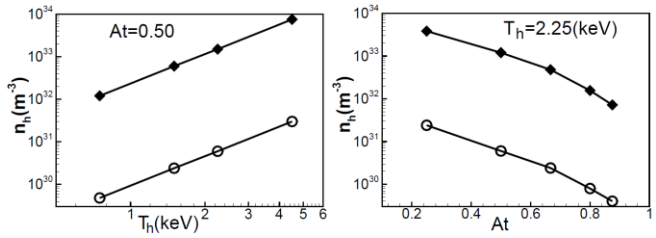

Figure 1: The variations of critical hot-spot number densities with hot-spot temperature and Atwood number.

Though a strong magnetic field (B~10^3T) is created by the Biermann battery effect, and its magnitude increases with Atwood number (fig.2a), for all simulations conducted in this study, the self-generated magnetic field is not sufficient to affect the flow dynamics or inhibit the electron thermal diffusion because of the extremely large plasma beta ($\beta > 10^5$) and small Hall parameter ($\omega_{ce}\tau_e \leq 10^{-2}$ in fig.2b).

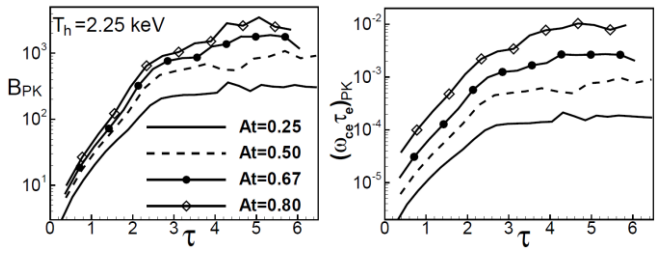

Figure 2: The evolutions of the peak values of self-generated magnetic field and Hall parameter at different Atwood numbers.

Acknowledgments: This work was supported by the Los Alamos National Laboratory under Contract No. 532498. provide acknowledgements for your work in this section.

References

[1] Z. Li and D. Livescu, Phys. Plasmas. **26**, 012109 (2019).
[2] S. Braginskii, Rev. Plasma Phys. **1**, 205 (1965).

Heat Transfer and Variable Transport Property Effects on the Compressible Rayleigh-Taylor Instability

K. Cherng[1,*], S. K. Lele [1] and D. Livescu[2]

[1]Dept. of Mechanical Engineering, Stanford University, Stanford, CA, USA
[2]Los Alamos National Laboratory, CSS-2, Los Alamos, NM, USA

[*]**Corresponding Author: kcherng@stanford.edu**

Mixing due to the Rayleigh-Taylor Instability (RTI) occurs in many applications such as supernovae explosions, Inertial Confinement Fusion (ICF) and Earth's mantle dynamics. In such extreme environments, there may be large variations in the fluid molecular transport properties of viscosity μ, thermal conductivity κ, and mass diffusivity D, occurring either from large temperature gradients or from the different properties of the fluids themselves [1]. How an abrupt emergence of large transport property differences, for example in response to rapid heating, affects the evolution of RTI flows remains an important open question.

Direct numerical simulations of the fully compressible RTI are performed with the PadeOps solver, which uses a high-order finite difference numerical scheme. We explore an idealized problem of RT unstable fluid layers composed of two materials at different temperatures - more specifically, a hotter, lower density gas layer pushing against colder, denser layer. To systematically isolate heat transfer and transport property effects, three configurations are considered: simulations that use constant properties, ones that use variable temperature-dependent properties and ones that begin with constant properties then transition to variable properties. The variable transport properties obey a plasma-type power law ($\mu, D, \kappa \propto T^{2.5}$). Once the constant-to-variable (transitional) transport property simulations reach a turbulent state, the transport coefficients are modified from the constant initial values to reflect the actual temperature field, approximating the sudden heating of a fluid; a similar procedure is used in [2]. This method of artificially altering the coefficients allows us to completely isolate transport property effects without introducing pressure waves or other complicating factors.

Results are presented for simulations at a variety of temperature ratios and transport property configurations. All simulations begin with the exact same random perturbations. With variable transport properties, especially at higher temperature ratios, we observe changes in timing for the onset of the self-similar mixing stage along with differences in the interface structure and mixing asymmetry. Furthermore, we find changes in the velocity fluctuation spectrum shape and the spatial intermittency of turbulence on the hotter fluid side. In the transitional property cases, when transport properties are adjusted, we detect a temporary flow transition stage in which the velocity and mass fraction gradients adapt and the system relaxes towards a final flow state, behavior supporting Taylor's dissipation-viscosity independence postulate for variable-viscosity mixtures as seen in [3].

Case Label	Temperature Ratio	Transport Property Configuration
A (baseline)	1	Constant
B	2	Constant
C	2	Variable
D	2	Constant-to-variable
E	3	Constant
F	3	Variable
G	3	Constant-to-variable

Table 1: The list of planned cases, with an Atwood number of 0.2 and Re=10000. The values of the other nondimensional parameters in the simulations follow those in [4].

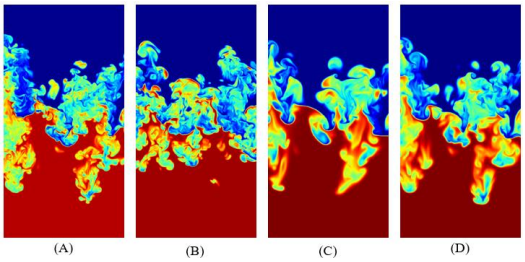

Figure 1: Mass fraction visualizations at a time after the transport property adjustment in case (D) for various simulation cases.

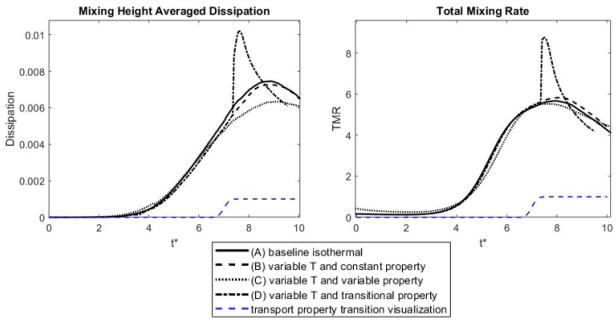

Figure 2: Time histories of the nondimensional mixing-zone averaged dissipation rate of turbulent kinetic energy and the total mixing rate $TMR = \int D \frac{\partial Y}{\partial x_i} \frac{\partial Y}{\partial x_i} dV$ for various simulation cases.

Acknowledgments: This work is supported by the Los Alamos National Laboratory under grant number 518570.

References

[1] S. Gerashchenko and D. Livescu, Physics of Plasmas **23**, 072121 (2016).
[2] D. Daniel and D. Livescu, *The Influence of Large Variations in Transport Properties on Homogeneous Turbulence Characteristics* (Los Alamos National Lab. (LANL), Los Alamos, CA, 2017).
[3] K. Lee, S.S. Girimaji, and J. Kerimo, Physical Review Letters **101**, (2008).
[4] B.L. Creurer and S. Gauthier, Theoretical and Computational Fluid Dynamics **22**, 125 (2008).

Direct numerical simulations of 2D multi-mode compressible Rayleigh-Taylor instability to explore the effects of different iso-thermal stratification strengths

Man Long Wong[1] and Denis Aslangil[2*]

[1]Los Alamos National Laboratory, Los Alamos, NM, 87545 USA
[2]Aerospace Engineering & Mechanics, The University of Alabama, Tuscaloosa, Alabama, 35487 USA

[*]**Corresponding Author: denis.aslangil@ua.edu**

Rayleigh-Taylor instability (RTI) occurs at the interface separating two fluids subjected to acceleration when the directions of the density gradient and the acceleration have opposite signs. Most of the previous scientific literature investigated the RTI under the incompressible assumption [1-3], while in many high-density-energy (HED) engineering applications and astrophysical phenomena such as inertial confinement fusion and supernova formations, the incompressible assumption may no longer be valid. In this study, the effects of the background iso-thermal stratification strength on multi-mode two-dimensional RTI are explored with fully compressible direct numerical simulations (DNS).

All DNS are performed to solve multi-species fully compressible Navier-Stokes Equations using Hydrodynamics Adaptive Mesh Refinement Simulator (HAMeRS) [4], (more details of the equations and the code can be found in [1]). The molar mass contrast between the mixing fluids known as Atwood number, $A = (W_1 - W_2)/(W_1 + W_2))$, is chosen to be 0.04 for all cases, where W_1 and W_2 are the heavy fluid and light fluid molar masses, respectively. Whereas, the strength of the background stratification is altered by the background iso-thermal Mach number, $Ma = \sqrt{g\lambda_0}/c_0$ where g is the acceleration, λ_0 is the characteristic wavelength and c_0 is the speed of sound. It is chosen as 0.3, 0.6, and 0.9 for weakly, moderately, and strongly stratified cases respectively. In addition, the time evolution of the investigated parameters is presented versus the normalized time, $t^* = t\sqrt{g/\lambda_0}$.

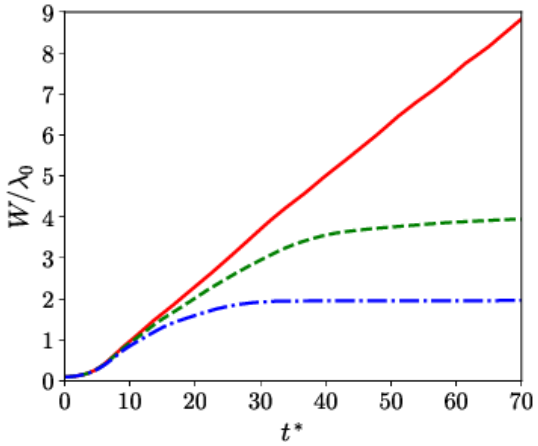

Figure 1: Time evolution of the normalized mixing width, W/λ_0. Red solid line: *Ma=0.3*; green dashed line: *Ma=0.6*; blue dash-dotted line: *Ma=0.9*.

Figure 1 shows that the increase in the flow compressibility through the strength of the background stratification suppresses the RTI growth and eventually, prevents the RTI mixing layer to grow further. This finding is similar to the single-mode 2D compressible iso-thermally stratified [5], in which a larger background Mach number also leads to a suppression on the RTI mixing layer growth. After reaching to the certain height of the mixing layer the flow tends to become well-mixed within the mixing layer. Figure 2 shows that an increase in background stratification leads to narrower and more homogeneously mixed mixing layers for the larger *Ma* compared to the weakly stratified case, and such effects are predominant for the strongly stratified case *Ma=0.9*. As a result of the enhanced mixing, the density gradients, which would feed the growth of the RTI mixing layer, decrease within the layer and the mixing growth saturates.

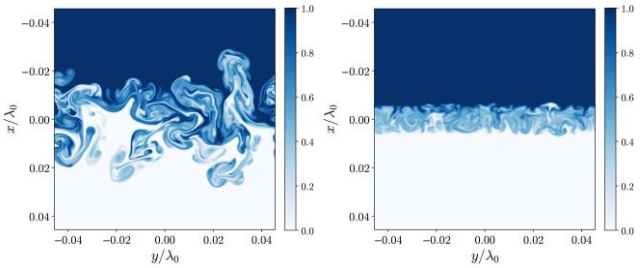

Figure 2: Heavier fluid mass fraction fields, Y_H, at $t^* = 50$. Left panel: *Ma=0.3*; right panel; *Ma=0.9*.

We will present detailed analysis of our DNS to study the flow compressibility through the strength of the background stratification and will compare the chaotic behavior of the multi-mode 2D RTI. Finally, we will show that that the findings of our study do not show any significant sensitivity to Reynolds number, Re_0, which suggests a more universal conclusion on the effects of background stratification on the flow instability.

Acknowledgments: For the computations, this work used the Extreme Science and Engineering Discovery Environment (XSEDE) [6], which is supported by NSF grant # ACI-1548562.

References

[1] Aslangil, D., Wong, M. L., "Study of iso-thermal stratification strength on 2D multi-mode compressible Rayleigh-Taylor instability", AIAA SCITECH 2022 Forum, 0456, (2022).

[2] Aslangil, D., Banerjee, A., and Lawrie, A., Numerical investigation of initial condition effects on Rayleigh-Taylor instability with acceleration reversals. Physical Review E, 2016. **94(5)**: p. 053114.

[3] Aslangil, D., Lawrie, A., and Banerjee, A., Effects of variable deceleration periods on Rayleigh-Taylor instability with acceleration reversals, under revision Physical Review E, 2022.

[4] Wong, M. L., "High-order shock-capturing methods for study of shock-induced turbulent mixing with adaptive mesh refinement simulations," Ph.D. thesis, Stanford University, 2019.

[5] Wieland, S. A., Hamlington, P. E., Reckinger, S. J., and Livescu, D., "Effects of isothermal stratification strength on vorticity dynamics for single-mode compressible Rayleigh-Taylor instability," Phys. Rev. Fluids, **Vol. 4**, 2019, p. 093905(2019).

[6] Towns, J., et al., "XSEDE: Accelerating Scientific Discovery", Computing in Science & Eng. **Vol. 16**, pp. 62–74.17 (2014).

Energy Pathways of Rayleigh-Taylor driven Mixing and Implications on Implosion Modeling

Dongxiao Zhao[1,2], Riccardo Betti[1,2] and Hussein Aluie[1,2,*]

[1]Department of Mechanical Engineering, University of Rochester, Rochester, New York, USA
[2]Laboratory for Laser Energetics, University of Rochester, Rochester, New York, USA

[*]**Corresponding Author: hussein@rochester.edu**

We identify two main processes for energy transfer across scales in Rayleigh-Taylor (RT) flows: baropycnal work Λ, due to pressure gradients, and deformation work π, due to flow strain. We show how these fluxes exhibit a quadratic-in-time self-similar evolution similar to RT mixing layer. Λ is a conduit for potential energy, transferring energy non-locally from the largest scales to smaller scales where π takes over. In 3D, π continues a persistent cascade to yet smaller scales, whereas in 2D, π re-channels the energy back to larger scales. This gives rise to a positive feedback loop in 2D-RT (absent in 3D) in which mixing layer growth and the associated potential energy release are enhanced relative to 3D, yielding the well-known larger α values in 2D simulations. Despite higher bulk kinetic energy levels in 2D, small scales are weaker than in 3D. We also find that net upscale cascade in 2D tends to isotropize the large-scale flow, in stark contrast to 3D-RT. These fundamental differences pinpoint the misleading physics inherent to 2D-RT simulations in ICF modeling. Our findings also indicate the absence of net upscale energy transfer in 3D-RT as is often claimed; growth of large-scale bubbles and spikes is not due to "mergers" but solely due to baropycnal work Λ.

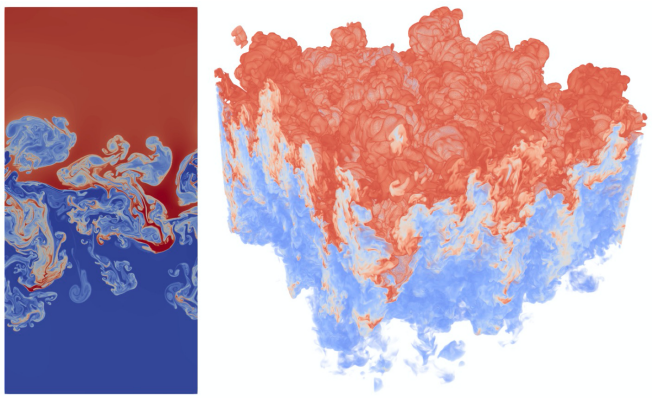

(a) 2D4096 snapshot (b) 3D1024 snapshot

Figure 1: Density visualizations from the 2D and 3D simulations from [1].

Acknowledgments: This research was funded by DOE FES grants DE-SC0014318and DE-SC0020229.

References

[1] D. Zhao, R. Betti and H. Aluie, "Scale interactions and anisotropy in Rayleigh-Taylor turbulence," *Journal of Fluid Mechanics,* p. A29, 2022.

Molecular dynamics simulations as a helpful tool to understand the phenomenology of formation and fragmentation of shock-induced hydrodynamic instabilities

Olivier Durand[1,2*] and Laurent Soulard[1,2]

[1]CEA, DAM, DIF, F-91297 Arpajon, France
[2]Université Paris Saclay, CEA, Laboratoire Matière en Conditions Extrêmes, Bruyères-le-Châtel 91680, France

[*]**Corresponding Author: olivier.durand@cea.fr**

It is now commonly accepted that the interaction of a shock wave with the surface defects of a metal causes the geometric inversion of the latter and can be at the origin, according to the shock conditions, of the development of so-called Richtmyer-Meshkov instabilities (RMIs). During their development, these instabilities can fragment in the form of particles (ejecta) and thus greatly disturb the progress of shock confinement experiments or the operation of measurement diagnostics located nearby. It is therefore necessary to properly characterize this phenomenon, called micro-jetting. In particular, we seek to determine the size and velocity distributions of the ejected particles as well as their total mass.

To simulate micro-jetting, the most classic approach is to use continuum mechanics (CM) because it deals with the same spatial and temporal scales as experiments. However, surface tension and viscosity effects, which are of great importance, are difficult to model and implement in computer codes. Furthermore, there is no fragmentation model either.

For about ten years, we at CEA have chosen to explore a complementary path and to treat the phenomenon by means of an atomistic method based on classical molecular dynamics (MD). Unlike CM, this method makes it possible, for a number of atoms exceeding a few million, to process not only the hydrodynamic aspects but also the fragmentation of the RMIs. It directly describes the behavior of matter at the atomic level and thus intrinsically takes into account the effects of surface tension and viscosity, provided that the interatomic potential chosen makes it possible to properly reproduce the behavior of matter under impact. It also does not suffer from mesh problem. The representativeness of MD therefore depends on the quality of the potential energy function used.

The main limitation of this type of approach is that the maximum size of the samples that can be simulated is typically 1 μm^3, significantly lower than the dimensions of the experimental samples. Furthermore, the effects of surface tension, for example, can be exacerbated. The comparison between the experiment and MD can therefore only be qualitative, but we show that the latter can constitute a powerful phenomenological tool which makes it possible to apprehend a large part of the physical mechanisms at work in the particular case of the micro- jetting, and to propose a modeling of it.

For our work, we mainly process tin. The first simulations were carried out with the Stamp code, developed at CEA, using a relatively simple interatomic potential, of the EAM (embedded atom model) type. Samples containing more than 100 million atoms could thus be processed [1-5]. The impressive progression of computing means now allows us to process samples containing more than a billion atoms by means of a potential of the MEAM (modified EAM) type, more physical in its description of tin under shock than the EAM potential, but also about 10 times more computationally expensive [6]. The simulations are carried out using the ExaStamp code, also developed at the CEA. Our work so far concerns the case of jets propagating in vacuum following the reflection of a supported shock.

The phenomenology of the rupture of the RMIs proposed by MD is as follows: below a critical thickness e_{cr}, the instability (jet of matter) during development becomes unstable. Holes then begin to appear, which grow, coalesce and percolate, thus leading to the formation of more or less cylindrical and elongated ligaments of liquid metal in the direction of extension of the jet (see fig. 1).

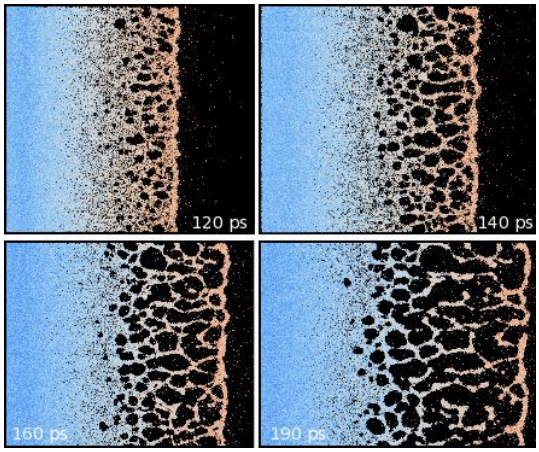

Figure 1: MD simulations of a RMI when it begins to break-up using an EAM potential. Below a critical thickness e_{cr}, holes appear, grow, coalesce, and ligaments of liquid metal are formed.

If they have enough kinetic energy, the longest of the ligaments created can in turn fragment into several particles which ultimately adopt a spherical shape under the effect of surface forces.

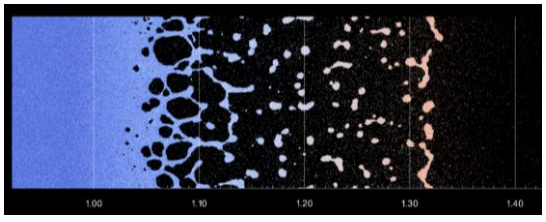

Figure 2: View of the RMI at a later time. The longest ligaments have fragmented in turn into secondary spherical particles.

As the jet becomes thinner during its development, the corresponding point e_{cr} moves, and the fragmentation zone counter-propagates from the jet tip towards the free surface. Two consequences can be deduced from this scenario: i) the fragmentation of the jet is neither instantaneous nor homogeneous, ii) the expansion rate of the

jet decreasing with time, the break-up occurs under dynamic conditions varying with time. In particular, it is possible to show, by simple energy considerations [7], that the particles created are all the larger the later they are produced, that is to say closer to the free surface. The volume distribution of the particles constituting the cloud is therefore not centered on an average value. The FZP (Fragmentation Zone Propagation) model proposed in [3,4] is the translation of these observations and allows, by taking into account the propagation of $_{ecr,}$ to calculate the ejected surface mass as a function of the velocity of the particles.

The observations from MD simulations using an EAM potential compare well with experimental observations of jet fragmentation, in particular that obtained by UV holography at Los Alamos [8] (compare fig. 2 and 3).

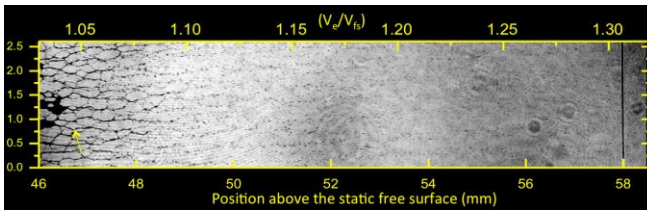

Figure 3: Hologram obtained by Sorenson et al. in [8] of the fragmentation of a liquid sheet of tin. Shock driven by explosive. A web-like structure and ligaments of tin, in black, are clearly visible and are similar to the structure simulated in fig. 2.

Other observations obtained by ultra-fast UV shadowgraphy at CEA [9] (fig. 4, left) and by X-ray imaging at Livermore [10] (fig. 4, right) show that the jet adopts a fairly complex double filamentary structure (large ligaments parallel to the direction of jet propagation, and a network of small ligaments between the large ligaments). As suggested by the MD simulations obtained with an MEAM potential [6], this double structure could result from the microstructure of the material induced by a solid/liquid phase change just after the shock has emerged from the bottom of the defect (see fig. 5).

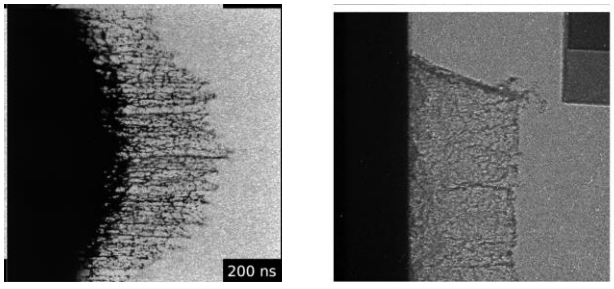

Figure 4: left) UV picosecond shadowgraph after shock driven by laser obtained by Sollier et al. in [9]); right) X-ray-imaging after shock driven by flyer plates obtained by Bober et al. in [10] of a tin jet as it fragments. A complex filamentary structure, similar to that simulated by MD in fig. 5 is observable.

It should be noted that the observations described above correspond to quite different stresses and sample sizes, which seems to indicate that the filamentary structure is quite general and not very dependent on the stress.

The evolution simulated by MD of the volume of the particles according to their velocity [3,4], after fragmentation, is also very similar to that observed experimentally [8]: the smallest particles are also the fastest, and they are located at the front of the jet, while the largest (slowest) are located near the free surface.

MD is therefore a powerful phenomenological tool which is of interest in the study of the development and fragmentation of hydrodynamic instabilities under shock. In addition to the CM, it offers an unprecedented interpretation of a certain number of experiments carried out at the CEA or in other laboratories, allowing, on its scale, an extremely fine description of the mechanisms of ejection of matter under impact and in particular the fragmentation of sheets of liquid metal. It also provides full physics reference solutions that any hydrodynamic simulation code must be able to reproduce [5].

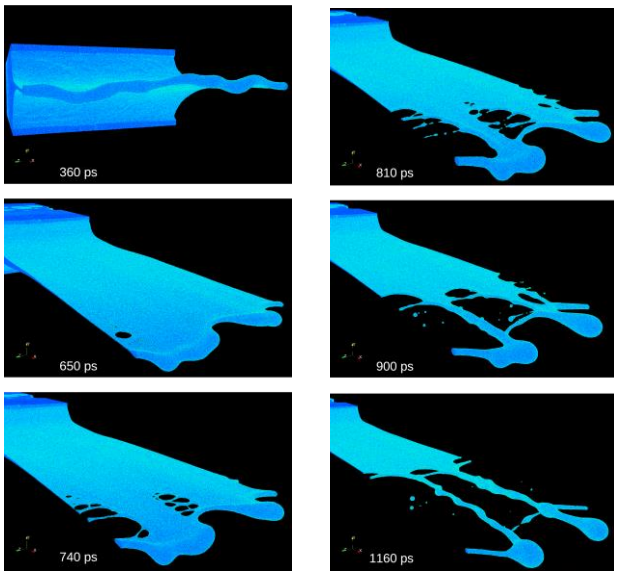

Figure 5: MD simulation of a RMI when it begins to break up using an MEAM potential. The ripples visible on the leading edge of the sheet, and the final filamentary structure may be explained by the phase change of tin as the shock has emerged from the bottom of the defect. This structure is similar to that of fig. 4.

References

[1] O. Durand and L. Soulard, J. Appl. Phys. **111**, 044901 (2012).
[2] O. Durand and L. Soulard, J. Appl. Phys. **114**, 194902 (2013).
[3] O. Durand and L. Soulard, J. Appl. Phys **117**, 165903 (2015).
[4] O. Durand and L. Soulard, J. Dyn. Behv. Mater **3**, 280 (2017).
[5] O. Durand, S. Jaouen, L. Soulard, O. Heuzé, and L. Colombet, J. Appl. Phys. **122**, 135107 (2017)
[6] O. Durand, L. Soulard, L. Colombet, and R. Prat, J. Appl. Phys. **127**, 175901 (2020).
[7] D.E. Grady, *Fragmentation of Rings and Shells* (Springer, New-York, 2006)
[8] Sorenson DS et al. Los Alamos National Laboratory technical Report No. LA-UR-15-25993 (2015)
[9] A. sollier and E. Lescoute, Int. J. Imp. Eng. **136**, 107177 (2020)
[10] D.B. Bober, K.K. Mackay, M.C. Akin, and F.M. Najjar, J. Appl. Phys. **130**, 045901 (2021)

Modeling the Shell Growth and Breakup of Hydriding Ejecta Particles

Frederick Ouellet[1,*], Alan K. Harrison[1] and Jonathan D. Regele[1]

[1]X-Computational Physics Division, Los Alamos National Laboratory, Los Alamos, New Mexico, USA

[*]**Corresponding Author: f.ouellet@lanl.gov**

Experiments performed at Los Alamos National Laboratory have shown that metal particles which are ejected from a shocked, perturbed surface exhibit different behaviors depending on whether the medium in which they are ejected is either inert or reactive. Particles ejected into an inert medium appear to show the reaction to hydrodynamic drag and break up via a standard liquid droplet breakup mechanism in cases in which they do break up. However, those ejected into a reactive, hydrogen-based medium are believed to form an outer hydride shell and exhibit a non-monotonic velocity response in recorded LDV data. One postulate for this behavior is that the surrounding hydride shell is brittle and small particles break off the shell as the ejecta experience hydrodynamic forces from the surrounding fluid. These small particles quickly equilibrate with the surrounding fluid and slow down which would then expose faster-moving, larger ejecta particles to the LDV. The specific physical processes which dictate the reactive phenomena are mostly unknown and are of interest to obtain accurate models for the trajectories of the ejecta after they form.

Three main topics are covered in this work. First, a set of point-particle simulations of the inert experimental configurations are discussed. The purpose of these simulations is to validate the currently implemented ejecta sourcing and momentum and energy coupling models used in the hydrocode in the inert cases before use for the reactive model development and testing. Next, a numerical solver for the inner and outer radii of the developing hydride shell around the ejecta due to the chemical reactions with the ambient gas is validated against experimental data using simulations with a single reacting particle. Finally, we present ongoing work on the creation of a model which is meant to simulate the shedding of small particles from the hydride shell as it interacts with the ambient gas through hydrodynamic forces. The reasoning for why a shedding mechanism is favored over liquid droplet breakup for modeling the reactive ejecta phenomenon of interest is also discussed.

Acknowledgments: Funding for this work is supported by Advanced Simulation and Computing Program, Physics and Engineering Models, Mix and Burn project.

LES of ejecta from irregular surfaces

M. A. Brown*, R. J. R. Williams

AWE, Aldermaston, Reading. RG7 4PR. United Kingdom

***Corresponding Author: matthew.a.brown@awe.co.uk**

A Lagrange-remap hydrocode is used to perform 3D Large Eddy Simulation (LES) of ejecta from multiply shocked surfaces on metal targets, with periodic and aperiodic surface amplitude profiles. Simulations investigate typical experimental conditions and assemblies.

Ejecta is often understood as the limit of a Richtmyer-Meshkov Instability (RMI) [1,2] in which the shock-driven acceleration of a material surface, in contact with vacuum or low density gas, leads to growth of solid or liquid spikes (jets) into the void. The shock-initiation of such growth, and the sourcing of material into the developing spike, should be influenced by structure below the surface. For instance, damage from a previous shock may influence the local shock behaviour during a subsequent re-shock (eg, recompaction of material fractured due to spall [3]).

For this work we investigate, with 3D LES, ejecta sourcing from irregular surfaces, including those with localized features, and for single and multi-modal periodic surfaces in two surface dimensions. We examine how surface profile and shock conditions influence the development of sub-surface structure, including due to spall, and how this can influence the eventual failure of the surface upon subsequent re-shocks.

References

[1] R. D. Richtmyer, Commun. Pure Appl. Math., **13**, 297 (1960).
[2] E. E. Meshkov, Fluid Dyn. **4,** 101 (1969)
[3] R. J. R. Williams and C. C. Grapes, J. dynamic behavior mater., **3**, 291 (2017)

UK Ministry of Defence © Crown Owned Copyright 2022/AWE

Dependence of Enstrophy Transport and Mixed Mass on Dimensionality and Initial Conditions in the Richtmyer–Meshkov Instability Induced Flows

Ye Zhou[1*], Michael Groom[2*], and Ben Thornber[2*]

[1]Lawrence Livermore National Laboratory, Livermore, CA 945506
[2]School of Aerospace, Mechanical and Mechatronic Engineering,
The University of Sydney, Sydney NSW 2006, Australia

[*]**Corresponding Authors:** michael.groom@sydney.edu.au, ben.thornber@sydney.edu.au, yezhou@llnl.gov

This paper presents a comparative study of the enstrophy budget and mixed mass between two- and three-dimensional flows induced by Richtmyer–Meshkov instability (RMI). Specifically, the individual contributions to the enstrophy budget due to the production from baroclinicity and from vortex stretching (which vanishes in two-dimensional (2D) flow) are delineated. This is enabled by a set of two- and three-dimensional computations at Atwood 0.5 having both narrow- and broad-band perturbations. A further three-dimensional (3D) computation is conducted at Atwood 0.9 using an identical narrowband perturbation to the Atwood 0.5 case to examine the sensitivity to density ratio [1]. The mixed mass is also considered with the goal to obtain insight on how faithfully a simplified calculation performed in two dimensions can capture the mixed mass for an inertial confinement fusion (ICF) or other practical application [2,3,4]. It is shown that the late time power law decay of variable density enstrophy is substantially different in two and three dimensions for the narrowband initial perturbation. The baroclinic production term is negligible in three dimensions (aside from the initial shock interaction), as vortex stretching is larger by two orders of magnitude. The lack of vortex stretching considerably reduces the decay rate in both narrowband and broadband perturbations in two dimensions. In terms of mixed mass, the lack of vortex stretching reduces the mixed mass in two dimensions compared to three in all cases. In the broadband cases, the spectral bandwidth in the 2D case is wider; hence, there is a longer time period of sustained linear growth which reduces the normalized mixed mass further.

Acknowledgments: This research was supported under Australian Research Council's Discovery Projects funding scheme (project number DP150101059). B. Thornber would like to acknowledge the computational resources at the National Computational Infrastructure through the National Computational Merit Allocation Scheme which were employed for all Flamenco cases presented here. This work was performed under the auspices of the U.S. Department of Energy by Lawrence Livermore National Laboratory under Contract DE-AC52-07NA27344.

References

[1] Y. Zhou, M. Groom, B. Thornber, J. Fluids Eng., 142, 121104 (2020).
[2] Y. Zhou, Phys. Rep. **720-722**, 1 (2017).
[3] Y. Zhou, Phys. Rep. **723-725**, 1 (2017).
[4] Y. Zhou, R.J.R. Williams, P. Ramaprabhu, M. Groom, B. Thornber, A. Hillier, W. Mostert, B. Rollin, S. Balachandar, P.D. Powell, A. Mahalov, and N. Attal, Rayleigh–Taylor and Richtmyer–Meshkov instabilities: a journey through scales. Physica D: Nonlinear Phenomena, 423, 132838 (2021)

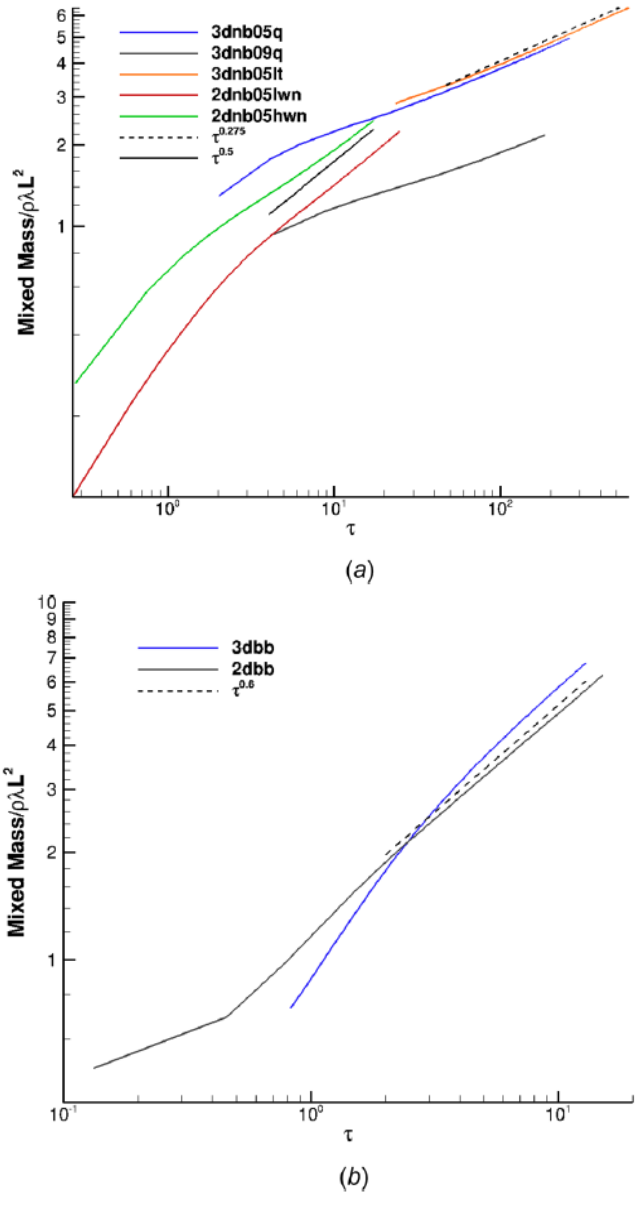

Fig. 1. Mixed mass for (a) narrowband and (b) broadband perturbations

Study of turbulence statistics and transport for Richtmyer-Meshkov instability with re-shock

Man Long Wong[1,2*], Jon R. Baltzer[2], Daniel Livescu[2], and Sanjiva K. Lele[1,3]

[1]Department of Aeronautics and Astronautics, Stanford University, Stanford, California 94305, USA
[2]Los Alamos National Laboratory, Los Alamos, New Mexico 87545, USA
[3]Department of Mechanical Engineering, Stanford University, Stanford, California 94305, USA

[*]**Corresponding Author: mlwong@alumni.stanford.edu, manlong.wong@nasa.gov**

The Richtmyer–Meshkov instability (RMI) and turbulence induced from it appears in many natural phenomena and engineering applications, such as supernova explosion, inertial confinement fusion and supersonic combustion. As alternatives to experiments, direct numerical simulation (DNS) or large-eddy simulation (LES) are powerful tools for studying turbulence generated from RMI. However, the need to resolve temporal-spatial scales fully or partially in these simulations limit the application of these methods to turbulent flows at lab-scale only, with simple configurations and relatively low Reynolds number. On the other hand, the Reynolds-averaged Navier–Stokes (RANS) simulation based on averaged equations with turbulence modeling of unclosed terms is a computationally less expensive method that can provide reasonable predictions for turbulent flows in complex engineering problems.

Large variable-density effects are commonly observed in flows induced by RMI when materials of moderate or large density ratios are turbulently mixed. Special models are hence required to deal with the variable-density effects that are absent in single-species incompressible flows. Besnard, Harlow, and Rauenzahn (BHR) [1] pioneered a RANS-based turbulence closure model for variable-density turbulence based on the averaged multi-species Navier–Stokes equations. Since then, many turbulence models for variable-density turbulence have been proposed. In many of these models such as the BHR-3 model [2], the transport equations of second-moments are modeled to close the averaged Navier–Stokes equations. The BHR-3 model shows reasonable comparison with experimental results of RMI but the comparison was limited to very few measurable quantities available from experiments, such as the mixing width. The experiments are also known to have many uncertainties in the initial conditions and measurements.

In this work, the budgets of second-moments and Reynolds stress for the variable-density turbulent flow induced by RMI at a twice- shocked mixing layer between SF_6 and air (Atwood number of 0.68) are studied based on the highest Reynolds number three-dimensional case presented in [3]. Results from adaptive mesh refinement simulations including a very high resolution run with a maximum of around 4.5 billion grid points are analyzed (more details of the equations and the code can be found in [4]). Fig. 1 visualizes the turbulent mixing region of the highest resolution simulation at different times after re-shock. The aim of the analysis is to study the mechanism of turbulence generated from RMI through the transport equations of second-moments, e.g. the turbulent mass flux, that can ultimately help improve existing turbulence models such as BHR-3 model using second-moment closure. Fig. 2 shows the spatial profiles of different terms in the transport equation of turbulent mass flux component in the inhomogeneous direction across the mixing layer at a late time after re-shock. The turbulent mass flux component, $\bar{\rho}a_1 = \overline{\rho' u'}$ plays an important role in transferring energy between mean kinetic energy and turbulent kinetic energy in the flow. In addition to turbulent mass flux, other second-moments such as the density-specific-volume covariance that mediates the turbulent mass flux production, and Reynolds stress tensor which is essential to close the averaged momentum equation are also examined with their budgets. Finally, the effects of the subfilter-scale stress on the budgets of the large-scale turbulent quantities with different degree of filtering are also discussed.

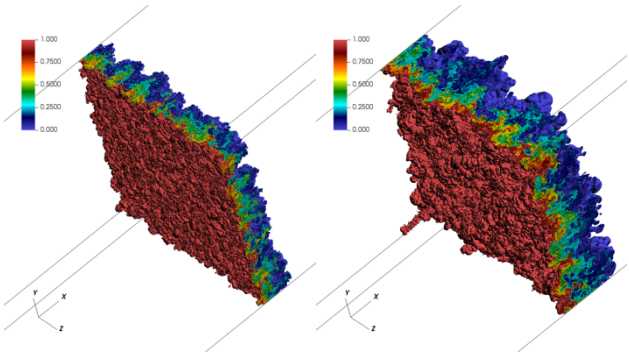

Figure 1: Isovolume of the SF_6 mole fraction at 1.2 ms (left) and 1.75 ms (right).

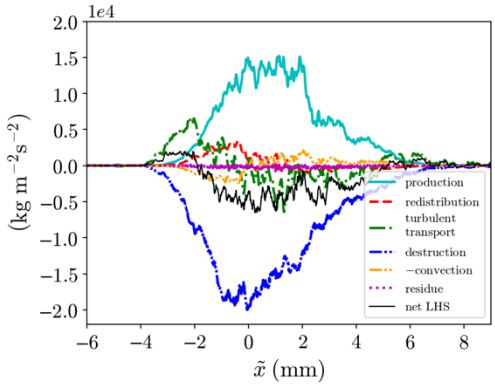

Figure 2: Budget of $\bar{\rho}a_1$ at 1.75 ms.

Acknowledgments: This work was performed under the auspices of U.S. Department of Energy. M. L. Wong and S. K. Lele were supported by Los Alamos National Laboratory, under Grant No. 431679.

References

[1] D. Besnard, F. Harlow, R. Rauenzahn, and C. Zemach, Tech. Rep. (Los Alamos National Lab., NM, United States), (1992).
[2] J.D. Schwarzkopf, D. Livescu, R.A. Gore, R.M. Rauenzahn, and J.R. Ristorcelli, Journal of Turbulence **12**, (2011).
[3] M.L. Wong, D. Livescu, and S.K. Lele, Physical Review Fluids **4**, (2019).
[4] M.L. Wong, J.R. Baltzer, D. Livescu, and S.K. Lele, Physical Review Fluids, (under review).

Permanence of large eddies in variable-density Richtmyer-Meshkov turbulent mixing zones

O. Soulard* and J. Griffond

CEA, DAM, DIF, F-91297 Arpajon, France

*Corresponding Author: olivier.soulard@cea.fr

At large times, turbulent mixing zones generated by the Richtmyer-Meshkov instability become self-similar [1]. In particular, their width grows according to a power law which exponent is usually denoted by θ. The value of θ is essential for engineering applications and its prediction is the object of many works, a summary of which can be found in [1].

In the Boussinesq limit, when density contrasts are very small, it has been shown [2] that θ is linked to initial conditions through the principle of permanence of large eddies. This principle originates from the study of homogeneous flows, and has first been applied to mixing zones in [3-4]. It relies on the idea that, under certain conditions, large eddies evolve on a time scale much larger than the one governing the growth of the zone. As a result, their initial information is preserved throughout the flow evolution. When this permanence is verified, the flow is constrained by large-scale initial conditions and its growth exponent θ can be expressed as a function of some large-scale initial parameter, such as s_0, the initial infrared exponent of the turbulent kinetic energy spectrum.

Whether large eddies are permanent or not depends on the long range correlations induced by non-linear terms. In a Boussineq flow, these terms involve quadratic products between the components of the velocity field, and their non-local propagation by the pressure field. Several models predict that these non-linear terms lead to a backscattering transfer of energy characterized by an infrared exponent of 4. As a result, for initial spectra satisfying $s_0 < 4$, large eddies are predicted to be permanent, while for $s_0 > 4$ they are not.

For strong density contrasts, a major difference arises: an additional non-linearity must be accounted for. Along with the usual quadratic term involving the velocity field, a non-linear product between the inverse density and the pressure gradient is also active. This additional non-linearity affects the way the pressure field transmits information over very long distances: the Poisson equation for pressure is indeed modified by its presence. Therefore, the long range correlations of the velocity field are possibly impacted by this additional non-linear term, along with the conditions under which large eddies are permanent. The purpose of this work is to clarify this issue.

To this end, we start by studying a simple example: we consider an isolated eddy displaying density variations. This setting is the same as the one first introduced in [5], except for the density not being uniform. Then, we show that density variations modify the asymptotic scaling of the pressure field. The main consequence is that the linear impulse of the eddy is not an invariant quantity, as opposed to the uniform density case. However, another invariant can be put forward, which is built upon the solenoidal component of the momentum.

A direct transposition of this result to the context of mixing zones can be achieved by considering a collection of independent variable-density eddies organized in the form of a one-dimensional layer. For such a mixing zone, it can be shown that the kinetic energy spectrum E is not invariant because of pressure correlations. By contrast, the spectrum Q of the solenoidal momentum exhibits invariant properties similar to those detailed previously.

To confirm these expectations, we perform a spectral analysis. In particular, we study the non-linear transfer terms governing the evolution of E and Q. We show that a backscattering transfer of energy occurs for Q, with an infrared exponent of 4, but not necessarily for E. As a result, the principle of permanence of large-eddies applies to Q but not to E. The main consequence is that, for strong density contrasts, the value of θ is not related to s_0 the infrared exponent of the turbulent kinetic energy spectrum E. Instead, it is related to s_q, the infrared exponent of the solenoidal momentum spectrum Q. Both exponents coincide in the Boussinesq limit. However, for strong density contrasts, one has in general $s_q \neq s_0$.

To verify these predictions, implicit large-eddy simulations of Richtmyer-Meshkov turbulent mixing zones are performed.

References

[1] Y. Zhou, Rayleigh-Taylor and Richtmyer-Meshkov instability induced flow, turbulence, and mixing. part I, Phys. Rep. **720** (2017) and part II, Phys. Rep. **723** (2017).
[2] O. Soulard, F. Guillois, J. Griffond, V. Sabelnikov, S. Simoëns, Permanence of large eddies in Richtmyer-Meshkov turbulence with a small Atwood number, Phys. Rev. Fluids **3** (2018) 104603.
[3] J. Chasnov, On the decay of inhomogeneous turbulence, J. Fluid. Mech. **342** (1997) 335–354.
[4] A. Llor, Invariants of free turbulent decay, 2006, arXiv/physics 0612220.
[5] G.K. Batchelor and I. Proudman. The large-scale structure of homogeneous turbulence. PTRSA, **248** (1956).

Linear stability investigations of the Richtmyer-Meshkov instability in an ideal two-fluid plasma

Yuan Li[1], Abeer Bakhsh[2], Ravi Samtaney[1,*]

[1] King Abdullah University of Science and Technology, Thuwal, Saudi Arabia
[2]Umm Al Qura University, Saudi Arabia

[*]**Corresponding Author: ravi.samtaney@kaust.edu.sa**

Inertial confinement fusion (ICF) is a promising method for the generation of fusion energy. By imploding the target to very high densities, it is expected that the fusion reactions occur and the fuel is confined by its own inertia. A key bottleneck towards the achieving goal of ICF is hydrodynamic instabilities, such as Richtmyer–Meshkov instability (RMI) which occurs when a perturbed density interface is impulsively accelerated. Due to the high temperature and high energy-density scenario in ICF, it is expected the materials to be in a plasma state, and thus could be influenced by a magnetic field. An effective fluid description for the plasma is two-fluid plasma (TFP). In this model, ions and electrons are treated as two separate fluids and are coupled to the full Maxwell equations. In addition, the electron inertia and light speed are finite. Unlike ideal MHD, the TFP model allows for non-zero self-generated electromagnetic fields.

Nonlinear simulations by Bond *et al.* [1, 2] showed that the TFP RMI differs significantly from the hydrodynamic case and the interface dynamics is extremely complex. In the spirit of a reductionist approach, we first develop the linear stability theory and perform simulations of the TFP RMI with a numerical method developed by Samtaney [3]. By splitting the solution U into the base flow $U^0(x,t)$ and perturbations $\epsilon\widehat{U}(x,t)e^{iky}$, the TFP equations of motion are separated into a base state and a set of linearized equations governing the evolution of the perturbations.

$$\frac{\partial U^0}{\partial t} + \frac{\partial F(U^0)}{\partial x} = S(U^0) \qquad (1)$$

$$\frac{\partial \widehat{U}}{\partial t} + \frac{\partial A(U^0)\widehat{U}}{\partial x} = \left(-ikB(U^0) + C(U^0)\right)\widehat{U}, \qquad (2)$$

$$\text{where } A = \left.\frac{\partial F}{\partial U}\right|_{U^0},\ B = \left.\frac{\partial G}{\partial U}\right|_{U^0},\ C = \left.\frac{\partial S}{\partial U}\right|_{U^0} \qquad (3)$$

Then the linear stability is numerically studied by solving Eqs. (1) and (2). In this model, two non-dimensional parameters arise: the referenced Debye length parameter $d_{D,0}$ (governs the different coupling regimes between the charged species) and β_0 (denotes initial magnetic field strength). When $d_{D,0}$ is large, the coupling between ions and electrons is sufficiently small that the induced Lorentz force is very weak and the two species evolve as two separate fluids. When $d_{D,0}$ is small, the coupling is strong and the induced Lorentz force is strong enough that the difference between state of ions and electrons is rapidly decreased by the force. As a consequence, the ions and electrons are tightly coupled and evolve like one fluid (see Fig. 1). We will present linear simulation results in the absence of an initial magnetic field and discuss the different coupling regimes by varying $d_{D,0}$. The growth rate of the perturbations is examined by varying β_0 for weak and strong coupling between the ions and electrons.

Some preliminary results with parameters $d_{D,0} = 0.1$ are plotted in Fig. 2. It shows that the RMI is suppressed in the presence of magnetic field.

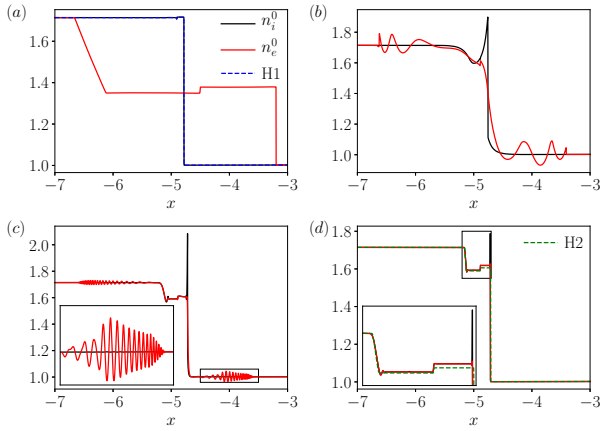

Figure 1: *Base number densities of ions and electrons at t = 0.157 for the cases with various reference Debye lengths; (a) $d_{D,0}$ = 10, (b) $d_{D,0}$ = 0.1, (c) $d_{D,0}$ = 0.01,(d) $d_{D,0}$ = 0.001. The results are compared with those of limiting hydrodynamic cases `H1' and `H2'.*

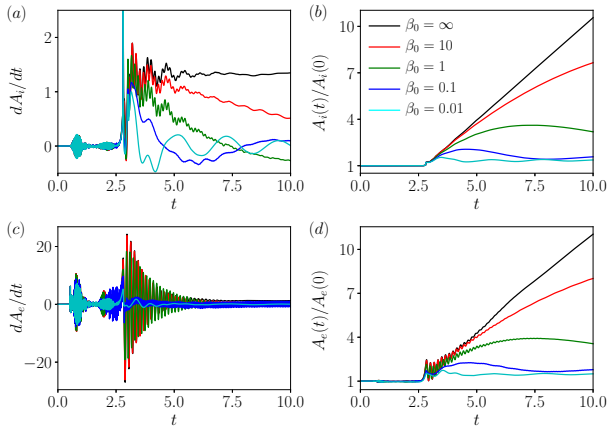

Figure 2: *Evolution of the growth rate and reference amplitude of the density interfaces for cases with $d_{D,0}$ = 0.1. (a) growth rate of ion interface, (b) amplitude of ion interface, (c) growth rate of electron interface, (d) amplitude of electron interface.*

Acknowledgments: This research was supported by the KAUST Office of Sponsored Research under Award URF/1/3418-01.

References

[1] D. Bond, V. Wheatley, R. Samtaney and D. I. Pullin, J. Fluid Mech., 833 (2017).
[2] D. Bond, V. Wheatley, Y. Li, R. Samtaney and D. I. Pullin, J. Fluid Mech., 903 (2020).
[3] R. Samtaney, J. Comput. Phys. 228(18), 6773–6783 (2009).

Numerical Simulations of a Perturbed Diffuse Interface Subjected to the Richtmyer-Meshkov Instability: Early Time and Transition to Turbulence

Sam Pellone[1*], Tiffany Desjardins[1], Carlos Di Stefano[1], John Charonko[1], Forrest Doss [1]

[1] Los Alamos National Laboratory, Los Alamos, NM, USA

*Corresponding Author: sampellone@lanl.gov

The Richtmyer-Meshkov (RM) instability plays an important role in inertial confinement fusion (ICF) because it may lead to mixing between the different layers inside ICF capsules, thus degrading their fusion yield. One design strategy aiming at mitigating the RM instability in ICF capsules is to use graded density layers [1], where the density varies continuously from one layer to another, as opposed to a sharp discontinuity. The presence of smooth density gradients in ICF may also originate from the absorption of electrons and x-rays by materials causing layers to expand before the arrival of the induced shock [2].

The literature on RM instability is vast but only a few studies have considered the effect of interface diffusion on the evolution of the instability. Some early work has shown that the kinetic energy initially imparted by the shock on perturbations and their subsequent growth rate is reduced when considering a smooth density gradient, as opposed to their sharp interface counterpart [3, 4]. However, these studies only focused on the early time evolution of the instability (linear and early non-linear regimes) without considering the transition of the flow to turbulence and mixing. Our objective is to investigate the role of the initial diffusion layer on perturbation growth and transition to turbulence for the RM instability.

Although direct numerical simulations would be helpful in understanding the underlying physics governing the late-time turbulent evolution of the flow, the computational cost is prohibitive due to the wide range of scales (especially for ICF-type problems). In this work, we perform numerical simulations using the BHR turbulence model implemented into the in-house code xRAGE. The BHR model is specifically designed to understand variable density effects in turbulent flows, which further serves our purpose of understanding the effect of smooth density gradients on the late-time evolution of the instability. As a preliminary study, we consider the evolution of a single-mode perturbation without the BHR model to validate our results and first understand the effect of the diffusion layer before the flow becomes turbulent. Our baseline case corresponds to the experiments of Collins and Jacobs [5] (single-mode perturbation of wavelength λ between air and SF_6) where we model the initial diffusion layer as a smooth density gradient over a distance δ. Fig. 1 shows an example of the time evolution of the interface for different values of the ratio δ/λ. Increasing the initial size of the diffusion layer reduces the initial growth rate of the perturbation and causes the fine structures in the roll-ups to be smeared out. The present study will focus on two parts: one part on the analysis of the growth rate before turbulence dominates the flow, and a second part dedicated to the evolution of the turbulent statistics and their dependence on the initial diffusion layer. The light-to-heavy and heavy-to-light cases will be discussed, along with multimode perturbations and reshock dynamics.

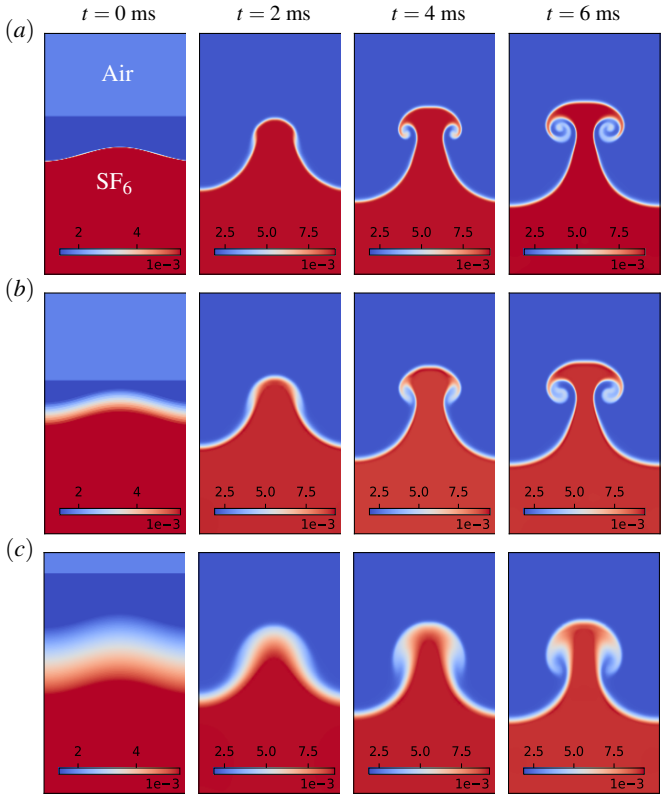

Figure 1: Evolution of the interface at different times represented by density contours (in g/cm^3) when the pre-shock interface is sharp (a), $\delta/\lambda = 0.1$ (b), and $\delta/\lambda = 0.3$ (c).

Acknowledgments: This work was supported by the U.S. Department of Energy through the Los Alamos National Laboratory (Triad National Security, LLC. Contract No. 89233218CNA000001).

References

[1] N.N. Vazirani et al., Phys. Plasmas 28, 122709 (2021).
[2] T. Desjardins, C. Di Stefano, E. C. Merritt, K. A. Flippo, and F. W. Doss, High Energy Density Phys. 39, 100937 (2021).
[3] P. Saffman and D. Meiron, Phys. Fluids 1, 1767 (1989).
[4] T. Pham and D. Meiron, Phys. Fluids 5, 344 (1993).
[5] B. Collins and J. Jacobs, J. Fluid Mech. 464, 1 13 (2002).

Linear Stability Simulations of Magnetohydrocynamic Richtmyer-Meshkov Instability of Double Interfaces in Cylindrical Geometry

[1,*]Abeer Bakhsh, [2]Ravi Samtaney

[1]Umm Al-Qura University, Makkah, Westren District, Saudi Arabia, [2]King Abdullah University of Science and Technology, Thuwal, Saudi Arabia

[*]**Corresponding Author: ahbaksh@uqu.edu.sa**

Richtmyer-Meshkov instability (RMI) occurs when a perturbed density interface between different fluids is impulsively accelerated by a shock wave [1]. RMI is important in inertial confinement fusion (ICF) [2, 3] wherein hydrodynamic instabilities are considered as a key bottleneck towards the achieving goal of ICF [4]. Bakhsh and Samtaney [5] investigated the linear analysis of magnetohydrodynamic (MHD) RMI in the presence of an azimuthal magnetic field in cylindrical geometry for a single interface, where it showed the suppression of the RM and Rayleigh-Taylor (RT) instabilities.

The present work investigates the suppression of the RMI of double interfaces in terms of linear analysis in cylindrical geometry. A converging shock interacts with the interfaces in three different cases, as shown in table 1, and the effect of varying magnetic field strength on the instability are presented.

Case number	Densities	Magnetic field strength β
C_1	$1:5:1$	HD, 256, 16, 4 and 2
C_2	$1:5:3$	HD, 256, 16, 4 and 2
C_3	$1:2:3$	HD, 256, 16, 4 and 2

Table 1: List of different cases of density interfaces C_1, C_2 and C_3. Linear simulations are performed in HD and in the presence of different magnetic field strengths β.

The results of the first case C_1, are presented below. Figure 1 displays the growth rate at the interfaces for hydrodynamics (HD) and different values of the magnetic strength. During the RMI phase of the instability, the normalized growth rate increases from zero and asymptotes to a value of unity. In the absence of a magnetic field (HD) it is clearly followed by an exponentially increasing growth characterizing the RTI phase of the instability. At the first interface, fig. 1(a), the Atwood number (A) is positive, A>0, and in the HD case the RTI is associated with a phase change. It can be seen that approximately after the scaled time $t \approx 115$, there is another impulse generated from the impact with a rarefaction fan, which is generated from the interaction of the transmitted shock and the second interface. Figure 1(b) represents the scaled growth rates of the second perturbed interface. For the second interface, A<0, there is a phase change associated RMI which is reinforced by the later exponential growth of RTI for the effect of HD. For the MHD case at both interfaces, the growth rates of the instabilities reduce in proportion to the strength of the applied magnetic field.

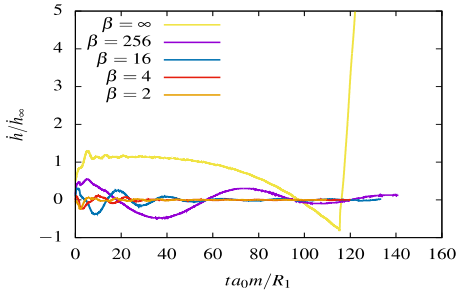

a) First interface

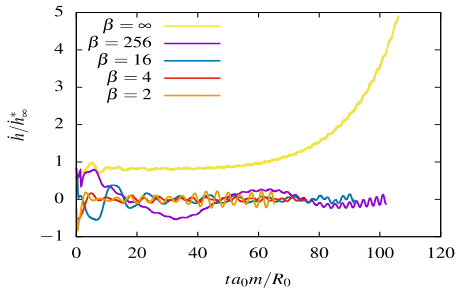

b) Second interface

Figure 1: Scaled growth rates at different magnetic strengths of (a) first interface (b) second interface for the case C_1.

Acknowledgments: KAUST Baseline Research Fund BAS/1/1349-01-01.

References

[1] R.D. Richtmyer, Commun. Pure Appl. math., 13, 297 (1960).
[2] T.H. Johnson, Proceedings of the IEEE 72, 548 (1984).
[3] R. Betti and O.A. Hurricane, Nature Physics 12, 435 (2016).
[4] J. Lindl, O. Landen, J. Edwards, and E. Moses, Physics of Plasmas 21, 020501 (2014).
[5] A. Bakhsh and R. Samtaney, Journal of Fluids Engineering 140, (2017).

A high-order, localized artificial diffusivity method for Eulerian simulation of multi-material elastic-plastic deformation with strain hardening

Jacob R. West[1,*], Michael C. Adler[2], and Sanjiva K. Lele[1,2,3]

[1]Department of Mechanical Engineering, Stanford University, Stanford, CA, USA
[2]Center for Turbulence Research, Stanford University, Stanford, CA, USA
[3]Department of Aeronautics and Astronautics, Stanford University, Stanford, CA, USA

[*]**Corresponding Author: jrwest@stanford.edu**

Shock-wave propagation through multi-material media is relevant to physical problems such as detonations, impact welding, and inertial confinement fusion (ICF). In ICF experiments, the development of hydrodynamic instabilities, including Richtmyer-Meshkov (RMI) and Rayleigh-Taylor, has been observed [1]. Material strength is of interest as a means of suppressing these instabilities and increasing the compression efficiency, and simulations are relied upon to target experimental campaigns. In solid materials, shock waves can create large deformations at high strain rates, resulting in strain hardening, thermal softening, and other inelastic phenomena. This requires a numerical method which can accurately resolve shocks, instability growth, material interfaces, and elastic-plastic deformation with complex material behavior in a unified framework.

In this work, an Eulerian finite difference method is presented which meets these requirements, building on work by Subramaniam, Ghaisas, and Lele [2-3], adding capabilities for modeling strain hardening and thermal softening through the tracking of additional kinematic tensors. 10^{th} order accurate compact differences are used for spatial derivatives, along with 4^{th} order RK timestepping. A multiplicative decomposition of the inverse deformation gradient tensor is assumed, and elastic and plastic kinematic tensors are tracked separately to compute elastic stresses and the effects of strain hardening. An implicit method is used to treat material yield, so that the simulation timestep is limited only by traditional CFL conditions. In this framework, the necessary input parameters for rate-dependent and rate-independent strain hardening models can be computed.

Discontinuities are treated with a localized artificial diffusivity (LAD) approach [4]. In addition to compressive shocks, contact surfaces, and material interfaces which occur in gasdynamics, solid materials can exhibit elastic-plastic shocks, as well as shear and tensile shocks, which are regularized by extending the LAD approach to the kinematic equations. Existing methods for artificial bulk viscosity are capable of treating elastic and plastic shocks in solids, so the extension of LAD to the kinematic equations is specifically targeted at the shear discontinuities which are unique to materials with strength. A diffuse interface approach is used to model multi-material phenomena, for its simplicity and its excellent conservation properties. Artificial species diffusion is used to regularize material interfaces. In the problems of interest, the time scale of deformation is short relative to the time scale of numerical diffusion, so no interface sharpening procedure is necessary.

This method has been validated on a wide variety of test problems, including using manufactured solutions to verify order of convergence, as well as 1-d elastic plastic impacts, and tests to verify that constraints on the kinematic tensors (zero curl and compatibility with the density field) are maintained. The simulation framework is used to study how the growth of the Richtmyer-Meshkov instability between metals is affected by strain hardening and thermal softening. In problems involving interface roll-up, the Eulerian framework is particularly useful, as it avoids the mesh distortion and remapping errors associated with Lagrangian methods. An example of copper-aluminum RMI with strain hardening is shown in Figure 1. At late times, it is clear that plastic strain is concentrated in regions of rollup, as well as the tips of bubbles and spikes penetrating into the other material.

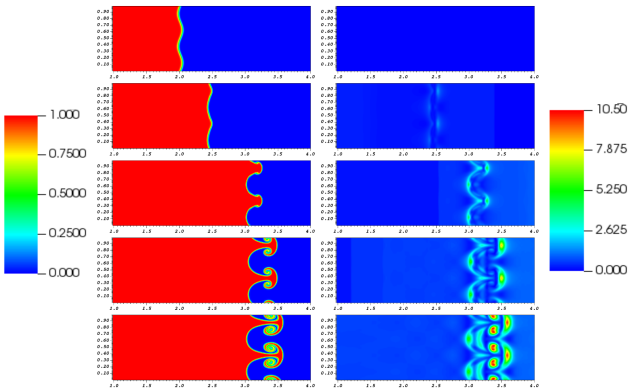

Figure 1: Time evolution of Richtmyer-Meshkov instability between copper and aluminum. Mass fraction of copper (left) and equivalent plastic strain in copper (right) are shown.

Acknowledgments: The authors appreciate the sponsorship of the U.S. Department of Energy Lawrence Livermore National Laboratory under contract DE-AC52-07NA27344 (monitor: Dr. A. W. Cook).

References

[1] Y. Zhou, Phys. Reports, 723 (2017).
[2] A. Subramaniam et al., J. Fluids Eng., **140**(5), 050904 (2018).
[3] N. Ghaisas et al., J. Comput. Phys., **371**, 452 (2018).
[4] A. Cook, Phys Fluids. **19**(5), 055103 (2007)

Ejecta physics induced by a downward impinging supersonic jet

Juan Sebastian Rubio[1], Miguel X. Diaz Lopez[1], Matt Gorman[1], and Rui Ni[*1]

[1]Johns Hopkins University, Baltimore, Maryland, United States of America

[*]**Corresponding Author: rui.ni@jhu.edu**

A high-speed jet impinging on a granular bed is important to understand the soil erosion and ejecta physics for missions to land on extraterrestrial bodies. This complex multiphase problem involves various physical mechanisms: shock-particle interaction within the jet core region, interaction between inertial particles and the jet shear layer, modulation of the gas phase turbulence by the particles, and the jet interacting with particle volume fractions from dilute to dense suspensions. These processes can significantly alter the jet flow dynamics, modify the pressure fluctuations, and generate flow instabilities [1]. In addition, the presence of an impingement region reduces the distance required for the flow to become unsteady, transitional, or turbulent, and it may amplify existing instabilities formed upstream of the impingement region [2]. The particles liberated from the soil surface are further subjected to drag and gravitational forces, influencing the ejecta behavior far from the impingement region. We present results for the ejecta motion in both a Martian and near-Lunar environment, where the ejecta physics change drastically between both cases during the transient phase of the impingement process.

Here, we present the results of a NASA experimental campaign aimed at understanding cratering and ejecta dynamics in vacuum environments. The primary motivation behind this campaign was to provide experimental data to validate numerical models of impinging supersonic jets on regolith. The experiments were conducted inside the TS-300 15-ft vacuum chamber at NASA Marshall Space Flight Center in Huntsville, Alabama. A half-width soil bin was used to secure the soil, with a windowpane that allowed for visualizing the ejecta particles being eroded from the soil surface. At the windowpane, a knife edge was used to split the flow exiting the supersonic nozzle in half. The inertial particles were visualized using particle shadow tracking with a HS Vision 1000 W LED. Two high-speed Phantom cameras were used to capture the ejecta in two fields of view near the jet impingement region at frame rates of 25 kHz and 775 kHz.

The key properties for the jet flow dynamics are the nozzle exit Mach number, M_e, and the Reynolds number, Re_D, where D is the nozzle diameter taken as the length scale of reference. For these tests, the Mach number was held constant at M_e = 5.3, and the order of the Reynolds number was varied from $O(10{,}000 - 100{,}000)$. The mass flow rate of the gas was varied from 0.32 to 8.6 g/s, and the ambient pressures tested ranged from Martian environments at P_{amb} = 4.5 torr to near-Lunar conditions at P_{amb} = 0.02 torr. The normalized nozzle height was varied from h/D = 3 to h/D = 13. Six different particle types were used in this study each with varying complexity. Table 1 lists the type of particles used and their corresponding mean particle diameters. For further details on the scaling analysis performed in this study to arrive at these flow conditions please refer to reference [3].

Case	Type	d_p (μm)
1	Monodisperse Sand (MDS)	150
2	Full Range Lunar (BP1)	1-500
3	Bidisperse Sand (BDS)	50,150
4	Tridisperse Mix (TRI)	50,150,300
5	Irregular Mixture (IRR)	300
6	Monodisperse Glass Beads (MGB)	150

Table 1: Particle types and corresponding particle diameter

Figure 1 shows preliminary results for the ejecta horizontal component of velocity and the ejecta particle count as a function of time for various soil types. Both sub-figures show data for particles first coming into the field of view and are tracked up to $t \sim 0.2$ s. The log-log plot reveals a scaling behavior in both the ejecta velocity and particle count, and both measures show a correlation with one another. We hypothesize that the steep drop in the particle velocity is influenced by the increase in particle density. The increase in particle concentration may modify the surrounding flow, and thus, decrease the drag that the particles are subjected to.

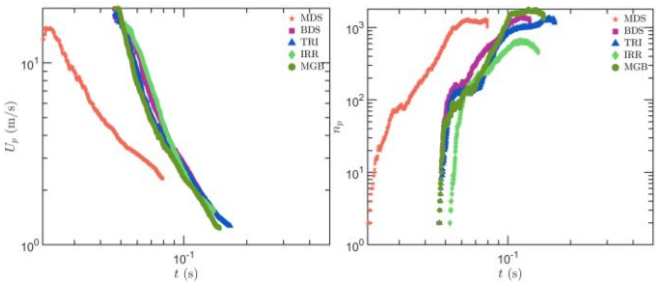

Figure 1: (a) Ejecta velocity and (b) ejecta particle count as a function of time for P_{amb} = 4.5 torr, $\dot{m}$ = 8.6 g/s, and h/D = 10.

This effort to understand ejecta physics is necessary to mitigate risks for future landers that will be sent to the Moon, Mars, and other planetary bodies in our solar system.

Acknowledgments: This work is supported by a NASA Space Technology Graduate Research Opportunity (Grant Number: 80NSSC20K1163).

References

[1] J. Capecelatro, International Journal of Multiphase Flow 150, 104008 (2022).

[2] J. Inman, P. Danehy, R. Nowak, and D. Alderfer, 47th AIAA Aerospace Sciences Meeting Including The New Horizons Forum and Aerospace Exposition (2009).

[3] A.M. Korzun, C.J. Eberhart, J. West, P. Liever, A. Weaver, J. Mantovani, A. Langton, B. Kemmerer, and A. Atkins, AIAA SCITECH 2022 Forum (2022).

Transition to Stable Plastic Regime of Rayleigh-Taylor Instability in Elastic-Plastic Solids

Aren Boyaci and Arindam Banerjee*
Department of Mechanical Engineering & Mechanics, Lehigh University, Bethlehem, PA 18015 USA
*E-mail: arb612@lehigh.edu

1. Introduction

Rayleigh Taylor instability (RTI) occurs between two materials when their density and pressure gradients are in opposite directions. In elastic-plastic solids, the instability is governed by various parameters like density (ρ), yield strength (Y), shear modulus (G), initial perturbation geometries at the interface, driving acceleration (a), material thickness (h), and others. Most of the past studies involving elastic-plastic (EP) materials have focused on estimating the instability threshold where the material yields and begins to flow [1]. The pure elastic to stable plastic phase transition occurs much earlier than the instability, signifies the first point where the mechanical properties start to vary dramatically and are rarely addressed in the literature [2, 3].

2. Results

In this work, the EP transition is explored using a rotating wheel experimental apparatus (see fig. 1). The test section attached to the wheel is filled with EP material, and air such that the free surface of the EP material is driven radially outwards by the centrifugal acceleration when the disk rotates. A backlit imaging analysis technique is used with a high-speed camera to track the evolution of the various phases of the instability. Mayonnaise, a soft solid, is chosen as the EP material and its mechanical properties, namely yield strength and shear modulus, are measured via rheological measurements [1].

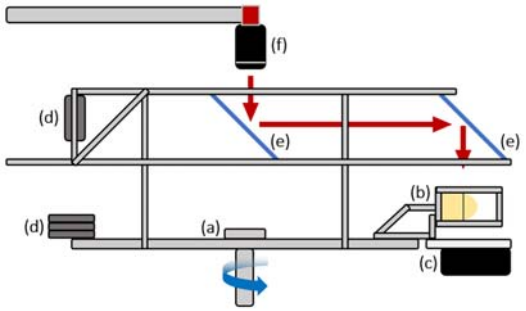

Figure 1: The rotating wheel experimental facility where (a): rotating disk, (b): test section, (c): LED light source, (d): counterweights, (e): mirror assembly, (f): high-speed camera [1].

The EP threshold acceleration (a_{EP}) and the maximum elastic strain that can be fully recovered (ε_{rec}) are explored for different 3D single-mode initial perturbation geometries and acceleration rates. The samples are first accelerated with a constant rate to a limit acceleration (a_{max}) and then decelerated (back to rest) at the same rate. The limit acceleration is chosen such that the sample does not become unstable where the material yields and flows and the process is irreversible [1]. On the contrary, we focus to remain in the stable regime and thereby measure the amount of recovery of the perturbation when the sample comes to rest. The limit acceleration value is thus systematically reduced for a sample until full elastic recovery is observed. In Fig. 2, snapshots from time evolution

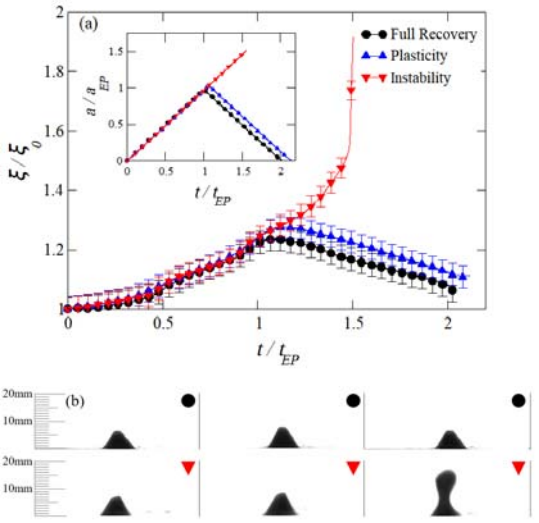

Figure 2: (a): Evolution of samples with full elastic recovery, plasticity and instability. (b): Snapshots of the perturbations showing samples with full elastic recovery, and instability at time instants t/t_{EP} = 0 s, t/t_{EP} = 1, and t/t_{end}, where a_{EP} = 49.7 m/s^2 and t_{EP} = 75 s.

histories of samples with full elastic recovery, stable plasticity and (irreversible) instability are presented.

We will explore relationships for non-dimensionalized a_{EP} and ε_{rec} as functions of the initial perturbation- wavelength (λ_o) and amplitude (ξ_o). These would allow us to expand upon exisiting models of similar flows based on non-dimensional amplitude ($\hat{\xi} = (\frac{\rho a \xi_0}{\sqrt{3}Y})$) and wavelength ($\hat{\lambda} = (\frac{\rho a \lambda_0}{4\pi G})$) [2]. In addition we will also discuss the perturbation growth in the stable plastic regime which will be explored by holding the driving acceleration constant at EP transition acceleration until irreversible instability is observed. The perturbation growth will be measured continuously, and the driving force estimated based on the perturbation mass and centrifugal acceleration to provide a more accuarate description of the force history on the sample.

Acknowledgments: Authors acknowledge financial support from LANL subcontract # 370333

References

[1] R. Polavarapu, P. Roach, A. Banerjee, Rayleigh-Taylor-instability experiments with elastic-plastic materials, Physical Review E, 99 (2019) 053104.
[2] A.R. Piriz, J.J.L. Cela, N.A. Tahir, Linear analysis of incompressible Rayleigh-Taylor instability in solids, Physical Review E, 80 (2009).
[3] S.A. Piriz, A.R. Piriz, N.A. Tahir, S. Richter, M. Bestehorn, Rayleigh-Taylor instability in elastic-plastic solid slabs bounded by a rigid wall, Physical Review E, 103 (2021) 023105.

The RM Instability After Reshock

Riccardo Bonazza*, Christopher Noble, Josh Herzog, Alex Ames, Raymond McConnell,
Jason Oakley and David Rothamer
Department of Engineering Physics, University of Wisconsin-Madison, Madison, WI, USA

*Corresponding Author: bonazza@engr.wisc.edu

The Richtmyer-Meshkov instability is investigated after reshock in the vertical shock tube of the Wisconsin Shock Tube Laboratory at the University of Wisconsin–Madison. The vertical, downward-firing shock tube is 9.2 m long and has square internal cross section, 25×25 cm^2. A planar shock impulsively accelerates a gas interface located about 1.2 m above the shock tube end wall. This initial condition (IC) is a broadband shear layer formed between a helium-acetone mixture and argon, with a nominal Atwood number A=0.52. The amplitude spectrum is highly repeatable in time but not so the phase spectrum. The interface is accelerated with an incident shock of nominal strength M=1.75. Examples of different ICs are shown in fig.1.

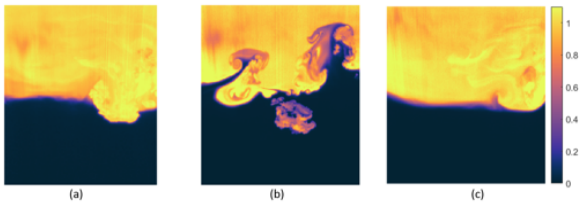

Figure 1: Examples of different IC immediately prior to reshock (He concentration fields).

Diagnostic techniques include planar laser-induced fluorescence (PLIF) and particle image velocimetry (PIV) to measure the concentration and velocity fields, respectively, in a vertical, planar cross section of the flow. Past experimental campaigns have included concurrent, single-shot PLIF/PIV experiments at four post-shock times [1,2]; concurrent single-shot PLIF/PIV at four post-reshock times; post-reshock high-speed PLIF [3,4]. Here we present results from a new campaign based on concurrent, high-speed PLIF/PIV performed on a reshocked interface. For PLIF, the fluorophore is the acetone vapor. For PIV, TiO_2 particles (200 nm in diameter) are added to both the helium-acetone and argon. The light source for both techniques is a pulse-burst laser that can deliver 10 ms pulse trains at up to 20,000 pulses/s, with each pulse containing 30 mJ at 266 nm (used for PLIF) and 60 mJ at 532 nm (used for PIV). The PLIF and PIV signals are recorded with high-speed digital cameras with 1 Mpix sensors, operated at 20,000 fps for an acquisition period of 5 ms. Because of the spatial resolution required to perform PIV, the field of view of the PIV camera is smaller than that of the PLIF camera and the two views are registered onto each other to ensure that measurements are available at the same physical locations within the flow. The results are ensemble-averaged over 20 repetitions.

Concurrent measurements of the concentration and velocity fields allow for the detailed analysis of many important quantities traditionally used in the study of turbulent flows. Particularly noteworthy is the ability to evaluate directly from the measurements all the terms in the transport equation for the energy spectrum of the scalar field. Indicating the spanwise and streamwise directions with x and z, respectively; the concentration field with ξ, its Fourier transform with $\hat{\xi}$, its complex conjugate with $\hat{\xi}^\circ$, the power spectrum of the scalar field with $E_\xi = \hat{\xi}\hat{\xi}^\circ$; the spanwise and streamwise velocity components with u and w, respectively, and the dimensionless time with τ, one obtains

$\frac{\partial E_\xi}{\partial \tau} = P_\xi + T_{\xi k} + T_{\xi z} + D_{\xi k} + D_{\xi z} - \chi_\xi$ where $P_\xi = -\left[\hat{\xi}\hat{w}^\circ + \hat{w}\hat{\xi}^\circ\right]\frac{\partial \bar{\xi}}{\partial z^*}$ is the scalar production, $T_{\xi k} = ik\left(\widehat{u\xi}\hat{\xi}^\circ - \widehat{u\xi}^\circ\hat{\xi}\right)$ is the scalar transport in the homogeneous (spanwise) direction, $T_{\xi z} = \frac{\partial}{\partial z^*}\left(\widehat{w\xi}\hat{\xi}^\circ + \widehat{w\xi}^\circ\hat{\xi}\right)$ is the scalar transport in the non-homogeneous (streamwise) direction, $D_{\xi k} = -\frac{k^{*2}}{Re\,Sc}E_\xi$ is the scalar diffusion in the homogeneous direction, $D_{\xi z} = \frac{1}{Re\,Sc}\frac{\partial^2 E_\xi}{\partial z^{*2}}$ is the scalar diffusion in the non-homogeneous direction, and $\chi_\xi = \frac{2}{Re\,Sc}\frac{\partial \hat{\xi}}{\partial z^*}\frac{\partial \hat{\xi}^\circ}{\partial z^*}$ is the scalar dissipation. Here time is nondimensionalized according to $\tau = \frac{th_0}{\dot{h}_0}$ where h_0 and $\dot{h}_0$ are the initial interface thickness and growth rate, respectively. The thickness is measured directly from the concentration field using $h = 4\int_{-\infty}^{\infty}\bar{\xi}\left(1-\bar{\xi}\right)dz$. The Reynolds and Schmidt numbers, Re and Sc, are calculated according to $Re = \frac{\dot{h}h}{\nu}$ and $Sc = \frac{\nu}{\mathfrak{D}}$, respectively. The kinematic viscosity is determined as an average value across the interface, using a Chapman-Enskog relation. Thanks to the concurrent measurements of the concentration and velocity fields, all the terms in the transport equation can be directly evaluated from the experiments.

It is then very interesting to carry out a time integral of the transport equation over the observation time. Here, following [5], the dimensionless time τ is replaced with $\ln h^*$, where $h^* = h(t)/h_0$. This allows to quantify the overall change in the energy content of the scalar field and to determine the contributions of the individual terms to that change. We express this as $\Delta E_\xi = \int_0^{ln\,(5)}\frac{\partial E_\xi}{\partial ln h^*}dln h^*$ and

$\Delta E_\xi = \mathcal{P}_\xi + \mathcal{T}_{\xi k} + \mathcal{T}_{\xi k} + \mathcal{D}_{\xi k} + \mathcal{D}_{\xi z} - X_\xi$

where all the symbols on the RHS indicate the same integration as in the definition of ΔE_ξ.

The results are shown in fig.2 where each term is presented as a function of the wavenumber and the vertical position within the interface, similarly to [6].

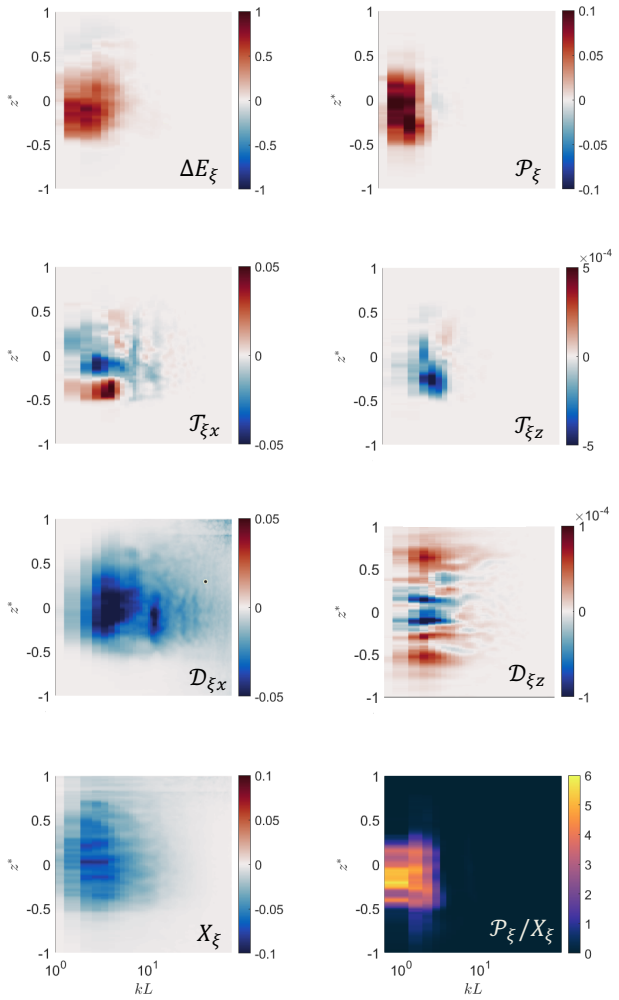

Figure 2: Time-integrals of the energy spectrum transport equation. L=25 cm is the shock tube width.

The physical meaning of these results, with particular reference to the sign and location of the main contributions, will be discussed in detail.

Acknowledgments: Work supported by DOE-NNSA grant DE-NA0003932.

References

[1] D.T. Reese, A. Ames, C.D. Noble, J.G. Oakley, D.A. Rothamer, R. Bonazza, JFM, **849**, 541, (2017).
[2] D. Reese, J. Oakley, A. Navarro-Nunez, D. Rothamer, C. Weber, R. Bonazza, EIF, **55**, 1823, (2014).
[3] C.D. Noble, J.M. Herzog, D.A. Rothamer, A.M. Ames, J. Oakley, R. Bonazza, JFE, **142**, 121102, (2020).
[4] C.D. Noble, J.M. Herzog, A.M. Ames, J. Oakley, D.A. Rothamer, R. Bonazza, Physica D, **410**, 132519, (2020).
[5] B.E. Morgan, B.J. Olson, J.E. White, J.A. McFarland, JOT, **18** (10), (2017).
[6] B. Thornber, Y. Zhou, Phys. Rev. E, **86**, 056302 (2012).

Diagnostics in extreme environments: a methodology for coupled velocity and scalar measurement

A. G. W. Lawrie[1*], J. T. Horne[1], R. J. R. Williams[2]

[1]Hele-Shaw Laboratory, Queen's Building, University of Bristol, University Walk, BS8 1TR, UK
[2]AWE Aldermaston, Reading, Berkshire, RG7 4PR, UK

[*]**Corresponding Author: andrew.lawrie@bristol.ac.uk**

There have been several attempts at developing simultaneous velocity and scalar field measurements in experimental fluid mechanics. Sometimes these have been performed with interleaved diagnostics, switching lighting conditions between frames of a video sequence to favour each technique in turn (see [1]). In extremely dynamic environments, such as moving reference frames, such methods are often impractical. Other approaches rely on a limited set of measured variables and solve an inverse problem to infer unobserved quantities [2]. A popular example of an inverse-problem-based approach to diagnosis in fluid mechanics is called Optical Flow (e.g. [3]), where scalar field data is obtained and from the spatial and temporal gradients a velocity vector map is computed. The system is highly underdetermined and some form of regularisation is required to approach any solution.

The method of inference of unobserved quantities, conceived originally by [4], lies at the heart of modern weather forecasting (e.g. [5-7]), and we adopt a complementary approach in this paper better suited to the information available in our problem.

Like optical flow, our approach also uses scalar field data as input, though the methods quickly diverge. We extract contours from the scalar field and use these to build a discrete model based on Lagrangian transport of fluid elements between pairs of frames in the recorded video sequence. We apply a flexible numerical method, derived from Hamiltonian fluid mechanics, on meshes constructed from the scalar contour field. This numerical method is advanced through all experimental time, but is iteratively corrected at each video frame by comparison of the numerical results with the evolution of the scalar contour field. The positional deviation of the numerical mesh from the experiment between pairs of frames is balanced against temporal smoothness of the numerical acceleration field and the resultant total error used to update the system Hamiltonian on a cell-by-cell basis. The method is constrained by a scalar-field-derived boundary condition that can be computed at any experimental time. We initially choose to compute the boundary condition at early-time and converge to a solution. The boundary condition is then applied at successively later times, converging to a solution at each, to build a converged, mass and momentum conserving numerical dataset over all experimental time. One may view this technique as a tightly-coupled simulation running in parallel with and nudged back towards an experimental ground-truth.

We apply our novel post-processing procedure to a number of test cases. Of particular interest are the experiments performed in a moving reference frame [8], where the scalar field is driven by a Rayleigh-Taylor-unstable interfacial flow between two miscible fluids as shown in fig. 1. We obtain our scalar field data by illuminating the tank with a diffuse back-light and measuring the attenuation of light due to a coloured dye dissolved in one of the layers of fluid. Matching our post-processing approach, we use a thin, O(1mm), Hele-Shaw-style tank to generate a quasi-two-dimensional flow. The flow is modelled by numerical simulation performed with MOBILE that includes a correction (introduced in [8]) for Ekman friction induced by the proximity of the boundaries. This generates well-matched numerical data against which our novel post-processing method can be validated.

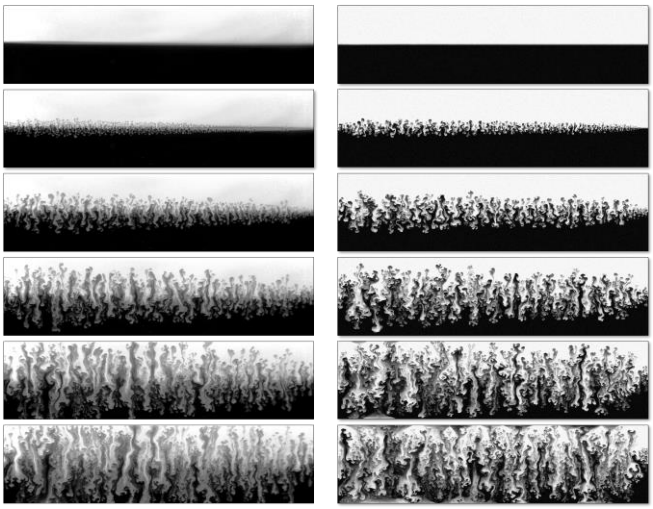

Figure 1: Scalar volume fraction field for experiments in [10] (left panels) and for matched MOBILE simulations (right panels) over a sequence of times after initialisation.

Acknowledgments: We would like to thank AWE for their support of this work.

References

[1] S. Dalziel, M. Carr, J. Sveen & P. Davies., Meas. Sci. Technol. **18,** 533 (2007).
[2] M. Galmiche, J. Sommeria, E. Thivolle-Cazat & J. Verron, CRAS **331,** 843 (2003).
[3] D. Corpetti, D. Heitz, G. Arroyo, E. Memin, & A. Santa-Cruz, Exp. Fluids **40**, 80 (2006).
[4] R. Kalman, J. Basic Eng. **82D**, 35 (1960).
[5] S. Hoang, R. Braille, O. Talagrand, X. Carton, & P. Mey, Dyn. Atmos. Oceans **27**, 257 (1998).
[6] F. LeDimet & O. Talagrand, Tellus **38**, 97 (1986).
[7] T. Vukicevic, M. Steyskal & M. Hecht, Mon. Wea. Rev. **129**, 1221 (2001).
[8] J. Horne & A. Lawrie, Physica D **406**, 132442 (2020).

UK Ministry of Defence © Crown Owned Copyright 2022/AWE

Recent Progress on Coarse Grained Simulations of Turbulent Mixing (+)

Fernando F. Grinstein *
Los Alamos National Laboratory, Los Alamos, NM 87545, USA

*Corresponding Author: fgrinstein@lanl.gov

We are interested in detailed understanding of the late-time consequences of mixing driven by hydrodynamical instabilities promoted by initial conditions at accelerated material interfaces, as in Inertial Confinement Fusion (ICF) capsule implosions. The flow physics is driven by flow instabilities such as Richtmyer-Meshkov, Kelvin-Helmholtz, Rayleigh-Taylor (RT), and vortex stretching. The initial conditions dependent flow involves transition to turbulence, turbulence decay, and non-equilibrium turbulence. Such flow physics can be captured with coarse-grained simulation (CGS) paradigms such as ILES [1], where small-scale flow dynamics is presumed enslaved to that of largest scales, and mix transition criteria and effective turbulence Reynolds numbers are used for macroscopic convergence metrics [2].

We revisit CGS strategies for turbulent material mixing applications, based on LANL's Radiation Adaptive Grid Eulerian (xRAGE) -- ILES, and Besnard-Harlow-Rauenzahn (BHR) – Reynolds-Averaged Navier-Stokes (RANS), using newly-available xRAGE HLLC numerical hydrodynamics options [3], including a Low-Mach Correction (LMC) [4] to address the well-known issue of excessive numerical diffusion of upwinding schemes for low Mach numbers [5]. The latter is a serious concern as most mixing of interest involves weakly compressible flow between shock events [6].

RANS typically presumes equilibrium turbulence and enstrophy production slaved to kinetic energy production, and 1D/2D computations are often involved [7]. There are outstanding problems using such standalone RANS for shock-driven turbulence, specifically: 1) transitional initial-conditions-dependent flow physics is 3D and non-equilibrium; 2) enstrophy generation is inherently very different from energy production; 3) transition to turbulence is driven by large-scale vortex dynamics, capturable with CGS, but not by single-point-closure RANS [8].

Dynamic BHR [9,10] bridging BHR and xRAGE for applications involving variable-density turbulent mixing applications was recently proposed. The bridging approach exploits the structure similarity of the RANS & ILES equations. It is based on the *Flow Simulation Methodology* [11], locally blending a high-resolution computational strategy with RANS modeling in terms of a contribution function $f = f(\Delta / L)$, ranging between $0 < f < 1$ – with $f \rightarrow 0$ denoting the high-resolution limit, and $f \rightarrow 1$ the pure RANS, at the low-resolution limit, and where Δ is the smallest grid size and L is a resolution reference length scale. *Dynamically solving for f* decomposing the full stress into modeled and resolved components – using a differential filter as secondary filtering operation [12] to define the resolved part, was first proposed in [13] and recently extended [9,10] by additionally requiring the resolved stress to approach the full stress with grid refinement to ensure realizability of the generated bridging-based LES. In contrast, classical FSM [11] defines $f(\Delta / L)$ explicitly in empirical *ad hoc* fashion.

We report progress with ILES and *Dynamic BHR* simulations for relevant test cases including, shock tube experiments [3,10,14,15] and RT driven flow and mixing [16,17]. We note the significant impact of the new HLLC numerical hydrodynamics in xRAGE with LMC [3,10,14,16,17], e.g. Fig.1, enabling higher-fidelity scale-resolving simulations on coarser grids.

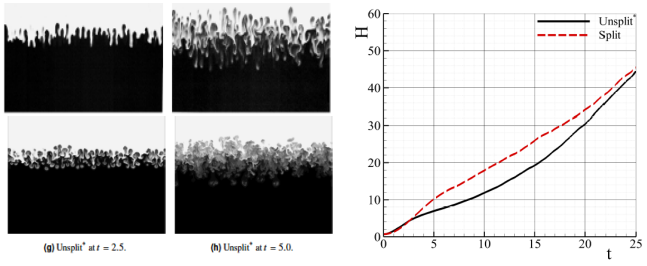

Figure 1. Mass density distributions and mix-width from *At-0.5 RT* xRAGE simulations (split on the top, unsplit* with LMC–below). Unsplit* capably captures: 1) early-time mix-width quadratic growth, 2) late-time RT small-scale mixing; 512^2 x 1536 simulations [16,17].

Acknowledgements
LANL is operated by TRIAD National Security LLC for the US DOE NNSA.

References
(+) LA-UR-22-21595
1. Grinstein F.F., *Coarse Grained Simulation and Turbulent Mixing*, Cambridge, 2016.
2.. Zhou Y., Grinstein F.F., et al., *PRE*, 89, 013303, 2014.
3. Grinstein, F.F., et al., *CAMWA*, 78, 437–458, 2019.
4. Thornber B., et al., *JCP*, 227(10):4873–4894, 2008.
5. Book, D.L., Grinstein, F.F., et al., *JSCP* 6:323–343, 1991; Guillard, H., Murrone, A., *CAF*, 33:655–675, 2004.
6. Youngs D.L., Williams R.J.R., *IJNMF,* 56:1597, 2008.
7. Schwarzkopf J.D., et al., *FTC*, 96:1-43, 2016.
8. George W.K., Davidson, L., *AIAA J.*, 42, 438-446, 2004.
9. Grinstein F.F., et al., *CAF* 199, 104430, 2020.
10. Grinstein F.F., et al., *PoF* 33, 035131, 2021.
11. Speziale C. G., *AIAA J.*, 36(2), 173-184, 1998; Fasel H.F., et al., *J. Appl. Mech.*, 73, 405-412, 2006.
12. Germano,M., *PoF* 29(6):1755-1757, 1986.
13. Germano M., *AIAA J.*, 36(9), 1766-1767, 1998.
14. Grinstein, F.F. and Pereira, F.S., *PoF* 33, 035126, 2021.
15. Mohaghar M., Ranjan D., et al., *JFM*, 871, 595, 2019,
16. Pereira F.S., Grinstein, F.F. et al., *PoF* 33:115118, 2021.
17. Grinstein F.F., Pereira F.S., and Rider W.J., Numerical Approximations Formulated as LES Models, Chapter 9 in, *Numerical Methods in Turbulence Simulation*, edited by R.D. Moser, Springer, 2022.

The subcritical transition to turbulence of Faraday waves in miscible fluids [1]

M. Cavelier[1], B.-J. Gréa[1,*] , A. Briard[1] and L. Gostiaux[2]

[1] CEA, DAM, DIF, F-91297 Arpajon, France

[2] Univ Lyon, CNRS, École Centrale de Lyon, INSA Lyon, Univ Claude Bernard Lyon 1, LMFA, UMR5509, F-69134 Écully, France

[*]**Corresponding Author: benoit-joseph.grea@cea.fr**

We study the development and the breaking process of standing waves at the interface between two miscible fluids of small density contrast (see Fig. 1). In our experiment, a subharmonic wave is generated by a time-periodic vertical acceleration via the Faraday instability. It is shown that its wavelength may be selected not only by the linear process predicted by the Floquet theory and favouring the most unstable modes allowed by the tank geometry, but also by a nonlinear mode competition mechanism giving the preference to subcritical modes. Subsequently, as the standing wave amplitude grows, a secondary destabilization process occurs at smaller scales and produces turbulent mixing at the nodes. We explain this phenomenon as a subcritical parametric resonance instability. Different approaches derived from local and global stability analysis are proposed to predict the critical wave steepness. These theories are then assessed against various numerical and experimental data varying the frequencies and amplitudes of the forcing acceleration.

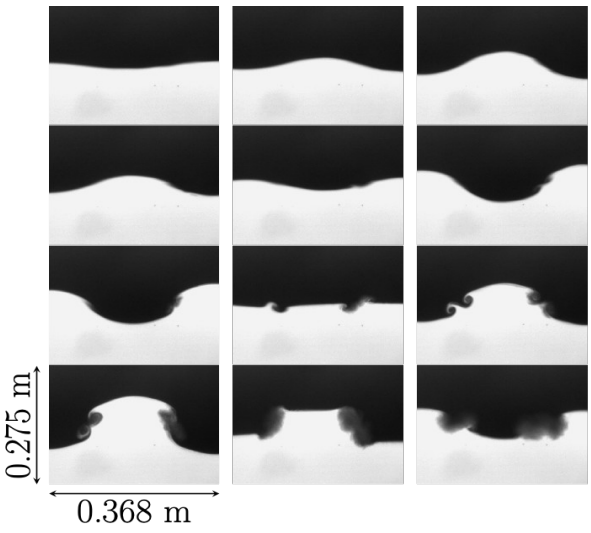

Figure 1: Growth and breaking of a Faraday wave in the FARAMIX experiment.

References

[1] Cavelier, M., Gréa, B., Briard, A., & Gostiaux, L. (2022). *Journal of Fluid Mechanics, 934*, A34.

Experimental 3D turbulent statistics in non-Boussinesq jet flows

D. Fratantonio[1*], E. G. Connor[1], A. Martinez[1], J. J. Charonko[1]

[1]Los Alamos National Laboratory, Physics Division, Los Alamos, New Mexico, USA

[*]**Corresponding Author: dfratantonio@lanl.gov**

Although great research efforts have been dedicated in the past century to variable-density turbulence [1], a complete experimental dataset offering simultaneous 3D velocity, density, and pressure fields is still missing. Such a comprehensive dataset is critically important to further understand how variable-density mechanisms affect turbulent mixing [2] and to validate RANS models such as BHR [3]. Practical challenges concerning the implementation of tomographic techniques have previously hindered the investigation of variable-density gas flows, despite the recent successful developments in tomographic techniques for other flows [4,5].

In this context, this work aims to provide the required experimental dataset by extending our previous low sampling rate measurements [2], employing high-speed stereoscopic particle image velocimetry and planar laser-induced fluorescence techniques to obtain simultaneous velocity and density measurements in a jet flow issued from a circular pipe into a coflow of air (Figure 1). Air and sulfur hexafluoride (SF_6) jets are used for the experimental comparison of Boussinesq and non-Boussinesq turbulent flows (At = 0.1 and 0.6, respectively). Measurements are taken in the pure jet region at several downstream distances from the jet source, between 2*D* and 16*D*, with *D* being the diameter of the pipe. Over this initial developing region of the jet, buoyancy effects are negligible and the fluid inertia is dominant in defining the development of turbulent mixing of the jet with the coflow. Additionally, because density gradients have the greatest magnitude in this momentum dominated region, the variable density effects on the turbulent mixing are particularly evident and useful for model validation.

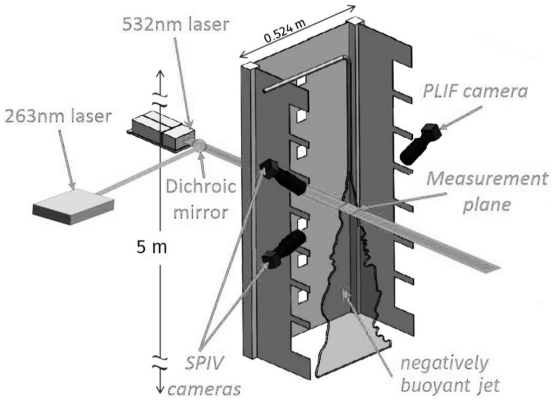

Figure 1: Schematic of the experimental setup.

By performing velocity and density measurements at several distances from the jet source, we scanned the spatial evolution of the turbulent statistics along the jet flow direction. Figure 2 reports a few instances of instantaneous density and velocity measurements taken at different locations in a SF6 jet with $Re_D = 15000$. By averaging at each location over 10000 fields, we are able to reconstruct 3D turbulent statistics, such as turbulent anisotropy, turbulent production, and turbulent diffusion fluxes, which we use to perform an energy budget analysis for the Reynolds stresses. In addition, by using a modified version of the Taylor's frozen turbulence hypothesis applicable to shear flows [6] in conjunction with time-resolved velocity/density acquisitions, we are able to compute from the measured planar data all components of the velocity gradient tensor and of the density gradient, thus giving access to the local three-dimensional features of turbulence. This access to time-varying 3D velocity and density further allows the estimation of the pressure field within the jet, and ultimately the computation of the velocity-pressure correlations. Such experimental data is extremely rare in the literature, but are key to the development of accurate turbulence closure models [7,8].

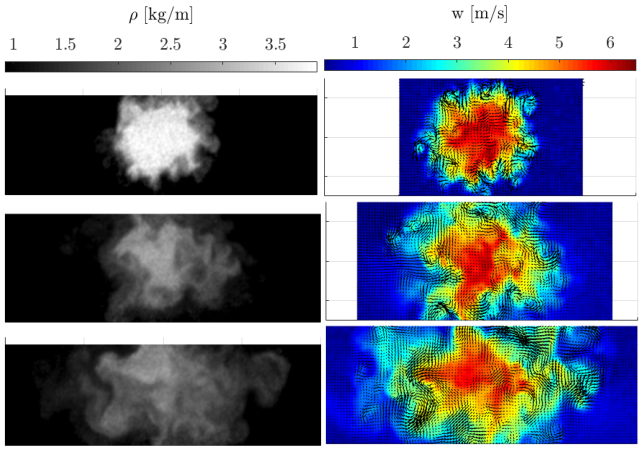

Figure 2: Instances of instantaneous (a) density and (b) velocity measurements at different distances from the jet source: (*top*) 2*D*, (*middle*) 6*D*, (*bottom*) 12*D*. The same velocity and density color scales are applied for all measurement locations.

References

[1] P. Chassaing, R.A. Antonia, F. Anselmet, L. Joly, S. Sarkar. Kluwer Academic Publisher (2002).
[2] J.J. Charonko and K. Prestridge. J Fluid Mech **825**, 887-921 (2017).
[3] J. D. Schwarzkopf, D. Livescu, J. R. Baltzer, R. A. Gore, and J. R. Ristorcelli. Flow Turbul Combust **96**, 1-43 (2016).
[4] G.E. Elsinga, F. Scarano, B. Wieneke, and B. W. Van Oudheusden. Exp Fluids **41**, 933-947 (2006).
[5] Y. Wu, W. Xu, Q. Lei, and L. Ma. Opt Extress **23**,33408-33418 (2015).
[6] D. Fratantonio, C.C.K. Lai, J.J. Charonko, and K. Prestridge. Exp Fluids **62**, 1-25 (2021).
[7] J. L. Lumley. Adv Appl Mech **18**, 123-176 (1979).
[8] B.E. Launder, G.J. Reece, and W. Rodi. J Fluid Mech **68**, 537-566 (1974).

Different initial composition ratio effects on variable-density turbulent mixing

Denis Aslangil[1*], Daniel Livescu[2] and Arindam Banerjee[3]

[1]Department of Aerospace Engineering and Mechanics, The University of Alabama, Tuscaloosa, AL, US
[2]Los Alamos National Laboratory, Computational Physics and Methods (CCS-2), Los Alamos, NM, US
[3]Department of Mechanical Engineering and Mechanics, Lehigh University, Bethlehem, PA, US

[*]**Corresponding Author: denis.aslangil@ua.edu**

The effects of different initial composition ratios on the evolution of homogeneous variable-density turbulence (HVDT) are studied by using high-resolution direct numerical simulations (DNS). VD turbulent mixing is of interest to the turbulence community due to its wide range occurrence in nature such as in astrophysics, oceanic and atmospheric flows and in engineering applications such as combustion engines and inertial confinement fusion [1-5]. In the scientific literature, HVDT flow has been mostly studied with equal initial amounts of the pure light and heavy fluids ([1, 3] and the references therein). However, VD mixing usually occurs between unbalanced amounts of pure fluids. In addition, different initial amounts of pure fluids pose a new challenge for mix models [4]. Thus, in this study, we alter the initial amounts of the fluids, which primarily aims to mimic the different locations of the mixing layer of the acceleration-driven Rayleigh-Taylor and shock-driven Richtmyer-Meshkov instabilities [4]. We investigate three cases with different initial compositional ratio (χ_0) that is defined as:

$$\chi_0 = \chi_l/\chi_h, \qquad (1)$$

where χ_l and χ_h are the mole fractions of the light and heavy fluids, respectively. (i) **HF:** heavy dominated flow where around three-quarters of the flow initially composed of heavier fluid $(\chi_0 = 1/3)$ (see Figure 1a), (ii) **SF:** initially symmetric distributed flow where the initial amounts of the lighter and heavier fluids are similar $(\chi_0 = 1)$ (see Figure 1b), and (iii) **LF:** light fluid dominated flow where around three-quarters of the flow initially composed of lighter fluid $(\chi_0 = 3)$ (see Figure 1c) for both low (1.1:1) and high (7:1) density-ratio case.

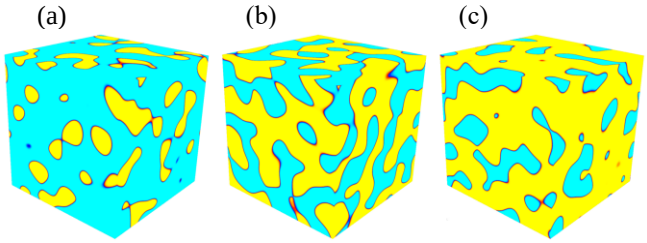

Figure 1: Initial configuration of the density field for (a) heavy fluid dominated flow ($\chi_0 = 3$), (b) symmetric distribution ($\chi_0 = 1$), and (c) light fluid dominated flow ($\chi_0 = 1/3$), where yellow color represents the pure light fluid ($\chi_h = 1$) and blue color represent the pure heavy fluid ($\chi_l = 1$).

Figure 2 presents the evolution of the Favre averaged turbulent kinetic energy (TKE) for LF, SF and HF cases with high density-ratio (7:1). As it is seen, light fluid dominated flow leads to larger TKE values. This is attributed to the smaller inertia of the light fluid regions, which enables to move these regions easier than to move the heavy fluid regions [3]. As a result, light fluid regions accelerate faster and so the TKE generation is enhanced for LF compared to SF and HF cases at high-density-ratio (7:1) [4].

We will present detailed analyses of the turbulent evolution and local turbulent structure. Our main findings can be summarized as [4]:

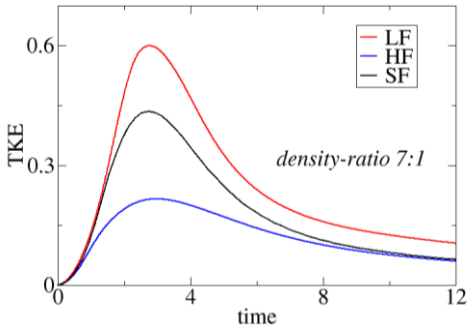

Figure 2: The evolution of $TKE = \rho^* u_i'' u_i'' / < \rho^* >$ for LF, SF and HF cases with high density-ratio (7:1) case where ρ^* is the density, u_i^* is the velocity in direction i, and Favre (density-weighted) fluctuations are represented by $''$ such that $u_i^* = \widetilde{U}_i + u_i''$ with $\widetilde{U}_i = < \rho^* u_i^* > / < \rho^* >$ the angle bracket is used for mean value.

- The initial composition ratio has a limited effect on both the flow evolution and structure for the low density-ratio case.
- For large density-ratio cases, the large inertial differences between the light and heavy fluid regions lead to significant differences between LF, SF and HF cases.
  - Compared to HF and SF cases, LF case reaches larger TKE values during the flow evolution.
  - Heavy fluid regions stay compact longer compared to light fluid regions as it is more difficult to stir heavy fluid regions due to their larger inertia.
- During the late time decay of the HVDT, the initial composition effects become minimal for both low and high density-ratio cases.

Acknowledgments: AB acknowledges financial support from the National Science Foundation Early CAREER Program Grant No. 1453056 and DOE/NNSA Grant No. DENA0003195. This work is co-authored by an employee of Triad National Security, LLC which operates LANL under Contract No. 89233218CNA000001 with the U.S. DOE/NNSA. Computational resources were provided by the IC Program at LANL and the Argonne Leadership Computing Facility at ANL through a 2017 ALCC Award.

References

[1] Livescu, D., Ristorcelli, J.R. *"Buoyancy-driven variable-density turbulence."* J. Fluid Mech. **591**, 43–71 (2007).
[2] Livescu, D. *"Turbulence with large thermal and compositional density variations."* Annu. Rev. Fluid Mech. **52**, 309-341, (2020).
[3] Aslangil, D., Livescu, D., Banerjee, A. *"Atwood and Reynolds numbers effects on the evolution of buoyancy-driven homogeneous variable-density turbulence."* J. Fluid Mech. **895**, A12 (2020).
[4] Aslangil, D., Livescu, D., Banerjee, A. *"Variable-density buoyancy-driven turbulence with asymmetric initial density distribution."* Physica D. **406**, 132444 (2020).
[5] Saenz, J.A., Aslangil, D., Livescu, D. *"Filtering, averaging, and scale dependency in homogeneous variable-density turbulence"* Physics of Fluids **33**, 025115 (2021).

The impact of temperature and material mixing heterogeneities on thermonuclear reactions

Brian M. Haines[1,*], B. J. Albright[1], T. J. Murphy[1], M. R. Douglas[1], J. H. Cooley[1], T. H. Day[1], N. A. Denissen[1], C. Di Stefano[1], P. Donovan[1], S. L. Edwards[1], J. Fincke[1], C. Forrest[2], V. Yu. Glebov[2], L. M. Green[1], L. Goodwin[1], R. A. Gore[1], M. A. Gunderson[1], J. R. Haack[1], C. E. Hamilton[1], E. P. Hartouni[3], K. C. Henderson[1], N. V. Kabadi[4], S. Khan[2], P. M. Kozlowski[1], Y. Kim[1], M. N. Lee[1], R. Lester[1], T. Morrow[1], J. A. Oertel[1], R. E. Olson[1], B. M. Patterson[1], T. Quintana[1], R. B. Randolph[1], D. W. Schmidt[2], R. C. Shah[2], J. M. Smidt[1], A. Strickland[1], C. Wilson[1], and L. Yin[1].

[1]Los Alamos National Laboratory, Los Alamos, NM, USA
[2]University of Rochester Labortory for Laser Energetics, Rochester, NY, USA
[3]Lawrence Livermore National Laboratory, Livermore, CA, USA
[4]Massachusetts Institute of Technology Plasma Science and Fusion Center, Cambridge, MA, USA

[*]**Corresponding Author: bmhaines@lanl.gov**

Inertial confinement fusion (ICF) implosions are subject to hydrodynamic instabilities and material jetting that can introduce contaminant material into the fuel region or otherwise disrupt the process of hot spot formation. These processes interact with thermonuclear burn at sub-micron scales that are computationally expensive to resolve in simulations. We report on experiments performed at the National Ignition Facility (NIF) and OMEGA laser facility as well as detailed high-resolution 3D simulations to understand how mixing impacts thermonuclear burn.

Our experiments [1,2] involve the implosion of capsules containing deuterated foams with controlled geometry (Figure 1) whose pores are filled with mixtures of hydrogen and tritium (HT) or argon and tritium (ArT). We control the heterogeneity of the mixing by varying the pore sizes. By separating the deuterium and tritium (DT) reactants, the DT reaction yield provides a diagnostic for the level to which the reactants are mixed. Furthermore, experiments on the NIF [2] provide reaction-weighted temperature measurements, so that the difference between the DT- and DD-reaction weighted temperatures provides information about the relative temperatures of the reactants.

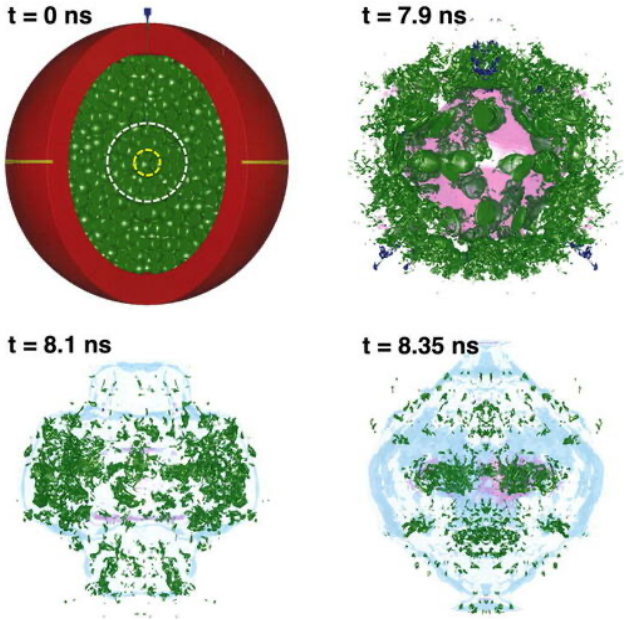

Figure 2: Visualizations of shock (magenta) interaction with pores (green) during implosion.

Our results (Figure 2) demonstrate that flow development is faster than thermal equilibration between reactants, so that temperature variations between the reactants dominates the impact of heterogeneity of their mixing [3,4] on reactivities. Furthermore, by changing the gas fill from HT to ArT, we are able to successfully suppress the temperature separation between reactants [5] and isolate the impact of mixing heterogeneity on thermonuclear burn. In this regime, we can successfully apply models [2,6] adapted from the chemically reactive flow literature (e.g., [7]) to account for sub-grid reactant distributions when evaluating the reactivities. In a future campaign, we plan to collect data necessary to extend models to account for temperature separation.

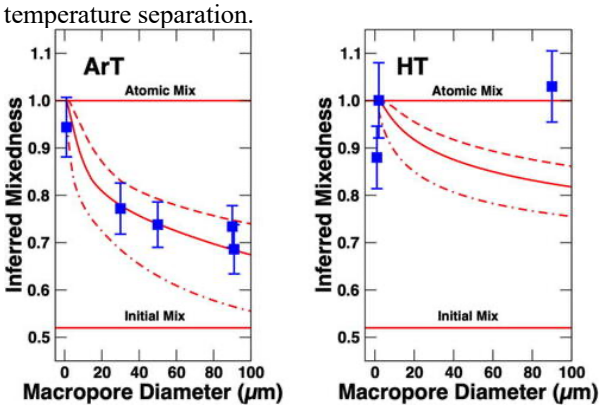

Figure 2: Inferred reaction mixedness vs. pore size for experiments with ArT (left) and HT (right) fills. The HT fill case appears to be fully atomically mixed for all pore sizes due to reactant temperature separation

Acknowledgments: This work was performed under the auspices of the U.S. Department of Energy by Triad National Security, LLC, operator of the Los Alamos National Laboratory under Contract No. 89233218CNA000001.

References

[1] R. E. Olson et al, Phys. Plasmas **27**, 102703 (2020).
[2] T. J. Murphy et al., High Energy Phys., **38**, 100929 (2021).
[3] B. M. Haines et al., Nature Commun. **11**, 544 (2020).
[4] B. M. Haines et al., Phys. Plasmas **27**, 102701 (2020).
[5] B. J. Albright et al., Phys. Plasmas **29**, 022702 (2022).
[6] N. A. Denissen and J. R. Ristorcelli, LANL report LA-UR-14-28935 (2014).
[7] A. W. Cook and J. J. Riley, Phys. Fluds **6**, 2868 (1994).

Transition to Turbulence and Multiphysics in 3D ICF Capsule Implosions (+)

F.F. Grinstein*, V. Chiravalle and B.M. Haines
Los Alamos National Laboratory, Los Alamos, NM 87545, USA

*Corresponding Author: fgrinstein@lanl.gov

Underlying longstanding design challenges in inertial confinement fusion (ICF) capsule-implosion experiments is recognizing the need for realistic 3D initial conditions and high-fidelity 3D modeling to predict transition to turbulence, late-time turbulent characteristics, and quantities of interest (e.g., yield). ICF capsules are unique with regards to hydrodynamic instabilities: 1) the time-scales are short relative to turbulence development, so understanding the transition is particularly important; 2) as the core heats, viscosity becomes important so that there is not much scale separation between the outer length scale and the viscous dissipation length scale; 3) jetting is a unique and critical phenomenon to ICF applications that arises due to Rayleigh-Taylor (RT) instability growth in a thin shell. Arguably the most important algorithm in the ICF simulation model is the hydrodynamics method, responsible for evolution of material position – and setting environment for the multiphysics.

High energy density and ICF capsule experiments at laser platforms such as OMEGA at University of Rochester and the National Ignition Facility (NIF) al LLNL, include *3D* features and defects. This creates a new urgency for assessing the new computational paradigms and the verification and validation of their *3D* modeling aspects in the research codes. ICF capsule experiments involve prominent *3D* features such as, *Defect-Induced-Mix-Experiment* capsules with equatorial trenches [1], *Marble* capsules with *3D* porous foam [2], and NIF *High-Foot-Implosion* capsules including a tent supporting structure and fill tubes [3]. Also noteworthy in this framework, are unexplained discrepancies for *Direct-Drive capsule-implosions* at OMEGA [4] – where role of missed 3D effects in state-of-the-art 1D simulations remains unknown.

Transition is driven by flow instabilities such as Richtmyer-Meshkov, Kelvin-Helmholtz, RT, Bell-Plesset, and vortex stretching – which also play an important role in the subsequent development of the turbulence. Multiple-shocked ICF capsule flow physics can be captured with a well-designed coarse-grained simulation paradigm [5], presuming spectral cascade transfer of energy determined by the initial and boundary-condition constrained large-scale vortex dynamics, and using mixing transition criteria and effective turbulence Reynolds numbers (Re) for macroscopic convergence metrics [6]. Effects of temperature-dependent plasma viscosity growing as $\sim T^{2.5}$ have been shown to suppress turbulent mixing in the hot spot of ICF capsules at bang time [7]. However, capturing these viscous effects has been explored for few other experiments [8].

We build on prior ICF simulations work, using *a Navier-Stokes based plasma viscosity model* [9] in conjunction with LANL's new xRAGE HLLC hydrodynamics with *directionally unsplit algorithms and low-Mach-number correction* (LMC), enabling higher fidelity scale-resolving simulations *on coarser grids* [9,10] – e.g., Fig.1. We simulate two ICF experiments: 1) OMEGA 50997 [4], involving an SiO_2 glass shell filled with a mixture of D_2 and ^3He and Kr impurities added to the gas, where 13.5 kJ of energy is deposited within the SiO_2 shell during 1ns, approximating the direct-drive laser absorption process in the experiment. 2) an indirect-drive NIF cryogenic capsule experiment, N170601 [8,11] requiring multi-group radiation diffusion to transport x-ray energy from the *Hohlraum* to the target capsule.

The 3D simulation model involves miscible (gas / plasma Schmidt number ~ 1) material interfaces and 3T plasma physics treatments [12]. We use relatively coarse 2D runs through onset of turbulence, followed by mapping to highly resolved 3D mesh with 3D seed-perturbations [12]. We assess ILES [9,10] and *Dynamic BHR* [13] ICF predictions with the new xRAGE numerical hydrodynamics. Challenges coupling 3D hydrodynamics and multiphysics (radiation-diffusion, 3T physics, plasma viscosity and diffusivity) are discussed in this context.

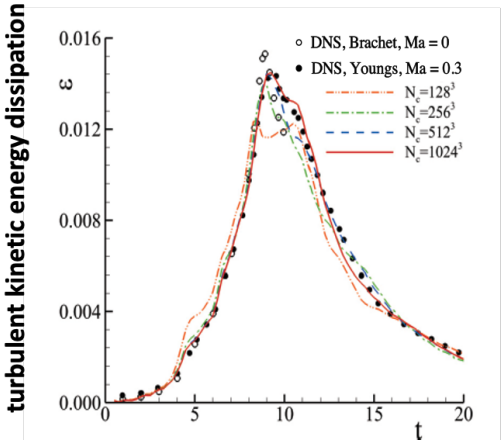

Figure 1. Turbulent KE dissipation for the Ma=0.3, Re=3000 Taylor-Green vortex [9]. LMC HLLC xRAGE exhibits fast convergence, and accurate resolution of viscosity and compressibility effects.

Acknowledgements

LANL is operated by TRIAD National Security LLC for the US DOE NNSA.

References

(+) LA-UR-22-21584
1. M.J. Schmitt et al., *PoP* 20, 056310, 2013.
2. B. M. Haines et al., *PoP* 27, 102701, 2020.
3. D. S. Clark et al., *PoP* 23, 056302, 2016.
4. E. S. Dodd et al., *PoP* 19, 042703, 2012.
5. F.F. Grinstein et al., *Coarse Grained Simulation and Turbulent Mixing*, Cambridge, 2016.
6. Y. Zhou, F.F. Grinstein, B.M. Haines, et al.,*PRE*, 89, 013303, 2014.
7. C. R. Weber et al., *PRE* 89, 053106, 2014.
8. D. S. Clark et al., *PoP* 26, 050601, 2019.
9. F.F. Grinstein and F.S. Pereira , *PoF* 33, 035126, 2021.
10. F.S. Pereira, F.F. Grinstein et al., *CAF*, 201, 104487, 2020; *PRE* 103, 013106, 2021.
11. Haines, B. M., et al., *PoP*, 27(8), 082703, 2020.
12. B.M. Haines, F.F. Grinstein, J.R. Fincke, *PRE* 89, 053302, 2014; B.M. Haines, et al., *PoP* 23, 072709, 2016.
13. F.F. Grinstein et al., *CAF*, 104430 (2020); *PoF* 33, 035131, 2021.

Computational study of shock-induced instability growth and mixing at high energy density

Jason D. Bender*, Oleg Schilling, Kumar S. Raman, Robert A. Managan,
Britton J. Olson, and Shon T. Prisbrey

Lawrence Livermore National Laboratory (LLNL), Livermore, CA, USA

*Corresponding Author: jbender73@gmail.com

Recent experiments at the National Ignition Facility (NIF) at LLNL investigated instability growth and mixing in the high-energy-density (HED) regime, in which pressures exceeded 1 Mbar [1, 2]. Each experiment featured a multimode initial perturbation at the interface between two different-density solid materials: iodine-doped plastic and carbonized resorcinol formaldehyde foam. The interface was impacted by a laser-driven first shock, which converts the solids to plasmas, and a subsequent laser-driven reshock. The perturbation grew via the Richtmyer–Meshkov and Rayleigh–Taylor instabilities. This presentation highlights recent developments in the computational modeling and analysis of the shocked and reshocked mixing layers, building on research previously presented at the 16th International Workshop on the Physics of Compressible Turbulent Mixing, Marseille, France, 2018 (IWPCTM-16). The work was recently published in the Journal of Fluid Mechanics [3].

New three-dimensional simulations using the LLNL radiation hydrodynamics code ARES are reported. The governing equations for a compressible multispecies plasma, with energy stored in ions, free electrons, and radiation, are solved numerically. A multimode initial perturbation is imposed at the modeled plastic–foam interface, using a new computational scheme designed to capture key characteristics of the experimental perturbation. The simulations incorporate non-ideal-gas equations of state and physical models for the transport coefficients of mass diffusivity, viscosity, and thermal conductivity. No explicit subgrid-scale model is included. Adaptive mesh refinement is leveraged to reduce computational cost. Despite the many modeling challenges posed by the HED regime, numerical simulations using the current capabilities of ARES can illuminate the physics of mixing and turbulence at HED conditions.

The simulations are shown to be in reasonable agreement with experimental data from the NIF, including measurements of the mixing-layer width at several times. Before the reshock event, the calculated flows exhibit nonlinear instability growth and vortex formation and breakdown. After reshock, they exhibit a broadening spectrum of length scales and other canonical features of turbulent mixing. Statistical quantities are presented and analyzed, including the turbulent kinetic energy, enstrophy, and the anisotropy of the Reynolds stress tensor. Fig. 1 shows a visualization from one of the simulations. Advances over the earlier research presented at IWPCTM-16 are highlighted. Comparisons are made with computational studies of non-HED reshocked mixing layers (e.g., [4]), and the impacts of HED-specific physics phenomena on mixing are isolated and elucidated. Sensitivity to mesh resolution is considered throughout the discussion. The talk concludes with perspectives on ongoing research efforts to understand mixing at extreme conditions.

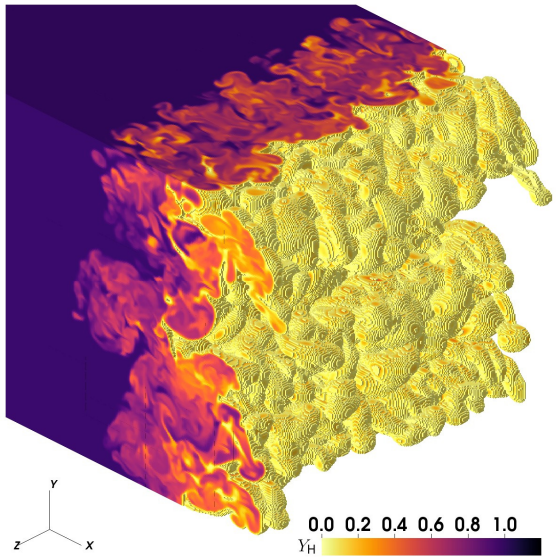

Figure 1: Contours of the simulated heavy-material mass fraction Y_H in a reshocked, HED mixing layer.

Acknowledgments: The authors thank Thomas Brunner, Alejandro Campos, Andrew Cook, Sean Copeland, Leland Ellison, David Erskine, Jeffrey Greenough, Channing Huntington, Stephan MacLaren, Brandon Morgan, Sabrina Nagel, Brian Pudliner, Philip Sterne, Christopher Wehrenberg, and Ye Zhou for important contributions and many helpful discussions. This work was performed under the auspices of the U.S. Department of Energy by Lawrence Livermore National Laboratory under Contract No. DE-AC52-07NA27344.

References

[1] S.R. Nagel, K.S. Raman, C.M. Huntington, S.A. MacLaren, P. Wang, M.A. Barrios, T. Baumann, J.D. Bender, L.R. Benedetti, D. M. Doane, S. Felker, P. Fitzsimmons, K.A. Flippo, J.P. Holder, D.N. Kaczala, T.S. Perry, R.M. Seugling, L. Savage, and Y. Zhou, Phys. Plasmas **24**, 072704 (2017).

[2] C.M. Huntington, K.S. Raman, S.R. Nagel, S.A. MacLaren, T. Baumann, J.D. Bender, S.T. Prisbrey, L. Simmons, P. Wang, and Y. Zhou, High Energ. Dens. Phys. **35**, 100733 (2020).

[3] J.D. Bender, O. Schilling, K.S. Raman, R.A. Managan, B.J. Olson, S.R. Copeland, C.L. Ellison, D.J. Erskine, C.M. Huntington, B.E. Morgan, S.R. Nagel, S.T. Prisbrey, B.S. Pudliner, P.A. Sterne, C.E. Wehrenberg, and Y. Zhou, J. Fluid Mech. **915**, A84 (2021).

[4] D.J. Hill, C. Pantano, and D.I. Pullin, J. Fluid Mech. **557**, 29 (2006).

Code Validation of Radiative Shock Propagation through a Porous Foam

Lauren M. Green[1], Brian M. Haines[1], Yong Ho Kim[1], Pawel M. Kozlowski[1], Thomas J. Murphy[1], Brian J. Albright[1]

[1]Los Alamos National Laboratory, Los Alamos, NM, USA

The MARBLE campaign at Los Alamos National Laboratory (LANL) is a series of inertial confinement fusion (ICF) capsule implosion experiments employing plastic foams with engineered macro-pores designed to investigate heterogeneous material mixing during laser driving implosions [6]. Accurately modeling the dynamics of these foams is challenging for radiation hydrodynamics codes due to the complex geometry that stresses multi-material modeling of equation of state (EOS), opacity, thermal conduction, and thermonuclear burn. We employed xRAGE, a LANL Eulerian radiation hydrodynamics code, to perform the simulations and study the material effects and shock propagation in comparison with the results of companion MARBLE Void Collapse experiments performed on the OMEGA laser at the Laboratory for Laser Energetics (LLE) [3-5,7]. Our simulations are in good agreement with the experimental shock wave speeds, the primary observable in these experiments. We will present the conditions necessary for accurate simulation of these experiments and discuss modeling implications.

In our previous work, xRAGE demonstrated the capability to simulate macro-pore foam implosions in 2D using two modeling approaches: (1) a homogenized foam approximation where the foam is a mixture of carbon and hydrogen with an average density and (2) a toroidal-pore foam approximation where the spherical macro-pores are modeled as toroids in a 2D cylindrical geometry [1]. Both models have shown to predict bulk behavior of the shock with good agreement to experiment, however without a full 3D simulation we cannot fully understand the energy loss due to the Richtmyer-Meshkov instabilities [2] and transverse flow generated from the shock interacting with the pores. Thus, we ran a third simulation in 3D that adopts a more realistic foam geometry with spherical macro-pores to better understand how the shock interacts with the pores and how that interaction might affect shock behavior.

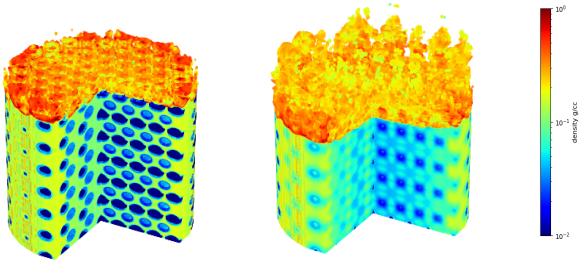

Figure 1: Density profile of simulated 3D foam with spherical macro-pores.

Figure 1 shows a density profile of the 3D simulation with spherical macro-pores at four and seven nanoseconds. Simulation results of the complex geometry show details of macro-pore behavior such as shock front distortion, pore collapse, and development of turbulent flow. The 3D simulation has a shock speed that is 7km/s faster than the 2D toroidal model. We think this difference in shock speed may be attributed to the difference in the development of turbulent flows created when the shock interacts with a toroidal pore versus a spherical pore. Although the two models produce different shock speeds, the difference is not measurable, sine the difference is smaller than the experimental uncertainty of the measured shock speeds.

In summary, MARBLE void collapse experiments have been performed at the OMEGA laser facility to evaluate our ability to model shock propagation through inhomogeneous media. Simulations of these experiments using both homogenized foam models as well as detailed models including foam pores show good agreement with experimental observables. 3D simulations allow us to study the development of turbulent flow generated from shock pore interactions, but are not necessary to predict bulk shock behavior in complex foam geometries. These results give us confidence in our ability to correctly model shock propagation through foams in more complicated MARBLE implosion experiments.

Acknowledgments: The authors acknowledge the support of the OMEGA Laser Facility operations team at Laboratory for Laser Energetics. This work was performed by the Los Alamos National Laboratory, operated by Triad National Security, LLC for the National Nuclear Security Administration (NNSA) of U.S. Department of Energy (DOE) under Contract No. 89233218CNA000001. MARBLE is supported by the DOE NNSA Office of Experimental Sciences (No. NA-113) SAT and PAT Programs.

References

[1] Y. Kim et al., Phys. Plasmas 28, 012702 (2021).
[2] E.E. Meshkov, Fluid Dyn. 4, 101 (1969).
[3] B. Haines et al., Phys. Plasmas 24, 052701 (2017).
[4] B. Haines et al., Comp. Fluids 201, 104478 (2020).
[5] J. Marozas et al., Phys. Plasmas 25, 056314 (2018).
[6] T. J. Murphy et al., J. Phys. Conf. Ser. 717, 012072 (2016).
[7] M. Gittings et al., Comput. Sci. Discovery 1, 015005 (2008).

Miscible Experiments on the Rayleigh-Taylor Instability in the Linear Induction Motor Drop Tower

C. J. Withers[1,*] M. J. Mokler[1], and J. W. Jacobs[1]

[1]The University of Arizona, Tucson, Arizona, United States of America

[*]**Corresponding Author: claytonwithers@email.arizona.edu**

1. The Linear Induction Motor Drop Tower (LIMDT)

Miscible experiments on the Rayleigh-Taylor Instability (RTI) in the Linear Induction Motor Drop Tower (LIMDT) at the University of Arizona are presented. The LIMDT (Figure 1) consists of a vertical tower that uses high density polyethylene rails to guide a test sled that is accelerated using linear induction motors. The experimental fluid pairs are prepared and placed into a test chamber attached to the sled. The sled is then accelerated vertically, against gravity at a rate of approximately 11g. The resulting Rayleigh-Taylor instability is imaged using planar laser induced fluorescence (PLIF) by seeding the heavy fluid with fluorescein dye that is illuminated by a scanning laser beam and imaged with a CMOS camera.

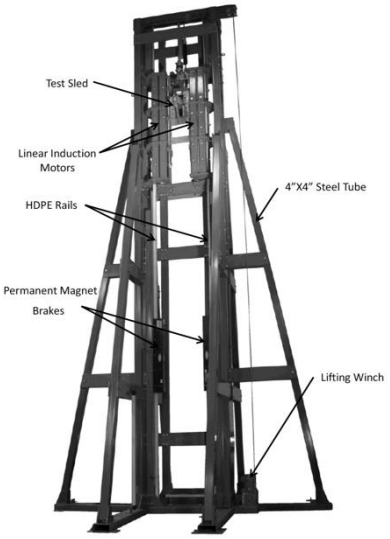

Figure 1: The linear induction motor drop tower

2. Index of Refraction Matched Miscible PLIF Experiments

Index of refraction (IOR) variation during miscible RTI experiments results in blurred images despite using pure fluids having perfectly matched IOR. As a result, this IOR variation negatively impacts the ability to extract measured quantities such as concentration in PLIF experiments and velocity using PIV experiments. In order to attempt to mitigate this effect, the index of refraction for experimental fluid pairs is modeled as a nonlinear fluid property with respect to fluid concentration and mixed ratio utilizing the method of McDougall [1]. Fluid combinations are then chosen that minimize the IOR variation, according to the model. RTI experiments are then performed by placing the miscible, aqueous fluid pair in the test chamber. The fluid with larger density is added first, resulting in an initially stable stratified fluid configuration. The fluids are then linearly accelerated producing the RTI. Mixing occurs and image sequences are then captured using the PLIF setup described above.

3. Results

It is found that the maximum index of refraction variation is nonlinearly proportional to the Atwood number. The variation in index of refraction with respect to the mixedness ratio is then minimized by evaluating different fluid combinations with Atwood numbers ranging from $0.1 \leq A \leq 0.2$. It was found that lowering the Atwood number by a modest amount results in a significant improvement in imaging. Figure 2 shows side-by-side comparison illustrating the imaging improvement achieved. The experimental images are then processed to extract mixed width and growth rate measurements. Figure 3 shows preliminary mixed width results from one experiment. Mixing width is extracted from the concentration profile using the integral expression below, where h is the mixed width and C is the concentration of the fluid pair.

$$h = \int_{0.05}^{0.95} C(1-C)dy \qquad (1)$$

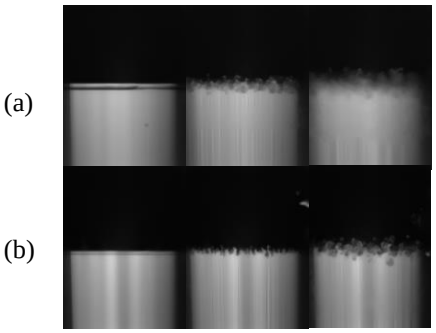

Figure 2: Image montage of (a) A= 0.216 (b) A=0.15 miscible Rayleigh-Taylor experiments

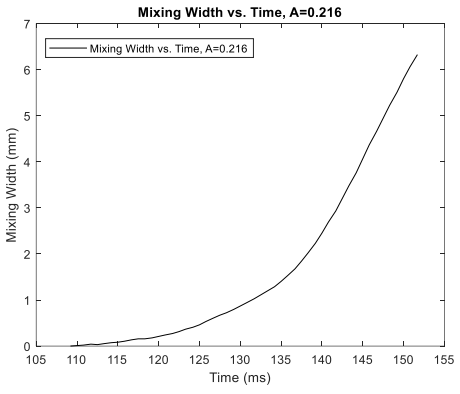

Figure 3: Preliminary mixed width measurement

Acknowledgments: The authors would like to acknowledge the support of Department of Energy NNSA Grant Number (DE-NA0003903) for funding this research.

References

[1] McDougall, T. J. 1979. "On the elimination of refractive-index variations in turbulent density-stratified liquid flows" Journal of Fluid Mechanics **93**, pp. 83-96.

Single-mode Richtmyer-Meshkov Instability

R. J. R. Williams[1,*], M. G. Probyn[2,3], B. Thornber[4], D. Drikakis[5], D. L. Youngs[6]

[1]AWE, Aldermaston, Reading, RG7 4PR, United Kingdom
[2]Centre for Fluid Mechanics and Computational Science, Cranfield University, MK43 0AL, United Kingdom
[3]Frazer-Nash Consultancy, United Kingdom
[4]School of Aerospace, Mechanical and Mechatronic Engineering, University of Sydney, NSW 2006, Australia
[5]University of Nicosia, Nicosia, CY-2417, Cyprus
[6]Formerly AWE, Aldermaston, Reading, RG7 4PR, United Kingdom

[*]**Corresponding Author: robin.williams@awe.co.uk**

We present results from an extensive study [1] of the development of single-mode Richtmyer-Meshkov [2, 3] instability performed using the Lagrange-remap hydrodynamics code TURMOIL [4].

In this work, we measured the early-time post-shock growth rate of the instability, and compared it with a number of approximate analytic forms for the growth rate, bubble-spike asymmetry and nonlinear suppression proposed in the literature.

We also studied the very late-time behaviour of the instability growth. We found that the bubble-squaring discussed by previous authors for light-to-heavy RM is the initial stage of a quasi-oscillatory behaviour, in which jets alternately appear at the position of the peak and trough of the initial perturbation. This alternation appears to be the result of a vortical structures deposited downstream of the interface by the passage of the curved transmitted shock being advected towards the surface as a result of loss of material to the growing jets.

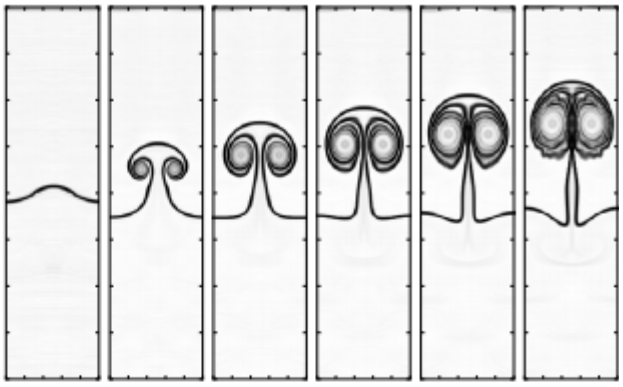

Figure 1: Edge contrast plot for single-mode light-to-heavy RM, with post-shock Atwood number 0.5 and amplitude 0.01 times the wavelength. The shock is incident from above on these axes.

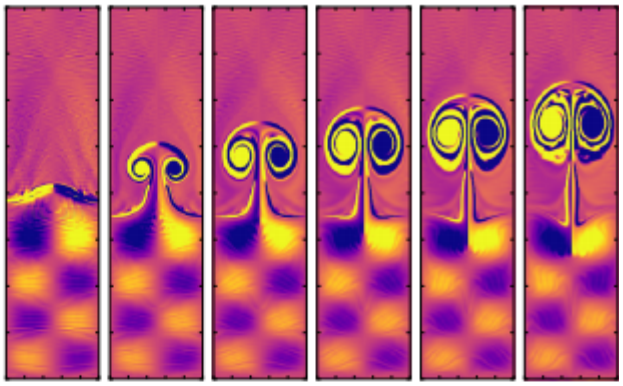

Figure 2: Flow vorticity for the same conditions as Figure 1, showing the relationship of 'bubble squaring' to the downstream deposited vorticity.

References

[1] M. G. Probyn, R. J. R. Williams, B. Thornber, D. Drikakis, D. L. Youngs, Physica D: Nonlinear Phenomena **418**, 132827 (2021).
[2] R.D. Richtmyer, Commun. Pure Appl. math., **13**, 297 (1960).
[3] E.E. Meshkov, Fluid Dyn. **4**, 101 (1969).
[4] D. L. Youngs, Physics of Fluids A **3**, 1312 (1991).

UK Ministry of Defence © Crown Owned Copyright 2022/AWE

Plasma transport dissipation in turbulent instability mixing

Erik Vold[1,*], Jan Velechovsky[1], and Susan Kurien[2]

[1]XCP-2: Eulerian Codes, LANL, Los Alamos, New Mexico, USA
[2]T-3: Fluid Dynamics and Solid Mechanics, LANL, Los Alamos, New Mexico, USA

[*]**Corresponding Author: elv@lanl.gov**

We examine mixing in a fuel/ablator interface during late time Rayleigh-Taylor deceleration inside a simplified Inertial Confinement Fusion (ICF) target. Resolved scale simulations (RSS) with and without plasma transport [1] are compared to a turbulence mix model (BHR) [2], including the effects of dissipation by plasma transport through plasma viscosity and species mass diffusion [3]. The simulations are run using LANL's multi-material multi-physics Eulerian code, xRage [4]. A model is proposed to include dissipation by plasma transport in the turbulent mixing and the initial implementation examines dissipation of a turbulent density self-correlation parameter, $b = <\rho><1/\rho> - 1$, which acts as a source term for the turbulent fluctuations.

The plasma dissipation model assumes that a turbulent length maintains the scale of the divergence of the fluctuation and plasma velocities, and that a plasma transport velocity term adds to the turbulent velocity within that divergence. The turbulent kinetic energy, $K_{trb,}$ determines the turbulent velocity, $v_{trb} \sim K_{trb}^{1/2}$, and the plasma velocity, v_{pls}, is set by a diffusive transport coefficient divided by a plasma scale length. Transport coefficients can include combinations of viscosity or mass diffusivity, and the respective scale lengths are the Kolmogorov or Batchelor scales. These scales are determined by a combination of the turbulent dissipation rate, $\varepsilon = -dK/dt$, and a plasma transport coefficient, η_{pls}, for example, the viscous scale length becomes the Kolmogorov scale, L_K, estimated as $L_K \sim (\eta_{pls}^3/\varepsilon)^{1/4}$. The ratio of the plasma velocity to the turbulent velocity is a measure of the plasma dissipation and this ratio is shown to scale with a turbulent Reynolds number, $Re_{trb} = (v_{trb}L_{trb}/\eta_{pls})$ as

$$v_{pls}/v_{trb} = Re_{trb}^{-1/4}.$$

This quantity is plotted in Fig.1 and demonstrates that the 'dissipation' from the plasma contribution is equal to the turbulent dissipation when Re decreases to unity, as expected.

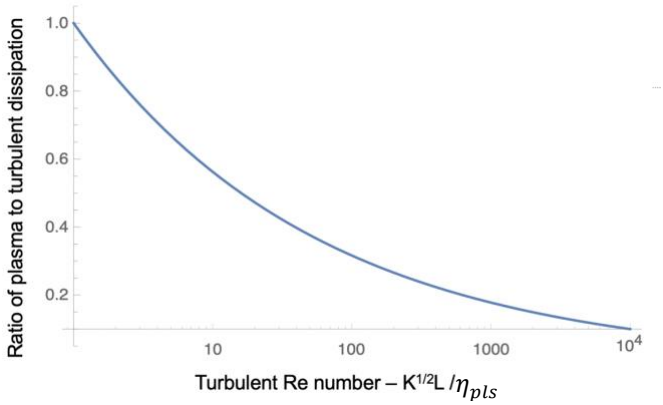

Figure 1: Plasma/turbulent dissipation versus Re_{trb}

As the flow speed increases, the ratio of plasma to turbulent dissipation decreases but the ratio remains a significant fraction even at high Re numbers, indicating that plasma transport remains a significant contribution to the mixing dynamics, even for the higher speeds at late time during instability growth.

The time evolution of the density self-correlation, 'b' was examined in an ICF R-T deceleration mixing layer, with and without plasma transport dissipation in a 1D approximation. Results in the BHR turbulence model are consistent with the plasma dissipation scaling in Fig.1, showing a significantly increased decay of *b* due to the plasma dissipation at early times when the mix velocities and turbulent Reynolds number are small, and a smaller but still significant decrease in *b* at later times.

These 1D turbulent mix model results do not recover all the dynamics of the RSS simulations [1], wherein the density self-correlation is seen to increase in time under some conditions. This is attributed to the smallest initial scales decaying rapidly and the larger wavelength modes growing at later times. Specifically, the current version of the turbulent model shows a monotonically decreasing value in time of the density self-correlation, *b*, for this R-T instability case, and the plasma dissipation acts to increase that rate of decrease in *b*. A scale-dependent turbulence model, LWN [5], may help resolve this discrepancy as that model can potentially represent the mode dependence of the plasma dissipation.

Acknowledgments: Los Alamos National Laboratory is managed by Triad National Security, LLC for the U.S. Department of Energy's NNSA under Contract No. 89233218CNA000001. Funding is provided by the Mix and Burn Project within NNSA's Advanced Simulation and Computing (ASC) Program, PEM (Physics and Engineering Models).

References

[1] J. Velechovsky, et.al., these proceedings.
[2] D. Besnard, et.al., LANL Report, LA-UR-12303 (1992).
[3] E. Vold, et.al., Phys. Plasm., **28**, 092709 (2021).
[4] M. Gittings, et.al., Comput. Sci. Disc., **1**, 015005 (2008).
[5] P. Narita, et.al., Phys.Rev.E,104(2), 025105 (2021).

Experimental investigation of Rayleigh-Taylor mixing in gases using simultaneous PIV-LIF

Prasoon Suchandra*, Mark Mikhaeil, Gokul Pathikonda, Devesh Ranjan

George W. Woodruff School of Mechanical Engineering, Georgia Institute of Technology,
801 Ferst Drive, Atlanta, GA 30332-0405, USA

*Corresponding author: prasoon.suchandra@gmail.com

The dynamics of molecular mixing and the energy transfer process in the Rayleigh-Taylor instability (RTI) are studied through the collection and analysis of simultaneous density-velocity field measurements. Statistically stationary experiments are performed in the "convective-type" gas tunnel facility, with density contrast achieved through the injection of helium into the bottom stream. To observe the structure of the self-similar regime, three experiments at Atwood number $\mathcal{A} \approx 0.1$ are captured at three outer-scale Reynolds numbers (Re$\sim h\dot{h}/\nu$): 520, 2260 and 4050, where h and ν are mixing width and viscosity respectively.

To study the mixing and dynamics of the flow, both particle image velocimetry (PIV) and laser induced fluorescence (LIF) are employed simultaneously. This allows, for the first time in an RTI flow with gases, the simultaneous field measurement of velocity and density. Together, these are used to measure statistics of velocity, density and velocity-density cross-correlated terms. The experimental understanding of the interaction between the large-scale motion of the RTI bubble and spike structures, and the resulting mixing and energy transfer serves as a useful validation tool for predictive turbulence models. This helps develop our understanding of a variety of physical phenomena, most importantly the ignition of Type Ia supernovae and the implosion of the inertial confinement fusion (ICF) fuel target.

Statistics of the density and velocity show self-similar profiles at large Reynolds number (Re > 2000). Flat velocity profiles indicate homogeneous turbulence characteristics in the core of the mixing region. Significant anisotropy develops in the flow, with horizontal velocity fluctuations being only 60% of the vertical velocity fluctuations. Turbulent mass flux, the leading term in the production of turbulent kinetic energy in the flow, is shown to be asymmetric with increased peak towards the spike.

Measurements of the molecular mixing show that mixing is maximized at the core of the flow, and increases with increase in Reynolds number. However, the rate of mixing peaks at Reynolds number around 2260, suggesting a regime transition in the flow around this Reynolds number. The analysis of the density-specific-volume correlation, b, shows that the potential for mixing is mostly limited in the flow by the relative concentrations of the top and bottom fluid. The transport equation of b shows that it is mostly produced in the core of the mixing region, but that the spatial evolution of its profile is the result of transport by bulk motion of the bubble and spike.

Energy transfer from gravitational potential energy to turbulent kinetic energy and viscous dissipation is observed to occur in the experiment, with a ratio of dissipated energy to potential energy released of 38%. The analysis of the turbulent kinetic energy transport equation budget reveals that production is the dominant mechanism towards the growth of turbulent kinetic energy of the flow, and is asymmetrically skewed towards the spike. The viscous dissipation is also skewed towards the spike, suggesting that it serves as a balancing mechanism for the growth rate of turbulent kinetic energy. The budget of turbulent kinetic energy (fig. 1) reveals the nature of the energy transfer process in the flow, from the production of turbulent kinetic energy at the core of the flow to its transport to the edges by large scale fluctuations of the bubble and spike structures.

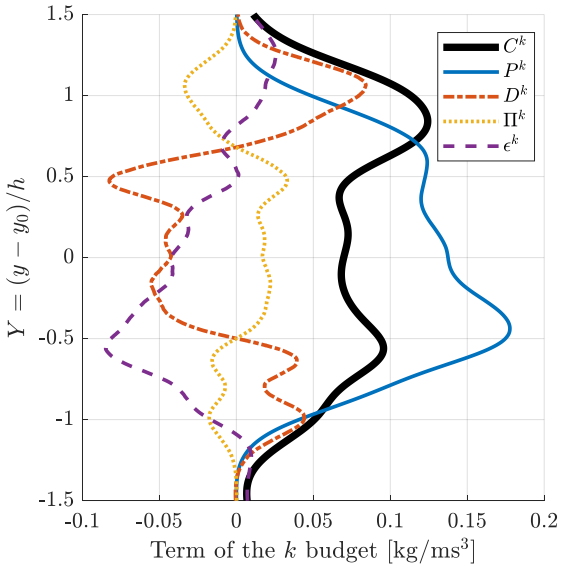

Figure 1: Profiles of the terms of turbulent kinetic energy budget, evaluated for Re = 4050 case.

Acknowledgment: This work has been supported by DOE grant GR00000566.

References

[1] Akula & Ranjan. "Dynamics of buoyancy-driven flows at moderately high Atwood numbers" *J. Fluid Mech* 795 (2016): 313-355.

[2] Akula et al. "Dynamics of unstably stratified free shear flows: an experimental investigation of coupled Kelvin–Helmholtz and Rayleigh–Taylor instability" *J. Fluid Mech* 816 (2017): 619-660.

[3] Mikhaeil. "Simultaneous velocity and density measurements of fully-developed Rayleigh-Taylor turbulent mixing" *PhD Dissertation* (2019), Georgia Institute of Technology.

[4] Mikhaeil Suchandra et al. "Simultaneous velocity and density measurements of fully developed Rayleigh-Taylor mixing" *Phys. Rev. Fluids* 6 (2021): 073902.

Simulations of Multimode Perturbations Driven by Same-Sided Successive Shocks

R.F. Sacks[1,*], F.W. Doss[1], C.A. Di Stefano[1], E.C. Merritt[1], H. Robey[1]

[1]Los Alamos National Laboratory, Los Alamos, New Mexico, USA

[*]**Corresponding Author: rsacks@lanl.gov**

In order to ensure physically complete simulations of high-energy density (HED) systems and inertial confinement fusion (ICF), investigation of turbulent mix models is of high importance. Mixing in ICF systems can lead to quenching of fuel by the injection of cold material into hot fuel, and the loss of confinement due to aneurisms developing in the compressed shell. ICF experiments contend with a number of complicated seeds that can lead to instability growth, including successive shocks. There is currently a lack of both analytic and modeling work in this regime since copropagating shocks are difficult to achieve with conventional (non-HED) drivers, and analyzing successive shocks requires the investigation of a large parameter space for instability growth. Ideal theory predicts fifteen separate growth cases for a single mode under successive shocks [1]. This increases to an even larger space of growth cases when multi-mode cases applicable to ICF systems are considered since they can include both coherent and nonlinear effects.

The current phase LANL multi-shock (MShock) campaign on the National Ignition Facility (NIF) is designed to study both Richtmyer-Meshkov (RM) growth and the subsequent transition to turbulence under successive shocks. MShock leverages the laser drive and large energy available at NIF to be the first experiment able to probe a wide portion of the successive shock parameter space, due to our ability to create independent and controllable successive shocks. One of the main reasons for this platform is to test LANL's BHR [2] mix model in the xRAGE[3] code. To this end, we require simulations of single and multimode perturbations with the BHR model. The simulations are both a design prerequisite to experiments and provide for a comparison to experimental data. Due to the large design and parameter space, we have developed a reduced complexity simulation using simplified drives and geometries, which allows us to do a large model initialization study at lower computational and time expense while maintaining the ability to independently alter relative shock strength, relative shock timing, and perturbation geometry. We present both a simulation comparison to single-mode successive shock experiments to establish the viability of our simulations, and a design study of multi-mode perturbation initial conditions and the application to BHR.

Acknowledgments: Los Alamos National Laboratory is operated by Triad National Security, LLC for the U.S. DOE under contract 89233218CNA000001, LA-UR-22-21687.

References

[1] K. Mikaelian, Phys. Rev. A, **31**, 410 (1985)
[2] J. D. Schwarzkopf *et al.*, Flow Turbulence Combust, **96,** 1-43 (2016)
[3] M. Gittings *et al.*,Comp. Sci. Disc. **1**, 015005 (2008)

A density fluctuation analysis for HED Richtmyer-Meshkov experiments

E.C. Merritt[1,*], F.W. Doss[1], J.M. Levesque[1], T. Desjardins[1], C.A. Di Stefano[1], K.A. Flippo[1], H. F. Robey[1], R. Sacks[1], D.W. Schmidt[1], L. Kot[1], and T. Perry[1]

[1]Los Alamos National Laboratory, Los Alamos, New Mexico, USA

[*]**Corresponding Author: emerritt@lanl.gov**

The applicability and implementation of turbulent mix models in the high-energy-density regime is a fundamental question for inertial confinement fusion (ICF). The impact of mix includes, the quenching of ignition experiments by mixing hot fuel with cold external materials. There is no consensus in the community on whether the development of mix is even inevitable, or if it is possible to "outrun" the mixing through rapid drives, or if plasma effects may anomalously damp the mixing process.

The LANL multi-shock (MShock) campaign on the National Ignition Facility is developing an experimental suite capable of studying RM growth and transition to turbulence in the ICF-relevant regime of multiple thin-layers driven with multiple, varying strength shocks from multiple directions. A fundamental focus is to test the applicability and performance of the BHR mix model [1] in this complex, HED regime.

Re-shocking an imperfect interface with a counter-propagating shock increases the Richtmyer-Meshkov instability growth rate and hastens a system's transition to turbulence [2]. This will only complicate already complex feedthrough effects on interface instability evolution. Similarly, shocking a single-interface multiple times from the same side should change the interface instability growth and mixing properties. We present platform overviews and results from two phases of Mshock experiments:

(1) a thin-layer under shock-reshock conditions [3], and
(2) a single-interface shocked successively from the same-side.

Both phases examine RM growth under both single-mode and multi-mode initial interface conditions, which consists of high-frequency broad-band noise imposed on a low-frequency single-mode sinusoid. Machined interfaces allow a significant separation of scales between the high-frequency broad-band noise and the low-frequency single-mode sinusoid. This has led to observations of separate regions of mixing along the thin-layer, and motivates a data analysis method capable of differentiating between the regions. Radiography images resolve enough interface structure that we can extract some 2D evolution information in addition to the traditional 1D mix-widths.

We will present a new analysis method to extract statistics of density fluctuations from radiographs and comparison of the experimental results to xRAGE simulations with a variety of initializations of BHR. Based on work by Kurien *et al.* [4], we use measurements of density fluctuations to calculate the BHR density-specific-volume covariance,

$$b = -\overline{\rho' v'} = -\overline{\rho'(1/\rho)'} \qquad (1)$$

where ρ' is the density fluctuations and v' is the specific volume fluctuations, and the fluctuations are ensemble averaged. The imposition of a low-mode sinusoid on the initial interface allows us to extract both 1D and 2D estimates of b (Fig. 1), for comparison to model performance in both 1D and 2D simulations. Early comparisons have shown our analysis has the ability to qualitatively distinguishing between BHR initializations. The analysis development has illuminated deeper questions of how to model systems with large separation of scales and lead to a discussion of the subtleties of equivalency between data and model quantities. Specifically what instability scales must be resolved directly and what can be captured by the model, and how that is reflected in what averaging domains we choose in the data when measuring statistical quantities.

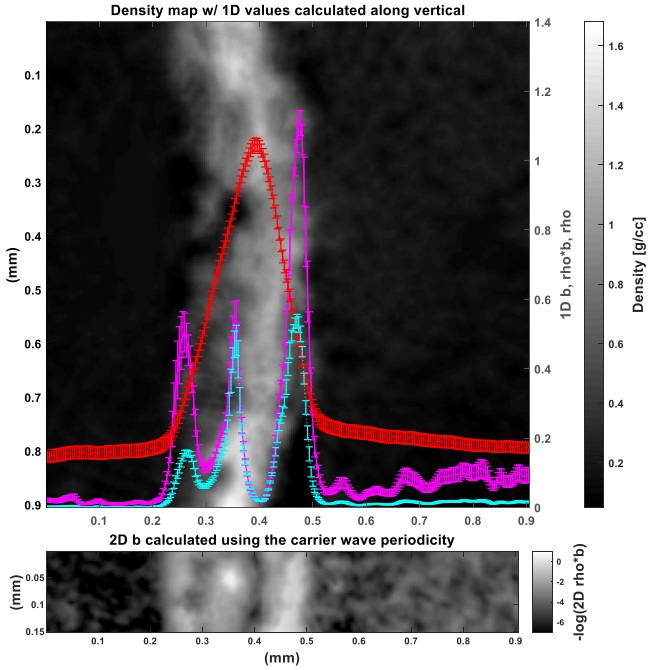

Figure 1: (Top) Density of the post-reshock thin-layer with a lineout of the calculated 1D ρ (red), b (magenta), and ρb (cyan) with the ensemble average along the vertical axis. (Bottom) Calculated 2D ρb with the ensemble average over a single wavelength of the low-frequency carrier mode.

Acknowledgments: Los Alamos National Laboratory is operated by Triad National Security, LLC for the U.S. DOE under contract 89233218CNA000001.

References

[1] J. D. Schwarzkopf *et al.*, Flow Turbulence Combust, **96,** 1-43 (2016)
[2] T. R. Desjardins *et al.*, High Energy Density Phys., **33**, 100705 (2019)
[3] E. Leinov *et al.*, J. Fluid Mech., **626**, 449-475 (2009)
[4] S. Kurien *et al.*, Physica D, in review (2020)

Wall Vortices Induced by Re-Shock in RMI Shock Tube Experiments

Raymond McConnell*, Chris Noble, Alex Ames, Jason Oakley, David Rothamer, and Riccardo Bonazza

Department of Engineering Physics, University of Wisconsin-Madison, Madison, WI, USA

*Corresponding Author Email: rmcconnell2@wisc.edu

The Richtmyer-Meshkov instability (RMI) is often studied in shock tubes. The walls and relatively narrow cross sections in these devices introduce boundary layers that can influence the development of the RMI. Most of the experimental RMI analysis assumes statistically two-dimensional flow and sufficient distance from wall effects. It is known that upon re-shock vortices form where the material interface meets the wall due to vorticity deposition in the boundary layer [1]. The goal of this research is to quantify the extent to which these vortices affect the flow in RMI experiments.

Experiments investigating the wall vortices formed upon re-shock were conducted in the Wisconsin Shock Tube Laboratory at UW-Madison. The shock tube facility is vertical, downward-firing, with a square cross section with a side length of 25 cm. Experiments were performed using planar laser-induced florescence (PLIF) with acetone as a tracer. Acetone was mixed with helium at a 3% volume fraction and was layered above argon giving a nominal Atwood number A=0.75. This interface was then accelerated by a Mach 1.8 shockwave and the vortices formed upon re-shock were imaged via PLIF. Figure 1 shows the boundary layer at the material interface present prior to re-shock with the right-hand boundary of the image aligned with the wall of the tube.

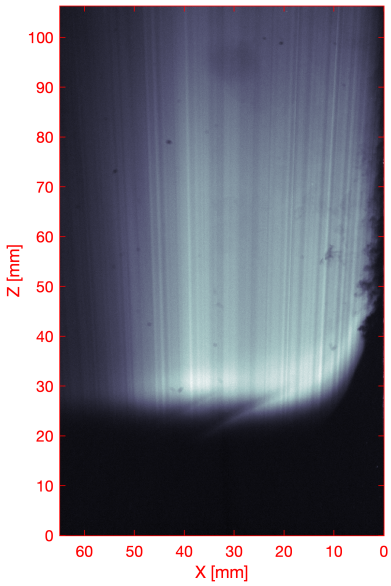

Figure 1: Acetone PLIF data showing the material interface boundary layer 50 μs prior to re-shock.

Here the focus is on the geometry of the wall vortex and its development over time. Figure 2 shows the time evolution of the wall vortex formation captured via PLIF. Geometric parameters determined from this data and analysis are combined with vortex models and with *Miranda* simulations. Comprehensive, quantitative conclusions will be presented on the vortices' impact on the RMI occurring away from the wall.

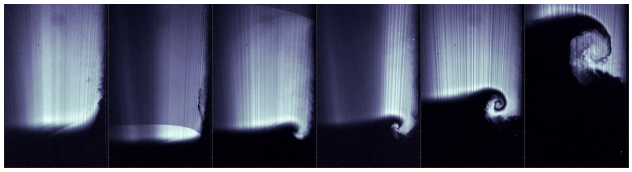

Figure 2: Temporal development of wall vortex after re-shock captured via PLIF.

Acknowledgments: Work supported by DOE-NNSA grant DE-NA0003932 and under the auspices of the US Department of Energy by Lawrence Livermore National Laboratory under Contract DE-AC52-07NA27344.

References

[1] M. Brouillette, & R. Bonazza, Physics of Fluids, **11**, 1127 (1999).

Simulation of shock-tube experiments using a well-characterised initial gas separation

Jérôme Griffond[1,*], Marta Rasteiro dos Santos[2], Yannick Bury[2], Stéphane Jamme[2] and Denis Souffland[1]

[1]Commissariat à l'énergie atomique et aux énergies alternatives, CEA, DAM, DIF, F-91297 Arpajon, France
[2]Institut Supérieur de l'Aeronautique et de l'Espace (ISAE), Université de Toulouse, Toulouse 31400 France

[*]**Corresponding Author: jerome.griffond@cea.fr**

The prediction of turbulent mixing zones (TMZ) evolution after interaction with a shock wave, is a crucial issue in different domains, ranging from astrophysics to inertial confinement fusion. But it remains challenging. Since decades, shock tube experiments have been used to bring to light the different mechanisms involved. An interface between initially separated gases undergoes Richtmyer-Meshkov instability after interacting with the shock stemming from the burst of the diaphragm between the high and the low-pressure sections. Depending on the initial conditions, the interface may evolve into a TMZ before being striked a second time by the shock front reflected from the aft-end of the shock tube, that is referred to as the "reshock". Such a configuration is therefore of major interest to study the shock/TMZ interaction.

Recently, an innovative way to separate both gases and generate an interface between them before the arrival of the first shock wave has been set-up in a 130x130mm^2 shock-tube at ISAE. This mechanism, called Micro Rotating Shutter System (MR2S), is composed of 13 thin plates rotating by 90 degrees around their central axis [1,2]. Before rotation, they separate the driven section (filled with air) from the visualization chamber (filled with helium) and their rotation generates an interface with a shape depending on the opening time.

As the MR2S avoids the use of membranes, the facility is well-suited to high-resolution measurements. Detailed concentration and velocity flow fields can be obtained by tomoscopy and PIV at the end of shutter opening. They are used here to initialize numerical simulations. The dynamics of the TMZ are then experimentally studied by three-component-PIV and high-speed schlieren photography [3].

Numerical investigations with the Triclade code [4] reported here are confronted with experimental data. Only three shutters are treated in the simulations, as fixed internal reflective boundary conditions, over a limited slice of the tube section. We will discuss in this poster several physical issues concerning :

- the three-dimensionalization of the initially deterministically 2D interface with unknown initial 3D perturbation seed;
- the subsequent transition from a statistically 2D to a statistically 1D behavior.

Both questions are illustrated in Fig. 1, that presents Triclade results for (a) the deterministically 2D interface (slightly perturbed) soon after shock crossing, (b) the statistically 2D TMZ some time later and (c) the (roughly)-statistically 1D TMZ after interaction with the reshock.

The methodology of the numerical 3D perturbation seed to be imposed to the 2D measured initial fields will be detailed. Since quantities of interest are of statistical nature, and collected over multiple experimental shots, the relevant way of comparing them to numerical predictions is questionable, depending on the expected kind and dimensionality of the interface/TMZ. These aspects will also be addressed in this study.

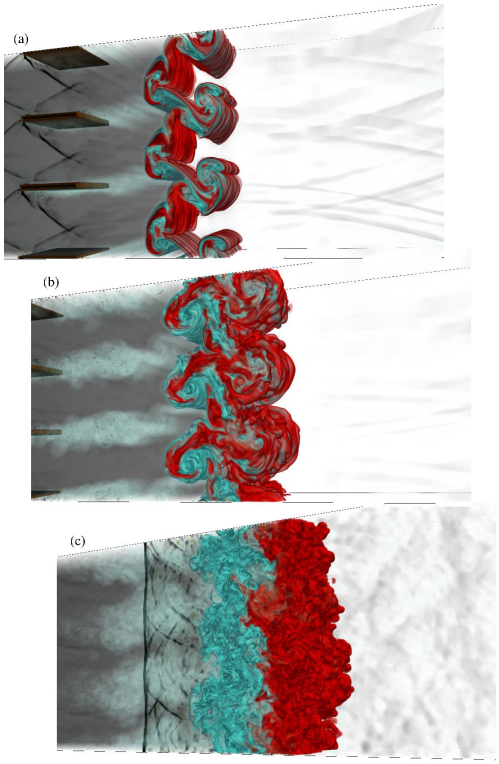

Figure 1: Volume rendering of the concentration and velocity divergence fields. Rotating shutters on the left. (a)- soon after main shock interaction; (b)-three-dimensionalization of the flow; (c)- just after reshock interaction.

Acknowledgments: This work is supported by CEA,DAM under Grant No. CAJ-18-59/C33893.

References

[1] P. Graumer, PhD thesis, Université de Toulouse, Toulouse, France (2019).
[2] Y. Bury, P. Graumer, S. Jamme and J. Griffond, Phys. Rev. Fluids **5** (2), 024101 (2020) .
[3] M. Rasteiro dos Santos, Y. Bury, S. Jamme and J. Griffond, AIAA SciTech, San Diego CA, 3-7 Jan 2022
[4] B. Thornber, J. Griffond, O. Poujade *et al.* Phys. Fluids **29** (10), 105107 (2017)

Exploring Shock and Interface Physics to Measure Viscosity

Sonya Dick[1,*], Tyler Perez[2], June Wicks[2], Marius Millot[3] and Eric Johnsen[1]

[1]University of Michigan, Ann Arbor, MI, USA
[2]Johns Hopkins University, Baltimore, MD, USA
[3]Lawrence Livermore National Laboratory, Livermore, CA, USA

[*]**Corresponding Author: scdick@umich.edu**

Mantle dynamics drive a wide range of processes that shape terrestrial planets including Earth and super-Earths. Processes such as plate tectonics, magnetic field generation, and planetary structure are affected by the mantle material transport properties. The viscosity of the mantle is a critical transport property necessary to model and understand these processes. However, the viscosity of mantle materials, mostly oxides and silicates, is not well characterized at relevant pressures (>100 GPa).

Thus, constraining mantle material viscosity at high pressures is important to increase the fidelity of models. High-energy laser facilities can shock relevant materials to pressures of interest. For example, the OMEGA laser facility has obtained pressures of up to 500 GPa in MgO for equation of state experiments. Thus, this work builds a platform to generate laser-shocked materials at relevant pressures to study material viscosity.

The evolution of a perturbed shocked interface is dependent on the material viscosity. Similarly, the evolution of the resulting corrugated shock amplitude is dependent on material viscosity. We aim to use this dependence to study material viscosity under extreme conditions (i.e., pressures up to 500 GPa).

This work focuses on the theoretical and computational development to aid in experimental design and interpretation of experimental results. We follow theoretical results for the viscous Richtmyer-Meshkov interface [1] and the viscous decay of a corrugated shock [2]. This theory is applied to design the experiments to obtain the optimal signal to noise ratio. Additionally, simulations of a corrugated shock are performed to study the underlying dynamics. We use an in-house Recovery-assisted discontinuous Galerkin code. An inviscid comparison of these simulations is compared with the theory from [2] and presented in fig. 1.

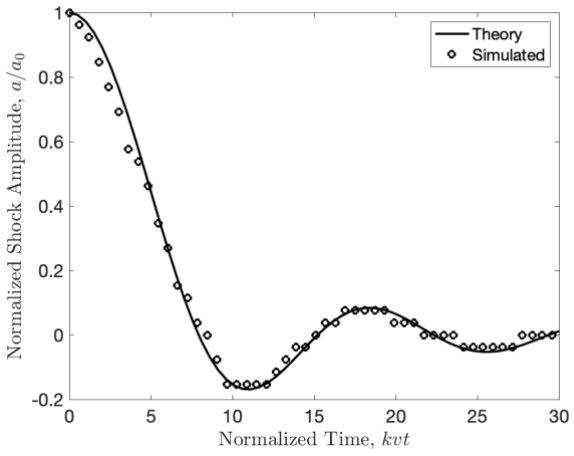

Figure 1: Shock amplitude decay from simulations and theory [2].

Acknowledgments: This work is supported by LLNL under subcontract B632749, the XSEDE Comet system under grant TG-CTS130005, and the NSF GRFP under Grant No. DGE 1256260. Part of this work was prepared by LLNL under Contract DE-AC52-07NA27344.

References

[1] K. O. Mikaelian, Effect of viscosity on Rayleigh-Taylor and Richtmyer-Meshkov instabilities, Phys. Rev. E 47 (1993) 375-383.
[2] G. H. Miller and T. J. Ahrens, Shock-wave viscosity measurements, Rev. Mod. Phys. 63 (1991) 919-498.

Numerical investigation of compressibility and Atwood number effects on the single-mode iso-thermally stratified Rayleigh-Taylor Instability

Tyler Prine[1], Denis Aslangil[1*] and Man Long Wong[2]

[1]Aerospace Engineering & Mechanics, The University of Alabama, Tuscaloosa, Alabama, 35487 USA
[2]Los Alamos National Laboratory, Los Alamos, NM, 87545 USA

[*]**Corresponding Author: denis.aslangil@ua.edu**

Rayleigh-Taylor Instability (RTI) consists of mixing two fluids with different molar masses that are initially separated by a thin perturbed layer subject to a gravitational force. This initial thin layer starts grow in and converts to a thicker mixing layer in the case that the acceleration is subjected to the opposite sign of the density gradient. It is observed in flows ranging from the oceanic, atmospheric, and geologic flows to astrophysical and in engineering applications such as with high energy density (HED) [1-4]. In the case where incompressible assumption holds, the growth of RTI mixing layer width, W, is well predicted by the self-similar equation: $W \approx \alpha A g t^2$ where α is the growth rate constant, g is the acceleration, and t is the time. In addition, A $(= (W_1 - W_2)/(W_1 + W_2))$ is the Atwood number, with W_1 and W_2 being the molar masses of the heavy and light fluids, respectively. One of the main weaknesses of the self-similar projection is the ignorance of the compressibility effects which may play an important role in astrophysical phenomena and HED applications such as ramjets [1]. Earlier studies which focus on the effects of the strength of the isothermal background stratification suggest a slow-down in the growth of the mixing layer due to increase in the compressibility of the mixing fluids. The purpose of this study is to extend the analysis to cover the coupled effects of Atwood and Mach numbers on the fully compressible 2D single-mode RTI by using direct numerical simulations (DNSs).

Multi-species fully-compressible Navier Stokes Eq.s are solved by using HAMeRS code (more details of the equations and the code can be found in [1]). In addition to the Atwood number, we also altered the iso-thermal Mach Number $Ma = \sqrt{g\lambda_0}/c_0$ where λ_0 is the characteristic wavelength and c_0 is the speed of sound. To compare the evolution of these different cases, we benefit from the well-established parameter for the non-dimensional time t^* as defined in [1,4] as $t^* = t\sqrt{g/\lambda_0}$ [1,4]. In this study, we alter its definition to include the A number effects. Modified time scale is defined as $t^* = t\sqrt{gA/\lambda_0}$. It is found that the new time scaling is capable of accurately accounting for the effects of A in the case of compressible RTI (not shown here for brevity).

In incompressible RTI problems the pure fluid penetrations become highly asymmetric when the A is larger (usually $A > 0.2$). This is related to having different inertia in the light and heavy fluid regions [2]. Such an asymmetric behavior has not been tested in the case of strong background stratifications ant it poses the question of whether this trend continues for the compressible RTI. To answer this question, multiple DNSs were performed with identical initial conditions, but with different Ma and A. A baseline case with a low A of 0.04 is taken, where the pure fluid penetrations stay approximately symmetric with different Ma. At a higher A of 0.25, this is no longer the case, as can be observed in figure 1 between a Ma of 0.3 and 1.5.

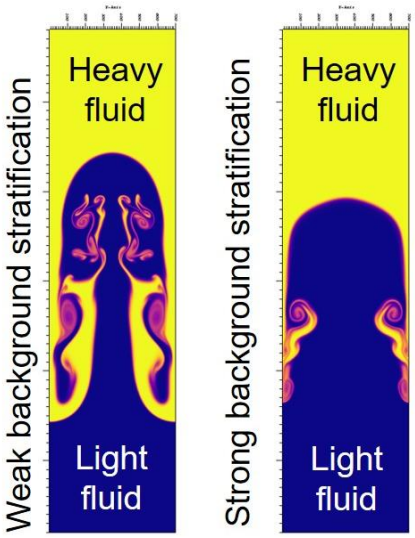

Figure 1: Comparison of cases with Ma=*0.3* (left) and 1.5 (right) with $A = 0.25$.

Figure 1 shows that the growth of the perturbations for a Ma of 0.3 is much greater than for a Ma of 1.5. This finding extends Wieland et al's [4] study to a higher Atwood number. An interesting observation for the cases with different Ma at this higher A is that there is an enhanced asymmetry between the mixing layer growths of heavy and light fluids for the case of large Ma number. At low Ma, this asymmetry does not appear as pronounced. However, at higher Ma value for the same A, we noticed much higher asymmetry between the growth of bubble and spikes. This finding suggests that the largely asymmetric growth of the RTI mixing layer can also be observed at relatively small A for case under strong background stratification. In this presentation, we will show detailed analysis for different A and Ma numbers to explore their coupled effects on the flow evolution.

Acknowledgments: For the computations, this work used the Extreme Science and Engineering Discovery Environment (XSEDE) [5], which is supported by NSF grant # ACI-1548562.

References

[1] Aslangil, D., Wong, M.L..,*"Study of iso-thermal straitification strength on 2D multi-mode compressible Rayleigh-Taylor instability"*, AIAA SCITECH 2022 Forum, 0456, (2022).

[2] Aslangil, D., Livescu, D., Banerjee, A.,*"Effects of Atwood and Reynolds numbers on the evolution of buoyancy-driven homogeneous variable-density turbulence"*, Journal of Fluid Mechanics **895**, A12, (2020).

[3] Aslangil, D., Livescu, D., Banerjee, A.,"Variable-density buoyancy-driven turbulence with asymmetric initial density distribution", Physica D: Nonlinear Phenomena **406**, 132444, (2020).

[4] Wieland, S. A., Hamlington, P. E., Reckinger, S. J., and Livescu, D., "*Effects of isothermal stratification strength on vorticity dynamics for single-mode compressible Rayleigh-Taylor instability,*" Phys. Rev. Fluids, **Vol. 4**, 2019, p. 093905.(2019)

[5] Towns, J., et al., *"XSEDE: Accelerating Scientific Discovery"*, Computing in Science & Eng. **Vol. 16**, pp. 62–74.17 (2014).

NOVEL PANS MODEL FOR VARIABLE DENSITY TURBULENCE

Filipe S. Pereira[1*], Fernando Grinstein[2,] and Daniel Israel[3]

[1]Los Alamos National Laboratory, Theoretical Division, Los Alamos, New Mexico, USA
[2] Los Alamos National Laboratory, X-Division, Los Alamos, New Mexico, USA

[*]**Corresponding Author: fmsoarespereira@gmail.com**

Modeling and simulation of variable density and mixing flows are rife with challenges. These problems feature transient and laminar flow, coherent structures and instabilities, onset and development of turbulence, non-equilibrium turbulence, density fluctuations, production of turbulence kinetic energy by shear and buoyancy mechanisms, and kinetic energy decay. This set of features is difficult to accurately model with one-point RANS closures.

For this reason, we recently derived the bridging partially-averaged Navier-Stokes equations (PANS) turbulence model for variable density flow and material mixing problems [1]. This formulation aims to compute complex flows efficiently (cost vs. accuracy) by only resolving the flow scales not amenable to modeling. The remaining turbulence scales are represented through a scale-aware closure. In this presentation, we summarize our work on PANS for variable density and mixing flow. The framework to extend PANS closures to such a class of variable-density problems is presented, and applied to derive the governing equations of the scale-aware PANS BHR2 closure [1]

The model is validated through the prediction of the Taylor-Green Vortex at Re=3000 and the Rayleigh-Taylor at At=0.50 benchmark flows. The results illustrate that the PANS method can accurately predict the complete flow evolution of these flow problems, which comprises of laminar, transitional, and turbulent flow, as well as coherent structures and instabilities. The flow evolution of the RT is presented in Fig 1. Most notably, the results confirm that the new model can predict these flows as accurately as Large-Eddy or Direct Numerical Simulations (LES and DNS). This is illustrated in Fig. 2. However, the model only resolves a fraction of the flow scales, reducing the computational cost significantly. Considering the TGV flow and ILES, PANS reduces the computational cost by more than fourteen times. This confirms the potential and accuracy of the model to efficiently predict variable density and mixing flows. A new verification and validation technique is also discussed.

Acknowledgments: Los Alamos National Laboratory (LANL) is operated by TRIAD National Security, LLC for the US DOE NNSA.

References

[1] F.S. Pereira, F.F. Grinstein, D.M. Israel, R. Rauenzahn, S.S. Girimaji – Partially-Averaged Navier-Stokes Closure for Variable-Density Turbulent Flow. Physical Review Fluids, **6**, 084602, 2021;
[2] F.S. Pereira, F.F. Grinstein, D.M. Israel, R. Rauenzahn, S.S. Girimaji – *Modeling and Simulation of Transitional Rayleigh-Taylor Flow with Partially-Averaged Navier-Stokes Equations*. Physics of Fluids, **33**, 115118, 2021;
[3] F.S. Pereira, F.F. Grinstein, D.M. Israel, R. Rauenzahn, S.S. Girimaji – *Modeling and Simulation of Transitional Taylor-Green Vortex with Partially-Averaged Navier-Stokes Equations*. Physical Review Fluids, **6**, 054611, 2021;
[4] F.S. Pereira, F.F. Grinstein, D.M. Israel, L. Eça – Verification and Validation: the Path to Predictive Scale-Resolving Simulations of Turbulence (submitted to Journal of Verification, Validation, and Uncertainty Quantification – minor revisions);

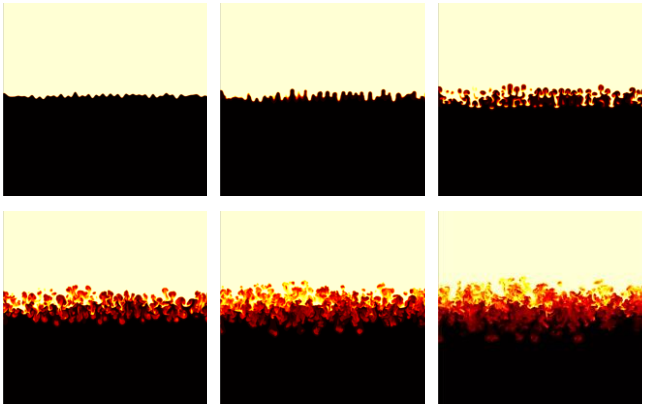

Figure 1: Flow evolution of the Rayleigh Taylor Flow. 2D slices of density field.

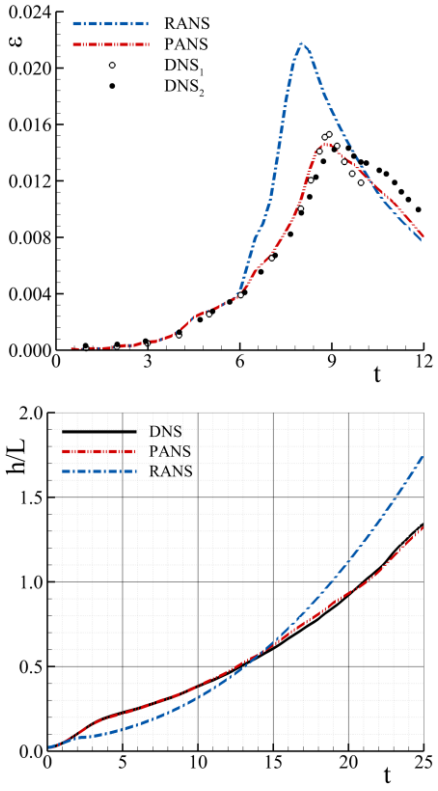

Figure 2: Dissipation of turbulence kinetic energy (TGV) and mixing layer height (RT) predicted with different turbulence models.

Learning closure models for turbulence

Ismael Boureima*, Vitaliy Gyrya, Juan Saenz, Susan Kurien, and Marianne Francois

Los Alamos National Laboratory, Los Alamos, NM, U.S
*Corresponding Author: iboureima@lanl.gov

We present a new data-driven methodology for the dynamic calibration of parametric differential equation (PDE) models with application to turbulence. The approach is inspired by deep learning techniques, and consists of forming an objective function based on mismatch between ground truth and time integral model predictions, and minimizing this objective function using backpropagation techniques. The identified objective function and the corresponding minimization formulation form a basis for systematic and objective calibration of parametric PDE models.

We demonstrate the performance of this calibration methodology on a particular turbulence closure model BHR 3.1 [2] that belongs to the BHR family, so named after the original version proposed by Bernard, Harlow and Rauenzahn [1]. These are Reynolds-Averaged Navier-Stokes (RANS) closure models consisting of a system of (nonlinear) differential equations

$$\frac{\partial}{\partial t}U = G[U;\theta] = G(U, U_x, U_{xx};\theta) \qquad (1)$$

for a vector state variable U with prescribed model form $G[U,\theta]$ dependent on a set of parameters θ. The coefficients θ, historically, have been calibrated by hand based on several canonical turbulence flows for which direct numerical simulation (DNS) data was available. In [2] manual calibration of BHR 3.1 has been performed against DNS data of homogeneous variable density turbulence (HVDT) flow, Kelvin-Helmholtz (KH) and Rayleigh-Taylor (RT) turbulence flows. We present our approach and the results of calibration against similar data but using a different metric.

We compare and contrast two approaches: i) a *static* approach, and ii) a *dynamic* approach. The static approach considers (and minimizes) the instantaneous rate of deviation of the model from the DNS data, while the dynamic approach considers the deviation over a finite (vs. infinitesimal) time interval. The static approach reduces to a large overdetermined system of (typically linear) equations that could be solved in the least square sense. In this approach, for BHR models we observe decoupling of equations which further simplifies the practical implementation of the method and the analysis of the results. The static method produces a reasonable approximation to the reference DNS data only for short times of the dynamics. In contrast, in the dynamic approach we express the BHR model in the form of a residual neural network, which, starting from a set of initial conditions at a time t_0, predicts the evolution of the model's dynamical variables up to a later time t_1. The difference between the network prediction and the DNS statistics [3,4] is minimized by optimizing the BHR coefficients in an optimization problem in which we minimize a loss or objective function. To this end, the gradient of the loss function with respect to the model coefficients are computed using automatic differentiation of the computational graph of the neural network, and then used to adjust the model coefficients in the next iteration. This approach was found to be fast and effective for solving the type of calibration problems formulated above for dynamical systems.

The performance of our proposed ML data driven approach compared to the standard and manual approach, using benchmarked test on HVDT, KH and RT DNS data sets at various Atwood numbers is illustrated with the results shown in Figure (1). Figure (1a) shows the overall (global) loss, along with the individual (local) losses relative to the different DNS data sets, obtained with the optimized coefficients as a function of training iteration. Plots are scaled by $\mathcal{L}_0$, the corresponding loss obtained with the default coefficients. We note a 50% reduction in model prediction error (black line) only after about 1000 training iterations. The least improvement is obtained for the prediction of HVDT-A=0.50 (orange line) which is now about 35% more accurate, and the best improvement is obtained for the prediction of KH-A=0.75 (purple line) which is now about 60% more accurate. The 35% improvement obtained for HVDT-A=0.50 is qualitatively illustrated in Figure (1b) where weighted profiles [5] of BHR dynamical variables R_{33} (blue), R_{22} (orange), a_3 (green) and b (red) from DNS (solid lines) are compared to profiles obtained with the default coefficients (dotted lines) and those obtained with the optimized coefficients (dashed lines), Statistics from DNS [3,4] are used as the ground truth.

We discuss various challenges and decisions that were made along the way. In particular we will discuss the merits of different flavors of dynamic approaches together with their limitations and suggest possible remedies.

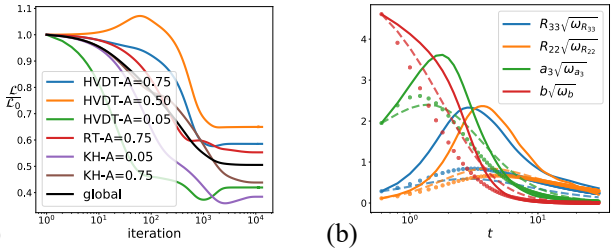

Figure 1: Optimized losses scaled by the loss obtained with default coefficients $\mathcal{L}_0$ vs training iteration in (a), and profiles of BHR weighted dynamical variables (dashed line) are compared to DNS (solid line) and profiles obtained with default coefficients (dotted lines) in (b).

Acknowledgments: This research was supported by the NNSA Advanced Simulation and Computing (ASC) program at Los Alamos National Laboratory through the Physics and Engineering Models-Mix & Burn, and the Advanced Technology Development and Mitigation –Machine Learning projects.

References

[1] D. Besnard, LANL Tech. Report, LA-10911-MS, (1987).
[2] J.D. Schwarzkopf, Flow Turbulence Comb., 96, (2015).
[3] D. Aslangil et al., JFM, 895:A12, (2020).
[4] J. Baltzer et al., JFM, 900:A16, (2020).
[5] I. Boureima et al., JCP, 457,110924 (2022)

High−Resolution Simulations of Transitional Triple−Point Shock Interactions

Alboreno Voci[1], ∗, Sanjiva Lele[1], Fernando Grinstein[2], Vincent Chiravalle[2] and Jonathan Regele[2]

[1]Stanford University, Stanford, California 94305, USA
[2]Los Alamos National Laboratory, Los Alamos, New Mexico 87545, USA

Corresponding Author: albovoci@stanford.edu

This work concerns the evolution of the Ritchmyer−Meshkov instability (RMI) in a rather unconventional setting: the classic triple−point canonical problem [1], commonly used as a 2D test case for validation and verification of multi−species flow solvers. The problem is defined here in 3D by periodically extending the out−of−plane direction. A cross section with all relevant initial conditions is given in Figure 1. The simulation includes reshock, making this a case which hasn't been studied before. The problem provides an excellent framework for studying shock induced transition to turbulence as well as other instability mechanisms such as secondary baroclinic instability.

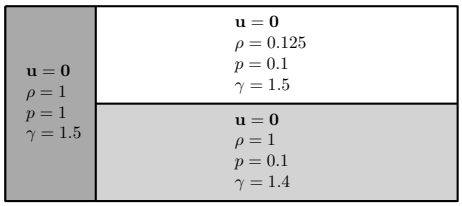

Figure 1: Planar $(x_1 - x_2)$ view of the triple−point problem.

The nature of the transition to turbulence in this problem depends on initial conditions. We have analysed this dependence by running an ensemble of configurations with different initial conditions using the *Legion* programming system [2] − a novel approach to simulating a large number of (multifidelity) simulations asynchronously.

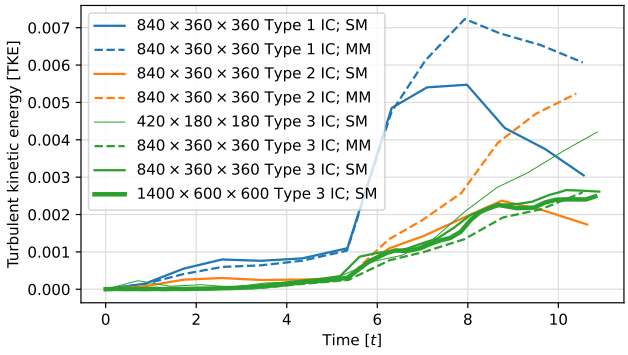

Figure 2: TKE for various runs with different initial conditions in Figure 1; perturbation level typically involved 1% of the corresponding mean initial values: *Type 1:* mass−density gradient 3D perturbations in the interface separating the two horizontal slabs, with variations only in the x_3 direction. *Type 2:* mass−density gradient 3D perturbations in the interface separating the two horizontal slabs, with variations in both x_1 and x_3 directions. *Type 3:* 3D perturbations in the pressure field in the high pressure region on the left.

For each set of initial conditions, bulk turbulence statistics (e.g. TKE) are postprocessed and compared. Several cases are shown in Figure 2. We found that multimode perturbations did not yield significantly different results from comparable single mode perturbations, and the most effective perturbations for promoting transition were of the *Type 1* kind.

Mesh sensitivity study for an arbitrary case (*Type 3* initial conditions) was performed. TKE plots for 3 different meshes (in each case the grid spacing was approximately halved) are also shown in Figure 2, we note that the plots nearly collapse for the finer meshes, thus demonstrating convergence. We were interested in observing the development of the flow, in particular the flow dynamics (comparison with 2D case) and vortical structures prior to reshock. Our findings are consistent with the theoretical relation between vorticity $\boldsymbol{\omega}$ and the gradients in the density ρ and pressure p, namely $\frac{D\boldsymbol{\omega}}{Dt} \propto \frac{1}{\rho^3}\nabla\rho \times \nabla p$. At early times we observe vorticity being deposited along the slip−sheet in the post−shock regions, and a slightly less on the main roller head. At late times, we see the nonlinear effects start to take over and the formation of vortical ribs aligned vertically. It is the interaction of the reshock with these structures, stretching and deforming them, which triggers transition to turbulence.

Turbulent mixing is studied using two species segregated in the initial condition, using multi−component mixture transport with constant properties (chemical effects are ignored). The mass fractions are plotted below at different times in Figure 3. A mixing indicator function is used to quantitatively measure the evolution of bulk mixing, and it was observed that the resulting trend follows the ones for TKE and enstrophy quite closely.

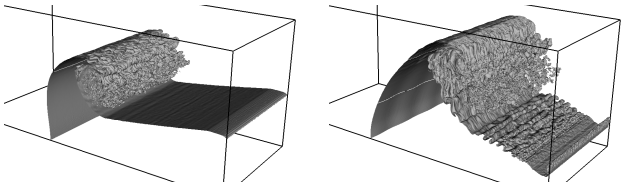

Figure 3: Mass fractions prior & post reshock for *Type 3* case.

Acknowledgements: The authors would like to thank Stanford's INSIEME project under PSAAP III supported by the DOE, NNSA under Award Number DE-NA0003968. They would also like to thank Stanford's HPCC center for providing access to computing resources and HTR's [3] code development team for multiple fruitful discussions.

References

[1] V. D'Yachenko, "A new method for the numerical solution of nonstationary problems of gas dynamics with two spatial variables," *Zh. Vychisl. Mat. Mat. Fiz.*, vol. 5-4, pp. 680–688, 1965.

[2] M. Bauer, S. Treichler, E. Slaughter, and A. Aiken, "Legion: Expressing locality and independence with logical regions," in *Int. Conf. High Perform. Comput.*, IEEE, 2012, pp. 1–11.

[3] M. Di Renzo, L. Fu, and J. Urzay, "HTR solver: An open-source exascale-oriented task-based multi-GPU high-order code for hypersonic aerothermodynamics," *Comput. Phys. Commun.*, vol. 255, p. 107 262, 2020.

Implicit large Eddy Simulations and Analytical Modelling of Shock-Induced Turbulent Mixing in Spherical Implosions

Moutassem El Rafei[1] and Ben Thornber[1,*]

[1]School of Aerospace, Mechanical and Mechatronic Engineering, The University of Sydney, NSW 2006, Australia

[*]**Corresponding Author: ben.thornber@sydney.edu.au**

Compressible turbulent mixing evolving from Richtmyer–Meshkov and Rayleigh–Taylor instabilities and Bell–Plesset effects has been investigated using high-resolution implicit large eddy (ILES) simulations of fundamental spherical implosion problems. Turbulent mixing in spherical geometries has been studied to a lesser extent compared to planar geometries which has been extensively investigated in the literature. however, planar cases lack the effect of geometric convergence that changes the growth of perturbations in spherical geometries. Moreover, the experimental diagnosis in many spherical compressible mixing applications is very challenging due to the extreme mixing environment. Thus, numerical simulations are important to further understand the effect of instabilities on the mixing process in a wide variety of turbulent mixing in spherical geometries applications, such as inertial confinement fusion (ICF).

For that purpose, high-resolution spherical algorithms have been designed carefully to study accurately the physics of mixing in spherical geometries. The choice of spherical coordinates is important to avoid unphysical perturbations that are introduced when studying such problems with non-spherical solvers. A semi-Lagrangian moving mesh algorithm is implemented to move the mesh and cluster the nodes within the mixing layer for a better resolution of the different length scales involved. The different algorithms were validated against benchmark test cases that are typically used for the validation of hydrodynamic codes, including the Sod shock tube problem, the Sedov blast and Noh problems. The numerical methods used here showed higher level of performance against non-moving and non-spherical (solving Cartesian momenta) algorithms.

Multimode narrowband (NB) and broadband (BB) initial perturbations consisting of spherical harmonics and multimode cosine perturbations are considered. A high Atwood number (At = 0:9) corresponding to a density ratio of 20 is examined and the implosion model corresponds to a moderate convergence ratio Cr = 3:6. This model approximates the late non-linear stages of the ICF process. Fig. 1 shows a visualization of the three-dimensional problem which is represented in the contours of distribution of volume fraction within the mixing layer in the NB and BB cases at different times of the implosion. This figure shows the evolution of the mixing layer in time and the growth of the perturbations due to the passage of the shock waves at the interface.

Several integral growth quantities, mixedness parameters and turbulence statistics are presented to provide a detailed understanding of the mixing process and the effect of the initial spectrum of perturbations on the subsequent mixing. Furthermore, this research is one of the few efforts to examine turbulent transport and budgets of turbulent kinetic energy, turbulent mass flux and density self-correlation, considering high-Atwood spherical implosion configurations and different initial perturbations spectra. The budgets are investigated while also quantifying the contribution from numerical dissipation and diffusion to the transport equations. This is important for the understanding of transition to turbulence and asymmetries across the mixing layer and for the validation of Reynolds-averaged closure models.

Different analytical mix models have been developed for the prediction of mixing layer growth and amount of mixing that occurs. The first model, denoted as the Bell-Plesset model, is an extension of a single mode perturbation growth model, that is based on small amplitude and linear growth assumptions, to multimode perturbations and reshocks. The results showed that this model was in good agreement with simulations as long as the long wavelength perturbations were not saturated. Bubble and spike growth is modelled using a Buoyancy-Drag (BD) approach that uses ordinary differential equations to model the different stages of the mixing process. Modification to the BD model are applied to introduce an effective length scale in the drag term to consider the initial conditions and early stages of the mixing process. The BD model was adapted to the spherical implosion case considered here and the effect of geometric convergence was also added to the model. The BD model results showed a very good agreement with the NB and BB results before and past reshock, proving the ability of this model to accurately estimate the different stages of the mixing process.

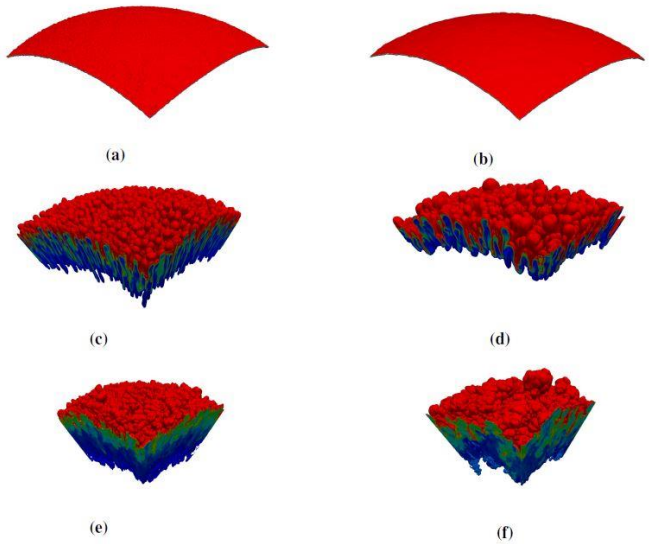

Figure 1: Iso-surfaces of mass fraction showing the mixing layer evolution at different times (t=0, 1.8 and 2.5 ns) in both the BB (b,d,f) and NB (a,c,e) cases.

High-resolution front tracking simulations of single-mode Richtmyer-Meshkov Instability

Tulin Kaman[1,*]

[1] Department of Mathematical Sciences, University of Arkansas, Fayetteville, AR 72701 USA

[*]**Corresponding Author: tkaman@uark.edu**

Turbulent mixing due to hydrodynamic instabilities occurs in a wide range of science and engineering applications. The experimental, theoretical, and numerical studies help us to understand the dynamics of hydrodynamically unstable interfaces between fluids [1,2]. In this paper, we present an increasingly accurate and robust front tracking method for the numerical simulations of Richtmyer-Meshkov Instability (RMI) to estimate the growth rate, V_{RM} ,

$$V_{RM} = kh_0 A\Delta U \qquad (1)$$

where k is the wave number, h_0 is the initial perturbation amplitude, A is the Atwood number and ΔU is the interface velocity [3].

The simulations based on the classical fifth order weighted essentially non-oscillatory (WENO) scheme of Jiang and Shu [4] with Yang's artificial compression [5] are compared with Collins and Jacobs (2002) [6] shock tube experiments. We investigate the effects of incident shock strength on the two-dimensional RMI of an air/SF_6 interface using front tracking method [7] and fifth order WENO scheme. The stable and high order WENO schemes are widely used in turbulent mixing [8]. The front tracking (FT) is a way to track the interface explicitly with high order accuracy. FT is a unique method to avoid systematic errors in an important class of problems around turbulent mixing [9, 10, 11]. This technique stores and dynamically evolves a meshed front that partitions a simulation domain into two or more regions, each representing a different material or physics mode.

For validation study, the model and input parameters used in our two-dimensional (2D) RMI simulations are set according to Collins and Jacobs shock tube experiments [6] for the Mach number $M = 1.11$ and $M = 1.21$. The parameters that are not specified in the experiments are set according to Latini, Schilling and Don's numerical studies [12]. While validation is through comparison to experiments, verification is through mesh refinement. The fine grid simulations on a uniform grid that has 256 grid points per initial perturbation wavelength.

The accurate and robust front tracking simulations with the classical fifth order WENO scheme and artificial compression reveal agreement with experimental data. Our validation studies show excellent agreement between the fine grid simulation and the Mach number $M = 1.11$ experiments (see Figure 1 left). We observe 9% discrepancy on the early-time growth rate for the Mach number $M = 1.21$ experiments (see Figure 1 right). For high Mach numbers, we present new results that show high spatial resolutions are needed to reduce the discrepancy between simulation and experiments at late time. For Mach 1.21 air/SF_6 shock-tube experiments, FT simulation with 512 grid points per initial perturbed interface gives the best agreement between the simulation and experiment. The uncertainty quantification studies to investigate the effect of model and input parameters on the growth rate and model improvement to capture the vortices at the interface are under development.

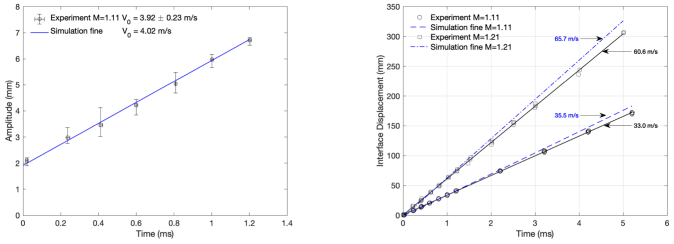

Figure 1: Comparison between experiments and simulations. Left: Amplitude at early time for $M = 1.11$. Each experimental data with error bar comes from five experiments of Collins and Jacobs. Right: Interface displacement and velocity for $M = 1.11, 1.21$.

Acknowledgments: It is a great pleasure to thank Dr. Jeffrey W. Jacob for providing experimental data for detailed comparison studies, Dr. James Glimm for many helpful comments and discussions. The author acknowledges support of the Lawrence Jesser Toll Jr. Endowed Chair at the Department of Mathematical Sciences in the Fulbright College of Arts & Sciences at the University of Arkansas. This research is supported by the Arkansas High Performance Computing Center which is funded through multiple National Science Foundation grants and the Arkansas Economic Development Commission.

References

[1] Y. Zhou, Physics Reports, **720-722**, 1 (2017).
[2] Y. Zhou, Physics Reports, **723-725**, 1 (2017).
[3] R.D. Richtmyer, Commun. Pure Appl. math., **13**, 297 (1960).
[4] G.S. Jiang and C.W. Shu, Journal of Computational Physics, **126**, 202, (1996).
[5] H. Yang, Ph.D. thesis, Dept. fo Mathematics, UCLA, (1988).
[6] B.D. Collins and J.W. Jacobs, Journal of Fluid Mechanics, **464**, 113, (2002).
[7] J.Glimm, J.W. Grove, X.-L. Li, K.-M. Shyue, Q. Zhang, and Y.Zeng, SIAM J. Sci. Comput., **19**, 703, 1998.
[8] C.W. Shu, Acta Numerica, 29, 701, (2020).
[9] J. Glimm, B. Cheng, D.H. Sharp, and T. Kaman, Physica D: Nonlinear Phenomena, **404**, 132346, (2020).
[10] J. Glimm, D.H. Sharp, T. Kaman, and H. Lim, Phil. Trans. R. Soc. A, **371**, 20120183, (2013).
[11] H. Zhang, T. Kaman, D. She, B. Cheng, J. Glimm, and D. H. Sharp, Pure and Applied Mathematics Quarterly, **14**, 193, (2018).
[12] M. Latini, O. Schilling, and W.S. Don, Journal of Computational Physics, **221**, 805, (2007) .

Ejection of vortex rings from shock-accelerated interfaces

Michael Wadas[1,*] and Eric Johnsen[1]

[1]University of Michigan, Ann Arbor, MI, USA

[*]**Corresponding Author: mwadas@umich.edu**

The mixing that results from the passage of a shock wave through an interface separating two dissimilar fluids is of critical importance in many scientific and engineering applications including astrophysics, inertial confinement fusion (ICF), and scramjet combustion [1]. Due to the misalignment of the pressure gradient, which points normal to the shock wave, and the density gradient, which primarily points normal to the interface, baroclinic vorticity is deposited onto the interface and causes perturbations to grow in a process known as the Richtmyer-Meshkov instability (RMI) [2]. As the instability progresses, the mixing becomes increasingly complex and may eventually develop into a state of asymptotic turbulence, though many questions about the conditions required to achieve such a state remain [3].

Though they have long been observed in shock-accelerated flows, the effects of vortex rings on the development of the RMI have only recently been explored. In addition to providing a precise mechanism that may explain the emergence of stellar core material in the outer layers of supernova remnants [4] and their importance in ICF fill-tube dynamics [5], vortex rings may more generally affect the development of the RMI through their propensity to transport energy out of the fluid mixing region, possibly inhibiting the transition of the flow to a turbulent mixing state [6].

While the importance of vortex rings in RMI flows is only beginning to be understood, their behavior in a more classical context (e.g., vortex rings generated with a piston-cylinder device submerged in water) is well established. Their scaling is based on principles of impulse, circulation, and energy conservation such that those properties are fully saturated for a ring generated by the ejection of a column of fluid with a length-to-diameter aspect ratio of $(L/D)_{sat} \approx 4$, known as the formation number, through an orifice [7].

Our objective is to uncover the mechanism for the formation of vortex rings and determine their scaling in RMI flows. Analogous to the classical literature [7, 8], we consider rings generated by the shock-acceleration of an interface separating light and heavy fluids along which there is a hole of depth L and diameter D filled with the heavy fluid. The passage of the shock from the heavy fluid to the light fluid causes the hole to invert and eject a vortex ring back into the heavy fluid. Consistent with classical studies, we find that, for small L/D, the circulation of the ejected ring increases with increasing L/D, but beyond a critical $(L/D)_{sat}$, the circulation, along with the energy and impulse, saturate, as shown in fig 1 for four sets of eight simulations each varying the hole depth for different shock strengths and interface density ratios.

We develop a model for the formation number that extends the conservation principles of the classical literature [8] with additional parameters obtained analytically from one-dimensional gas dynamics theory. We find that the formation number of such rings is related to the classical formation number by a parameter, σ, which is a function of the shock strength and interface density ratio. The inset of fig 1 shows that the formation number inferred from simulations agrees with the prediction of our model, given in units of 3.8σ.

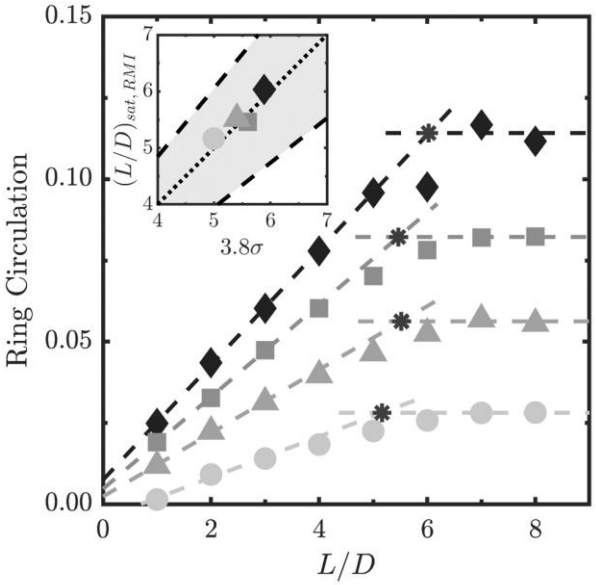

Figure 1: The vortex ring circulation versus the initial hole aspect ratio for four sets of simulations with different shock strengths and interface density ratios. The * shows the inferred formation number for each set, which is compared to the prediction of our model in the inset. The shaded region bounded by the dashed lines shows the predicted formation number range in terms of the classically reported range of $3.0 < (L/D)_{sat} < 4.6$ [7, 8].

Acknowledgments: This work is supported by the Lawrence Livermore National Laboratory under Subcontract No. B632749 and the U. S. Department of Energy (DOE) as part of the Stewardship Science Graduate Fellowship Program under Grant No. De-NA0003960. Computational resources were provided by the Extreme Science and Engineering Discovery Environment Comet system, USA under grant TG-CTS130005 and the Oak Ridge Leadership Computing Facility, a DOE Office of Science User Facility supported under Contract DE-AC05-00OR22725.

References

[1] Y. Zhou, Phys. Rep. **720-722**, 1 (2017).
[2] E. Meshkov, Fluid Dyn. **4**, 101 (1969).
[3] E. Swewll et al., J. Fluid Mech. **917**, A41 (2021).
[4] T. Dotani et al., Nature (London) **330**, 230 (1987).
[5] B. Hammel et al., Phys. Plasmas **18**, 056310 (2011).
[6] B. Thornber et al., Phys. Rev. E **86**, 056302 (2012).
[7] M. Gharib et al., J. Fluid Mech. **360**, 121 (1998).
[8] K. Mohseni et al., Phys. Fluids **10**, 2436 (1998).

On the stability of non-isolated steady shock waves

Andrés Calvo-Rivera[1], César Huete[1,*], Gustavo Wouchuk[2], and Alexander L. Velikovich[3]

[1]Grupo de Mecánica de Fluidos, Dpto. de Ingeniería Térmica y de Fluidos, Universidad Carlos III de Madrid, 28911, Leganés, Spain.
[2]Universidad de Castilla-La Mancha (retired), 13071 Ciudad Real, Spain.
[3]Plasma Physics Division, Naval Research Laboratory, Washington, DC 20375, USA.

[*]**Corresponding Author: chuete@ing.uc3m.es**

The studies of shock compression and shock-front stability started simultaneously in the 1940s within nuclear weapons projects. Notwithstanding the impressive progress made in both fields since then, the fundamental shock-front instability theoretically discovered by D'yakov [1] and Kontorovich [2] (DK) still challenges the understanding of shock compression, since the associated unstable range typically lies outside the conventional gas dynamics realm.

What is well established is the small-amplitude theory for planar isolated shocks: for $-1<h<h_c$, where h is the DK parameter, h_c is its critical value corresponding to the onset of the instability, any small perturbation on the shock shape will decay in time with the power law $t^{-3/2}$ ($t^{-1/2}$ in the strong-shock limit). For $h_c<h<1+2M_2$, a simple Fourier analysis dictates the perturbed shock will evolve with constant-amplitude oscillations in the long time, with the associated spontaneous acoustic emission (SAE). This analysis stems from the fact that the perturbation-free solution is steady, which implies the presence of a supporting mechanism (typically a solid piston) driving the shock. However, for the isolated-shock configuration to be practical, the shock must be sufficiently far from the piston, which translates into paradoxically assuming that the shock is stable, even in the range $h_c<h<1+2M_2$. Then, we can safely conclude that Fourier analysis is not sufficient for the stability of steady (i.e., supported) planar shocks. We must solve an initial-value problem (IVP) instead.

Previous works devoted to shed light on the IVP arrived at different conclusions. The stability analysis in Ref.[3] did not find any qualitative distinctness in the shock front perturbation behavior for $h_c<h<1-2(M_2)^2$, beyond the fact that the shock oscillates with multiple frequencies because of the acoustic reverberation and the Doppler shift effect. On the other hand, Ref.[4] found instability, a linear growth of shock perturbations in the whole range $h_c<h<1+2M_2$. Then, up to date there is no clear consensus about the shock dynamics in the marginally stable/SAE range when a supporting mechanism is considered.

In this work, we present an analytical and numerical work on the shock stability in either planar, cylindrical, and spherical configurations, where the corresponding eigenvalues associated with the shock perturbation growth rate are analyzed in detail. For expanding steady shocks, we have found that the DK instability of cylindrical and spherical shock waves drives a power-law growth of shock ripples and the associated flow perturbations in the range deemed marginally stable in the classic theory [5]. The difference between this case and the classic case of isolated planar shocks is due to the consideration of the supporting mechanism, here represented with the center of symmetry (2D) or center (3D). Per the planar piston-driven shock problem, our latest results obtained via numerical integration of the Euler equations by the method of characteristics, with the linearized RH equations being analytically provided, suggest that the shock is effectively unstable in the rage $h_c<h<1+2M_2$. We find that shock perturbations grow in time with a power law that depends on shock properties, in consonance with the results given by the Noh problem [5] and in contraposition with previous works. The numerical solution has been previously validated with known analytical solutions for $-1<h<h_c$ and via mesh.

Figure 1 shows the numerical solution of the shock pressure perturbations as a function of the dimensionless time in log scale, with different distinguished values of the DK parameter and for a piston-driven planar shock. It is observed that for the stable range, $1<h<h_c$, the qualitative evolution of the shock front is the same as that found in isolated-shock conditions. This is an expected result since the amplitude of the pressure perturbations in this range decays exponentially with the distance from the shock, thereby making the acoustic coupling ineffective in the long time. For the SAE range, however, there is a distinct evolution when the piston is involved: perturbations seem to grow with time and the growth rate is not linear. We are still working in providing the analytical expression for the growth rate and we are confident that results will be ready at the time the conference is held.

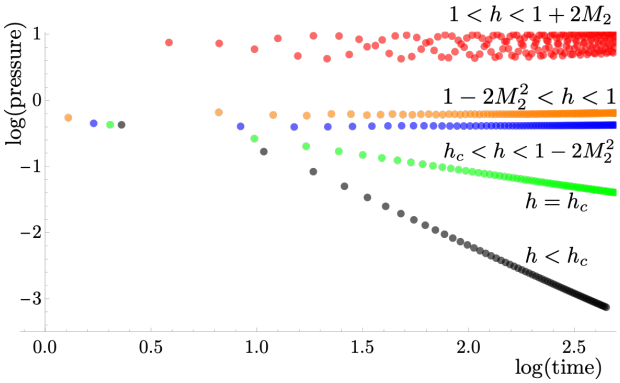

Figure 1: Shock pressure perturbations vs time.

Acknowledgments: A.C.R and C.H. work has been supported with projects PID2019-108592RB-C41 (MICINN/FEDER, UE) and (H2SFE-CM-UC3M). A.L.V. work has been supported by the National Nuclear Security Administration of the U.S. Department of Energy.)

References

[1] S. D'yakov, Zh. Eksp. Teor. Fiz 27, 288 (1954).
[2] V. Kontorovich, Zh. Eksp. Teor. Fiz 33, 1525 (1957).
[3] J. Wouchuk and J. L. Cavada, Phys. Rev. E 70, 046303 (2004).
[4] J. Bates, Physical Review E 91, 013014 (2015).
[5] C. Huete, A. L. Velikovich, D. Martínez-Ruiz, and A. Calvo-Rivera, J. Fluid Mech. 927, A35 (2021).

Shock Acceleration of a Multifluid Vortex Ring

Alex Ames*, Chris Noble, Ray McConnell, Jason Oakley, David Rothamer, Riccardo Bonazza

Department of Engineering Physics, University of Wisconsin-Madison, Madison, Wisconsin, U.S.A.

***Corresponding Author: aames@wisc.edu**

Vortices are a well-known mechanism of transport across stratified interfaces. When repeatedly shocked, preexisting vorticity-driven deformation of the interface provides greater leverage for baroclinic torque under subsequent acceleration. The locally axisymmetric baroclinic vorticity deposition is a primary source in the turbulent energy cascade, leading to anisotropically-oriented eddies at the inertial scale, producing deleterious interfacial mixing. In particular, the assembly of a uniform fusion hotspot in inertial confinement fusion capsules is disrupted by the protrusion of a cold vortical bubble arising from the remains of the fill tube [1].

More generally, during the intermediate stages of Richtmyer-Meshkov instability development prior to the onset of turbulence, vortical flow structures are commonly observed at the outer extents of the mixing region. The evolution of these structures upon reshock may play an important role in the tails of the mixedness distribution, but they are difficult to study repeatably because of the inherently unstable mixing process. To capture these vortex-shock interaction events in isolation, an ensemble of simultaneous PLIF/PIV measurements were acquired at 20 kHz following the firing of a small, open-ended, argon-filled shock tube upwards into ambient nitrogen, a configuration known to produce isolated vortex rings [2]. The measurements capture the initial propagation of the argon vortex ring as well as its perturbation upon interaction with a M = 1.75 shock and subsequent reshock.

In parallel, computations of an equivalent set of shock-vortex interaction have been conducted using the *MIRANDA* hydrodynamics code. From these experimental and computational data, vortex evolution, baroclinic production during and following shock interaction, behavior of secondary vortices, and mixing intensification are detailed across a range of vortex strengths and Atwood & Mach numbers.

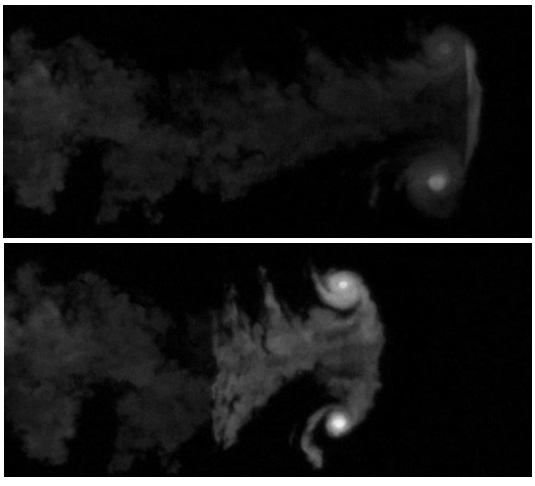

Figure 1: Planar laser-induced fluorescence image of an argon vortex ring during and following shock interaction.

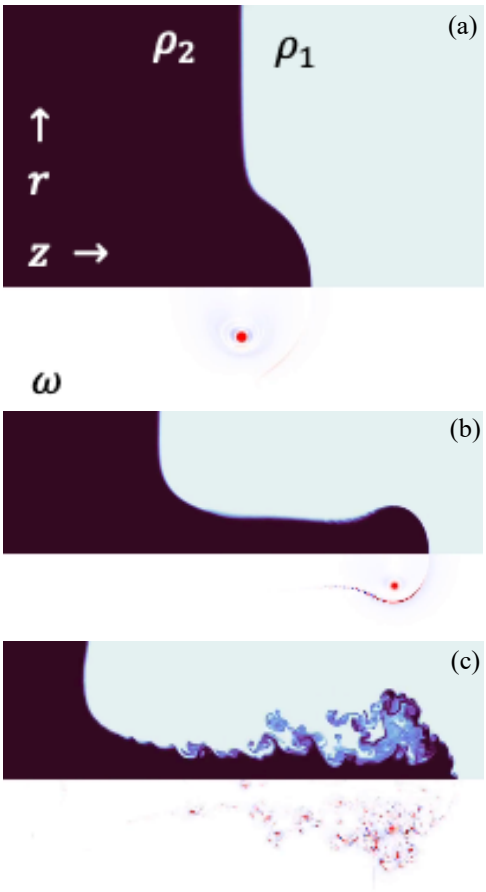

Figure 2: *MIRANDA* simulation of shock-vortex interaction. (a) Propagation of a compressible vortex ring from argon into helium. (b) Late-stage vortex-driven interface growth. (c) Disintegration of interface following shock interaction.

Acknowledgments: Support was provided by NSF Grant #1939809. Portions of this work were performed under the auspices of the US Department of Energy by Lawrence Livermore National Laboratory under Contract DE-AC52-07NA27344.

References

[1] G.R. Bennett *et al.*, PRL **99**, 205003 (2007).
[2] F.K. Elder, N. De Haas, J. Appl. Phys. **23**, 10, 1065 (1952).

Investigating high-speed velocity measurements in the Blast-Driven Instability

Samuel J. Petter[1], Dr. Benjamin C. Musci[1], Dr. Gokul Pathikonda[2], and Dr. Devesh Ranjan[1*]

[1]Georgia Institute of Technology, Atlanta, Georgia,
USA [2]Arizona State University, Tempe, Arizona, USA
[*]Principle Investigator

[*]**Corresponding Author: devesh.ranjan@me.gatech.edu**

The Rayleigh-Taylor (RT) and Richtmyer-Meshkov (RM) hydrodynamic instabilities share no shortage of interest due to their presence in a variety of engineering applications like fuel/pellet mixing in inertial confinement fusion, as well as natural phenomena. The combination of these two instabilities are of interest to astrophysicists studying supernova-type mixing, as the RT & RM instabilities are thought to contribute to mass from the core being ejected.

The Blast Wave Facility at Shock Tube and Advanced Mixing laboratory aims to resolve the important spatial-temporal scales of hydrodynamic mixing at a laboratory scale in the blast-driven instability. Statistical description of turbulent mixing from these experiments will offer models an experimentally validated parameter set for estimations of variable density turbulent mixing in such flows, such as in outer layer evolution of supernovae. The facility uses a blast wave generated from a "point-source," which is used to induce mixing between two fluids (N_2/CO_2) forming a stably stratified interface. As the blast wave interacts with the interface, the combined RMI and RTI growth from a blast-wave can be observed in a cylindrical geometry.

To better understand the development of the mixing as it pertains to its initial conditions, this work discusses ensembles of stochastic interface conditions driven impulsively by blast waves. Dynamics of blast driven instability are investigated using high-resolution high-speed particle image velocimetry (1Mpix, 4.75kHz, PIV), where vector resolution of 0.8 mm per vector is achieved (Fig. 1 and 2). Implementing PIV gains a quantitative understanding of the development of the velocity field on spatial scales where dissipative effects become important.

Post-PIV analysis includes a comparison to vorticity models, and the development of probability density function of velocity fluctuations in time. Additionally, the progression of positive and negative circulation is examined alongside the velocity and acceleration of the mixing region where the turbulence intensity is highest. Furthermore, the transition to turbulence and its corresponding vorticity (Fig. 3) and the positive/negative circulation of the flow-field will be examined.

Estimations of the turbulence intensity (TI) are made from velocity fluctuations; from this, a dominant trend in the temporal evolution of the turbulence intensity is observed. The turbulence intensity at the interface of the Blast Driven Instability is found to be proportional to the mixing width growth rate. Additionally, the growth rate parameter, Θ, is found to be 0.49 during its late-time nonlinear growth.

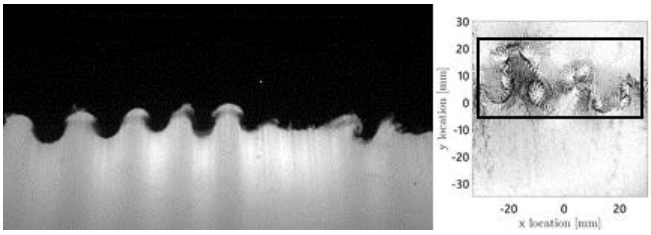

Figure 1: Transition in diagnostics from Mie scattering to vector fields from PIV.

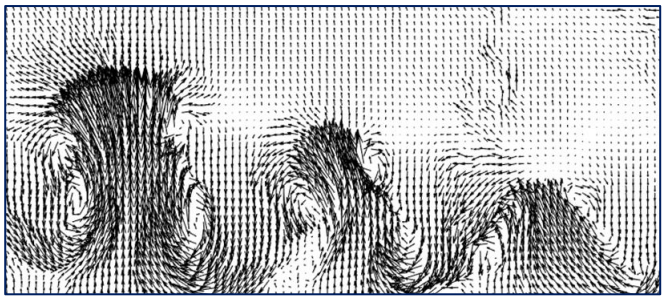

Figure 2: Enlarged vector field showing bubble/spike pairs forming the mixing width

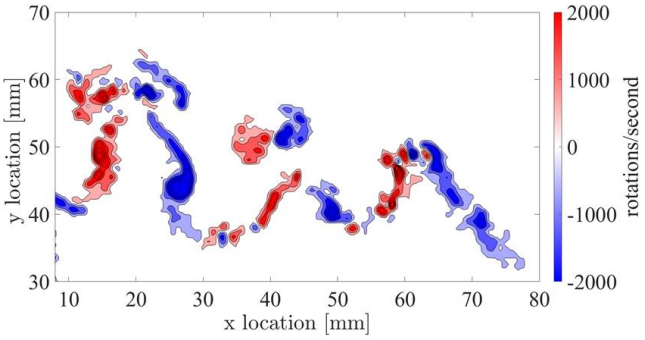

Figure 3: Colormap of calculations of vorticity (curl of velocity) from vector fields.

Acknowledgments: We thankfully acknowledge support from the U.S. DOE for funding this research in the form of grant DE-SC0016181.

References

[1] Musci, B., Petter, S., Pathikonda, G., Ochs, B., & Ranjan, D. (2020). Supernova hydrodynamics: A lab-scale study of the blast-driven instability using high-speed diagnostics. *The Astrophysical Journal*, *896*(2), 92.

[2] Remington, B. A., Kane, J., Drake, R. P., Glendinning, S. G., Estabrook, K., London, R., ... & Fryxell, B. (1997). Supernova hydrodynamics experiments on the Nova laser. *Physics of Plasmas*, *4*(5), 1994-2003.

[3] Kuranz, C. C., Park, H. S., Huntington, C. M., Miles, A. R., Remington, B. A., Plewa, T., ... & Drake, R. P. (2018). How high energy fluxes may affect Rayleigh–Taylor instability growth in young supernova remnants. *Nature communications*, *9*(1), 1-6.

Influence of the Shock-To-Reshock Time on the Richtmyer-Meshkov Instability in a Dual-Driver Vertical Shock Tube

K. J. Ferguson[1,*] and J. W. Jacobs[1]

[1]The University of Arizona, Tucson, Arizona, United States of America

[*]**Corresponding Author: kjfergus@email.arizona.edu**

1. The Dual-Driver Vertical Shock Tube (DDVST)

Experiments on the Richtmyer-Meshkov Instability in the Dual-Driver Vertical Shock Tube (DDVST) conducted at the University of Arizona are presented. The layout of the DDVST is presented schematically on the left side of Fig. 1. The DDVST is a 10 m long shock tube that consists of two vertically opposed drivers (A,F) and driven (B,E) sections oriented on opposite sides of a 1 m test section (C,D) in which an initially stationary interface is formed utilizing the method of Jones and Jacobs [1]. The gas column is vertically oscillated using two voice coil actuators to form random, multi-modal Faraday waves on the interface. The pressurized drivers are separated from the driven sections by thin polypropylene diaphragms. The region above the interface (B,C) is filled with the light gas, Air, and the region below the interface (D,E) is filled with the heavy gas, Sulfur Hexaflouride (SF_6). The experiments presented here use a light gas shock Mach number of $M_L = 1.2$ and with a heavy gas shock Mach number $M_H = 1.23$ chosen to arrest mean interface motion after the second shock wave arrival. The mixing region is illuminated using a 70 W 527 nm Nd:YLF laser.

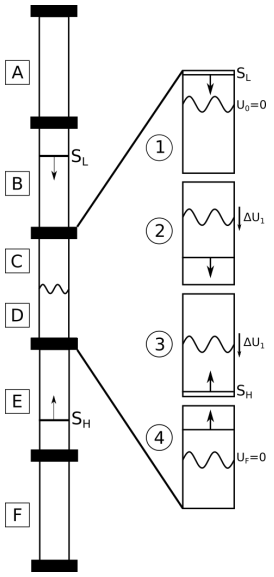

Figure 1: Schematic Layout of the DDVST (Left) along with example experimental progression (Right)

2. Experimental Configuration

The present work utilizes a set of 4 APX-RS Fastcam High Speed Cameras oriented in a 4x1 grid (See Figure 2) for imaging. Experiments are conducted with a range of shock-to-reshock times, and in both a traditional light shock first, and a heavy shock first configuration. The cameras are operated at a frame rate of 1500 Hz in double frame mode with 100 μs inter-frame time for the PIV diagnostic. The frame rate was chosen to allow the cameras to operate at their maximum resolution of 1024x1024 pixels. This results in a final vector spacing of 0.37 mm. Vegetable glycerin droplets with a mean diameter of approximately 2 μm are seeded into both test gasses to serve as the tracer particle.

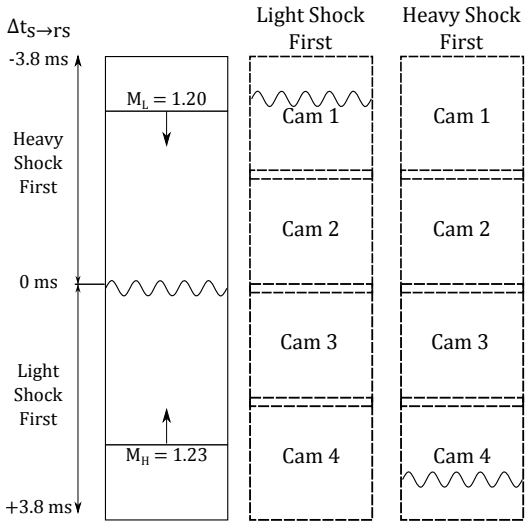

Figure 2: Illustration of camera layout with the initial condition. Dashed lines indicate regions where camera views overlap

3. Results

Analysis of the growth of the RMI as well as characteristics of the turbulent mixing zone are presented. The influence of the shock-to-reshock time on the values of these parameters is examined. Quantities of interest include the value of the growth exponent, θ, the rate of decay of turbulent kinetic energy and its relationship to the value of the growth exponent [2], the anisotropy ratio of the mixing region, and the spectral distribution of scales in the mixing region versus time.

Acknowledgments: The authors would like to acknowledge the support of Department of Energy NNSA/SSAA Grant Number DE-NA0003903 for funding this research.

References

[1] Jones, M. A. and Jacobs, J. W. 1997. “A membrane less experiment for the study of Richtmyer-Meshkov Instability of a shock-accelerated gas interface.” Physics of Fluids **9**, pp. 3078–3085.

[2] Thornber, B. 2010. "The influence of initial conditions on turbulent mixing due to Richtmyer-Meshkov instability.". J. Fluid Mech **654**, pp 99-139.

Shocked Variable-Density Turbulence Studies

Tiffany Desjardins[1,*], Erin Connor[1], Adam Martinez[1], and John Charonko[1]

[1]Los Alamos National Laboratory, Los Alamos, NM, USA

[*]**Corresponding Author: tif_des@lanl.gov**

Supernova and inertial confinement fusion (ICF) implosions involve mixing and turbulent flows between different fluids. These mixing flow are subjected to shocks, which are expected to have effects on the mixing. The effect of shock-turbulence interactions (STI) have been well studied experimentally in single fluids [1]; these studies have shown that STI can affect the velocity and turbulent length scales, which could have important effects on mixing in a variable-density setting. However, STI in a variable-density setting has only been studied via limited simulations [2]. Tian *et al.* found in their simulations that the shock had stronger effects in a variable density setting than in a single fluid scenario, leading to much larger velocity fluctuation and smaller characteristic length scales.

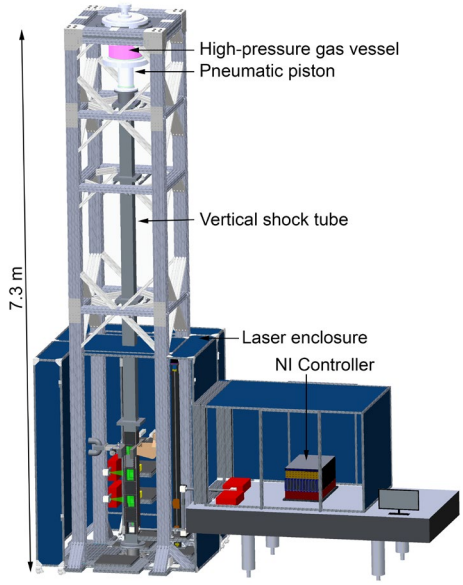

The Vertical Shock Tube (VST) at Los Alamos National Laboratory is a 7-m tall traditional shock tube with a piston driver. The VST is able to take over fifty shows a day, enabling large collection of shocked data for ensemble averaging to study turbulent statistics. The VST using an air-SF6 combination to study variable-density mixing and turbulent interactions. Both gases are seeded with 1-um size olive oil particles and illuminated with 1-mm thick 532-nm laser sheet to perform particle image velocimetry (PIV). Resulting images are processed to obtained 2D velocity fields. A single gas is seeded with acetone vapor, which is excited with a 266-nm laser sheet, leading to a 2D density field.

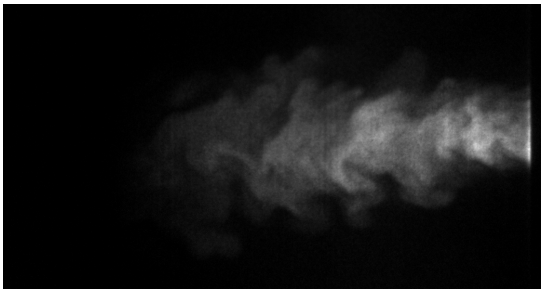

In order to study STI, pipe flow is used to create an SF6 jet seeded with acetone into a stagnant air background. To define our system as turbulent, we use the definition of the Reynold's number for a jet flow [3]:

$$Re = \frac{\rho u L}{\mu} \geq 10{,}000 - 20{,}000 \quad (1)$$

and the turbulent Reynold's number:

$$Re_\lambda = \frac{\rho u' \lambda}{\mu} = \frac{u'^2}{\lambda^2} \geq 100 - 140 \quad (2)$$

where ρ is the fluid density, u is the fluid velocity, L is a characteristic length, in this case the diameter of pipe used to generate the jet, and μ is the fluid viscosity. Prime indicates the fluctuating value, and λ is the Taylor microscale calculated from the experimental results.

Single fluid studies suggest that the Reynold's number of the turbulence, as well as the shock strength, may change the STI. In order to test this, we are able to adjust our setup from a weakly turbulent regime (Re ~ 10,000) to a strongly turbulent regime (Re>50,000). We are also able to adjust our shock speed, and obtain Mach numbers up to M = 1.5 in air. Our initial studies focus on a single Mach number, M~1.25, and focus on the effect of the Reynold's number. This talk will cover current progress and results to date.

Acknowledgments: Research presented in this presentation was supported by the Laboratory Directed Research and Development program of Los Alamos National Laboratory under project number 20210601ECR.

References

[1] Andreopoulos Y, Agui JH, Briassulis G. *Annual Review of Fluid Mechanics.* 2000;32(1):309-345

[2] Tian Y, Jaberi FA, Li Z, Livescu D. 2017;829:551–588-551–588

[3] Dimotakis, P. J. Fluid Mech. 409 (2000)

Experimental study of the Richtmyer-Meshkov instability in spherical geometry

M. Brasseur[1*], C. Mariani[1], D.C. Barros[1], G. Jourdan[1]
M. Vandenboomgaerde[2], D. Souffland[2]

[1] Aix Marseille Univ, CNRS, IUSTI, Marseille, France
[2] CEA, DAM, DIF, F-91297 Arpajon, France

[*]**Corresponding Author: mathieu.brasseur@univ-amu.fr**

When a shock wave propagates through a disturbed interface between different fluids, this interface becomes unstable and the Richtmyer-Meshkov instability (RMI) develops. This phenomenon has been widely investigated in the planar configuration. Recent investigations of the converging RMI were conducted in cylindrical geometry [1] using a conventional square section shock tube to explore the Bell-Plesset convergence effects [2, 3]. However, in the process of inertial confinement fusion (ICF), this instability occurs in spherical geometry. To the authors' knowledge, no canonical experimental study has been conducted for this case in a conventional shock tube. The aim of the present work is to investigate the RMI in 3D spherical geometry, following the experimental approach of Biamino *et al.* for the 2D configuration [4].

The first challenge in this project is to check whether the gas-lens method remains valid in the spherical case [5]. A new conical chamber coupled with an ellipsoidal 3D-printed grid acting as a gas lens is installed at the end of the small section shock tube T80 (see fig. 1). The trajectory and the shape of the shock wave are both monitored by planar Mie scattering coupled with a high-speed camera. A machine learning algorithm is used to correct the optical distortion of the cone, enabling the analysis of the shock focusing. Conserving the experimental parameters used in the previous 2D experiments, *i.e.* the gas combination (air / SF_6), the strength of the incident shock wave (M_{is} = 1.15), the half apex angle (15°) and the elliptical shape of the interface, we check the validity of this approach in the 3D case. A comprehensive validation test campaign will be presented during the workshop.

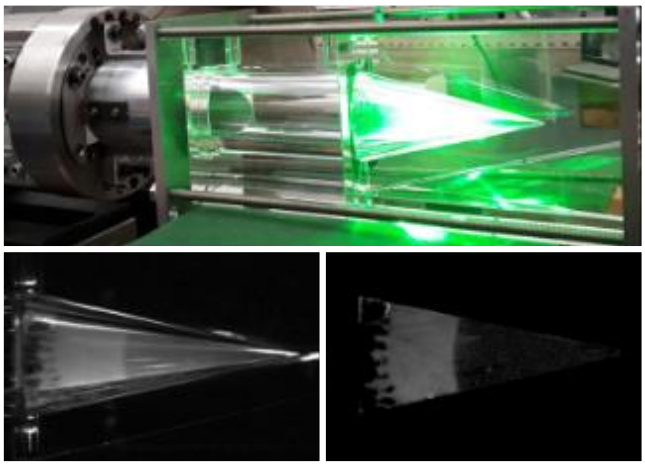

Figure 1: View of the convergent test section installed at the end of the 80x80 mm^2 square cross section shock tube T80 (upper part). Spherical converging shock wave recorded during its propagation in the conical chamber, before (left) and after (right) machine learning image processing (lower part).

The second challenge is to study the RMI by adding a second shaped interface within the downstream section of the cone. New investigations are being conducted on the larger T200 shock tube to optimize flight time and optical access (see fig. 2). During the conference, we will present pioneering experimental results conducted in a spherical configuration.

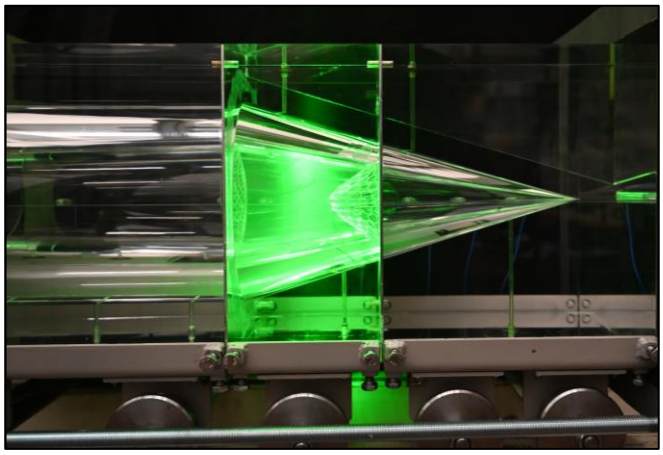

Figure 2: View of the conical test chamber implemented on the larger shock tube T200 (200x200 mm^2 square cross section).

Acknowledgments: This work is supported by CEA/DAM/DIF under contract #BACO/AJ-20-73/C37653.

References

[[1] M. Vandenboomgaerde, P. Rouzier, D. Souffland, L. Biamino, G. Jourdan, L. Houas, C. Mariani, Phys. Rev. Fluids, **3**, 014001 (2018).

[2] G.I. Bell, Los Alamos Scientific Laboratory Report No.LA-1321 (1951).

[3] M.S. Plesset, J. Appl. Phys., **25**, 96 (1954).

[4] L. Biamino, G. Jourdan, C. Mariani, L. Houas, M. Vandenboomgaerde, D. Souffland, Journal of Fluids Engineering, American Society of Mechanical Engineers, **136**, 10.1115/1.4026562, (2014).

[5] M. Brasseur, M. Vandenboomgaerde, C. Mariani, D.C. Barros, D. Souffland, G. Jourdan, Exp. Fluids, **62**(7), 1-8 (2021).

[6] C. Mariani, M. Brasseur, L. Biamino, D. Barros, G. Jourdan, L. Houas, M. Vandenboomgaerde, D. Souffland, P. Rouzier, Proc. Of the 32nd ISSW, Singapore (2019).

Local Wavenumber Model for Inhomogeneous Two-Fluid Mixing

Nairita Pal*, Ismael Boureima, Noah Braun, Susan Kurien, Praveen Ramaprabhu, Andrew Lawrie
Los Alamos National Laboratory, Los Alamos, NM 87545, USA
University of North Carolina – Charlotte, Charlotte, NC 28223, USA,
University of Bristol, University Walk, Clifton BS8 1TR UK

We present here a turbulence closure model to calculate density and velocity fluctuations of variable–density flows in a typical Rayleigh Taylor configuration. The model, known as the local wavenumber (LWN) model, is a two–point spectral closure model. The Rayleigh–Taylor instability is generated by the relaxation of a statically-unstable density stratification. Model outcomes are validated against data from 3D simulations of the RT instability. We compute the time-evolution of the spectral distribution in wave number k of the correlation of density and specific volume $b(k)$, the velocity associated with the turbulent mass flux $a(k)$, and the turbulent Reynolds stress $R_{nn}(k)$, along a number of horizontal layers of the system, using a set of coupled equations. We investigate two forms for a source term for the evolution of the spectrum of density–specific-volume covariance b for the LWN model. The first includes an empirically motivated calibration of the source to achieve the final asymptotic state of constant b. The second form does not require calibration but, in conjunction with enhanced diffusion and drag captures the full evolution of all the dynamical quantities, namely, the mix–layer growth, turbulent mass–flux velocity, Reynolds stress, as well as the desired behavior of b. This model is envisioned as a practical option for applications requiring multi-physics simulations in which statistical hydrodynamics quantities such as Reynolds stresses, turbulent kinetic energy, and measures of mixing such as density-correlations and mix-width evolution, need to be captured with relatively high fidelity ([1, 2, 3]).

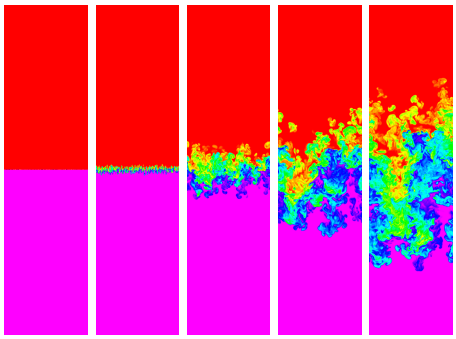

Figure 1: Visualization of the density field in the MOBILE simulation run `R3` at non–dimensionalized times (a) $\tau = 0$; (b) $\tau = 0.42$; (c) $\tau = 3.164$; (d) $\tau = 5.19$ and (e) $\tau = 6.5$; (f) schematic of the LWN system, with a slice-through visualization from 3D simulations at $\tau = 5.19$.

References

[1] S. Kurien and N. Pal, Philosophical Transactions of the Royal Society A **380**, 20210076 (2022).

[2] N. Pal, S. Kurien, T. Clark, D. Aslangil, and D. Livescu, Physical Review Fluids **3**, 124608 (2018).

[3] N. Pal et al., Physical Review E **104**, 025105 (2021).

*nairita@lanl.gov

Advances in Reynolds-averaged Navier-Stokes modeling for reacting turbulent mixing

Brandon E. Morgan[1,*]

[1]Lawrence Livermore National Laboratory, Livermore, CA, USA

[*]**Corresponding Author: morgan65@llnl.gov**

Summary

Turbulent mixing layers are encountered in a variety of physical systems, including oceanic and atmospheric flows, astrophysical phenomena, and in applications of inertial confinement fusion (ICF). When mixing occurs in the context of reacting turbulence, whether the reactions are chemical or nuclear in nature, accurate prediction of the statistics of scalar transport are vital to understanding the impact of turbulence on reaction rate [1].

In classical Rayleigh-Taylor (RT) mixing, two fluids mix when they are subject to an acceleration gradient that is opposite in direction to the mean density gradient. For problems of two-fluid mixing, second-moment statistics of a passive scalar can be characterized with a single scalar variance [1, 2]. In practical problems of engineering interest, however, it is frequently the case that more than two components will be involved in the mixing process. In the so-called "CD Symcap" ICF experiments, for example, tritium-filled capsules were surrounded by a silicon-doped plastic ablator, and a deuterated plastic (CD) layer was either placed against the tritium gas or recessed within the ablator by up to 8 μm [3]. In problems such as this, a single scalar variance is not sufficient to fully describe the multicomponent mixing process that occurs between the gas, the CD plastic, and the surrounding plastic ablator which acts as a non-reacting contaminant.

Since Reynolds-averaged Navier-Stokes (RANS) modeling remains a common tool for the design and analysis of ICF targets, the development and improvement of RANS models for variable density and reacting turbulent mixing remains a problem of significant interest. This talk will discuss some efforts by the author in recent years to improve RANS modeling approaches at Lawrence Livermore National Laboratory for problems of reacting turbulent mixing. Topics will include: development of the *k-L-a-V* RANS model and comparisons with large-eddy simulation (LES) of a reacting RT mixing layer in a spherical geometry [1]; improvement of the *k-L-a-V* model for prediction of scalar mixing in Kelvin-Helmholtz shear layers [2]; development of the *k-ϕ-L-a-V* RANS model to admit self-consistent, high-order spatial profiles [4]; and extension of the *k-L-a-V* and *k-ϕ-L-a-V* models for problems of reacting turbulence involving multicomponent mixing [5] such as the CD Symcap experiments.

Acknowledgments: This work was performed under the auspices of the U.S. Department of Energy by Lawrence Livermore National Laboratory under contract DE-AC52-07NA27344.

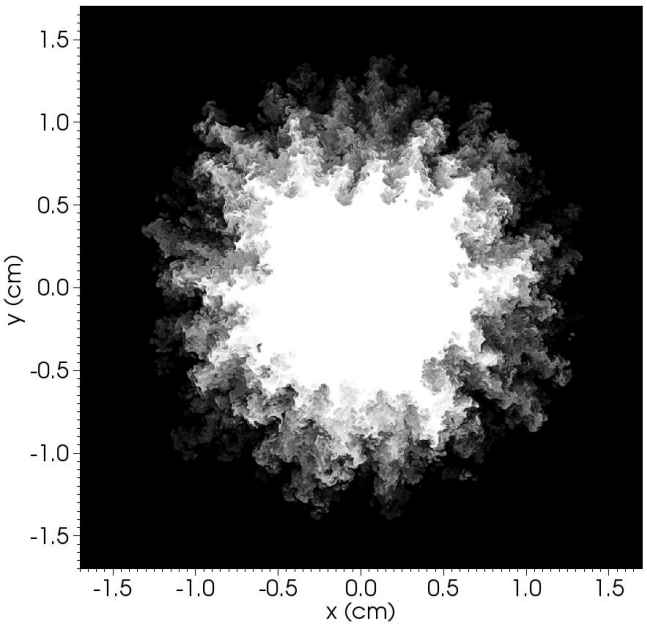

Figure 1: Slice of heavy material mass fraction (Y_H) contours at the onset of thermonuclear burn in spherical RT simulation from [1]. Contours are illustrated between $Y_H = 0$ (white) and $Y_H = 1$ (black).

References

[1] B. E. Morgan, B. J. Olson, W. J. Black, and J. A. McFarland, "Large-eddy simulation and Reynolds-averaged Navier-Stokes modeling of a reacting Rayleigh-Taylor mixing layer in a spherical geometry," Phys. Rev. E **98**, 033111 (2018).

[2] B. E. Morgan, "Scalar mixing in a Kelvin-Helmholtz shear layer and implications for Reynolds-averaged Navier-Stokes modeling of mixing layers," Phys. Rev. E **103**, 053108 (2021).

[3] D. T. Casey, V. A. Smalyuk, R. E. Tipton, *et al.*, "Development of the CD Symcap platform to study gas-shell mix in implosions at the National Ignition Facility," Phys. Plasmas **21**, 092705 (2014).

[4] B. E. Morgan, "Self-consistent, high-order spatial profiles in a model for two-fluid turbulent mixing," Phys. Rev. E **104**, 015107 (2021).

[5] B. E. Morgan, "Simulation and Reynolds-averaged Navier-Stokes modeling of a three-component mixing problem with thermonuclear burn," Phys. Rev. E. (under review).

Calibration of Local Wave-Number Turbulence Model using Machine Learning Techniques

Ismael Boureima, Vitaliy Gyrya*, Juan Saenz, Susan Kurien

Los Alamos National Laboratory, Los Alamos, NM, U.S
*Corresponding Author: vitaliy_gyrya@lanl.gov

Local Wave-Number (LWN) turbulence model is a two-point spectral turbulence closure model [1]. It aims to address the deficiency of single-point models, such as Reynolds-averaged Navier-Stokes (RANS) family of models with predicting phenomena such as strong transients and density variations since single-point models do not have information on the multiple scales generated by nonlinearities intrinsic to turbulence. Two-point model allows to retain information about scales through variable dependence on correlation between two distinct spatial points.

In the general settings LWN is a system of (nonlinear) differential equations

$$\frac{\partial}{\partial t}U = G[U;\theta] = G(U, U_x, U_{xx}, U_k, U_{kk};\theta) \quad (1)$$

for a state vector variable U with prescribed model form $G[U,\theta]$ dependent on a set of parameters θ. The model $G[U,\theta]$ is a nonlinear function of U and its first and second order derivatives in the physical space variable x and the frequency cross-correlation variable k.

The calibration problem consists of finding the optimal set of coefficients θ for which the model (1) results in the best fit to the ground truth data. In our case the ground truth data is coming from a set of canonical flows. Specifically, we consider direct numerical simulation (DNS) data for homogeneous variable density turbulence (HVDT) flows in a box with periodic boundary conditions in x and y directions and quasi-periodic boundary conditions in the (vertical) z direction. The turbulence is driven by gravity and the difference in density between fluid components. The quasi-periodicity in z direction indicates that instead of imposing periodicity in pressure we impose periodicity in pressure gradient. The average pressure differential across the height of the computational box is uniquely determined by the hydrostatic pressure.

In the HVDT settings the general LWN model simplifies to a reduced form

$$\frac{\partial}{\partial t}U = G[U;\theta] = G(U, U_k, U_{kk};\theta), \quad (2)$$

where the model no longer has dependence on the physical space variable x. The terms in the model function $G(U, U_k, U_{kk};\theta)$ could be arranged to represent reaction, advection and diffusion terms. The numerical treatment of these terms would be different. We consider the Kurganov-Tadmor [3] discretization due to its low numerical dissipation properties. This scheme relies on uniform spatial discretization which is computationally inefficient for the spectral variable k. To address this issue, we consider change of variable $k(z)$, such that uniform discretization in z corresponds to an efficient non-uniform discretization in k. In the new variable z the model equation retains a form similar to (2) with the model function $G(U, U_z, U_{zz};\theta)$ containing reaction, advection and diffusion terms dependent on the choice of nonlinear rescaling $k(z)$.

Historically, calibration of turbulence models has been done by hand based on a hierarchy of simplifying assumptions. In our calibration approach we follow a different strategy inspired by the Machine Learning (ML) techniques. We form an *objective function* $L(\theta)$ also referred to as *loss function* and minimize it as a function of the choice of parameters θ. The objective function $L(\theta)$ is computed as a mismatch between the ground truth data and the model prediction over a time interval window of length dT. For the initial conditions for the model (2) we use the exact ground truth data. The choice of metric in forming the loss function is essential for the outcome of the optimization. We will discuss various design choices, their benefits and drawbacks.

To solve the optimization problem:

$$\text{find} \quad \text{argmin } L(\theta)$$

we implement a numerical time integration scheme for (2) in PyTorch [4] following the approach described in [2]. Thus, the outcome of the time integration scheme and the value of the loss function are represented as a custom deep, convolutional, residual Neural Network (NN) with parameters θ corresponding to some learnable weights in this NN. Optimization of this NN can then be done using the gradient descent type methods based on PyTorch built-in back-propagation tools for computing of gradients.

We demonstrate the performance of the optimization approach and quantify the necessary computational effort. We then present the results of the optimization and analyze properties of the calibrated model. We then present a sensitivity analysis of the objective function with respect to perturbation of the parameters θ around the found optimal values and draw conclusions about certainty of identified optimal parameters.

Acknowledgments: This research was supported by the NNSA Advanced Simulation and Computing (ASC) program at Los Alamos National Laboratory through the Physics and Engineering Models-Mix & Burn, and the Advanced Technology Development and Mitigation –Machine Learning projects. High-performance computing resources were provided by the ASC program at Los Alamos National Laboratory.

References:

[1] N. Pal et al., Pys. Rev. E, 3, 124608, (2021).
[2] I. Boureima et al., , JCP, 457,110924 (2022).
[3] A. Kurganov and E. Tadmor, JCP, 160, 241-282, (2000).
[4] A. Paszke et al., Automatic Differentiation in PyTorch, NIPS 2017 (2017).

Multi-fidelity validation of variable-density turbulent mixing models

Britton Olson[1], Benjamin Musci[2,1] and Devesh Ranjan[2]

[1]Lawrence Livermore National Laboratory, Livermore, CA, USA
[2]Georgia Institute of Technology, Atlanta, GA, USA

*Corresponding Author: olson45@llnl.gov

In this study, experimental data are presented and utilized to compare and validate two models used in the simulation of variable density, compressible turbulent mixing. Though models of this kind (Reynolds averaged Navier-Stokes and Large-Eddy Simulations) have been validated extensively with canonical flows in previous studies, the present approach offers novelty in the complexity of the geometry and the uniformity of the computational framework on which the models are tested. Moreover, experimental and computational results were collected by the same researchers which has led to a tightly coupled experimental configuration with its model or "digital twin." The experimental setup of the divergent shock tube is described as are the data acquisition methods. A two-dimensional computational Euler model which neglects the turbulent mixing at the interface is optimized to experimental data using a Gaussian process. This model then serves as the basis for both the RANS and the LES studies that make comparisons to the mixing layer data from the experiment. Mixing width, turbulent kinetic energy, density variance, and turbulent mass flux are among the mixing layer quantities that are extracted from the RANS and LES models and compared with experiment.

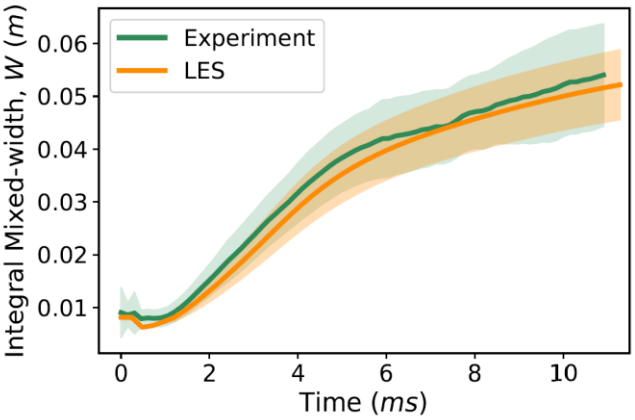

Figure 1: Comparison of the mixing layer width between LES and experiment for an ensemble (N=27) of initial conditions.

To validate the LES model, we generated a simulation ensemble of equal size to the experimental data ensemble. This allowed for the comparison of mean and variance trends for the mixing quantity of interest (QOI). While, the validated LES model had no model parameters to optimize it was shown to be sensitive to the method used for the characterization of the initial conditions. Directly inputting experimental ICs into the LES model led to much better overall agreement between the data ensembles for both mixing width and its growth rate. The LES model was shown to capture all of the relevant QOIs and physics present in the BDI experiments where the RANS model was only able to match experiment data for a limited subset of the QOIs for a limited time window. Late time behavior of the LES and the experiment data agree with Ritchmyer-Meshkov self-similar theory from the literature.

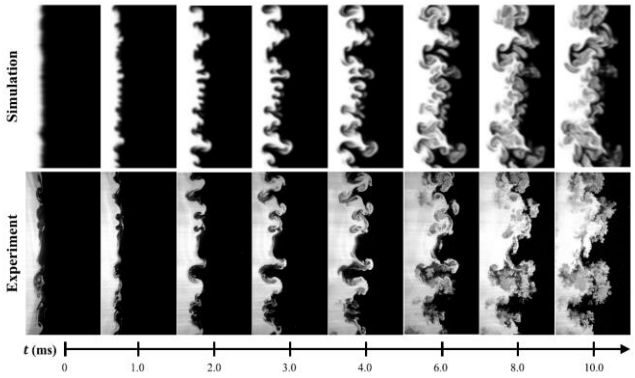

Figure 2: A comparison of the temporal evolution of mass fraction field, Y_h, taken from slices of simulation (top) and experiment (bottom). All images have been cropped and rotated from the original orientation to show the above comparison.

Acknowledgments: This work was performed under the auspices of the U.S. Department of Energy by Lawrence Livermore National Laboratory under Contract DEAC52-07NA27344.

References

[1] B. Musci, S. Petter, G. Pathikonda, B. Ochs, and D. Ranjan, Supernova Hydrodynamics: A Lab-scale study of the Blast-driven Instability Using High-Speed Diagnostics, The Astrophysical Journal 896, 92 (2020)

Plasma kinetic effects on the deceleration Rayleigh-Taylor instability

Jan Velechovsky[1,*], Erik Vold[1] and Susan Kurien[2]

[1]XCP-2: Eulerian Codes, LANL, Los Alamos, New Mexico, USA
[2]T-3: Fluid Dynamics and Solid Mechanics, LANL, Los Alamos, New Mexico, USA

[*]**Corresponding Author: jan@lanl.gov**

We present detail 3D simulations of mixing on a fuel/ablator interface inside a simplified Inertial Confinement Fusion (ICF) target. These simulations are run using LANL's multi-material multi-physics Eulerian code, xRAGE [1]. In particular, we are interested in the deceleration phase where a heavy Carbon ablator is supported by hot light Deuterium fuel while reaching maximal compression of the fuel. The resulting Rayleigh-Taylor instability and corresponding mixing are sensitive to plasma viscosity and species diffusivity at the interface [2]. Two cases are compared: 1) an inviscid hydrodynamic simulation govern by Euler equations with only numerical material mixing, and 2) a viscous hydrodynamic simulation with explicitly modeled plasma species diffusion. Simulated material distributions are shown in fig. 1 and fig. 2, respectively, showing only the computational cells containing more than 50% of Carbon colored by its mass fraction. Electron heat conductivity is included in both calculations.

Observed differences are used to improve a sub-grid turbulent mixing model, denoted BHR [3], in xRAGE, wherein mixing is governed by the evolution of the density-specific volume covariance. While the mixing width is not significantly affected by plasma kinetic effects, the absolute value of the density-specific volume correlation calculated from our 3D simulations is. This indicates that the increased atomic mixing, when plasma kinetic effects are properly accounted for, reduces the turbulent mixing leading to modified material distribution in the mixing layer.

Acknowledgments: Los Alamos National Laboratory is managed by Triad National Security, LLC for the U.S. Department of Energy's NNSA under Contract No. 89233218CNA000001. Funding is provided by NNSA ASC, Physics and Engineering Models, Mix and Burn project.

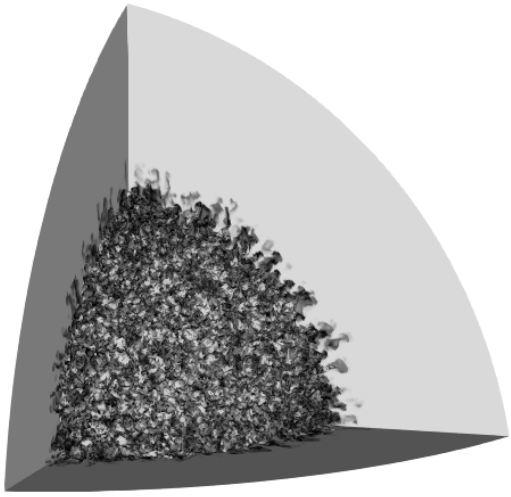

Figure 1: Simulated ablator for the inviscid case.

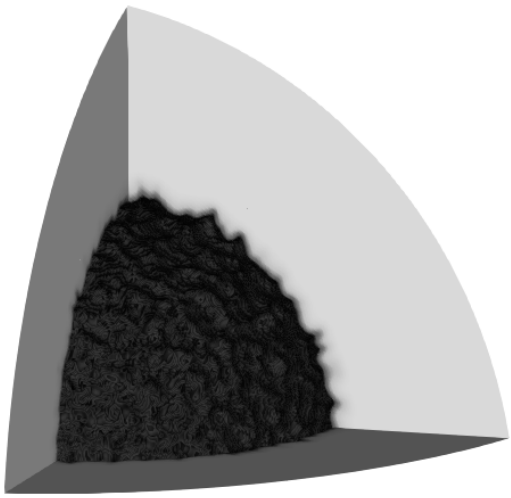

Figure 2: Simulated ablator for the plasma case.

References

[1] M. Gittings et al., Comp. Sci. Disc., **1**, 015005 (2008).
[2] E. Vold et al., Phys. Plasm., **28**, 092709 (2021).
[3] D. Besnard et al., LANL Rep., LA-UR-12303 (1992).

Analysis of Mix Using the Method of Separated Reactants on Indirect Drive Gas-Fill Implosions at the National Ignition Facility

A.R. Vazsonyi*, J.E. Pino, B.E. Morgan, and K.K. Mackay

[1]Lawrence Livermore National Laboratory, Livermore, CA, USA

***Corresponding Author: vazsonyi1@llnl.gov**

The "C-D Mix" platform at the National Ignition Facility (NIF) was developed with the intent of studying the effect of mix on indirect drive implosion performance through the method of separated reactants. [1] The targets are fabricated with a plastic (C-H) shell, where a small layer of the shell uses deuterated plastic (referred to as C-D). The target is filled with a gas comprised of a 75%/25% hydrogen-tritium (H-T) mixture. Therefore, during implosion, any measured 14 MeV deuterium-tritium (D-T) neutron output is a result of gas-shell mixing, whereas the 5-10 MeV T-T neutron output is uniquely a measure of core fusion performance, and D-D neutron output is largely a measure of fusion performance in the warm shell region. [2] C-D Mix experiments at the NIF used a recessed 3.26μm layer of C-D plastic in the Two-Shock capsule design. By varying the C-D recession depth, the measured D-T and D-D yields provide a means of probing the relative extent and characteristics of the gas-shell mix. The shots considered in this study are given in Table 1.

Shot number	C-D Recession Depth (μm)
150503	0.0
170416	0.5
170430	1.0

Table 1: Depth of C-D recession across the NIF shots considered in this study.

In this study, one-dimensional numerical analyses of these shots are carried out in the radiation-hydrodynamics code, Ares. A discrete ordinate radiation model is used to capture the energy delivery to the capsule. A variety of mix models are considered, including a Multi-Component Navier Stokes diffusion model (MCNS) and the k-L-a-V and k-φ-L-a-V Reynolds-Averaged Navier Stokes (RANS) models. [3,4]

Results using the RANS model demonstrate that both D-T and D-D yields are sensitive to initialization parameters of the mix model. In particular, the choice of initial length scale of the turbulence (L_0), a free parameter in the model, has a strong influence on the predicted yields. A value for L_0 is specified at time zero of the simulation at the various material interfaces of the capsule.

In Figure 1, Ares is run with the k-φ-L-a-V RANS model, where L_0 is allowed to vary between $50-350$nm for the shots given in Table 1. A larger L_0 increases the predicted D-T yield, yet this comes at the expense of a reduced D-D yield. This is an expected result, as larger L_0 values indicate increased mixing into the hotspot H-T gas from the C-D capsule shell layer. Also of note are the trends in ion temperature; the D-T ion temperature decreases with increasing yield, while the D-D ion temperature increases with increasing yield. This is because, as the C-D layer moves farther from the fill gas, D-T interactions are largely due to tails of the deuterium ion distribution, while D-D interactions take place further from the hotspot.

The model does not simultaneously predict the correct D-T and D-D yield; when the D-T yield agrees, within experimental error, to the measured value, the D-D yield is consistently underpredicted. To address this discrepancy, a variable initial turbulent length scale is implemented such that the length scale prescribed at the gas-shell interfaces ($L_{E,0}$) may be different from the length scale at the internal shell-shell interfaces ($L_{I,0}$). The intent of this approach is to find simultaneous agreement with D-T and D-D yields through better capturing the level of mixing at each interface.

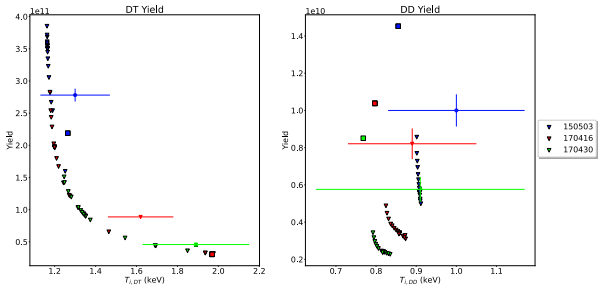

Figure 1: Experimental (circles), k-φ-L-a-V RANS (triangles), and MCNS (squares) D-T and D-D yields for varying C-D layer recessions.

This study analyzes the efficacy of mix model choices for various recession depths in the C-D Mix campaign. An analysis of the two-term initial turbulent length scale approach and comparison with experiment is conducted. The validity of the two-term initial length scale approach is assessed via analytic estimates of the Atwood number at the internal versus external capsule interfaces. This study also considers the efficacy of the MCNS model compared with the RANS model for various C-D layer recession depths. The results of these analyses are discussed in the context of other campaigns at the NIF and the relative role of mix in shot performance.

Acknowledgments: This work performed under the auspices of the U.S. DOE by Lawrence Livermore National Laboratory under Contract DE-AC52-07NA27344.

References

[1] V.A. Smalyuk et. al., PRL **112**, 025022. (2014)
[2] K.K Mackay and J.E. Pino, Phys. Plasmas **27**, 092704. (2020)
[3] B.J. Olson and J. Greenough. Phys. Fluids **26**, 044103. (2014)
[4] B.E. Morgan, Phys. Rev. E. **104**, 015107. (2021)

Demonstration of a Divergent Shock-Bubble Interaction in a High Energy Density Plasma

Pawel M. Kozlowski[1*], Yongho Kim[1], Brian M. Haines[1], Joseph M. Smidt[1], Tana Morrow[1], Shaun G. Newman[1], Thomas J. Murphy[1], Melissa R. Douglas[1], Brian J. Albright[1]

[1]Los Alamos National Laboratory, Los Alamos, NM, USA

[*]**Corresponding Author: pkozlowski@lanl.gov**

Supersonic flows in inhomogeneous media are ubiquitous, from the scale of inertial confinement fusion implosions to that of supernova remnants interacting with the interstellar medium [1]. The many interactions between reflections, transmissions, lensing, etc. off a multitude of pores make it difficult to probe a fully imhomogeneous system in experiments. Shock-bubble interaction (SBI) experiments are a building block for understanding supersonic flows in inhomogeneous media by isolating these complex systems down to a single inhomogeneity (bubble) in an ambient medium, which interacts with an incoming shock wave. Although SBI have been studied extensively in low energy hydrodynamic systems, data in the high energy density (HED) plasma regime have focused primarily on convergent regime SBI, where the bubble is of higher acoustic impedance, $Z = \rho c$, than the ambient medium, typically due to the use of a higher density material for the bubble [2-4]. These convergent regime SBI experiments have importantly demonstrated connections between the classical hydrodynamic theory of incompressible fluids (e.g. Widnall instability) and HED plasmas, but have not yet shown such connections in the divergent SBI regime.

We present the Marble VC platform, fielded on Omega-60, for studying divergent regime SBI in HED plasma flows. We believe these are the first successful divergent regime SBI experiments fielded on an HED platform, wherein the acoustic impedance of the bubble is lower than that of the ambient medium. This lower impedance causes the bubble to act as a divergent acoustic lens on the incoming shock, while the bubble itself is compressed the shock, as well as inverted into a vortex ring due to the deposition of baroclinic vorticity.

In order to study this system, we have developed a novel computer vision based analysis pipeline in order to clean and segment experimental radiographs to identify key features of interest [5]. Using these computer vision techniques we have extracted both shock front and bubble contours throughout the SBI, as can be seen in Figure 1. The identified features are characteristic of divergent SBI, and can be directly compared to highly constrained radiation-hydrodynamic simulations produced by LANL's xRAGE code. Using the initial target and laser conditions, with no additional energy or flux limiter tuning, we have found good agreement with features identified in experiment. Though we note here that achieving this level of agreement required refinement to the quiet start routine used to suppress fluid motion prior to arrival of the shock.

This work connects the classical hydrodynamic theory of SBI, based on acoustic impedance and baroclinicity, to the HED plasma regime via identification of features characteristic of divergent SBI, and thereby provides a basis for understanding generalized plasma flows through inhomgeneous media using the classical theory. This has implications for plasma flows through porous media, as observed in NIF Marble separated reactants experiments [6].

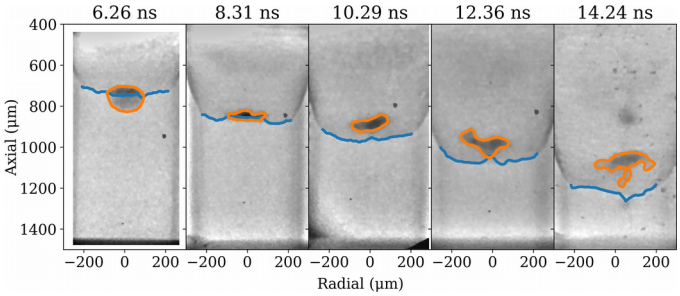

Figure 1: Sequence of radiographs from the Marble experiment campaign on Omega-60 showing the progression of a divergent regime SBI in an HED plasma. Shock front contours (blue) and bubble perimeter contours (orange) were extracted via computer vision analysis techniques.

Acknowledgments: This work was performed under the auspices of the US DOE by LANL under contract number 89233218CNA000001. LA-UR-22-21731

References

[1] D. Ranjan, et al. Anuu. Rev. Fluid Mech. **43**, 117 (2011).
[2] D. Ranjan, et al. Phys. Fluids **20**, 036101 (2008).
[3] H. F. Robey, et al. Phys. Rev. Lett. **89**, 8 (2002).
[4] J. F. Hansen, et al. Phys. Plasmas **14**, 056505 (2007)
[5] P. M. Kozlowski, et al. Rev. Sci. Instrum. **92**, 033532 (2021).
[6] B. J. Albright, et al. Phys. Plasmas **29**, 022702 (2022).

The Impact of Fill Tube Geometry on Recent High Yield Implosions on the National Ignition Facility

John Kuczek[1,*], Brian M. Haines[1]

[1]Los Alamos National Lab, Los Alamos, New Mexico, US

[*]**Corresponding Author: jkuczek@lanl.gov**

Implosions on the National Ignition Facility have recently achieved ignition [1]. These capsules achieve high yield through the absorption of alpha particles produced by the DT fusion reaction that heats the fuel, thus increasing reactivities further in a thermodynamic instability. Nevertheless, capsule implosions with significant alpha heating are particularly sensitive to asymmetries such as the fill tube.

Fill tubes are used to insert deuterium and tritium gas into inertial confinement fusion capsules at NIF. Fill tubes have been shown to introduce jets of contaminant and high-density fuel into the hot spot and reduce fusion yield by introducing a low-density pathway into the central fuel region [2]. The addition of this complex nonlinear flow leads to a challenge of modeling the evolution of the fill tube jet in implosion experiments. The impact of fill tube geometry on fusion yield has been well documented from both experiments [3-6] and simulations [7-8]; although there have been seemingly counter-intuitive results, such as larger contaminant jets arising from nominally smaller fill tubes as shown in fig. 1. A quantitative relationship between fill tube geometry and fusion yield has not yet been derived. We aim to understand how variations in the fill tube geometry and x-ray drive can impact capsule performance.

This study analyzes recent high yield shots at NIF through the use of the radiation-hydrodynamics code xRAGE. We intend to develop a more direct relationship between fusion yield and geometric details and pulse shape variations. We explore how the differences in bore hole and fill tube geometry influence capsule performance. The experimental results are given alongside simulated comparisons in: 1D, 2D with surface roughness, 2D with surface roughness and varying fill tube and bore hole geometries.

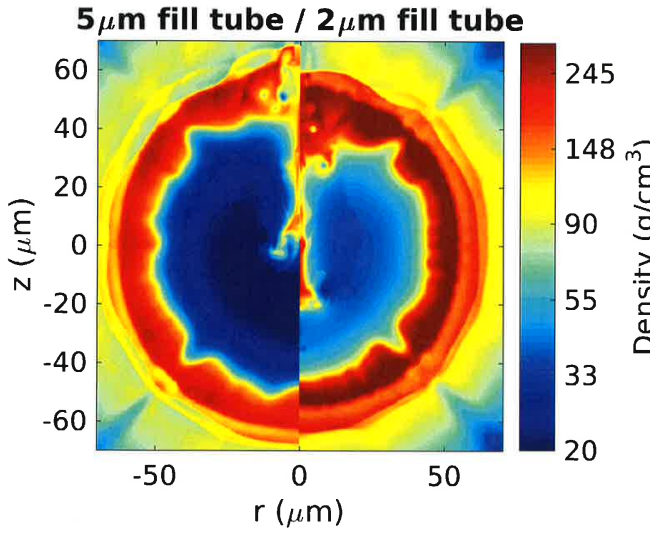

Figure 1: Comparison of fill tube jet at peak compression for two capsule implosions at bang time. This demonstrates that changing the details of the fill tube geometry and pulse shape can lead to larger jet from a smaller fill tube.

Acknowledgments: The authors would like to thank the NIC team for providing data necessary to simulate these experiments. This work was performed by the Los Alamos National Laboratory, operated by Triad National Security, LLC for the National Nuclear Security Administration (NNSA) of U.S. Department of Energy (DOE) under Contract No. 89233218CNA000001.

References

[1] D. Callahan et al., Bull. Am. Phys. Soc. AR01.00001 (2021).
[2] B. M. Haines et al., Phys. Plasmas. 27, 082703 (2020).
[3] S. Le Pape et al., Phys. Rev. Lett. 120, 245003 (2018).
[4] L. Divol et al., Phys. Plasmas. 24, 056309 (2017).
[5] A. G. MacPhee et al., Phys. Plasmas. 25, 054505 (2018).
[6] C. R. Weber et al., Phys. Plasmas. 27, 032703 (2020).
[7] A. Pak et al., Phys. Rev. Lett. 124, 145001 (2020).
[8] D. S. Clark., Nucl. Fusion. 59, 032008 (2019).

Experimental investigation of the multilayer Rayleigh-Taylor instability

Prasoon Suchandra*, Devesh Ranjan

George W. Woodruff School of Mechanical Engineering, Georgia Institute of Technology,
801 Ferst Drive, Atlanta, GA 30332-0405, USA

***Corresponding author: prasoon.suchandra@gmail.com**

Statistically stationary experiments are performed to study the effect of complex stratification pattern on the Rayleigh-Taylor instability (RTI). Experiments are conducted in a newly built, blow-down 3-layer gas tunnel facility. Mixing between three gas streams are studied, where the top and bottom streams comprise of air, and the middle stream comprises of air-helium mixture, giving Atwood numbers in the range $\mathcal{A}_{12}$~0.1-0.6 at the unstable interface between the top and middle streams. There is no shear between these streams. Two experimental cases are investigated, with one middle stream thickness (G ~ 3 cm) and two Atwood numbers ($\mathcal{A}_{12}$~ 0.3 and 0.6). The growth of the middle layer is measured using back-lit visualization and Mie-scattering techniques. The dynamics of the flow is investigated using particle image velocimetry (PIV) for velocity measurements and laser induced fluorescence (LIF) for density measurements. In addition to extracting quantities of statistical importance from our measurements, we address questions regarding the self-similarity, scaling, energetics and molecular mixing.

Figure 1 shows the evolution of mixing width h with nondimensional time $\tau = \left(\sqrt{\mathcal{A}_{12}g/G}\right)t$, normalized with middle layer thickness G, for the two Atwood number cases, and is compared with the mixing width obtained from the experiments of Jacobs & Dalziel (2005) at $\mathcal{A}_{12}$~0.002. We observed that at late times, the linear growth of the mixing width is observed. This linear growth was also suggested by self-similarity analysis of Jacobs & Dalziel (2005) for 3-layer RTI in the limit $\mathcal{A}_{12} \ll 1$. Other results from our experiments will be presented at the conference.

These experiments are of immense significance for engineering applications like inertial confinement fusion (ICF) as well as atmospheric and oceanic sciences, and they provide turbulence statistics which can be used to develop and validate variable density turbulence models. Since the ICF targets are multilayered, it is important to study hydrodynamic instabilities in multilayer configurations. Another important question is to check if the RTI during the ICF process can be suppressed due to the presence of multiple layers of materials.

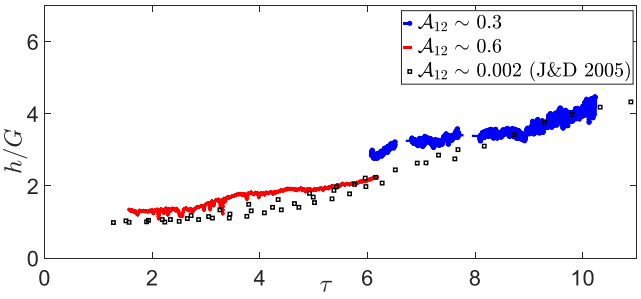

Figure 1: Normalized mixing width h/G vs nondimensional time $\tau = \left(\sqrt{\mathcal{A}_{12}g/G}\right)t$.

Acknowledgment: This work has been supported by DOE-NNSA grant DE-NA-0003912.

References

[1] Jacobs & Dalziel. "Rayleigh-Taylor instability in complex stratifications" *J. Fluid Mech* 542 (2005): 251-279.

[2] Akula et al. "Dynamics of unstably stratified free shear flows: an experimental investigation of coupled Kelvin–Helmholtz and Rayleigh–Taylor instability" *J. Fluid Mech* 816 (2017): 619-660.

[3] Mikhaeil, Suchandra et al. "Simultaneous velocity and density measurements of fully developed Rayleigh-Taylor mixing" *Phys. Rev. Fluids* 6 (2021): 073902.

Stratified flows under variable global acceleration

J. T. Horne[1,*], A. G. W. Lawrie[1]

[1]Hele-Shaw Laboratory, University of Bristol, Queen's Building, University Walk, Bristol, BS8 1TR, UK

[*]**J.T. Horne: jonathan.horne@bristol.ac.uk**

1. Introduction

The mixing behaviour of two-fluid stratified fluid systems is driven by the acceleration imposed on these fluids. The ability to manipulate this acceleration significantly enhances our insight into the behaviour of such systems. While relatively simple to imitate in numerical simulation, implementing well-diagnosed experiments with variable acceleration poses numerous challenges in apparatus design and there have been only a small number of preceding studies exploring this important regime.

In this work we present a new experimental apparatus facilitating repeatable and configurable variable acceleration experiments for stratified flows.

2. Variable acceleration apparatus

Experiments in this study are performed using the CAMPI rig, a novel apparatus that subjects saline-solution-based stratifications to apparent accelerations of up to 5g. A high speed, two-directional closed-loop winch accelerates a 0.4m x 0.2m x 0.2m tank along a track (see figure 1). The use of water as the base fluid enables high resolution diagnostics such as planar laser induced fluorescence (PLIF) to be used on miscible low Atwood number experiments. High Atwood immiscible experiments are also straightforward to implement in our configuration. The accelerations we generate are sufficiently high, and the track sufficiently long to evolve unstable flows into the strongly nonlinear regime of interest, and can rapidly switch from de-stabilizing to stabilizing acceleration. We believe that this offers unrivalled capability to diagnose the behaviour of this class of stratified flows.

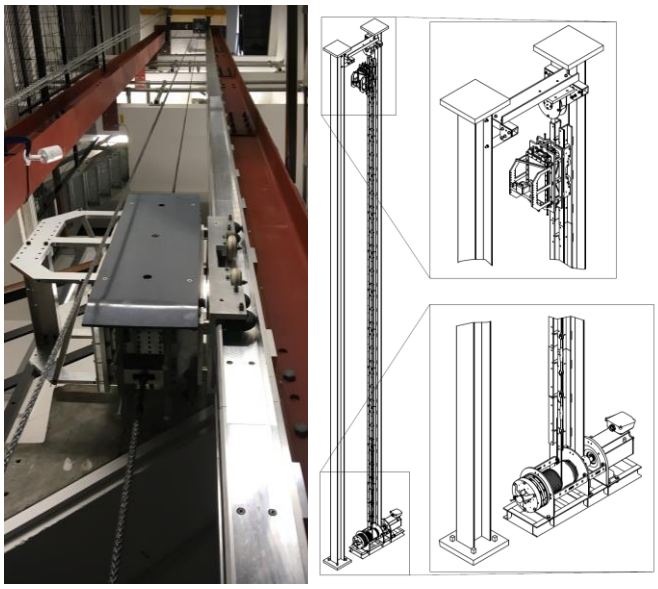

Figure 1: The CAMPI rig, a variable acceleration apparatus for multiphase flows.

3. Flows under variable global acceleration

We present closely coupled experiments and simulations of the evolution of Rayleigh-Taylor instability under a range of variable acceleration profiles. This work builds on the numerical work of Ramaprabhu et. al [1], as well as on earlier experimental studies by Dimonte et. al [2]. Our capability covers both sinusoidal acceleration and a variety of accel-decel and accel-decel-accel profiles. Example experimental output from an accel-decel acceleration profile is shown in figure 2, where initial acceleration ceases at 0.85 s.

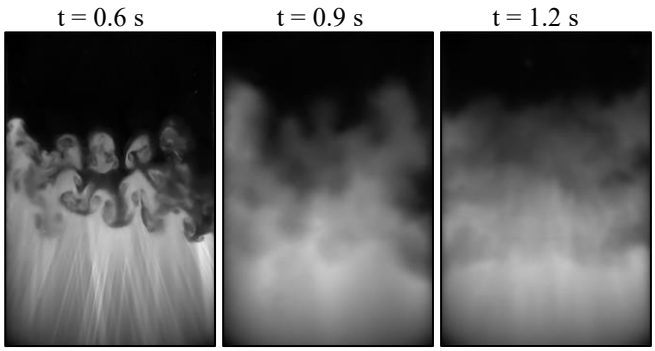

Figure 2: Accel-decel profile experimental output

Keywords

Variable acceleration, multi-phase systems, Rayleigh-Taylor, experimental.

Acknowledgments: We would like to thank AWE for their support of this work, in particular Robin Williams and Chris Batha.

References

[1] P. Ramaprabhu, V. Karkhanis, and A.G.W. Lawrie, "The Rayleigh-Taylor Instability driven by an accel-decel-accel profile", Physics of Fluids 25(11), 115104 (2013).

[2] G. Dimonte, P. Ramaprabhu, and M. Andrews, "Rayleigh-Taylor instability with complex acceleration history", Physical Review E 76(4), 046313 (2007).

UK Ministry of Defence © Crown Owned Copyright 2022/AWE

Abstract for the 17th IWPCTM

Shock-Particle Interaction and Explosive Dispersal of Particles

S. Balachandar[1],

[1]Department of Mechanical & Aerospace Engineering, University of Florida, Gainesville, FL, 32611, USA

[*]**Corresponding Author: bala1s@ufl.edu**

Shock-particle interaction is fundamental to explosive dispersal of particles, as it occurs in many natural and human-made systems. Euler-Lagrange point-particle (EL-PP) technique has been increasingly employed for solving such complex flows. Since flow around the individual particles is not resolved, the accuracy of the technique depends on the fidelity of the force law used for representing the fluid-particle momentum exchange that occurs at the microscale.

The talk will take a reductionist approach and address the following sequence of increasingly more complex problems: (i) We will first discuss the generalized Faxen form of the force law, which allows accurate accounting of the coupling between the flow and an isolated particle even under complex conditions, where the length and time scales of the flow are comparable to those of the particle (such as during shock-particle interaction). (ii) We will then consider shock interaction over a structured and random array of particles. Here we will focus on the effects of particle-particle interaction as mediated by the flow in between. The effect of this interaction both on particle force as well as gas-phase pseudo turbulence will be discussed. (iii) Finally, we will address the physics of explosive dispersal of particles. Of particular interest are the instability mechanisms responsible for the generation of fascinating mesoscale structures in the dispersing particle cloud.

The talk will also look at this complex problem at varying length and time scales: at the microscale around individual particles, at the mesoscale of instabilities, and the system-level macroscale. At each scale detailed comparisons with companion experiments performed at the National laboratories will be discussed. These validations are critical for the continuous improvement of the modeling framework.

Acknowledgments: This work was supported by the U.S. Department of Energy, National Nuclear Security Administration, Advanced Simulation and Computing Program, as a Cooperative Agreement under the Predictive Science Academic Alliance Program, under Contract No. DE-NA0002378 and also under the Stewardship Science Academic Alliances funding. The author of this invited talk would like to acknowledge Yash Mehta, David Zwick, Fred Ouellet, Bertrand Rollins, Goran Marjanovic, Kyle Hughes, Rahul Koneru, Giselle Frenandez, Josh Garno, Bradford Durant, Jacob Behrendt, Smyther Hsia, and Sam Briney, whose dissertation work is being summarized here.

Numerical investigation of drag and turbulence in compressible flows through particle suspensions

Archana Sridhar[1, *], Mehdi Khalloufi[2] and Jesse Capecelatro[1,2]

[1]Depatment of Aerospace Engineering, University of Michigan, Ann Arbor, MI, USA
[2]Department of Mechanical Engineering, University of Michigan, Ann Arbor, MI, USA

[*]**Corresponding Author: arsridha@umich.edu**

Shock-particle interactions are observed in a variety of natural phenomenon and engineering applications, including detonation blasts [1], volcanic eruptions, plume-surface interactions (PSI) during spacecraft landings [2], solid-propellant rockets [3] and pulse-detonation engines. A detailed understanding of the fluid dynamics at finite Reynolds number, Mach number, and volume fraction is currently lacking. Over the past several decades, significant progress has been made towards developing a theoretical understanding and numerical models for turbulent particle-laden flows in the incompressible regime. Yet, significantly less attention has been paid to compressible gas-particle flows. Coarse graining (or averaging) the viscous compressible Navier—Stokes equations results in unclosed terms in the form of drag and turbulence induced by particles (termed pseudo-turbulent kinetic energy, PTKE). Meanwhile, models for drag and PTKE at finite Mach numbers and volume fractions do not yet exist.

Particle-resolved numerical simulations represent the most comprehensive method to model these interactions as all of the sub-grid scale dynamics are directly captured. While computationally expensive, particle-resolved simulations provide a wealth of information that can be used to inform physics-based models. In this work, we present a high-order and computationally efficient framework for simulating compressible flows in moderately dense particle suspensions. The viscous compressible Navier—Stokes equations are discretized using high-order narrow stencil finite-difference operators that satisfy the summation-by-parts (SBP) property. The SBP scheme is combined with the simultaneous approximation term (SAT) treatment at the domain boundaries to ensure global energy stability, and skew-symmetric splitting of the inviscid fluxes is used for kinetic energy preservation. Boundary conditions at the surface of each particle are handled using a ghost-point immersed boundary method. Localized artificial dissipation is used for shock capturing and modified for presence of particles.

The framework is applied to two systems: statistically homogeneous flow through a suspension of particles and shock-particle interaction that is statistically one-dimensional. In the former, a database of simulations is generated across a wide range of volume fractions and Mach numbers. The drag force acting over the suspension of particles is quantified, and a correlation is proposed. Figure 1 shows an example of the homogeneous flow with a volume fraction of 0.1 and Mach number of 0.8. We show that compressibility effects on drag arise at lower Mach numbers as particle volume fraction increases. A model based on an effective Mach number is proposed that varies with the mean volume fraction.

In addition, we consider the problem of a planar shock wave interacting with a moderately dense suspension of particles. The budget of turbulent kinetic energy is quantified with special attention paid to production due to drag. A two-equation model is proposed in which PTKE and its dissipation are transported, providing a robust means of capturing fluid velocity fluctuations originating within the interstitial space between particles. The models being developed are designed for integration into coarse-grained simulations such as Euler-Euler and Euler-Lagrange methods.

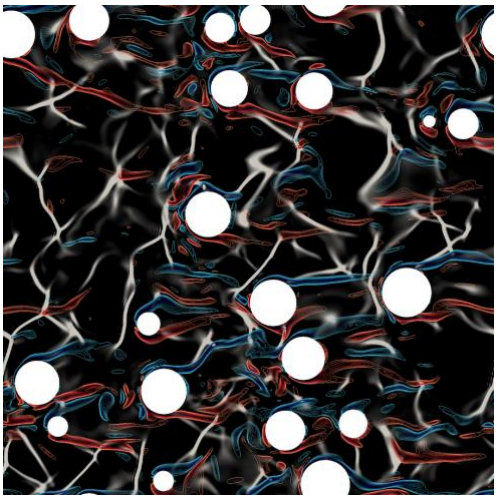

Figure 1: Compressible flow past a random assembly of fixed spheres showing a 2D cross-section of the 3D flow highlighting dilatation (black/white) and vorticity (red: positive, blue: negative).

Acknowledgments: This work is supported by NASA under grant no. 80NSSC20K1868 and SBIR contract no. 80NSSC20C0243

References

[1] F. Zhang, P. Thibault, and R. Link, Proc. Of The Royal Society of London. **459**, (2003).
[2] J. Capecelatro, Modeling high-speed gas-particle flows relevant to spacecraft landings, International Journ. Of Multiphase Flows, vol. **150**, (2022)
[3] J. Dupays, M. Prevost, P. Tarrin, and F. Vuillot, Effects of particulate phase on vortex shedding driven oscillations in solid rocket motors, (1996).

An Euler--Lagrange Approach for Turbulent Particle-laden Compressible Flows

Meet Patel[1,*] and Jesse Capecelatro[2]

[1]Research Assistant, University of Michigan, Ann Arbor, Michigan, 48109.
[2]Assistant Professor, University of Michigan, Ann Arbor, Michigan, 48109.

[*]**Corresponding Author: meetm@umich.edu**

Turbulent compressible flows laden with solid particles are ubiquitous in nature and engineering applications. Examples include volcanic eruptions, detonation of solid material, and supernovae. Plume-surface interactions (PSI) during spacecraft landing is particularly complex (see Fig. 1) as it involves dilute to dense suspension of particles, subsonic to supersonic flow, strong shock structures, and high Reynolds number turbulence. The wide range of length- and timescales and multi-physics aspects associated with PSI introduces many challenges in predicting the corresponding erosion, ejecta, and cratering.

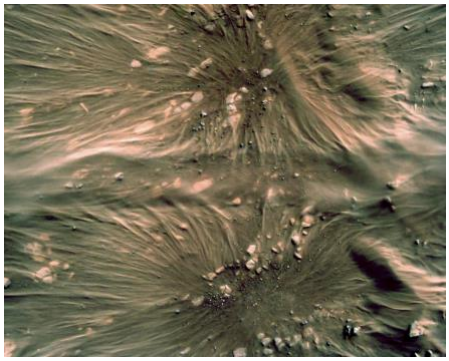

Figure 1: PSI during landing phase of Mars-2020 mission. Image adapted from NASA. A top-down view from perseverance rover.

In this work, we present a novel, high-order, low dissipative Euler—Lagrange framework for simulating such complex flows. The viscous compressible Navier—Stokes equations are solved for the gas phase using a volume-filtered approach [1]. The effects of the particle phase are accounted through volume fraction and interphase momentum- and heat-exchange terms. Individual particles tracked in a Lagrangian manner. Particle collisions are accounted for through a soft sphere collision model [2] that employs an efficient nearest-neighbor detection algorithm. This framework allows for simulations from dilute to dense suspense of particles while capturing the underlying gas phase turbulence.

The gas-phase equations are discretized with high-order narrow stencil finite difference operators that satisfy the the summation-by-parts (SBP) property. Boundary conditions are weakly imposed via simultaneous approximation terms (SAT) to achieve energy stability [3]. Additionally, a skew-symmetric splitting [4] of the inviscid fluxes taking into account the local volume fraction enables kinetic energy preservation at low Mach number. Localized artificial dissipation [5] is used for shock capturing. Complex geometries are accounted for using a ghost-point immersed boundary method (IBM) [6] based on a signed-distance levelset function.

Using this framework, simulations of PSI are performed with a nozzle of a diameter D situated at a distance h above a bed of monodisperse particles. The computational grid is uniform in the vicinity of the jet in all direction and then stretched in span-wise directions beyond $5D$ from the jet centerline. The setup involves approximately 193 M grid points and 44 M particles. In this study, we consider 3 different nozzle pressure ratios (NPR) chosen in such a way that under-expansion at nozzle exit is attained. Other parameters are kept constant (e.g., Reynolds number, h, D) to isolate sensitivity of crater morphology to NPR and corresponding turbulent mixing within crater. Two of the cases are shown in Fig. 2, depicting a 2D slice of the gas-phase Mach number highlighting the jet structure and 3D iso-contour of particle volume fraction of shows the crater shape. Note that the high NPR results in a finite size Mach disk that alters the cratering process. Further details on the framework, problem setup, and results will be presented at the conference.

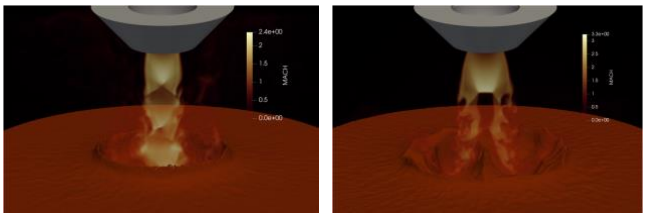

Figure 2: NPR=4.08 (left). NPR=6.12 (right).

Acknowledgments: This work is supported by an Early-Stage Innovations (ESI) Grant Award number: 80NSSC20K0295 under a contract with the NASA.

References

[1] Shallcross, G. S., Fox, R. O., & Capecelatro, J. (2020). A volume-filtered description of compressible particle-laden flows. *International Journal of Multiphase Flow*.
[2] Cundall, P. A., & Strack, O. D. (1979). A discrete numerical model for granular assemblies. *Geotechnique*.
[3] Svärd, M., & Nordström, J. (2008). A stable high-order finite difference scheme for the compressible Navier–Stokes equations: no-slip wall boundary conditions. *Journal of Computational Physics*.
[4] Pirozzoli, S. (2011). Stabilized non-dissipative approximations of Euler equations in generalized curvilinear coordinates. *Journal of Computational Physics*.
[5] Cook, A. W., & Cabot, W. H. (2005). Hyperviscosity for shock-turbulence interactions. *Journal of Computational Physics*.
[6] Chaudhuri, A., Hadjadj, A., & Chinnayya, A. (2011). On the use of immersed boundary methods for shock/obstacle interactions. *Journal of Computational Physics*.

Comparisons of Explosive Dispersal in Static and Supersonic Conditions

Bradford Durant[1*], Frederick Ouellet[2], S. Balachandar[1], and T. Jackson[1]

[1]University of Florida, Gainesville, Florida, USA
[2]Los Alamos National Laboratory, Los Alamos, New Mexico, USA

[*]**Corresponding Author: neoncrash@ufl.edu**

Explosive dispersal is a challenging and rich topic of research in the multiphase flow community. How explosive dispersal changes when subjected to a supersonic background environment raises interesting questions. In this work, the explosive dispersal is simulated with a barrel in an axisymmetric configuration with the explosive particulate dispersal occurring at the flat end of the cylindrical barrel into the ambient. For each ambient configuration, both particle-laden cases and gas only cases are simulated. The particle cases consist of a bed of steel particles placed in between the explosive and the barrel exit. This configuration was used to study and compare the interaction of the blast wave with a cylindrical packet of particles at the mesoscale in various ambient environments. These Euler-Lagrange simulations are carried out in a finite volume code.

The ambient state is in three different configurations: a static ambient case and then incoming Mach 3 and Mach 6 flows. The detonation of the explosive is modeled by a reactive burn model obtained by solving the reactive Euler equations. The resulting burn profile was used to provide the initial conditions for the explosive material in the mesoscale simulations. A mixture equation is used to model the equation of state of the fluid mixture containing the products of detonation and the ambient air. For the high-speed conditions, a bow shock is allowed to form over the barrel as an additional initial condition before the explosive dispersal is simulated. Virtual probe plates are configured in three different locations downstream of the barrel exit to capture incipient flow and particle metrics for analysis at various times during the simulations.

Acknowledgments: This work was also supported in part by the U.S. Department of Energy, National Nuclear Security Administration, Advanced Simulation and Computing Program, as a Cooperative Agreement under the Predictive Science Academic Alliance Program, under Contract No. DE-NA0002378; and in part by NSWC Crane under Contract No. N00164-20-1-2006.

Break up and Evaporation in Shock Driven Multiphase Mixing

Vasco O. Duke W.[1], Calvin J. Young[2,] *Jacob A. McFarland[3]

[1-3]Texas A&M University, College Station, Texas, United States

*Corresponding Author: mcfarlandja@tamu.ed

High-speed liquid droplet breakup and evaporation phenomena occur in a variety of technologies of interest, such as multiphase ejector pumps, liquid-fueled detonation engines, and explosive droplet dispersals. This phenomenon occurs concurrently with larger scale hydrodynamic mixing such as the Shock Driven Multiphase Instability (SDMI), a multiphase variation of the Richtmyer-Meshkov instability.

The SDMI often involves many concurrent multiphase phenomena that occur simultaneously across many length scales from the microscale (droplet-scale) to mesoscales (cloud scale). At the mesoscale, insight into the multiphase mixing phenomena can be quantified by droplets sizes, bulk vapor production, and pressure and density gradients. At the microscale, droplet-scale mixing can be isolated to study the combined phenomena of breakup and evaporation. Due to the complexity of the problem, simulations may be used to along with experimental data to capture the relevant physics.

With this in mind, new experimental equipment, methodologies, and techniques are utilized to investigate the impulsively accelerated heterogeneous shock-driven multiphase mixing. Due to the complexity of the problem, significant attention is paid to the initial conditions of the experiment. A curtain of particles perpendicular to the incident shock direction creates the multiphase interface. Particles are generated with variable ultrasonic atomizer nozzles with the size distribution measured utilizing a Phase Doppler Particle Analyzer system.

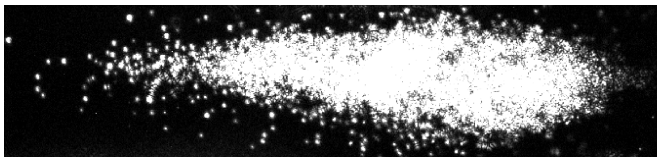

Figure 1: Child droplet from a 15 um droplet at 66 us after shock arrival.

Laser illuminated measurements are taken of both the droplet and vapor species. Particles are imaged by Planar laser Mie scattering as they are accelerated and break up as shown in fig. 1. Planar Laser-Induced Fluorescence images are taken simultaneously to measure vapor concentrations. These measurements allow characterization of the droplet breakup and survival times and vapor production rates. With data from these experiments, breakup and evaporation models used in simulations can be validated and tuned for higher accuracy, providing insight into the coupled physics behind these phenomena.

Acknowledgments: This work was funded by grants from the the Office of Naval Research (ONR:N00014-20-1-2796) and the National Sciences Foundation (NSF:2044767).

Abstract for the 17th IWPCTM

Modeling of Droplet Breakup and Impact in Supersonic Flight

Sam Briney[1], S. Balachandar[2,*]

[1]Graduate Student, Department of Mechanical & Aerospace Engineering, University of Florida, Gainesville, FL, 32611, USA
[2]Professor, Department of Mechanical & Aerospace Engineering, University of Florida, Gainesville, FL, 32611, USA

[*]**Corresponding Author: bala1s@ufl.edu**

Air vehicles traveling at supersonic and hypersonic speeds may encounter particles or rain drops in the atmosphere, which are capable of causing damage to the surface of such vehicles at sufficient speeds. In the case of a blunt body as shown in fig. 1, particles or droplets encounter a bow shock prior to either being diverted from colliding with the body by the post shock flow or, given sufficient particle inertia, collide with the blunt body. The time between a droplet encountering a shock wave and a possible collision is long enough in some cases to result in droplet breakup due to the step change in flow conditions and subsequent high relative velocity.

In order to simulate this problem using an Euler-Lagrange (EL) methodology, a droplet breakup model is integrated into a particle tracking code to obtain physical results. The existing droplet breakup literature is extensive and provides insight into the breakup process which is complex but widely understood to be driven by Rayleigh-Taylor and Kelvin-Helmholtz instabilities [1]. The literature also provides and several reduced order models suitable for EL simulations.

Presently, we implement breakup models into the highly scaleable particle tracking library ppiclF [2]. Furthermore, we modify these models to account for stochasticity in the breakup process. Statistics of droplet collisions with the air vehicle are predicted and reported using multiple droplet breakup models for comparison.

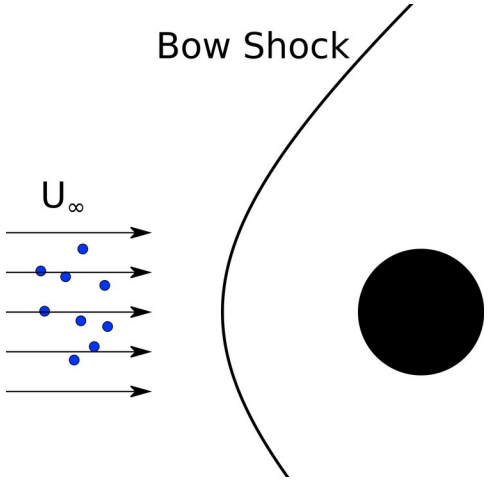

Figure 1: Droplets before encountering a bow shock when approaching a blunt body at supersonic velocity.

Acknowledgments: This work was supported by the U.S. Department of Energy, National Nuclear Security Administration, Advanced Simulation and Computing Program, as a Cooperative Agreement under the Predictive Science Academic Alliance Program, under Contract No. DE-NA0002378 and also under the Stewardship Science Academic Alliances funding, and also by Sandia National Laboratories with Campus Exec Funding.

References

[1] T. G. Theofanous, Annual Review of Fluid Mechanics. **43,** 661 (2011).
[2] D. Zwick, Journal of Open Source Software. **4** (37), 1400 (2019).

Multiphase Phenomena in Heterogeneous Detonations

Calvin J. Young[1], Vasco O.D. Walker[2,] *Jacob A. McFarland[3]

[1-3]Texas A&M University, College Station, Texas, United States

*Corresponding Author: mcfarlandja@tamu.edu

Heterogeneous or multiphase detonation and blast phenomena are of interest in a variety of field, from advanced air-breathing engines for sustained super- and hyper- sonic flight vehicles to explosive particulate and droplet dispersal of ordnance and explosion safety in combined spaces. While detonations in homogenous gaseous mixtures and heterogeneous solid particle suspensions have received much attention, the problem of a detonation in a multiphase mixture consisting of liquid fuels and gaseous oxidizer has yet to be sufficiently investigated.

The multiphase detonation consists of several coupled phenomena occurring over simultaneous time and length scales. Liquid droplets are able deform and break up into smaller child droplets due to aerodynamic forces incident shock of the detonation, experiencing hydrodynamic instabilities as a result. As the droplets undergo this deformation they are simultaneously heated and vaporized, shrinking in size while contributing vapor to the flow field. The vapor species in turn limit the reactions, which contribute heat to continue to process of vaporization. Concurrently larger scale hydrodynamic phenomena may be present , such as the multiphase Richtmyer-Meshkov instability, due to system features such as fuel injection sites and inhomogeneities in the flow field, as well as gradients in equivalence ratio due to spatial variations in droplet number density and size distribution.

The complexity of the problem quickly escalates to the point that a direct simulation of more than one droplet undergoing this process becomes infeasible. To simulate the problem it thus becomes necessary to employ breakup, vaporization, and reaction models. Sophisticated models exist for each separate phenomenea, such as those of Reitz [1] for breakup and Abramzon [2] for droplet heating and evaporation, as well as numerous reaction models of varying complexity. To accurately model the phenomena occurring simultaneously requires reliable experimental data for verification and validation.

Here a multiphase detonation tube facility is constructed, with experiments measuring the bulk properties of a multiphase detonation. Significant attention is given to characterization of the initial conditions inside the experiment, such as equivalence ratio and spatial droplet size distribution. Results consist of pressure profiles and velocities of the detonation wave.

With this data from this experimental facility, breakup, vaporization, and reaction models used in concert may be tuned to greater accuracy than previously possible, granting insight into the underlying physics involved in multiphase detonations. Further refinement of the models will be attained through data collected with optical diagnostics, such as droplet survival times and vapor production rates. With these improved capabilities simulations will be able to accurately predict complex system behaviors.

Acknowledgments: This work was funded by grants from the the Office of Naval Research (ONR:N00014-20-1-2796) and the National Sciences Foundation (NSF:2044767).

References

[1] Reitz, R.D., Beale, J.C., 1999. Modeling spray atomization with the kelvin-helmholtz/rayleigh-taylor hybrid model. Atomization and Sprays 9, 623–650.

[2] Abramzon, B., Sirignano, W., 1989. Droplet vaporization model for spray combustion calculations. Int. J. Heat Mass Transfer 32, 1605–1618.

Jet initiation from shock wave-induced microbubble collapse

Guillaume T. Bokman*, Luc Biasiori-Poulanges, Daniel W. Meyer and Outi Supponen

Institute of Fluid Dynamics, Department of Mechanical and Process Engineering,
ETH Zürich, Zürich, Switzerland

*Corresponding Author: bokmang@ethz.ch

The interaction of shock waves and microbubbles can lead to a non-spherical bubble collapse, which sometimes produces high-speed jets in the direction of the wave propagation. This occurs in a wide range of applications involving shock waves and liquid-gas media. The violent consequences of such an encounter can be beneficial in therapeutic shock wave lithotripsy [1], ultrasonic cleaning or reaction initiation [2]. The separation of a small quantity of gas from the main body of the bubble at the liquid jet tip has also been previously reported [3], offering a possible method for *in vitro* microinjections of bubble gas content. However, the small spatial and temporal scales at which such dynamics take place pose significant experimental challenges, and therefore only few experiments with a limited resolution have been reported thus far. Here, experiments with unprecedented detail are conducted, where gas microbubbles interact with laser-induced shock waves in water. The resulting dynamics are resolved using high-speed imaging with a microscopic zoom lens. The shock pressure signals are characterized using a needle hydrophone. The use of high-power flash lamps reveals the interior of the bubbles during the motion of the liquid jet, offering details on the position and shape of the jet before it reaches the distal side of the bubble. This work probes the initial conditions required to initiate jetting and characterizes the jet quantities to increase control over such events.

By generating bubbles of a few tens of microns by electrolysis and hundreds of microns by a co-flow microfluidic device, a whole range of bubble sizes are investigated. A broad range of shock wave peak pressures is also considered by varying the laser power. A parameter space investigation is conducted which shows a clear limit between jetting and non-jetting dynamics. Results are contrasted to numerical methods of different levels of complexity such as a segmented version of the Rayleigh-Plesset model, the boundary integral method, or an open-source volume-of-fluid code (ECOGEN) to predict the onset of jetting based on initial parameters only. The bubble shape evolutions computed with the distinct methods are directly compared with the experimental visualisations and are all found to agree well although to a different extent. Taking advantage of both the high spatial and temporal resolution of the experiments, bubble and jet quantities are extracted and compared to previous numerical studies, when available, to deepen the understanding of jet control and get closer to achieving on-demand micro-injections. The collapse time of shocked microbubbles is compared to the ones found numerically for planar shock waves [1] and found to scale with the length of the temporal full width at half maximum of the shock wave. The liquid jet speed is found to scale with the peak pressure, independently of the initial bubble size, confirming previous numerical studies [4]. The size of the gas pocket ejected from the main bubble by the jet tip is observed and shows the presence of liquid encapsulated in the ejected gas body. An empirical law has been derived to describe this process and suggests that the ejection mechanism scales with the initial speed of the jet when breaching the distal side of the bubble. Finally, the above-mentioned code, ECOGEN, is used to better understand the non-linear behaviour of impulse shock driving, such as those generated by extra-corporal shock wave lithotripters or optical laser breakdown in liquids used in biomedical applications. This is achieved by modelling a spherically propagating shock wave and by accounting for its energy dissipation over time.

This study offers a better understanding of the mechanisms linked to shock wave-induced bubble jets and how to tune them on-demand. By probing this limit, it is possible to control the size of the gas ejection, thus allowing for controlled *in vitro* microinjection of gaseous contents in cells by adjusting the acoustic driving parameters.

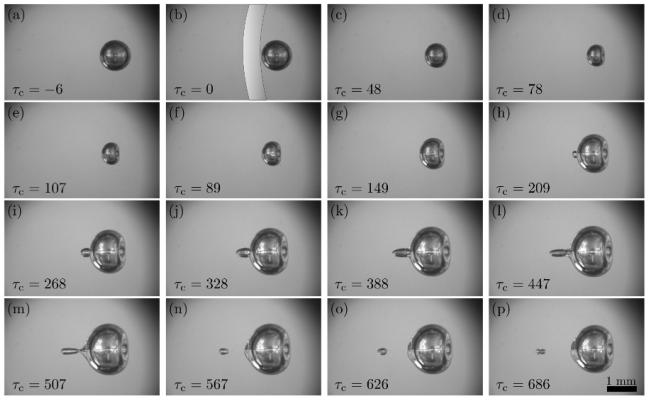

Figure 1: Bubble dynamics resulting in a high-speed liquid jet after the interaction of a bubble of initial radius $R_0 = 500$ um with a shock wave of peak pressure $P_s = 40$ MPa. The characteristic time is $\tau_c = tc_L/R_0$, where c_L is the sound speed in the liquid.

Acknowledgments: Authors acknowledge financial support from ETH Zurich.

References

[1] E. Johnsen and T. Colonius. Journal of Fluid Mechanics **629** (2009).
[2] J. P. Dear *et al.* Nature **332**, 6164 (1988).
[3] C. D. Ohl and R. Ikink. Physical Review Letters **90**, (2003).
[4] S.-W. Ohl *et al.* Interface Focus **5**, 5 (2015).

Shock-induced release of a gas-encapsulated droplet

Luc Biasiori-Poulanges*, Guillaume Bokman, Enea Baumann and Outi Supponen

ETH Zürich, Institute of Fluid Dynamics, Zürich, Switzerland

*Corresponding Author: lbiasiori@ethz.ch

Gas-encapsulated liquids consist of a gas bubble immersed in an ambient liquid and encompassing a droplet. These 3-fluid components stand out as a promising candidate for fluid transport, especially for drug delivery where the encapsulated droplet contains the payload. The process for experimentally generating such structures having been recently validated [1], this work assesses the ability of shock waves to release and disseminate thick-shelled gas-encapsulated drops. Two types of shock-driving are examined: a laser-induced divergent shock and a plane sustained shock wave.

The interaction of a planar shock wave with a gas-encapsulated droplet is numerically investigated using the open-source compressible multiphase flow code ECOGEN [2]. The examination of the resulting flow discontinuities reveals the intricate dynamics of the bubble rupturing. When the bubble interface comes into contact with the encapsulated droplet by experiencing a non-spherical collapse, a water-hammer shock is initiated both inside the droplet and the surrounding liquid. Consequently, a succession of sheet jetting fragmentating the bubble is triggered and overcomes the ongoing collapse. This phenomenon, referred to as *jet cascade*, occurs alongside with the generation of a region of tension inside the droplet caused by the internal reflections of the water hammer wavefront at the droplet interface. The evaluation of the magnitude of the produced tensions shows that the local pressure drops down to 2 times the homogenous cavitation threshold (~134 MPa) predicted by the classical nucleation theory, suggesting the occurrence of shock-induced cavitation inside the droplet.

The initial water-hammer pressure produced inside the droplet is analytically derived from the original high-speed liquid-to-solid impact equation of Huang et al. [3], modified by accounting for the bubble wall velocity as predicted by the Rayleigh collapse equation, and the surrounding flow properties considering the Rankine-Hugoniot jump relations. Due to the non-spherical nature of the bubble collapse, this model yields substantial discrepancies even though it is able to predict the order of magnitude. This is corrected by replacing the Rayleigh collapse solution for the bubble wall velocity with a segmented formulation of the Keller-Miksis equation, where a very good agreement with numerical measurements is found. The high pressure resulting from the water hammer shock drives the surrounding liquid into the gas bubble and forms the first sheet jet. Based on the acoustic impedance ratio of the various phases involved, the jet velocity is theoretically approximated and obeys to a linear law where the particle velocity behind the water-hammer shock is the variable. When this first jet interacts with the bubble boundary, the liquid-gas interface rupturing initiates a second water-hammer shock that eventually triggers a second sheet-jet. This is the recurrent process – the jet cascade – that eventually leads to the bubble rupturing. By all converging to the bubble axis, sheet jets generate a high-pressure region at the rear of the bubble, reaching up to tens of GPa for a shock wave Mach number of 2.1, which deforms the droplet from the back in a bowl-like shape.

The initial droplet's center-of-mass displacement along the shock's direction of propagation is modelled assuming the droplet as a non-deformable spherical particle of constant mass and acceleration, from which the characteristic transport time for the droplet is found to be $\tau = R_{d,0}\sqrt{\rho_{d,0}/(p_2 - p_{b,0})}$, where $R_{d,0}$ is the initial bubble radius of pressure $p_{b,0}$, $\rho_{d,0}$ is the initial droplet density and p_2 is the post-shock density of the surrounding fluid. The dissemination of the droplet inside the surrounding fluid is eventually investigated, albeit with caution due to the simulation limits and the possibility of phase change that was not accounted for, and found to increase in a power law fashion as time proceeds.

This numerical study opens experimental opportunities to elucidate the release mechanisms of a gas-encapsulated droplet, which are formed with a mixing microfluidic setup into a water tank. To shed light on a valuable alternative to sustained shock waves, the interaction of the gas-encapsulated droplet with a shock wave produced by a laser-induced optical breakdown is first investigated. Intricate processes are thus imaged and similarities with the above-described simulations are found despite the different shock natures. Depending on the exact location of the droplet inside the bubble, the interaction between the bubble wall and the droplet results in significantly different phenomena. Mainly three distinct regimes are identified: (1) the eccentricity of the droplet is too large to affect the canonical bubble collapse; (2) the eccentricity is moderate which deflects the main transverse jet of the bubble; (3) the eccentricity is small so that the main transverse jet violently impacts the droplet that subsequently deforms into a crown-like shape with an azimuthal periodic distribution of ligaments.

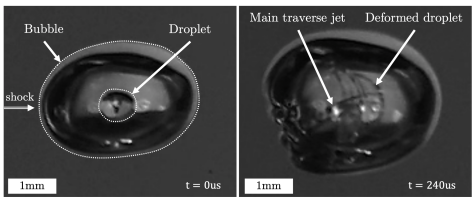

Figure 1: Interaction of a 35 MPa laser-induced shock with a gas-encapsulated droplet.

Acknowledgments: Authors acknowledge the financial support from ETH Zurich and the ETH Zurich Postdoctoral Fellowship programme.

References

[1] Y. Shen *et al.*, Physical Review Letters **5**,120 (2018).
[2] K. Schmidmayer *et al*., Comp.Phys. Com. **251**, (2020).
[3] Y. C. Huang *et al.*, J. Appl. Phys. **44**, (1973).

Effect of surface instabilities on evaporation rates of shock-driven droplets

Prashant Tarey[1], Praveen Ramaprabhu[2,*] and Jacob McFarland[3]

[1,2]University of North Carolina, Charlotte, NC, USA
[3]Texas A&M University, College Station, TX, USA

[*] **Praveen Ramaprabhu: pramapra@uncc.edu**

Instability-driven breakup and droplet evaporation play an important role in liquid fuel droplet combustion. The different droplet breakup regimes are governed by the Weber number (We), which is the ratio of hydrodynamic and surface tension forces. In Pulse Detonation Engines (PDEs) and Rotating Detonation Engines (RDEs), the fuel droplet size can vary from 5 μm to 50 μm[1-4], with corresponding Weber number ranges of 10 - 10^4, encompassing a wide range of regimes of droplet breakup, from bag breakup (We ~ 10) to catastrophic breakup (We$\gtrsim 10^3$). Recent experimental work by Theofanous et. el.[5-7], has pointed to the existence of two dominant modes of droplet breakup, namely Rayleigh Taylor Piercing (RTI) for We<10^2 and Shear Induced Entrainment (SIE) for We>10^3, with a mixed RTI and SIE regime for intermediate Weber numbers ~10^2 to10^3.

In this work, through detailed numerical simulations, of a 2D axisymmetric JP-10 fuel droplet, the effect of surface instabilities on the evaporation rate are investigated. The Weber number for all the simulations was set at We = 100, representing flow conditions relevant to fuel droplets in RDEs and PDEs. The simulations were performed in 2D to ensure the dominant KH wavenumbers, which follow the scaling ~ We/3 are adequately resolved. The cases simulated, involved a 10 μm droplet, processed by an impinging shockwave, for different Mach numbers of M=1.47 and M=3, with and without evaporation.

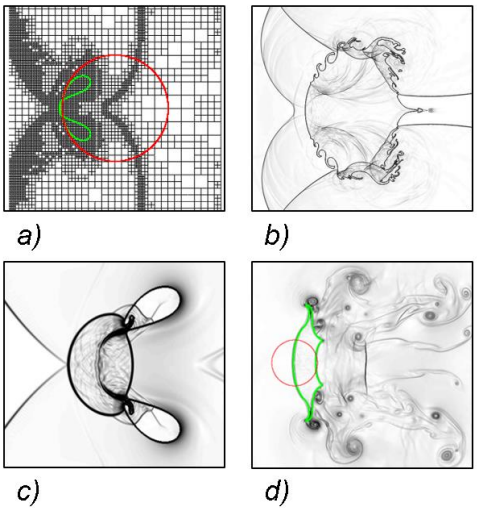

Figure 1: Sample results from IMPACT : a) R22 bubble collapse in Air, b) AMR mesh capabilities c) Shock-bubble interaction d) Shock-Droplet interaction.

The simulations were performed using IMPACT[8], a multiphase shock physics code that employs a 5th order WENO scheme to solve the Euler Equations with Adaptive Mesh Refinement. The interface between the liquid and gaseous phase was tracked using the Level Set method, and a Riemann Ghost Fluid Method (RGFM)[9] integrated with a multi-medium Riemann solver used to couple the two phases. The evaporation (or condensation) rates were computed using the Schrage-Knudsen[10] evaporation law, while the liquid phase saturation pressure (required to calculate evaporation rate) was obtained from the Antoine equation[11]. For the present simulations, the thermal conductivity and mass diffusivity coefficients were treated as constants.

Simulations were performed for different shock Mach numbers to isolate the effects of surface tension and evaporation on droplet breakup. It was observed that the first appearance of KH instabilities occurs near the equatorial points of the droplet, where shear is maximum. The evaporation simulations were initialized with a layer of vapors surrounding the initial droplet surface to avoid impulsive evaporation at $t^* = 0$. The evaporation rate of the shock-driven droplets were found to increase with the Mach number of the incident shock, due to the higher post shock temperature at higher Mach numbers.

Acknowledgments: This material is based upon work supported by the National Science Foundation under Grant No. 1933479.

References

[1] J. Kindracki, J. Power Technologies (2), 80-89 (2012).
[2] J. Kindracki, Aerosp Sci Technol **43**, 445-453 (2015).
[3] K. Kailasanath, in *39th AIAA/ASME/SAE/ASEE Joint Propulsion Conference and Exhibit* (2003).
[4] J. S. Gong and H. Ma, Int J Aerospace Eng (2020).
[5] T. G. Theofanous, G. J. Li and T. N. Dinh, J Fluid Eng-T Asme **126** (4), 516-527 (2004).
[6] T. G. Theofanous and G. J. Li, Phys Fluids **20** (5) (2008).
[7] T. G. Theofanous, Annual Review of Fluid Mechanics, Vol 43 **43**, 661-690 (2011).
[8] P. Bigdelou, C. Liu, P. Tarey and P. Ramaprabhu, Comput Fluids **233** (2022).
[9] P. Das and H. S. Udaykumar, J Comput Phys **405** (2020).
[10] R. W. Schrage, *A Theoretical Study of Interphase Mass Transfer*. (Columbia University Press, 1953).
[11] E. P. O. F. Douglas A. Schwer, Jr.* and David A. Kessler, 2018.

Buoyancy–Shear–Drag–Scalar-Based Turbulence Modeling for Rayleigh–Taylor, Reshocked Richtmyer–Meshkov, and Kelvin–Helmholtz Mixing: Applications

Oleg Schilling*

Lawrence Livermore National Laboratory, Livermore, California, United States

*Corresponding Author: schilling1@llnl.gov

A phenomenological turbulence model for Rayleigh–Taylor, reshocked Richtmyer–Meshkov, and Kelvin–Helmholtz instability-induced mixing developed using a general buoyancy–shear–drag model is applied to constant-acceleration Rayleigh–Taylor, impulsively reshocked Richtmyer–Meshkov, and variable-density Kelvin–Helmholtz mixing layers to demonstrate its utility [1]. Analytic solutions to the model equations corresponding to each instability were derived and used to calibrate the model coefficients to predict specific values of the mixing layer growth parameters and exponents. The buoyancy–shear–drag equations for the bubble and spike mixing layer widths are then solved numerically, and a turbulent diffusivity (or viscosity) is constructed as the product of the mixing layer width, h, and its time-derivative, dh/dt. Surrogate turbulent fields are then constructed by multiplying a presumed, approximate self-similar spatial profile by appropriate functions of h and dh/dt.

This model was applied to a Rayleigh–Taylor mixing layer with Atwood number 0.5, a reshocked Richtmyer–Meshkov mixing layer with Atwood number 0.67, and a variable-density Kelvin–Helmholtz mixing layer [1]. It was shown that the numerical solutions of the model calibrated using specific values of the instability growth parameters and exponents: (1) produces mixing layer widths in agreement with the expected self-similar growth power-laws; (2) gives turbulent fields that are expected and consistent with previous results; (3) predicts the expected power-law behavior of the spatially-integrated turbulent fields, and; (4) gives mean fields that are expected and consistent with previous results.

Additional applications of this model, extended to include scalar fluctuations, are described here. Models consisting of both bubble and spike width evolution equations, as well as of just the total width are considered. In particular, Rayleigh–Taylor mixing with both passive and active scalar fluctuations is considered. In the passive case, the scalar fluctuations are decoupled from the buoyancy–drag equations, and the scalar variance is determined by the assumed value of the molecular mixing parameter (for example, estimated from experimental or simulation data). In the active case, the scalar fluctuations are coupled to the buoyancy force, and modify the value of the growth parameter α from the passive (classical) case. The properties of the analytic solutions of the model equations for the mixing layer width and scalar variance are discussed. The spatiotemporal evolution of the profiles of the turbulent fields will be discussed.

Figure 1 shows the temporal evolution of the mixing layer width and (scaled) normalized density fluctuation $\Theta(t) = \rho'/\overline{\rho}$ and normalized density variance $S(t) = \Theta(t)^2$ for a Rayleigh–Taylor mixing layer obtained by numerically solving the buoyancy–drag and scalar fluctuation ordinary differential equations. The fluctuation and variance attain constant values determined by the balance between scalar production and destruction. Figure 2 shows the temporal evolution of the molecular mixing parameter (calibrated to a value of 0.8) obtained from the density variance for a Rayleigh–Taylor mixing layer. With turbulent fields constructed using the procedure described in the previous presentation, it is shown that their evolution is similar to that obtained from the solution of partial differential Reynolds-averaged turbulence models. Potential applications of this buoyancy–shear–drag–scalar model paradigm are discussed.

The more general formulation of the model to complex turbulent flows, in which the mean flow equations closed using expressions constructed from the turbulent fields are solved numerically, is also briefly described.

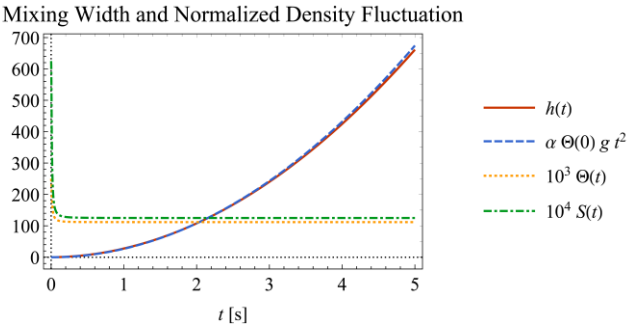

Figure 1: Temporal evolution of the mixing layer width and (scaled) normalized density fluctuation and normalized density variance for Rayleigh–Taylor mixing.

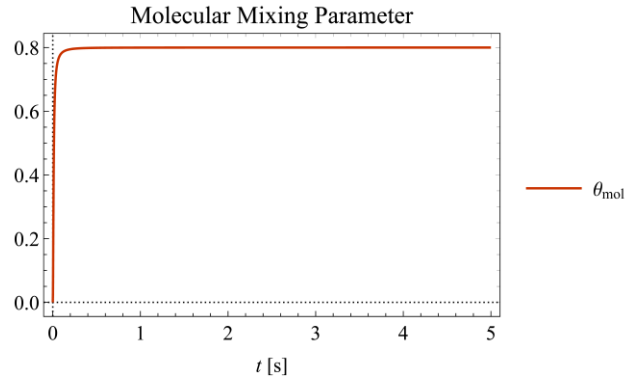

Figure 2: Temporal evolution of the molecular mixing parameter for Rayleigh–Taylor mixing.

Acknowledgments: This work was performed under the auspices of the U.S. Department of Energy by Lawrence Livermore National Laboratory under contract DE-AC52-07NA27344.

References

[1] O. Schilling, Physica D **402**, 132238 (2020).

Three- and Four-Equation Reynolds-Averaged Navier–Stokes Modeling of a Small Atwood Number, Transitional Rayleigh–Taylor Mixing Experiment

N. J. Mueschke[1] and Oleg Schilling[2,*]

[1]Southwest Research Institute, San Antonio, TX, United States
[2]Lawrence Livermore National Laboratory, Livermore, CA, United States

[*]**Corresponding Author: schilling1@llnl.gov**

The physical understanding of acceleration-induced hydrodynamic instabilities and the resulting turbulent mixing arising at material interfaces is essential to investigating various applications in science and engineering, including core-collapse supernovae, nonlinear and potentially turbulent mixing in inertial confinement fusion capsule implosions, and mixing processes in the atmosphere and oceans. Buoyancy-driven turbulent mixing is induced by the growth of the Rayleigh–Taylor (RT) instability occurring when a less dense fluid is accelerated into a denser fluid across a perturbed interface initially separating the fluids. Various aspects of RT unstable mixing have been investigated over the last several decades using experiments, numerical simulations, and modeling.[1] A review, synthesis, and perspective on efforts to simulate and model RT experiments was recently presented.[2]

In the realm of Reynolds-averaged turbulence modeling, most studies conducted thus far have focused on predicting the basic properties of self-similar RT mixing, such as the quadratic in time growth of the mixing layer width. However, there have been exceptionally few studies that have applied such models to experimental data to validate them and quantify their predictive capabilities.[3] A four-equation K–ε–S–χ mechanical–scalar turbulence model based on the turbulent kinetic energy and mass fraction variance (K and S) and their dissipation rates (ε and χ) was proposed and validated *a priori*[4] using direct numerical simulation (DNS) data corresponding to a detailed model of a small Atwood number, transitional RT water channel experiment.[5] The model equations were recently solved analytically in the statistically one-dimensional, self-similar, small Atwood number approximation in the context of Rayleigh–Taylor, Richtmyer–Meshkov, and Kelvin–Helmholtz mixing.[6]

The present study applies this turbulence model (calibrated both using the DNS data and self-similar solutions) *a posteriori* and compares the predictions to the experimental mixing layer growth and molecular mixing evolution. A three-equation model using an algebraic model for χ is also applied. Model predictions using constant and optimized time-dependent coefficients, and initialized using DNS data and simple analytical initial conditions, are compared. The values of quantities predicted by the models are also compared, such as the ratio of kinetic energy to released potential energy, production-over-dissipation/destruction ratios, and other self-similar quantities.

In general, and as expected, the model using time-dependent coefficients and DNS initial conditions captures the early-time and transitional behavior of the mixing layer evolution better than the model using constant coefficients and simplified initial conditions. However, the differences in the results obtained using DNS and simplified initial conditions are quite small. Also, the predictions of the three-equation model are remarkably similar to those of the four-equation model. Figures 1 shows a comparison of the time-evolution of the mixing layer widths and molecular mixing parameters from experiment, DNS, and the models using the two types of initial conditions and time-dependent coefficients. Larger differences in the predictions are observed between the three- and four-equation models when constant coefficients are used instead, as shown in Fig. 2.

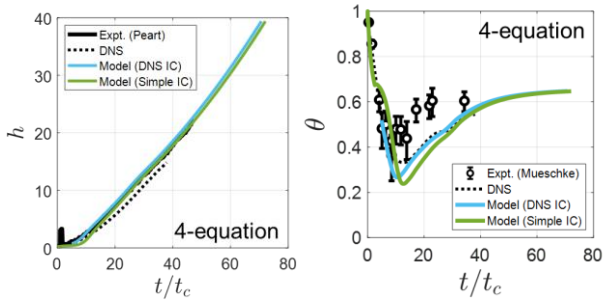

Figure 1: Mixing layer widths (left) and molecular mixing parameters (right) from experiment, DNS, and the four-equation model using time-dependent coefficients and the two types of initial conditions.

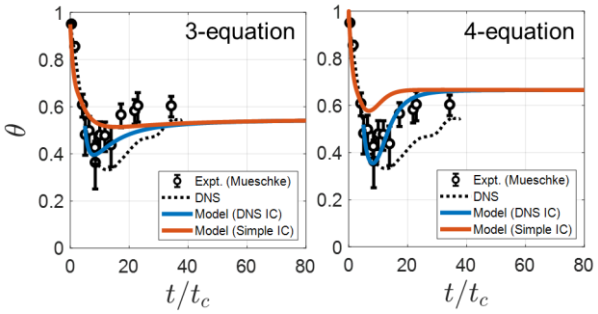

Figure 2: Molecular mixing parameters from experiment, DNS, and the three-equation (left) and four-equation (right) model using constant coefficients and the two types of initial conditions.

Acknowledgments: This work was performed under the auspices of the U.S. Department of Energy by Lawrence Livermore National Laboratory under Contract DE-AC52-07NA27344.

References

[1] Y. Zhou, Phys. Rep., **720-722**, 1 (2017); Y. Zhou, Phys. Rep., **723-725**, 1 (2017).
[2] O. Schilling, ASME J. Fluids Eng., **142**, 120802 (2020).
[3] D. M. Snider and M. J. Andrews, ASME J. Fluids Eng., **118**, 370 (1996); G. Dimonte and R. Tipton, Phys. Fluids, **18**, 085101 (2006).
[4] O. Schilling and N. J. Mueschke, Phys. Rev. E, **96**, 063111 (2017).
[5] N. J. Mueschke and O. Schilling, Phys. Fluids, **21**, 014106 (2009).
[6] O. Schilling, Phys. Fluids, **33**, 085129 (2021).

Convergence problem of Reynolds-averaged Navier-Stokes modeling in case of shock waves

Maksim Igorevich Boldyrev[1,*], I.V. Glazyrin[1] and N.A. Mikhailov[1]

[1]Russian Federal Nuclear Center – Zababakhin All-Russia Research Institute of Technical Physics, Snezhinsk, Russian Federation

[*]**Corresponding Author: boldyrevmi@vniitf.ru**

An implementation of *a k-ε-a-b* [1] turbulence model in the Eulerian 3D hydrocode FOCUS [2] had faced the problem of the solution convergence in tests of Richtmeyer-Meshkov (RM) [3, 4] instability. The source of the problem – an influence of the shock wave on the production of the turbulent quantities and its' diffusion through shock discontinuity.

To achieve the convergence and agreement with experiments, limitations are imposed on the deviatoric part of the Reynolds tensor in production terms and some of diffusion coefficients. A limiting function has following form [5]:

$$\theta_S = 1 \Big/ \sqrt{1 + \left(\frac{4 \cdot C_\mu}{3 \cdot C_S} \cdot \frac{k}{\varepsilon} \cdot \left(\nabla \cdot \vec{U} \right) \right)^2} \qquad (1)$$

Multiplication of the deviatoric part of the Reynolds tensor and diffusion coefficients by this function decreases turbulence generation on the shock discontinuity and diffusion of turbulent quantities through it.

Simulations of various experiments on Richtmeyer-Meshkov and Raleigh-Taylor [6] instabilities are performed to assess an effect of these limitations on the solution and agreement with experimental data.

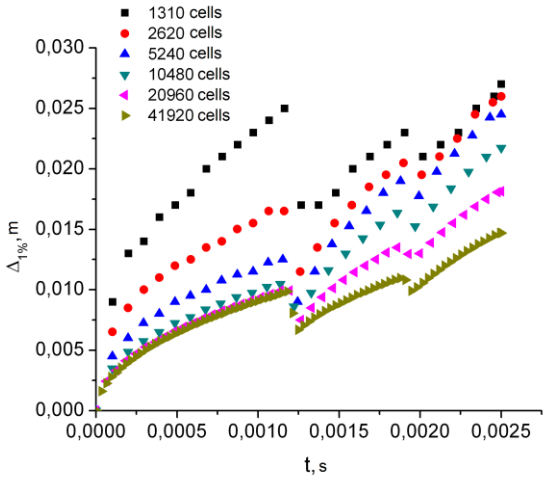

Figure 1: Modeling of Poggi RM experiment [7]. Solution diverges without limitations.

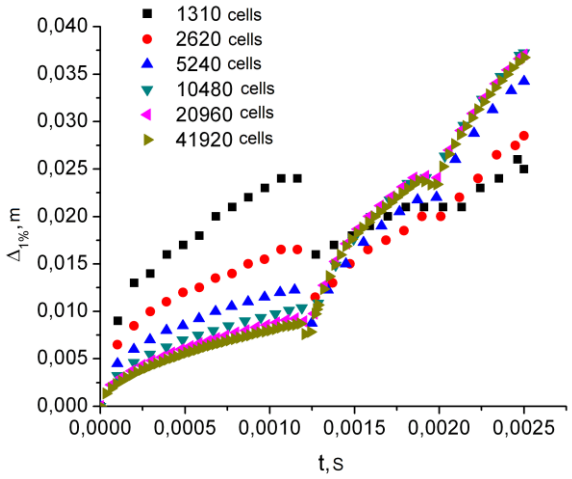

Figure 2: Modeling of Poggi RM experiment. Solution converges with limitations.

References

[1] D. Besnard, F.H. Harlow, R.M. Rauenzahn, and C. Zemach, LA-UR-12303, Los Alamos National Laboratory, Los Alamos, NM (1992).

[2] N.A. Mikhailov, I.V. Glazyrin, Zababakhin Scientific Talks: Proceedings of XII International Conference, 20-24 March, 2017, RFNC-VNIITF, p. 326 (2017).

[3] R.D. Richtmyer, Commun. Pure Appl. math., **13**, 297 (1960).

[4] E.E. Meshkov, Fluid Dyn. **4**, 101 (1969).

[5] M.I. Avramenko, About k-ε turbulence model, RFNC-VNIITF, Snezhinsk (2010, in Russian).

[6] G.I. Taylor, Proc. R. Soc., Ser. A, **201**, 192, London (1950).

[7] F. Poggi, M.-H. Thorembey, G. Rodriguez, Phys. Fluids **10**, 2698-2700 (1998)


49
ERS


GT